Design and modeling of an experimental tilapia and African catfish recirculating aquaculture system

by

Ruan Pretorius

Thesis presented in partial fulfilment
of the requirements for the Degree

of

MASTER OF ENGINEERING
(CHEMICAL ENGINEERING)

in the Faculty of Engineering
at Stellenbosch University

Supervisor

Neill Jurgens Goosen

March 2020

DECLARATION

By submitting this thesis electronically, I declare that the entirety of the work contained therein is my own, original work, that I am the sole author thereof (save to the extent explicitly otherwise stated), that reproduction and publication thereof by Stellenbosch University will not infringe any third party rights and that I have not previously in its entirety or in part submitted it for obtaining any qualification.

Date: March 2020

PLAGIARISM DECLARATION

1. Plagiarism is the use of ideas, material and other intellectual property of another's work and to present is as my own.

2. I agree that plagiarism is a punishable offence because it constitutes theft.

3. I also understand that direct translations are plagiarism.

4. Accordingly all quotations and contributions from any source whatsoever (including the internet) have been cited fully. I understand that the reproduction of text without quotation marks (even when the source is cited) is plagiarism.

5. I declare that the work contained in this assignment, except where otherwise stated, is my original work and that I have not previously (in its entirety or in part) submitted it for grading in this module/assignment or another module/assignment.

Student number: ……..

Initials and surname: ……..

Signature: ……..

Date: ……..

Abstract

This study aimed to design a new warm-water recirculating aquaculture system (RAS) that will have the flexibility to rear both African catfish (*Clarias gariepinus*) and Mozambique tilapia (*Oreochromis mossambicus*) using an engineering modeling approach. The facility was to be built within existing buildings and should maintain stable conditions when rearing either African catfish or Mozambique tilapia preferably at their commercial stocking densities of 200 kg/m^3 and 100 kg/m^3 respectively. Empirical data and verified models were obtained from literature to accurately describe the RAS. Unit operations were designed to achieve biofiltration by nitrification, solids removal, aeration, CO_2 degassing, UV sterilization and temperature control. The unit operations were sized for peak loading conditions which occur at the end of a trial when the feeding rate was highest. The stocking density was adjusted to 50 kg/m^3 due to limited footprint available for the wastewater treatment equipment required. At a peak biomass of 324 kg, the feeding rate was 10.3 kg/day and resulted in the estimated waste production rates of 505 g TAN/day, 2 333 g TSS/day, 1 256 g DOM/day, 3 490 g CO_2/day and oxygen consumptions of 2 538 g/day, 1 930 g/day and 2 028 g/day by fish, heterotrophic bacteria and autotrophic bacteria respectively.

The biofilters designed for the RAS were six moving bed bioreactors (MBBRs) of 1.0 m^3 each with 65% filling of 300 m^2/m^3 biomedia to maintain TAN concentrations in the fish tanks below 3.0 mg/L and were sized by considering both ammonium and oxygen reaction rate limiting substrates. A lamella settler with 5.5 m^2 settling area was designed to remove solids and was sized using experimentally measured settling rates of African catfish solids, which estimated a total suspended solids removal efficiency of 80%. A submerged in-tank aeration system for the fish tanks (110 std m^3/h) and MBBRs (25 std m^3/h) was designed using empirical data of various submerged diffuser depths and is estimated to maintain oxygen above the required minimum of 5 mg/L and limit CO_2 concentrations below 15 mg/L. The required recirculation flow rate to prevent accumulation of waste products in the fish tanks was estimated to be 12 m^3/h. Heat transfer models were used to estimate the heat loss from the process water and building air. The estimated peak heat loss of the water at 27°C was estimated to be 8.9 kW and is to be supplied by a heat pump. The largest heat loss contributor was evaporation at the fish tank surfaces.

The capital cost of the proposed RAS was estimated to be R 145 000. The annual operating costs of electricity (55.7% of total), make-up water (44% of total) and sodium bicarbonate for alkalinity control (0.2% of total) resulted in a total annual operating cost of R 79 000.

There was concluded that this study presents a thorough comparison of RAS technologies based on their advantages and disadvantages. The study also presents verified modeling methodology for conceptual RAS design and demonstrates the use by proposing a RAS design that is ready for implementation.

Opsomming

Hierdie studie het beoog om 'n nuwe warmwater hersirkuleringsakwakultuurstelsel (RAS) te ontwerp wat die buigbaarheid het om beide Afrika-baber (*Clarias gariepinus*) en Mosambiekse kurper (*Oreochromis mossambicus*) te kweek deur 'n ingenieursmodelleringsbenadering te gebruik. Die fasiliteit moes gebou word binne bestaande geboue en moet stabiele kondisies behou wanneer óf Afrika-baber óf Mosambiekse kurper verkieslik by hul kommersiële voorraaddigthede van 200 kg/m^3 en 100 kg/m^3 onderskeidelik gekweek word. Empiriese data en bevestigde modelle is verkry uit literatuur om die RAS akkuraat te beskryf. Bedryfseenhede is ontwerp om biofiltrasie deur nitrifikasie, verwydering van vaste stof, belugting, CO_2-ontgassing, UV-sterilisasie en temperatuur kontrole te bereik. Die bedryfseenhede is geskaal vir kondisies van spitslading wat plaasvind teen die einde van 'n toets as die voertempo op sy hoogste was. Die voorraaddigtheid is aangepas na 50 kg/m^3 as gevolg van beperkte staanoppervlakte beskikbaar vir die afvalwaterbehandeling se toerusting wat benodig word. By spitsbiomassa van 324 kg, was die voertempo 10.3 kg/dag en het die beraamde afvalproduksietempo's van 505 g TAN/dag, 2 333g TSS/dag, 1 256 g DOM/dag, 3 490 g CO_2/dag en suurstofgebruik 2 538 g/dag, 1 930g/dag en 2 028 g/dag deur visse, heterotrofiese bakterieë en outotrofiese bakterieë onderskeidelik tot gevolg gehad. Die biofilters ontwerp vir die RAS was ses bewegende bed-bioreaktors (MBBR) van 1.0 m^3 elk met 65% vulling van 300 m^2/m^3 biomedia om TAN-konsentrasie in die vistenks onder 3.0 mg/L te behou en is geskaal deur beperkende-substrate van beide ammonium- en suurstof-reaksietempo's in ag te neem. 'n Lamella besinker met 5.5 m^2 besinkingsarea is ontwerp om vaste stowwe te verwyder en is geskaal deur ekperimenteel-gemete besinkingstempo's van Afrika-baber se vaste stowwe te gebruik, wat 'n totaal verwyderingsdoeltreffendheid van hangende vaste stof van 80% beraam het. 'n Onderdompelde binne-tenk belugtingsisteem vir die vistenks (110 std m^3/h) en MBBRe (25 std m^3/h) is ontwerp deur empiriese data van verskeie onderdompelde verspreier dieptes te gebruik en is beraam om suurstof bo die vereiste minimum van 5 mg/L te handhaaf en CO_2-konsentrasies onder 15 mg/L te beperk. Die vereiste sirkulasie vloeitempo om akkumulasie van afvalprodukte in die vistenks te verhoed, is beraam om 12 m^3/h te wees. Hitte-oordragmodelle is gebruik om die hitteverlies van die proseswater en geboulug te beraam. Die beraamde spitshittteverlies van die water by 27°C is beraam om 8.9 kW te wees en is voorsien deur 'n hittepomp. Die grootste bydraer van hitteverlies was verdamping by die vistenkoppervlak.

Die kapitaalkoste van die voorgestelde RAS is beraam om R 145 000 te wees. Die jaarlikse koste van elektrisiteit (55.7% van totaal), aanvullingswater (44% van totaal) en koeksoda vir alkaliniteitbeheer (0.2% van totaal) het 'n totale jaarlikse bedryfskoste van R 79 000 tot gevolg gehad.

Daar is tot die gevolg gekom dat hierdie studie 'n deeglike vergelyking van RAS-tegnologieë lewer gebaseer op hul voordele en nadele. Die studie het modellering metodologie vir konsepsuele RAS-ontwerp bewys en stel die gebruik daarvan voor deur 'n RAS-ontwerp wat reg is vir implementasie.

Acknowledgements

Firstly, I would like to acknowledge the excellent support of my supervisor, Dr. Neill Goosen. Without his expert guidance, none of this work would have been possible.

My appreciation goes to the Department of Process Engineering at Stellenbosch University for the funding that made this study a reality.

I would like to acknowledge my dear friend Janus Louw for the many stimulating conversations that often helped me gain insight on details I was missing at the time.

Last, but certainly not least, I would like to the thank my parents, Johan and Francis Pretorius, for their continued loving support throughout my studies and for that I am eternally grateful.

Dedication

I dedicate this thesis to my loving wife and soul mate, Beth Pretorius. This undertaking would surely have failed without her undying support by picking me up when I'm down and spurring me on. Thank you for giving me the strength and showing me that sometimes it is worth it to just have a bit of faith.

Nomenclature - List of abbreviations

ADG	Average daily gain
AGR	Absolute growth rate
ASM	Activated sludge model
BOD	Biochemical oxygen demand
BOD_5	5-day biochemical oxygen demand
BP	Barometric pressure
BW	Body weight
CBOD	Carbonaceous biochemical oxygen demand
COD	Chemical oxygen demand
CSTR	Continuous stirred-tank reactor
DE	Diatomaceous earth
DO	Dissolved oxygen
DOM	Dissolved organic matter
DP	Differential pressure
FBB	Floating bead biofilter
FCR	Feed conversion ratio
FSB	Fluidized sand biofilter
HDPE	High-density polyethylene
HSL	Hydraulic surface loading rate
LLDPE	Linear low-density polyethylene
MBBR	Moving bed bioreactor
NR	Nitrogen retention
PFD	Process flow diagram
P&ID	Piping and instrumentation diagram
PM	Porous media
POM	Particulate organic matter
PVC	Polyvinyl chloride
RAS	Recirculating aquaculture system
RBC	Rotating biological contactor
SG	Specific gravity
SGR	Specific growth rate
STP	Standard temperature and pressure
TAN	Total ammonia nitrogen
TDS	Total dissolved solids
TGC	Temperature growth coefficient
TGP	Total dissolved gas pressure
TMY	Typical meteorological year
TSS	Total suspended solids
UV	Ultraviolet
VBGF	Von Bertalanffy growth function
WWT	Wastewater treatment
ZAR	South African Rand

Nomenclature - List of symbols

Symbol	Units	Description
A	m^2	Area
$A_{biofilm}$	m^2	Biofilm area
A_c	m^2	Cross-sectional area
A_s	m^2	Heat transfer surface area
A_{settle}	m^2	Horizontally projected settling area
AGR	g/day	Absolute growth rate
a_1	$g^{0.5}/(m^{0.5} \cdot day)$	Trickling filter model parameter
a_2	$g/(m^2 \cdot day)$	Trickling filter model parameter
a_3	$g/(m^2 \cdot day)$	Trickling filter model parameter
α	Dimensionless	Ratio of oxygen transfer coefficients at field and clean water conditions
β	Dimensionless	Ratio of oxygen saturation concentration at field and clean water conditions
B	$1/K$	Coefficient of volume expansion
$BOD_{5,prod}$	$g\ BOD_5/day$	Daily BOD_5 production
b	Dimensionless	Allometric exponent
BP	$mmHg$	Local barometric pressure
c_p	$J/(kg \cdot K)$	Specific heat capacity
$c_{p,w}$	$J/(kg \cdot K)$	Specific heat capacity of water
C	mg/L	Concentration
$C_{N,protein}$	$g\ N/g\ protein$	Nitrogen content of protein
C_{NH_3-N}	mg/L	Un-ionized ammonia concentration
$C_{NO_3-N,max}$	mg/L	Maximum allowable nitrate concentration
C_{CO_2}	mg/L	Dissolved carbon dioxide concentration
${C_{CO_2}}^{sat}$	mg/L	Saturation concentration of carbon dioxide in water
C_{O_2}	mg/L	Dissolved oxygen concentration
${C_{O_2}}^{*}$	mg/L	Reaction order transition oxygen concentration
${C_{O_2}}^{sat}$	mg/L	Saturation concentration of oxygen in water
$({C_{O_2}}^{sat})_{eff}$	mg/L	Mean effective dissolved oxygen saturation concentration
$({C_{O_2}}^{sat})_{CW}$	mg/L	Oxygen saturation concentration under clean conditions
$({C_{O_2}}^{sat})_{FW}$	mg/L	Oxygen saturation concentration under field conditions
$C_{protein}$	$g\ protein/g\ feed$	Feed protein content
C_{TAN}	mg/L	Total ammonia nitrogen concentration
${C_{TAN}}^{*}$	mg/L	Reaction order transition TAN concentration
D	m	Diameter
D_h	m	Hydraulic diameter of the geometry
D_p	m	Particle diameter
D_{inner}	m	Inner pipe diameter
D_{outer}	m	Outer pipe diameter
D_{pipe}	m	Pipe diameter
DP	$mmHg$	Difference between TGP and BP
ε	Dimensionless	Emissivity
ξ	m	Pipe surface roughness
F	$mmHg/(mg/L)$	Gas tension factor
f	Dimensionless	Darcy friction factor
Gr_L	Dimensionless	Grashof number

g	m/s^2	Gravitational acceleration
$\{H^+\}$	Dimensionless	Activity of hydrogen ions
HSL	$m^3/(m^2 \cdot day)$	Hydraulic surface loading rate
H	W	Heat transfer rate
H_{makeup}	W	Heat transfer rate due to make-up water addition
h	m	Height
$h_{diffuser}$	m	Diffuser depth
h_L	m	Head loss
h_{tf}	m	Distance from the top of the trickling filter
$K_L a_{CO_2}$	$1/day$	Overall carbon dioxide mass transfer coefficient
$K_L a_{O_2}$	$1/day$	Overall oxygen mass transfer coefficient
$(K_L a_{O_2})_{CW}$	$1/day$	Overall oxygen mass transfer coefficient under clean water conditions
$(K_L a_{O_2})_{FW}$	$1/day$	Overall oxygen mass transfer coefficient under field conditions
k_{death}	$1/day$	Mortality rate
k_{MBBR}	$g^{1-n_r} m^{3n_r-1}/day$	MBBR reaction rate constant
k_{VBGF}	$1/day$	Von Bertalanffy growth coefficient
κ	$W/(m \cdot K)$	Thermal conductivity
κ_{air}	$W/(m \cdot K)$	Thermal conductivity of air
κ_{wall}	$W/(m \cdot K)$	Thermal conductivity of wall material
λ_w	kJ/kg	Latent heat of vaporization of water
l	m	Fish length
L_c	m	Characteristic length of the geometry
L_{pipe}	m	Pipe length
$L_{plate\ length}$	m	Lamella settler plate length
$L_{plate\ width}$	m	Lamella settler plate width
L_{wall}	m	Wall thickness
m	g/day	Mass flow rate
m_{acc}	g/day	Mass accumulation rate
m_{CO_2}	g/day	Mass transfer rate of carbon dioxide into the water
$(m_{cons})_{CO_2}$	g/day	Carbon dioxide removed by aeration
$(m_{cons})_{O_2}$	g/day	Oxygen consumed by fish metabolism
m_{feed}	$g\ feed/day$	Feeding rate
m_{O_2}	g/day	Oxygen mass transfer rate
$(m_{prod})_{CO_2}$	g/day	Carbon dioxide excreted by fish
$(m_{prod})_{O_2}$	g/day	Oxygen added by aeration
$(m_{prod})_{TAN}$	g/day	Total ammonia nitrogen produced by feeding
$(m_{prod})_{TSS}$	g/day	Total suspended solids produced by feeding
$m_{recirc,in}$	g/day	Influent mass flow rate
$m_{recirc,out}$	g/day	Effluent mass flow rate
μ	$Pa \cdot s$	Dynamic viscosity
μ_w	$Pa \cdot s$	Dynamic viscosity of water
Φ	degrees	Lamella settler plate inclination with the horizontal plane
φ	Dimensionless	Submerged diffuser model parameter
η_a	Dimensionless	Absorption efficiency of aeration
η_{blower}	Dimensionless	Blower efficiency
N_{FW}	$lb\ O_2/(hp \cdot h)$	Oxygen transfer efficiency at field conditions
N_{std}	$lb\ O_2/(hp \cdot h)$	Oxygen transfer efficiency at standard conditions
Nu	Dimensionless	Nusselt number
NR	$g\ N\ retained/g\ N\ intake$	Nitrogen retention in the fish

n_i	N/A	Initial number of fish
n_t	N/A	Number of fish at time t
n_r	Dimensionless	Reaction order
P	Pa	Pressure
P_r	Dimensionless	Relative pressure
P_{blower}	hp or kW	Blower input power
P_{TAN}	$g\ N/day$	Total ammonia-nitrogen added to water
pK_a	Dimensionless	Acid dissociation constant
p_n	Dimensionless	Percentage of population that died in mortality data
ρ	kg/m^3	Density
ρ_p	kg/m^3	Particle density
ρ_w	kg/m^3	Density of water
$\rho_{stocking}$	kg/m^3	Peak fish stocking density
Q_{air}	m^3/h	Air volumetric flow rate at STP of 0°C and 101 325 Pa
Q_{makeup}	m^3/day	Make-up water volumetric flow rate
Q_{recirc}	m^3/day	Recirculation flow rate
Re	Dimensionless	Reynolds number
Λ	K/W	Thermal resistance
Λ_{cond}	K/W	Thermal resistance against heat transfer by conduction
$\Lambda_{cond,pipe}$	K/W	Thermal resistance against heat transfer by conduction through a circular pipe wall
Λ_{conv}	K/W	Thermal resistance against heat transfer by convective
Λ_{rad}	K/W	Thermal resistance against heat transfer by radiation
$\mathcal{H}$	$g\ H_2O/m^3$	Absolute humidity
$\mathcal{R}$	Dimensionless	Relative humidity
r_{TAN}	$g/(m^2 \cdot day)$	Nitrification reaction rate
$r_{TAN,max}$	$g/(m^2 \cdot day)$	Intrinsic nitrification reaction rate
SGR	$\%BW/day$	Specific growth rate
θ	Dimensionless	Temperature activity coefficient
T	K or °C	Temperature
T_{air}	K or °C	Air temperature
T_{film}	K or °C	Air film temperature
T_{makeup}	K or °C	Make-up water temperature
T_{PW}	K or °C	Process water temperature
T_s	K or °C	Surface temperature
T_∞	K or °C	Air temperature sufficiently far away from the surface
TGC	$g^{1/b}/(°C \cdot day)$	Temperature growth coefficient
TGP	$mmHg$	Total dissolved gas pressure
t	$days$	Production time
t_p	$days$	Length of production cycle of mortality data
τ	$mmHg$	Gas tension
u	m/s	Velocity
u_{avg}	m/s	Average flow velocity
u_o	m/s	Overflow rate
u_s	m/s	Settling velocity
V	m^3	Volume
v	m^2/s	Kinematic viscosity
v_w	m^2/s	Kinematic viscosity of water
w_{inf}	g	Asymptotic weight

w_i	g	Initial fish body weight
w_t	g	Fish body weight at time t
ψ	$W/(m^2 \cdot K)$	Heat transfer coefficient
ψ_{conv}	$W/(m^2 \cdot K)$	Convection heat transfer coefficient
ψ_{rad}	$W/(m^2 \cdot K)$	Radiation heat transfer coefficient
x	$g\ H_2O/kg\ dry\ air$	Mixing ratio
y	Dimensionless	Percentage reduction in nitrification rate relative to pH 8
Z	$g\ BOD_5/(m^2 \cdot day)$	Organic loading
ζ	m	Altitude of the site

Table of contents

Chapter 1. Introduction to recirculating aquaculture systems (RAS) 1
1.1 Introduction 1
1.2 Recirculating aquaculture systems (RASs) 2
1.3 Motivation for the study 3
1.4 Objectives and scope of the study 4
1.5 Structure of the thesis 5
Chapter 2. Literature survey of RAS technology 6
2.1 Water quality parameters 6
2.2 Biofiltration 15
2.3 Solids removal 20
2.4 Aeration and oxygenation 23
2.5 Carbon dioxide degassing 24
2.6 Disinfection 24
2.7 Water and air heating 25
2.8 Waste management 25
2.9 Conclusions 25
Chapter 3. Steady state RAS modeling methods 26
3.1 Introduction 26
3.2 Fish growth, mortality and feeding 27
3.3 Waste production models 34
3.4 Biofiltration modeling 38
3.5 Solids removal modeling 47
3.6 Aeration and degassing models 52
3.7 Pipe flow pressure drop 56
3.8 Fish tank mass balances 57
3.9 Water and air heat transfer models 59
Chapter 4. Conceptual design results 70
4.1 Design basis 72
4.2 Initial site layout 79
4.3 Fish tank design 80

4.4 Solids removal design 82
4.5 Biological filtration design 89
4.6 Aeration design 97
4.7 Water and air distribution design 102
4.8 Temperature regulation design 105
4.9 Disinfection design 107
4.10 Water quality measurements 108
Chapter 5. System design proposal 109
5.1 Required equipment and costs 109
5.2 Drawings of proposed facility 111
5.3 RAS dimensioning heuristics 112
5.4 RAS management plan 112
5.5 Conclusions 117
5.6 Recommendations for process optimization 118
References 120
APPENDIX A : Design variables 129
APPENDIX B : Equipment data sheets 132
B.1. Lamella settler data sheet 132
B.2. Moving bed bioreactor data sheet 132
B.3. Blower data sheet 133
B.4. Heat pump data sheet 133
B.5. Pump and blower performance curves 134
APPENDIX C : Piping and instrumentation diagrams (P&IDs) 136
APPENDIX D: Bill of quantities 138
APPENDIX E : Carbonate reaction equilibria 140
APPENDIX F : Gas properties 141
F.1. Nitrogen and oxygen properties 141
F.2. Air and water vapour properties 141
APPENDIX G : Lamella settler design 143
APPENDIX H: MBBR oxygen concentration optimization 145
APPENDIX I : Air distribution system sizing 147

List of tables

Table 2-1: Advantages and disadvantages of most commonly used biofilters (Eding et al., 2006; Timmons and Ebeling, 2007; Summerfelt, 2006; Kawan et al., 2016; Badiola et al., 2018) 18
Table 3-1: African catfish growth data and calculated TGC's 31
Table 3-2: Feeding levels and observed FCR's in African catfish systems 33
Table 3-3: Feeding levels proposed for African catfish growth from 10g to 1000g in 8 months (DAFF, 2018, p. 48) 33
Table 3-4: Protein content of fish feeds in literature 35
Table 3-5: Half-order/zero-order kinetics for nitrification reactions in a trickling filter (Bovendeur et al., 1987; Eding et al., 2006; Nijhof, 1995) 40
Table 3-6: Nitrification rates observed in an MBBR at various oxygen concentrations and organic loadings at a water temperature of 15°C (Hem et al., 1994) 44
Table 3-7: Nusselt number relations for natural convection over various geometries. Redrawn from Cengel and Ghajar (2015). 62
Table 4-1: List of equipment in the current existing RAS 72
Table 4-2: Experimental design of previous studies at Welgevallen 74
Table 4-3: Allowable stocking densities for tilapia RAS culture at different fish masses (Timmons and Ebeling, 2007, p. 121) 75
Table 4-4: Fish feed composition 76
Table 4-5: Chosen design water quality parameters for rearing tilapia and African catfish 77
Table 4-6: Relative humidity and absolute humidity with 5% probability of non-exceedance 79
Table 4-7: Disadvantages and potential applications of various solids removal configurations (Chen et al., 1994) 82
Table 4-8: Comparison of designs including and excluding a sand filter 87
Table 4-9: Initial sizing results for the MBBR design 93
Table 4-10: Biofilter sensitivity analysis 94
Table 4-11: Pump selection and operating costs for trickling filter RAS and MBBR RAS 95
Table 4-12: Final sizing results for the MBBR design 95
Table 4-13: Initial air diffuser sizing 97
Table 4-14: Fish tank and MBBR air flow sensitivity analysis 98
Table 4-15: Gas supersaturation results 101
Table 4-16: Cost-benefit analysis of a heat pump vs electric resistance heater 107
Table 5-1: Equipment list and capital costs 109
Table 5-2: Operating cost estimates 109
Table 5-3: RAS equipment sizing heuristics 112
Table 5-4: RAS troubleshooting guide 116
Table A-1: Input and output variables of the final RAS design 129
Table B-1: Lamella settler data sheet 132

Table B-2: Moving bed bioreactor data sheet 132
Table B-3: Blower data sheet 133
Table B-4: Heat pump data sheet 133
Table D-1: Bill of quantities for the proposed RAS design (pipes, pipe fittings and valves) 138
Table F-1: Nitrogen solubilities at different partial pressures, nitrogen and oxygen gas tension factors (Watten, 1994) 141
Table F-2: Ideal gas properties of air (Cengel and Boles, 2015) 142
Table H-1: Calculation results of blower operating costs 142
Table H-2: Calculation results of biofilter capital costs 142
Table H-3: Cashflow of various MBBR DO concentration cases 143
Table H-4: NPV over time of various MBBR DO concentration cases 143
Table I-1: Head loss calculation results of the fish tank air supply line 144
Table I-2: Head loss calculation results of the MBBR air supply line 145

List of figures

Figure 1-1: Global fish production from aquaculture and fisheries operations (FAOSTAT, 2017) 1
Figure 1-2: Block flow diagram of a typical RAS. 2
Figure 2-1: Predicted NH_3-N concentrations at different pH and temperature values and a constant TAN of 3 mg/L using equation (2.2) 9
Figure 2-2: Categorization of biofilter types. Redrawn from (Malone and Pfeiffer, 2006) 16
Figure 2-3: Particle size ranges with high solids removal efficiency of various processes. Redrawn from Chen et al. (1994) 20
Figure 2-4: Zones of a rectangular sedimentation tank (side view cross-section). Redrawn from Chen et al. (1994) 21
Figure 2-5: Tube- and lamella settler cross-section and flow. Redrawn from Timmons and Ebeling (2007) 22
Figure 3-1: Typical fish growth curve (Lugert et al., 2016) 27
Figure 3-2: Fish growth curve at 27°C with a TGC = 1.21 x 10^{-3} $g^{1/3}$/°C.day 32
Figure 3-3: Specific fish feeding rates estimated using DAFF feeding levels and FCR, both with TGC model estimated fish weights 34
Figure 3-4: Nitrification rates observed in literature compared to the TAN diffusion limiting model equation (3.16) 43
Figure 3-5: Percentage reduction in nitrification rates caused by lowered pH values 46
Figure 3-6: Experimental rig used to conduct a settling test for characterization of African catfish solids 49
Figure 3-7: Solids characterization of African catfish solids collected at Welgevallen, South Africa .. 50
Figure 3-8: Oxygen absorption efficiencies at various diffuser depths and DO saturation levels. Data by Mavinic and Bewtra (1976). Redrawn from Huguenin and Colt (2002) 54
Figure 3-9: Heat transfer paths through the ground 69
Figure 4-1: Temperature control conceptual design process 70
Figure 4-2: Wastewater treatment conceptual design process 71
Figure 4-3: Process flow diagram of current existing RAS 73
Figure 4-4: Total estimated daily feeding rate over time 77
Figure 4-5: Probability of non-exceedance of dry bulb temperatures from SAURAN dataset (SAURAN, 2019) during winter months (June – August) 78
Figure 4-6: Fish tank room layout before addition of WWT equipment (top view) 80
Figure 4-7: Fish tank inlet and outlet design cross sectional side view 81
Figure 4-8: Lamella settler drawing 84
Figure 4-9: Effect of TSS removal efficiency on TSS concentration in the fish tanks at peak loading 85
Figure 4-10: Effect of TSS production ratio on TSS concentration in the fish tanks at peak loading .. 86
Figure 4-11: Estimated conditions in the trickling filters 90

Figure 4-12: Proposed biomedia to be used as carriers in the MBBRs (Ecotao Enterprises, 2017) 91
Figure 4-13: Optimal MBBR oxygen concentrations as a function of investment period. Discount rate = 10% 92
Figure 4-14: First MBBR (BF-01) internals, piping and flow pattern design cross sectional side view 96
Figure 4-15: Chosen submerged air diffuser model HB016 99
Figure 4-16: CFW Fans regenerative blower model ZXB 710-3.0kW-50Hz performance curve showing the operating discharge air flow of the blower 100
Figure 4-17: BADU Porpoise 10 pump performance curve 102
Figure 4-18: Water and air piping layout 104
Figure 4-19: Building air heat losses at the design case 105
Figure 4-20: Process water heat losses at the design case 106
Figure 5-1: Process flow diagram of the proposed RAS design 111
Figure 5-2: African catfish stocking limits 113
Figure 5-3: Increase in TAN concentrations due to overfeeding 115
Figure B-1: BADU Porpoise 10, Porpoise 22 and Galaxy 23 pump performance curves 134
Figure B-2: CFW Fans regenerative blower model ZXB 710-3.0kW-50Hz performance curve 134
Figure B-3: SCL V4 1.1kW-50Hz regenerative blower performance curve 135
Figure C-1: Piping and instrumentation diagram of proposed RAS design wastewater treatment section 136
Figure C-2: Piping and instrumentation diagram of proposed RAS design fish tank section 137
Figure G-1: Lamella settler sheet metal cutting pattern on four 3000mm x 1500mm 304SS sheets . 143
Figure G-2: Lamella settler dimensions 144

Chapter 1. Introduction to recirculating aquaculture systems (RAS)

1.1 Introduction

Fish production is achieved by two different means. Firstly, wild fish are caught in the sea, lakes and rivers by fisheries. Secondly, fish are cultivated in farms (also known as aquaculture) employing a variety of production systems, including ponds, floating cages, flow-through raceways and recirculating aquaculture systems (RAS) (Timmons and Ebeling, 2007). Fish is an important food source that has been growing steadily in terms of consumption per capita, with global annual consumption increasing from 11.7 kg/capita in 1980 to 20.3 kg/capita in 2015 (FAOSTAT, 2017). Aquaculture is reported as the world's fastest growing agricultural industry with an average annual growth in global production of 8% (based on statistics from 1980 to 2015) (World Bank, 2011). The growth in aquaculture production versus fisheries production can be clearly seen in Figure 1-1 (FAOSTAT, 2017).

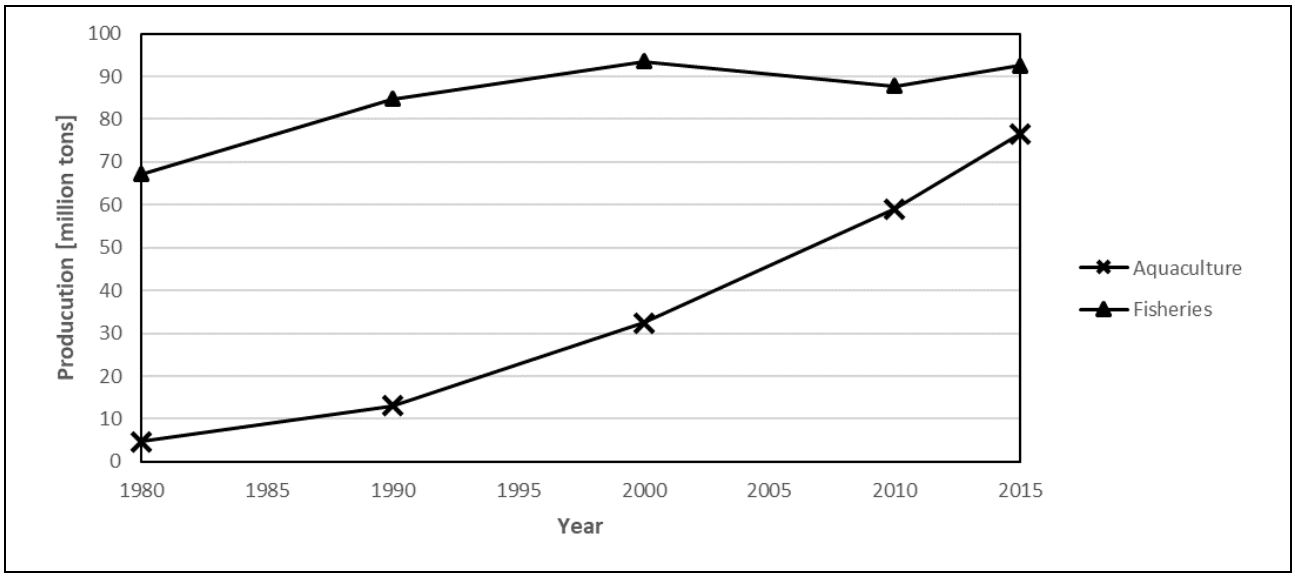

Figure 1-1: Global fish production from aquaculture and fisheries operations (FAOSTAT, 2017)

Figure 1-1 shows that the aquaculture industry has been growing rapidly when compared to fisheries that has experienced only very minor growth (>2%) since 1990. This stagnant output of wild capture fisheries has been a strong motivation for investment in aquaculture technologies. In terms of the South African context, studies suggest that growth in aquaculture industries in developing countries have a positive impact on the countries' economies. Although alleviation of poverty is a very complex issue, growth in aquaculture does help alleviate poverty to some extent (Béné et al., 2016).

1.2 Recirculating aquaculture systems (RASs)

Recirculating aquaculture systems (RAS) are, as the name implies, an aquaculture production system where the water used for culturing the animals is treated and then recirculated within the system. Effluent from the culturing tanks is treated using known wastewater treatment technologies, and mostly consists of solids removal, biological nitrification of ammonia to nitrate, degassing of dissolved CO_2, aeration to increase dissolved oxygen (DO) and UV irradiation for pathogen control (Timmons and Ebeling, 2007). A typical RAS flow scheme is shown in Figure 1-2.

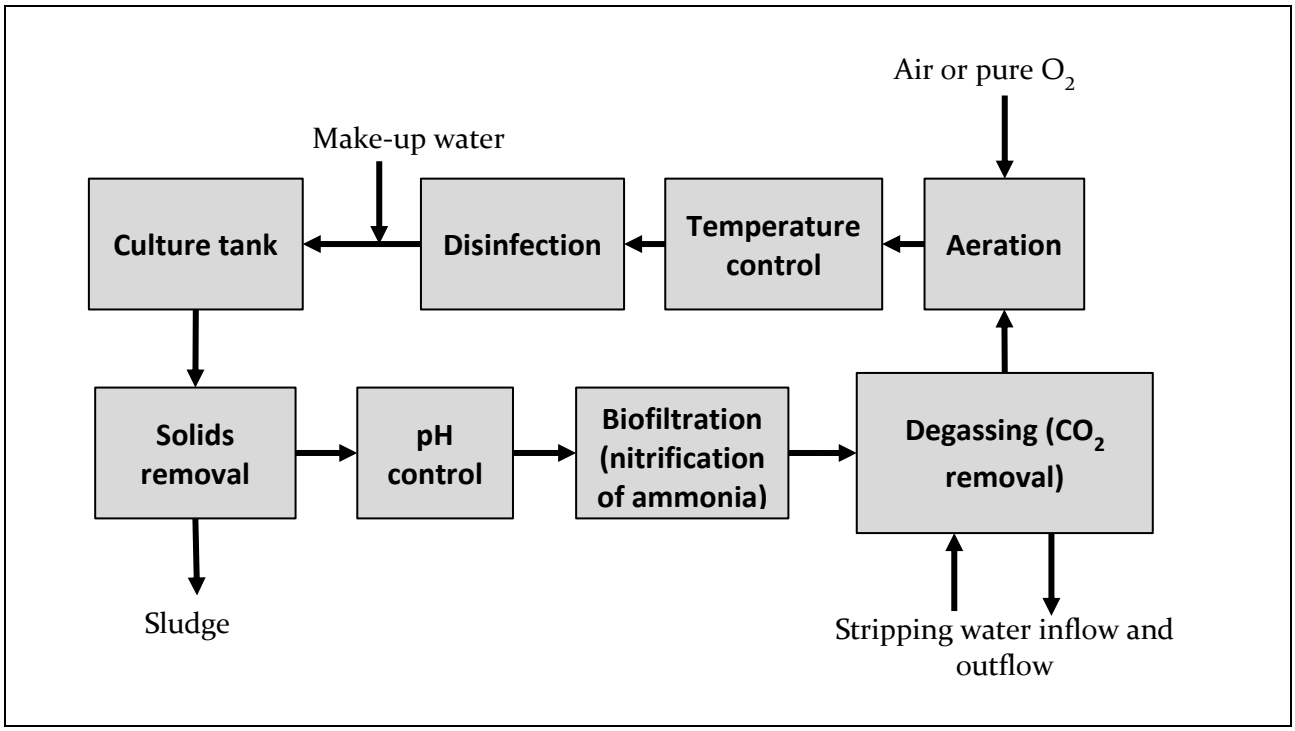

Figure 1-2: Block flow diagram of a typical RAS.

RASs have several advantages above flow-through systems and ponds. Flow-through systems do not reuse any water with the water only flowing through each tank once, which can be problematic if the area has a limited supply of freshwater. RASs recycle water by treating it, greatly reducing water requirements of the operation. Flow-through systems and ponds are mainly outdoors, which exposes them to the environment where diseases are easily introduced to the fish population. This is not a problem with RAS, which are indoor systems where pathogens can be better controlled to decrease the likelihood and impact of diseases. Another one of the main advantages of RAS is that water quality can be accurately controlled, resulting in a consistent water quality that facilitates predictable and year-round production (Lekang, 2007; Losordo and Timmons, 1994; Timmons and Ebeling, 2007). Due to the sustainability, biosecurity and high production rates, rearing of fish using RAS has become a popular method of aquaculture. Many experimental aquaculture systems at universities and research institutions use RAS technology for the increased control over water quality conditions needed to sustain reliable research (Bovendeur et al., 1987; Caraman et al., 2010; Goosen, 2014; Losordo et al., 2000; Terjesen et al., 2013).

1.3 Motivation for the study

Stellenbosch University owns an experimental facility at Welgevallen (33° 56' 34.8" S 18° 51' 57.6" E). This facility hosts various RAS for experimental work on Mozambique tilapia (*Oreochromis mossambicus*) and African catfish (*Clarias gariepinus*). Under conditions of high stocking density and multiple simultaneous trials, some of the experimental RAS have been unable to maintain optimal water quality standards. In experimental work it is especially crucial to consistently maintain water quality according to standards to gain conclusive results in terms of, for example, growth rates of cultured animals. Due to the inability to maintain water quality during high biomass loading, periodic water exchanges have been implemented to control water quality, which negates any advantages of lower water usage that RAS should provide. In recent years, the Western Cape (including Stellenbosch) has been subject to stringent water restrictions, thus having a well-functioning and high water-reuse RAS able to maintain high water quality standards for experimental work is particularly important to ensure high quality research which also utilizes water responsibly.

In the African context, better understanding of production of African catfish using RAS is crucial. African catfish is already grown in Nigeria using RAS, but production thereof is limited due to lack of knowledge of the technology and management of RAS (Akinwole and Faturoti, 2007). African catfish is a fast-growing fish that is relatively easy to culture, making it an attractive option for food production in developing countries. Interest has been shown in developing the market for African catfish in South Africa as well (DAFF, 2018).

RAS technology in general is poorly understood in South Africa (DAFF, 2018), with only a few small companies offering design work. Design of facilities producing high-end products such as Atlantic salmon have been outsourced to international companies due to lack of knowledge on both the fish species and the RAS technology (SalmonBusiness, 2018). Implementation of a commercial RAS requires large capital investments and operating costs to run when compared to wild caught fish. Therefore, high productivity in operations is required to make land-based fish production more sustainable.

Thus, better understanding of RAS technology and the Welgevallen experimental systems would be beneficial to research productivity and quality at Welgevallen and provide an opportunity for experimentation of the RAS itself. These points motivated the research question that this study attempted to answer: What methodology and parameters are appropriate for the design of an experimental RAS? This study set out to answer the research question by establishing a design methodology and demonstrating it practically by providing a design of a well-functioning RAS for use at Welgevallen.

1.4 Objectives and scope of the study

This study aimed to establish a design methodology and provide a design of a new RAS capable of culturing both African catfish and Mozambique tilapia.

Objective 1 - Determine through a literature survey the different technology options that can be used in RAS and evaluate the maturity, benefits and disadvantages of these technologies.

Objective 2 - Develop or compile mathematical models to describe (1) biomass growth and waste production, (2) the individual wastewater treatment unit operations, (3) fluid transport and (4) energy requirements in the RAS.

Objective 3 - Apply the RAS models to (1) evaluate the current Welgevallen RAS to identify equipment that can be reused or cost effectively altered and (2) design a new RAS based on retrofitting within existing infrastructure.

Objective 4 - Compile an operating guide to aid in successful operation of the designed RAS.

The scope of the design was limited to conceptual engineering design due to time constraints. The capital costs and operating costs of the proposed facility was to be determined. The design was to be described using:

1) Top-view layout of the RAS
2) Process flow diagram (PFD) of the RAS showing the major equipment and pipelines.
3) Piping and instrumentation diagram (P&ID) of the RAS showing all piping, valves and equipment in detail.
4) Data sheets of each major piece of equipment describing critical information.

1.5 Structure of the thesis

It should be noted that the work contained in this thesis was done using the engineering design method rather than the scientific method. As with the scientific method, the engineering design method focused on thoroughly defining the problem, identifying constraints and methods through a review of available literature. Where the engineering design method is different is that the study focused on formulating the final design package and product rather than observation and discovery of phenomenon through experimentation. The various chapters of this thesis show the design steps taken and presents the final design proposal at the end. Here follows a brief description of each chapter:

Chapter 1 Introduction to recirculating aquaculture systems (RAS)

The importance of RAS is motivated in this chapter along with the description of the project scope and objectives.

Chapter 2 Literature survey of RAS technology

Important water quality parameters are described in this chapter along with the allowable limits and measurement methods. Available RAS water treatment technologies are listed and discussed in this chapter.

Chapter 3 Steady state RAS modeling methods

All the models used for the sizing of the equipment are described in this chapter. This consists of the fish growth model, waste production estimates, biofilter reactor models, sedimentation model, sand filter model, aeration model and heat transfer modeling of the facility. Motivation for the use of a certain model is given where needed.

Chapter 4 Conceptual design results

The main design decisions are stated in this chapter. Motivation for the decisions are supported by use of the models described in Chapter 3. The selection of technologies and sizing of equipment is presented in this chapter. Sensitivity analyses are presented in this chapter that investigate the sensitivity of equipment sizes to changes in certain design parameters.

Chapter 5 System design proposal

A breakdown of sizes and costs for the redesigned system is presented and discussed. Drawings of the proposed facility is given. A management plan for successful operation of the proposed facility is given as well as possible areas of future process optimization.

Chapter 2. Literature survey of RAS technology

An overview of RAS technologies was essential to gain knowledge of the benefits and disadvantages of the various options for each unit operation and achieve Objective 1 of the study (see section 1.4). This allowed the choice of modeling methods to be more focused on specific technologies. Note that the technology choices are motivated in Chapter 4 as part of the design process narrative. The literature survey of RAS included water quality parameters, biofiltration, solids removal, aeration, degassing of carbon dioxide, UV irradiation, water heating, air conditioning and waste management.

2.1 Water quality parameters

Good management of water quality parameters in RAS culture is crucial. Fish species can only survive within a certain range of each water quality parameter with the ranges varying between different species. The water quality parameters for both the African catfish and Mozambique tilapia was investigated as the system was to be designed to be capable of culturing either species. Within the allowable range of a water quality parameter exists an optimal value where optimal growth and health of the fish is observed, which is required for optimal production performance and therefore economic performance. Considerable research has been devoted to determining the allowable limits for different species as well as the optimal parameter values. The aim of this section is to (1) define the critical parameters, (2) discuss why each of the critical parameters are important in fish production, (3) determine the allowable limits and optimal values reported in literature for African catfish and Mozambique tilapia and (4) state how each critical parameter is measured.

2.1.1 Dissolved oxygen concentration

Dissolved oxygen (DO) in the water is utilized by fish during respiration and is thus crucial for the survival of fish. A notable exception is the African catfish, which does have lungs capable of breathing air when crucially needed. However, the air breathing ability of African catfish was not considered in the design as it is only likely to occur at DO concentrations far below the optimal. Oxygen in fish drives all biological processes including digestion and growth. DO concentrations in water is important due to limited gill surface area that can take up oxygen, thus limiting the rate at which oxygen can be taken up (Tran-Duy et al., 2008), and sub-optimal DO concentrations impair growth rates of fish. Buentello et al. (2000) found that weight gain and feed intake both decreased with decreasing DO concentrations in channel catfish (*Ictalurus punctatus*) culture.

Timmons and Ebeling (2007) report a minimum safe DO concentration of 2 – 3 mg/L, below which fish can start suffocating. However, they recommend DO concentrations of 5 mg/L or higher to ensure optimal growth of warm-water freshwater fish. A DO concentration of 5 mg/L or higher is also recommended for commercial African catfish production (DAFF, 2018). Tilapia production is

recommended to have DO concentrations higher than 4 mg/L (Eding et al., 2006). For the purposes of designing a dual-purpose RAS, a design value of 5 mg/L would be suitable as it is optimal for both African catfish and tilapia.

DO levels have to be measured regularly due to the importance of oxygen for the survival of fish. Continuous monitoring is sometimes necessary if stocking densities are high. Monitoring of DO levels can be done analytically with the Winkler method or be measured using a DO probe, as is commonly done in RAS. DO meters work by placing an electrode in the water, which produces a signal that is proportional to the DO level in the water (Timmons and Ebeling, 2007).

2.1.2 Temperature

Fish are poikilothermic, which means that their body temperature is regulated by the surrounding water temperature. Therefore, there is only a certain temperature range for each fish species in which they can survive. There is also an optimum growing temperature for each fish. Fish are classified into 3 different groups:

- Cold-water = <15°C
- Cool-water = 15°C – 20°C
- Warm-water = >20°C

Both African catfish and tilapia are warm-water fish. Various recommendations for water temperatures are found in literature. Recommendations for African catfish are 25°C – 27°C (Eding et al., 2006) and 24°C – 26°C (Akinwole and Faturoti, 2007), while those for tilapia are 24°C – 30°C (Eding et al., 2006) and 28°C – 32°C (Timmons and Ebeling, 2007). When cultivated beyond these recommended ranges, animals will grow sub-optimally and be susceptible to disease. For example, in a trial with African catfish a high rate of mortalities was observed at water temperatures between 30°C and 35°C induced by high environmental temperatures (Oluwaseyi, 2016). The mortalities were proposed to be due to a condition called bloat that is a consequence of the high water temperatures (Oluwaseyi, 2016). This would suggest that the water temperature of 30°C was too high for African catfish, and a RAS should rather be controlled at the recommended temperatures of 24°C – 27°C when growing African catfish.

A suitable design temperature would be 27°C as it is within the recommended optimal ranges of both African catfish and tilapia. This is an acceptable choice as there is an example of an experimental RAS used to rear both African catfish and tilapia at 26.0°C ±0.7°C (Mota et al., 2015). African catfish has also been reared in an experimental system at 27.0°C (Schram et al., 2010).

The main method of measuring temperature is by using temperature probes included in DO meters and pH meters. Mercury thermometers are no longer used due to the risk involved with mercury leaks into the fish culture tanks (Timmons and Ebeling, 2007).

2.1.3 Ammonia, nitrite and nitrate concentrations

Nitrogenous wastes are pollutants that enter the water through various means, and mainly originate from the feed. Urea, uric acid and amino acids are excreted by fish through gill diffusion, gill cation exchange, urine and feces. Nitrogenous wastes can also enter the water through uneaten feed, decomposing biomass and nitrogen gas from the atmosphere. The most important nitrogenous waste found in aquaculture wastewater is ammonia (Timmons and Ebeling, 2007). Ammonia is mostly harmless in its ionized form, ammonium (NH_4^+), but is toxic to fish in its un-ionized form, ammonia (NH_3). Ammonium and ammonia are in equilibrium in water due to deprotonation of ammonia shown in equation (2.1).

$$NH_3 + H_2O \rightarrow NH_4^+ + OH^- \quad (2.1)$$

Thus, ammonia needs to be removed from the RAS water and is done through biofiltration, which involves the oxidation of ammonium (NH_4^+) to nitrite (NO_2^-) and nitrite to nitrate (NO_3^-) through the metabolism of autotrophic bacteria (see section 2.2.1).

For ease of calculation, inorganic nitrogen compounds are often expressed by the amount of nitrogen they contain, such as NH_3-N (un-ionized ammonia nitrogen), NH_4^+-N (ionized ammonium nitrogen), NO_2^-N (nitrite nitrogen), NO_3^-N (nitrate nitrogen) and TAN (total-ammonia-nitrogen), which is the sum of NH_3-N and NH_4^+-N.

2.1.3.1 Ammonia

The ratio of NH_3-N to NH_4^+-N is a function of pH, temperature and salinity. An equation for the prediction of un-ionized ammonia fraction was developed by Emerson *et al.*, (1975).

$$C_{NH_3-N} = \frac{C_{TAN}}{10^{(pK_a - pH)} + 1} \quad (2.2)$$

where

C_{NH_3-N}	=	Un-ionized ammonia concentration $[mg/L]$
C_{TAN}	=	Total-ammonia-nitrogen concentration $[mg/L]$
pK_a	=	Acid dissociation constant

pK_a can be estimated using equation (2.3):

$$pK_a = 0.0901821 + \frac{2729.92}{T} \quad (2.3)$$

where

T	=	Temperature $[K]$

Thus equations (2.2) and (2.3) can be used to predict the concentration of NH_3-N in freshwater when the pH and temperature is known. Figure 2-1 is a graphical depiction of equation (2.2), showing the effect of both pH and temperature on NH_3-N concentrations.

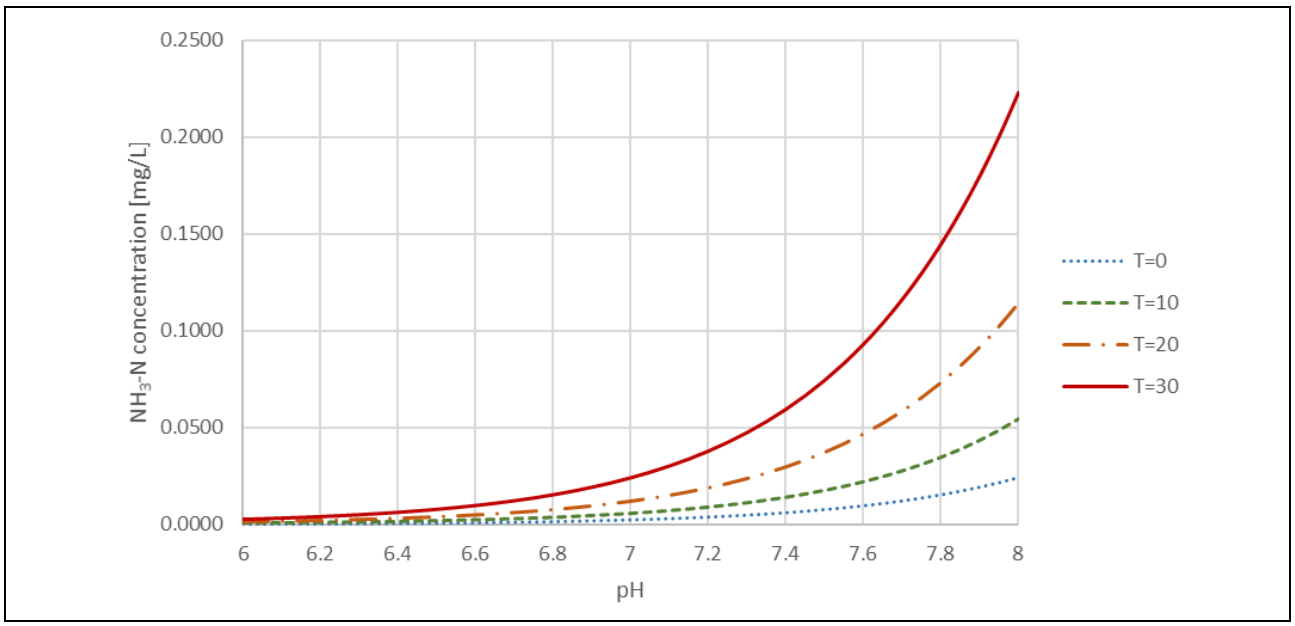

Figure 2-1: Predicted NH_3-N concentrations at different pH and temperature values and a constant TAN of 3 mg/L using equation (2.2)

As illustrated in Figure 2-1, ammonia is less soluble in water at higher temperatures. The NH_3-N concentration roughly doubles with an increase of 10°C at a constant pH. It can be calculated using equation (2.2) that in the range of 21°C to 30°C, the difference in NH_3-N concentrations at two temperatures 1°C apart is only 4%. This shows that if the water temperature can be maintained at a constant temperature with variations of up to 1°C, the NH_3-N concentration can only increase by 4%. As can be seen in Figure 2-1, pH also influences NH_3-N concentration where the NH_3-N concentration increases tenfold when pH is increased by 1. Thus, pH control is important as it can easily cause NH_3-N concentrations to increase beyond the recommended limits for healthy fish growth.

Timmons and Ebeling (2007) recommended that NH_3-N levels should be kept below 0.06 mg NH_3-N/L when rearing tilapia, and that total ammonia nitrogen (TAN) concentrations remain below 3.0 mg/L. Schram *et al.*, (2010) assessed the effects of elevated NH_3 concentrations on African catfish production and concluded that NH_3-N levels should not exceed 0.34 mg NH_3-N/L to prevent gill deterioration. From the above literature values, it was assumed that tilapia is the most sensitive species to ammonia. Although ammonia is the harmful nitrogenous substance, it was more useful for the purposes of modeling to define a limit for the TAN concentration rather than NH_3-N. This was due to TAN being a variable in biofilter modeling and the difficulty of estimating the pH of RAS water (Piedrahita and Seland, 1995). pH would have to be estimated in order to estimate NH_3-N concentrations. A maximum limit of 3.0 mg/L TAN was determined to be allowable for the culture of both African catfish and tilapia. This is supported by equation (2.2), that showed that the proposed tilapia NH_3-N limit of 0.06 mg NH_3-N/L will only be reached at a TAN concentration of 3.0 mg/L, pH of 7.5 and water temperature of 27°C.

Nesslerization is often cited as the standard method used for measuring ammonia concentrations (Timmons and Ebeling, 2007) and is a colorimetric method (Folin and Denis, 1916). Although

nesslerization is still used at existing facilities (Terjesen *et al.*, 2013; Fernandes, Pedersen and Pedersen, 2017), this method has been replaced as a standard quantification method due to the use of mercury in the analysis. Alternatives to nesslerization are an ammonia-selective electrode method and a phenate spectrophotometric method that can measure concentrations from 0.03 to 1400 mg NH_3-N/L and 0.02 to 2.0 mg NH_3-N/L respectively. The phenate method involves the formation of indophenol from ammonia, hypochlorite and phenol and is quantified using a spectrophotometer (APHA, 1998). Ammonia concentration measurements have also been done using ion chromatography, which is both expensive and time consuming (Brazil, 2006).

2.1.3.2 Nitrite

Nitrite (NO_2^-) is the intermediate product of nitrification (see Section 2.2.1) and has been proven to be toxic to fish (Hilmy et al., 1987). Freshwater fish must continually take up Cl^- ions through their gills to make up for ions lost through urine and passive efflux across the gills. The presence of nitrite causes the nitrite ions to preferentially be taken up instead of Cl^-. Nitrite ions enter the blood stream and diffuse into red blood cells, where these ions in the red blood cells react with iron found in hemoglobin, forming methemoglobin that reduces the overall oxygen carrying capacity of the blood. High levels of methemoglobin can cause fish mortalities (Kroupova et al., 2005). Fish have been shown to acclimatize to nitrite over time, increasing their resistance to toxic effects (Kroupova et al., 2005). However, a sudden increase in nitrite concentrations could be lethal.

Nitrite toxicity is affected by a range of factors namely: length of exposure, chloride concentration, bromide concentration, calcium concentration, sodium concentration, ammonia concentration, pH, dissolved oxygen, temperature, fish species and fish size (Kroupova et al., 2005). The most significant factor influencing nitrite toxicity is the chloride concentration. Nitrite toxicity has been found to greatly decrease when chloride ions are present in the water (Tomasso et al., 1979). Thus a certain ratio of chloride to nitrite must be maintained to prevent the toxic effects of nitrite on fish. Timmons and Ebeling (2007) recommended a 20 to 1 mass ratio of Cl^- to NO_2^- and that the NO_2-N concentration should be kept below 1.0 mg NO_2-N/L when rearing tilapia. Losordo et al. (2000) have successfully operated an intensive tilapia RAS by maintaining 100 mg Cl^-/L at an average NO_2-N concentration of 1.83 mg NO_2-N/L. These higher nitrite levels were reported to be typical of a biofilter that is still developing a stable biofilm. Thus, the steady state design nitrite concentration should be below 1.0 mg NO_2-N/L.

A colorimetric method is the most common method of measuring nitrite concentration in water and requires the use of a spectrophotometer or filter photometer (APHA, 1998). Ion chromatography was used for nitrite concentration measurements by Brazil (2006), which is both expensive and time consuming compared to other methods. As an alternative to the colorimetric method, a cadmium reduction method was used for nitrite concentration measurements by Losordo et al. (2000).

2.1.3.3 Nitrate

Nitrate (NO_3^-) is the final product of the nitrification process (see Section 2.2.1). Nitrate is only removed from a RAS through water exchange or denitrification (reduction of nitrate to nitrogen gas). If the RAS has a high water reuse ratio, nitrate can accumulate in the system (Timmons and Ebeling, 2007). Identically to nitrite, nitrate is suggested to be toxic due to uptake in the blood and the subsequent conversion of hemoglobin to methemoglobin. The uptake of nitrate is less profound than nitrite and is thus less toxic (Camargo et al., 2005).

Timmons and Ebeling (2007) recommended nitrate concentrations be maintained below 400 mg NO_3-N/L. Losordo et al. (2000) operated a tilapia farm at nitrate concentrations of 200 – 250 mg NO_3-N/L. Schram *et al.* (2014) assessed the effects of nitrate on the physiology, growth and feed intake of African catfish and recommended that nitrate concentrations should not exceed 140 mg NO_3-N/L. The design maximum nitrate concentration was thus chosen to be 140 mg NO_3-N/L.

Various methods can be used for nitrite measurements, namely (1) ultraviolet method, (2) ion chromatography, (3) capillary ion electrophoresis, (4) nitrate electrode method, (5) cadmium reduction method and (6) automated cadmium reduction methods (APHA, 1998). Ion chromatography was used for nitrate concentration measurements by Brazil (2006).

2.1.4 pH, alkalinity and hardness

pH is a measure of how acidic or basic a solution is and is defined in equation (2.4) (Stumm and Morgan, 1995):

$$pH = -\log\{H^+\} \quad (2.4)$$

where
$\{H^+\}$ = Activity of hydrogen ions (activity is the measure of the effective concentration of a species in a mixture)

pH is important in RAS for a variety of reasons. Both the fish and bacteria have a range of pH values that they can survive and thrive in. However, the most crucial effect of pH is its effect on the ratio of NH_4^+ to NH_3 (see section 2.1.3.1) At the maximum values of 0.06 mg NH_3-N/L and 3.0 mg TAN/L, the maximum allowable pH would be 7.5, calculated using equation (2.2). Timmons and Ebeling (2007) recommended an optimal pH range of 6.5 to 9.0 for freshwater fish. Tilapia has been successfully reared in a system with a pH varying between 6.9 and 7.4. (Losordo et al., 2000) Thus, a steady state design pH of 7.0±0.2 would be acceptable. pH is measured using pH meters calibrated using standard solutions (APHA, 1998).

Alkalinity is the acid neutralizing capacity of water and is defined as the amount of titratable bases present in the water. Alkalinity is expressed as the equivalent of milligrams calcium carbonate ($CaCO_3$) per liter (APHA, 1998). CO_3^- and HCO_3^- are the main ions contributing to alkalinity. Since HCO_3^- is consumed in nitrification reactions (see section 2.2.1), alkalinity often needs to be increased by adding

a supplement such as sodium bicarbonate ($NaHCO_3$) (Timmons and Ebeling, 2007; Bovendeur et al., 1987). Alkalinity, pH and carbon dioxide concentrations are linked and thus the required alkalinity depends on pH and carbon dioxide concentrations. Total alkalinity is measured using a titration technique by changing the pH to 8.3 first using a phenolphthalein indicator and then to 4.5 using a bromocresol green or a mixed bromocresol green-methyl red indicator (APHA, 1998).

Hardness is defined as the sum of the bivalent metal ions and is expressed as the equivalent of mg $CaCO_3$/L (APHA, 1998). Calcium and magnesium are important minerals for fish bone and scale growth (Wurts, 2002). Wurts (2002) recommended that calcium hardness in aquaculture water should range between 75 and 200 mg $CaCO_3$/L. Timmons and Ebeling (2007) recommended that total water hardness should be kept above the equivalent of 100 mg $CaCO_3$/L in a commercial fish tank. An EDTA titrimetric method is used to measure total water hardness (APHA, 1998).

2.1.5 Carbon dioxide concentration

Dissolved carbon dioxide in water can be inhibitory to fish health at high levels. The carbon dioxide concentration in the fish's blood can increase, decreasing the amount of oxygen that the hemoglobin in the blood can transport. This can lead to respiratory distress in fish (Timmons and Ebeling, 2007). An upper limit of 15-20 mg CO_2/L is recommended when rearing tilapia (Timmons and Ebeling, 2007) and 25 mg CO_2/L when rearing African catfish. (Eding et al., 2006). However, it was stated by these sources that carbon dioxide limits are difficult to define and should be used as rough guidelines. The chosen maximum allowable carbon dioxide concentration was 15 mg/L to remain conservative and allow for the system to be suitable for both African catfish and tilapia. Dissolved carbon dioxide is inferred using a nomograph which requires knowledge of the pH and total alkalinity (Timmons and Ebeling, 2007).

2.1.6 Solids concentration

Solids in water are classified into two main categories, namely total suspended solids (TSS) and total dissolved solids (TDS). TSS is defined as the solids larger than 2.0 µm and TDS as the solids smaller than 2.0 µm (APHA, 1998). TDS is also known as salinity (see section 2.1.7).

Feces and uneaten feed are the main sources of TSS in water. The presence of these particles increase biochemical oxygen demand in the water (BOD) and releases toxins such as ammonia into the water (Baccarin and Camargo, 2005). Suspended solids negatively affect biofiltration by attaching to the biofilm, increasing BOD and thereby decreasing nitrification rates (Eding et al., 2006). In other words, the presence of suspended solids decreases the efficiency of biofilters. Chapman *et al.* (1987) have shown suspended solids within the size range of 5 – 10 µm to be toxic to rainbow trout. No research on the effects of varying suspended solid particle sizes on either tilapia or African catfish was found. Suspended solids can negatively affect fish health by damaging gills and carrying pathogens. Current research suggests that generally the TSS concentration is not a critical parameter for fish health when compared to dissolved oxygen, carbon dioxide, temperature or ammonia (Timmons and Ebeling,

2007). However, the fact that suspended solids increases BOD, total ammonia nitrogen concentrations and decreases biofilter efficiency warrants the rapid removal of TSS within a RAS.

Timmons and Ebeling (2007) recommended an upper limit for TSS concentration at 25 mg/L and 10 mg/L for long-term operation of freshwater fish culture. 25 mg/L is recommended as the upper limit for African catfish (Eding et al., 2006). A limit of 15 mg/L has also been recommended (Chen et al., 1994). Tilapia have been reported to show no adverse effects in well-being when the TSS concentration was 80 mg/L with all other water quality parameters being acceptable (Timmons and Ebeling, 2007).

For TSS concentration data collection, TSS concentration is measured using standard method number 2540D, which is sampling, filtration of the sample through a glass-fiber filter, constant drying of the sample at 103 to 105°C and measurement of the filter mass increase (APHA, 1998).

2.1.7 Salinity

Salinity is the concentration of dissolved salts in the water (APHA, 1998) and is expressed as parts per million (ppm) or milligrams of salt per liter of water. Freshwater aquaculture systems are generally maintained at a salinity of 2000 to 3000 ppm. The TDS is equal to the salinity and commonly includes calcium, sodium, potassium, bicarbonate, chloride and sulfate (Timmons and Ebeling, 2007).

The most efficient methods of measuring salinity are indirectly using electrical conductivity, water density, speed of sound in the water, or refractive index. Electrical conductivity is the most precise and convenient of these methods and is thus the most used method for determining salinity (APHA, 1998).

2.1.8 Biochemical oxygen demand (BOD)

Biochemical oxygen demand (BOD) is defined as the oxygen that can be consumed through oxidation of organic matter by microorganisms. BOD can be expressed as either ultimate BOD (BOD_U) or 5-day BOD (BOD_5). BOD_U is a measure of the oxygen consumed when all carbonaceous and nitrogenous organic matter have been biologically oxidized. BOD_5 is a measure of the oxygen consumed by biological oxidation of organic matter after a 5-day incubation period at 20°C. Most of the carbonaceous organic matter is oxidized within the first 5 days of incubation, with minimal oxidation of nitrogenous organic matter by nitrifying bacteria (APHA, 1998). Thus, it can be assumed that BOD_5 is equal to the carbonaceous biochemical oxygen demand ($CBOD_5$), which is a measure of the oxygen consumed by heterotrophic biological oxidation of carbonaceous organic matter. BOD differs from chemical oxygen demand (COD), which is the oxygen consumed through oxidation of organic matter using a chemical oxidant. This means that COD accounts for both the biodegradable and non-biodegradable portions of the organic matter (APHA, 1998).

High levels of BOD_5 in RAS effluent can be harmful to the environment and requires further biological treatment before discharge can be permitted. High levels of BOD_5 in the recirculating water results in increased heterotrophic bacterial populations, inhibiting nitrifying bacteria in the biofilter through decreased availability of dissolved oxygen (Eding et al., 2006; Rusten et al., 2006). Specific limits for

BOD_5 in RAS were difficult to define as, by itself, it does not have any negative effects on fish production. The negative effect of BOD_5 occurs via impacts on the biofilter performance and has been accounted for in the biofilter modeling (see section 3.4.6.2).

2.1.9 Total dissolved gas pressure (TGP)

Supersaturation of gas in aquaculture water can cause gas bubble disease, usually leading to high mortality rates in fish populations (Weitkamp and Katz, 1980). Gas supersaturation can occur in a RAS when using submerged air diffusers due to hydrostatic pressure increasing the saturation concentrations of dissolved gasses at the diffuser location. The degree of gas supersaturation is determined by calculating the total dissolved gas pressure (TGP) by gas tensions (see section 3.6.2). The water is considered supersaturated with gas if the TGP exceeds the local barometric pressure (BP).

Allowable limits of TGP in fish tanks are defined by (1) the %TGP, which is the ratio between TGP and atmospheric pressure and (2) differential pressure (DP), which is TGP minus BP. For example, if TGP and BP equals 836 mmHg and 760 mmHg respectively, the %TGP will be 110%. A study observed no gas bubble disease at %TGP of 106% (Weitkamp and Katz, 1980). It is recommended that the DP in intensive warm-water RAS not exceed 20 mmHg (Watten, 1994).

2.2 Biofiltration

Biofiltration is the process of removing ammonia from wastewater through biological nitrification reactions. Nitrification is done by nitrifying bacteria that form part of a biofilm on solid media placed in biofilter units. Biofiltration is considered a crucial process step in RAS that requires careful design considerations (Timmons and Ebeling, 2007) and was thus a major focus of this thesis. Modeling of biofilters is discussed in section 3.4.

2.2.1 Nitrification

Nitrification is the oxidation of ammonia to nitrite, followed by the oxidation of nitrite to nitrate. The oxidation of ammonia to nitrite and nitrite to nitrate is done by the autotrophic bacteria *Nitrosomonas* and *Nitrobacter* respectively. These nitrification reactions are given by equations (2.5) and (2.6) (Henze et al., 1997).

Nitrosomonas: $$NH_4^+ + \frac{3}{2}\,O_2 \rightarrow NO_2^- + H_2O + 2\,H^+ \quad \textbf{(2.5)}$$

Nitrobacter: $$NO_2^- + \frac{1}{2}\,O_2 \rightarrow NO_3^- \quad \textbf{(2.6)}$$

Autotrophic bacteria use CO_2 as their carbon source. The reactions for cell growth is given in equations (2.7) and (2.8) with the compound $C_5H_7NO_2$ representing the bacterial biomass (Henze et al., 1997).

$$15\,CO_2 + 13\,NH_4^+ \rightarrow 10\,NO_2^- + 3\,C_5H_7NO_2 + 4\,H_2O + 23\,H^+ \quad \textbf{(2.7)}$$

$$5\,CO_2 + NH_4^+ + 10\,NO_2^- + 2\,H_2O \rightarrow 10\,NO_3^- + C_5H_7NO_2 + H^+ \quad \textbf{(2.8)}$$

In addition to using the carbonate equilibrium system (see APPENDIX E), equations (2.5) and (2.7) are combined to yield equation (2.9). Equations (2.6) and (2.8) are also combined to yield equation (2.10).

$$80.7\,NH_4^+ + 114.55\,O_2 + 160.4\,HCO_3^- \rightarrow C_5H_7NO_2 + 79.7\,NO_2^- + 82.7\,H_2O + 155.4\,H_2CO_3 \quad \textbf{(2.9)}$$

$$134.5\,NO_2^- + NH_4^+ + 62.25\,O_2 + HCO_3^- + 4\,H_2CO_3 \rightarrow C_5H_7NO_2 + 134.5\,NO_3^- + 3\,H_2O \quad \textbf{(2.10)}$$

Within a biofilter, the substrates for the metabolism reactions diffuse into the biofilm from the bulk water and subsequently the products of the reactions (metabolites) diffuse back into the bulk water. The two main substrates in equation (2.9) are ammonium (measured as TAN) and oxygen. Thus a biofilter can be either TAN diffusion limited or oxygen diffusion limited (Eding et al., 2006).

2.2.2 Types of biofilters

Different types of biofilters are commonly used in wastewater treatment and RASs. As previously mentioned, nitrifying bacteria are grown on solid media to form a biofilm, which is known as the fixed film type of biofilter. Biofilters operating without solid media are classified as suspended growth biofilters where heterotrophic bacteria are grown in suspension (Timmons and Ebeling, 2007) Suspended growth biofilters are considered to be less stable than fixed film biofilters (Malone and

Pfeiffer, 2006), but are regularly used for denitrification and elimination of organic matter in RAS effluent streams (Schneider et al., 2007). Fixed film biofilters were the focus of this design due to the wide knowledge base of the technology and the improved stability of the autotrophic bacterial populations. Fixed film biofilters can be categorized into four types according to the nature of their hydraulics, namely emergent, packed, expandable and expanded biofilters. These categories each have different types of biofilter configurations as shown in Figure 2-2 (Malone and Pfeiffer, 2006).

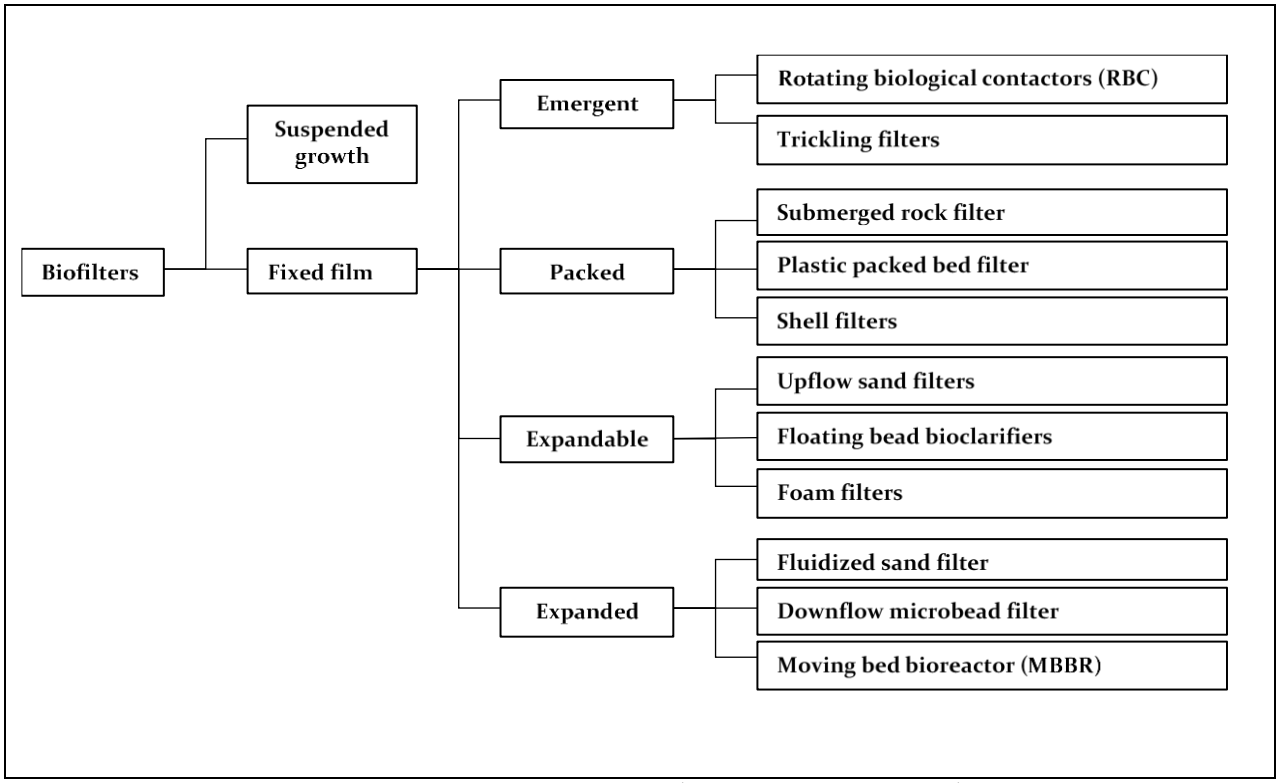

Figure 2-2: Categorization of biofilter types. Redrawn from (Malone and Pfeiffer, 2006)

The most commonly used types of biofilters are (1) trickling filters (Eding *et al.*, 2006; Akinwole and Faturoti, 2007; McMillan *et al.*, 2003; Bovendeur, Eding and Henken, 1987; Mota *et al.*, 2015; Losordo, Hobbs and DeLong, 2000), (2) rotating biological contactors (Brazil, 2006; Van Gorder and Jug-Dujakovic, 2004), (3) moving bed bioreactors (Terjesen et al., 2013), (4) fluidized sand biofilters (Guerdat *et al.*, 2010; Heinen *et al.*, 1996; Summerfelt *et al.*, 2004) and (5) floating bead biofilters. Only these biofilters were considered for the design due to their wide application in RAS and literature data available for modeling. The various advantages and disadvantages of the biofilters considered are listed in Table 2-1 in section 2.2.3.

2.2.2.1 Trickling filters

Trickling filters operate by distributing water over the top of a fixed bed of filter media. The water needs to be evenly distributed to ensure the entire biofilm grown on the filter media is wetted. Forced ventilation is often used to force air upwards in the column to supply O_2 to bacteria and strip CO_2. This is done to prevent air from being stagnant in the column which can lead to anaerobic conditions, which will reduce nitrification rates (Eding et al., 2006; Timmons and Ebeling, 2007). Typical trickling

filters used in RAS vary from 0.15 – 5.0 m high (Wheaton et al., 1994a). Practical aspects of trickling filter design and operations are described by Eding et al. (2006).

2.2.2.2 Rotating biological contactors (RBC)

A rotating biological contactor (RBC) is type of biofilter that consists of a rotating horizontal shaft attached to the centers of multiple disks, acting as the media where the biofilm grows. The shaft is located at the top of the water level with half of each disk being submerged. The disks are sufficiently spaced to be close enough to provide high specific surface area and far enough apart to prevent clogging (Wheaton et al., 1994a). The main aspect that sets RBC's apart from other biofilters is that it has mechanical moving parts, increasing the failure rate due to mechanical failure (Timmons and Ebeling, 2007). Hochheimer and Wheaton (2000) discussed all the practical aspects of RBC design and operation.

2.2.2.3 Fluidized sand biofilters (FSB)

Fluidized sand biofilters (FSB) are containers filled with a media of high specific surface area (usually a type of sand) and operated by pumping water through the filter of a sufficient velocity to fluidize the media. A mesh on the inlet pipe is installed to prevent backflow of media. The main costs associated with FSBs are pumping costs due to the head loss through the media and the fact that water must be pumped upwards through the filter (Wheaton et al., 1994a). FSBs are associated with systems required to maintain excellent water quality of 0.1 – 0.5 mg TAN/L and < 0.1 – 0.3 mg NO_2-N/L at the filter discharge (Summerfelt, 2006). The practical aspects of design and management of FSB's were described by Summerfelt (2006).

2.2.2.4 Floating bead biofilters (FBB)

Floating bead biofilters (FBB) are similar in construction to FSBs but contain 3 – 5 mm polyethylene beads as media with a specific gravity of roughly 0.91 and specific surface areas of 1150 – 1475 m^2/m^3. The low specific gravity causes the beads to float. FBBs are operated in an up-flow configuration. FBBs are also known as bioclarifiers due to the beads also acting as a granular filter (see section 2.3.2.2), requiring periodic backwashing (Timmons and Ebeling, 2007).

2.2.2.5 Microbead filter

A microbead filter is similar in construction to FSBs and FBBs, but differs in the biomedia used, which are polystyrene beads of a much lower density (16 kg/m^3 bulk density) and are 1 – 3 mm in diameter. Microbead filters are operated in a downflow configuration where water is distributed over the beads and allowed to trickle downwards (Timmons and Ebeling, 2007).

2.2.2.6 Moving bed bioreactors (MBBR)

A moving bed bioreactor (MBBR) consists of floating biomedia with a specific gravity of 0.95. These carriers are unlike floating bead filter and microbead filter media, as they are cylindrical structures with inner and outer fins to increase specific surface area. The biomedia is constantly agitated by aeration to achieve mixing of the water, supply oxygen and prevent clogging of the biofilm by abrasion

of the media against each other, which removes the need for backwashing. MBBRs have negligible pressure drop and are operated at atmospheric pressure. The outlet water can be recirculated to the fish tank by an overflow. The inlet is commonly located at the bottom of the tank to prevent bypassing of reactor volume. Both the inlet and outlet require a mesh to prevent biomedia from exiting the MBBR (Ødegaard, 1995). MBBRs are relatively new when compared to other biofilter types, but have shown commercial success in both wastewater treatment and aquaculture (Kawan et al., 2016; Rusten et al., 2006, 1995).

2.2.3 Advantages and disadvantages of various biofilters

The various types of biofilters described above each have their own advantages and disadvantages, which are listed in Table 2-1.

Table 2-1: Advantages and disadvantages of most commonly used biofilters (Eding et al., 2006; Timmons and Ebeling, 2007; Summerfelt, 2006; Kawan et al., 2016; Badiola et al., 2018)

Advantages	Disadvantages
Trickling filter	
Simple to design and operate	Relatively low volumetric nitrification rates, resulting in large reactor volumes and thus high capital cost
Wide knowledge base available on operations and modeling	
CO_2 stripping takes place within the tower	
Evaporation of water through forced ventilation can help with water cooling in the summer	Sloughing/shearing of biofilm
Most widely used biofilter type, reducing material costs and increasing material availability	Relatively high pumping costs
Relatively high stability	More susceptible to clogging
Rotating biological contactor (RBC)	
Aeration takes place within the reactor	Mechanical failure of RBCs is more likely due to wear on rotating bearings
Some degree of CO_2 stripping takes place	
Self-cleaning due to mechanical rotation and therefore does not clog easily.	Relatively low specific surface area, resulting in large reactor volumes and thus high capital cost
Relatively low operating costs	
No clogging	
Moving bed bioreactor (MBBR)	
Low head loss with only pumping requirement to pump to the top of the filter	Start-up of the filter can take relatively long
Relatively high media specific surface area	Efficiency of filter is sensitive to change in parameters such as temperature
No requirement for backwashing	
Low maintenance requirements	Efficiency highly dependent on media used
No clogging	

Table 2-1: Advantages and disadvantages of most commonly used biofilters (Eding et al., 2006; Timmons and **Ebeling**, 2007; Summerfelt, 2006; Kawan et al., 2016; Badiola et al., 2018) **(cont.)**

Fluidized sand biofilter (FSB)	
Relatively low capital cost due to high specific surface area of media and low cost of media. Allows for a more conservative design	Complex design procedure
	Non-aerating, increasing the need for aeration after the filter
Can be constructed from widely available materials	Does not strip CO_2, increasing the need for a CO_2-stripper after the filter
	Operating flow rate is limited due to bed expansion requirements. Flow rate must be within 10 – 30% of design flow rate.
Is not susceptible to clogging	Stagnation of flow for more than 6 – 24 hours can cause anaerobic conditions, decreasing nitrification rates
	Additional pumping costs to maintain fluidization of bed
Wide knowledge base available on operations and modeling, specifically in cold-water systems	Density in FSB changes over time as biofilm grows, requiring a management strategy
	Expensive plumbing to prevent back-flow of media into the pump during shutdown is a requirement for some designs
Floating bead biofilter (FBB)	
Widely available from different suppliers	Is undesirable for large scale RAS due to low specific surface area of media necessitating a large reactor and thus higher capital costs
Combination with other filters is possible for alternative designs	Relatively high head loss over the filter
	Variation in head loss requires use of variable speed drive pumps in certain cases
Also acts as granular filter, thereby providing additional solids removal	High residence time of solids in the filter (if not backwashed frequently or no additional filtration done before the filter) can increase BOD in the water

2.3 Solids removal

High total suspended solids (TSS) concentrations within a RAS can adversely affect water quality (increased BOD and ammonia) and biofilter efficiency (as discussed in section 2.1.6). Thus, solids removal is one of the critical process steps in RAS and needed to be thoroughly incorporated into the system design. Gravity separation, filtration and flotation are the three main mechanisms of solids removal that are most commonly employed in RAS (Timmons and Ebeling, 2007). TSS can be roughly classified into two classes, namely settleable solids (> 100 µm) and non-settleable solids (< 100 µm). Figure 2-3 shows the particle size ranges where various solids removal processes are most effective (Chen et al., 1994).

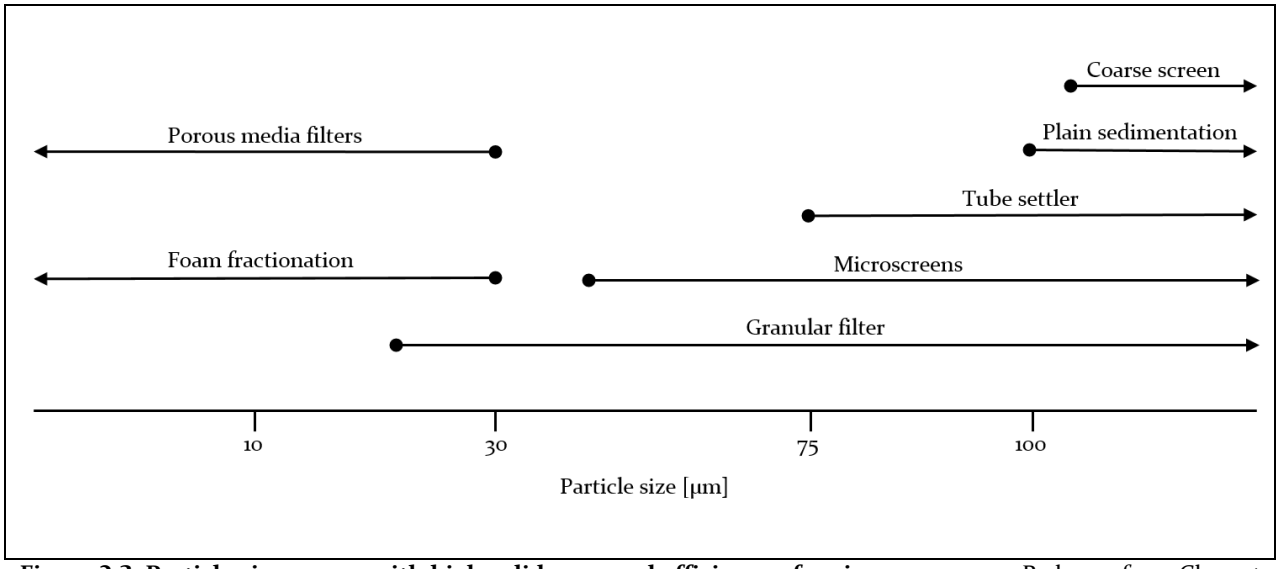

Figure 2-3: Particle size ranges with high solids removal efficiency of various processes. Redrawn from Chen et al. (1994)

2.3.1 Gravity separation

Gravity separation can only remove particles with a higher specific gravity than that of water and its removal efficiency is only significant with particles larger than around 100 µm. This is due to the slow settling velocities of fine particles that renders gravity separators inefficient. Centrifugal pumps have been found to cause breakage of particles, increasing the amount of smaller particles (60 – 100 µm) (McMillan et al., 2003). Gravity separators mainly remove particles larger than 100 µm and therefore centrifugal pumps would decrease the removal efficiency of gravity separators. A gravity separator is thus usually operated under gravity flow from the fish tank overflow to avoid pumping the particles to prevent particle breakup. The gravity separation unit types are swirl separators (not gravity flow), radial-flow settlers, rectangular sedimentation tanks, tube settlers and lamella settlers (Timmons and Ebeling, 2007).

2.3.1.1 Sedimentation tanks

Sedimentation tanks are mainly either rectangular or circular (radial-flow settlers). Any sedimentation tank (side view cross-section of rectangular tank shown in Figure 2-4) can be divided into four different zones: (1) inlet zone, (2) settling zone, (3) sludge zone and (4) outlet zone (Chen et al., 1994).

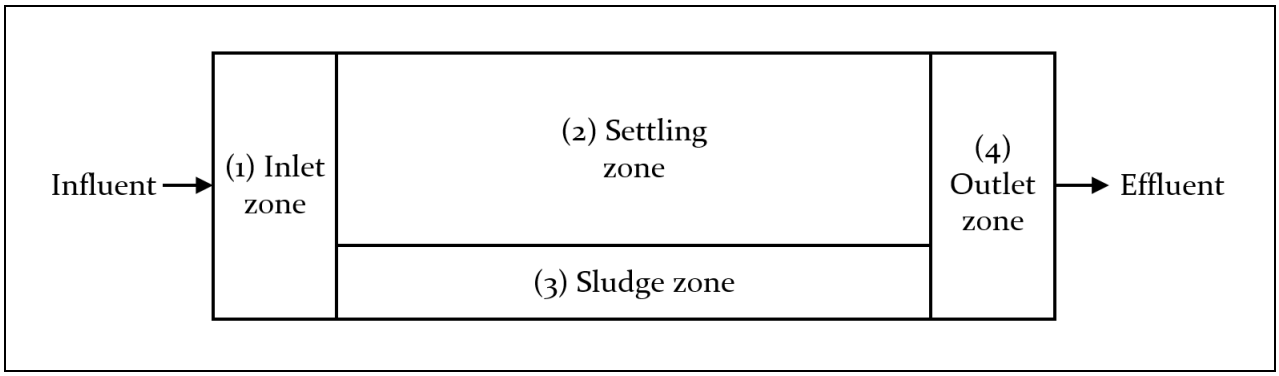

Figure 2-4: Zones of a rectangular sedimentation tank (side view cross-section). Redrawn from Chen et al. (1994)

The inlet zone uniformly distributes the suspension over the entire cross-section of the tank by flowing over a weir. The settling occurs in the settling zone where the particles settle down into the sludge zone. The clarified water flows over another weir into the outlet zone where the water is collected and discharged (Timmons and Ebeling, 2007). A radial-flow settler is a circular sedimentation tank where the inlet zone is in the center and the water flows over a weir on the outer edge of the tank. The water flows through a turbulence dampening cylinder in the center to reduce turbulence before being discharged into the tank (Davidson and Summerfelt, 2005). Sedimentation tanks require a large surface area within the settling zone for effective settling to occur and are thus limited in use by the available footprint. Turbulence in the tank will greatly reduce the solids removal efficiency (Timmons and Ebeling, 2007).

2.3.1.2 Swirl separators

Another solids removal technology utilizing gravity separation is the swirl separator. A swirl separator is cone shaped and operates by a tangential inlet flow which creates a vortex. This vortex creates a low-pressure zone along the center vertical axis. The particles in the water are subjected to two forces, an outward centrifugal force and inward drag force. The centrifugal force pushes the faster settling particles outwards where the water velocity is lower, where they settle to the bottom of the separator. The slower settling particles are carried inward by the drag force, where an inner upward vortex carries them up and out of the separator (Wills and Finch, 2016). A drawback of swirl separators are the high pumping requirements to overcome the high head loss (Chen et al., 1994). Pumping causes breakage of particles, reducing their size and settling rate and thus their settling potential. Davidson and Summerfelt (2005) found swirl separators to be less efficient than radial-flow settlers. They observed TSS removal efficiencies of 37.1 ± 3.3% and 77.9 ± 1.6% for swirl separators and radial-flow settlers respectively.

2.3.1.3 Tube settlers and lamella settlers

Due to the large surface area requirements of rectangular sedimentation tanks and radial flow settlers, a more space efficient solution needed to be considered. Tube- and lamella settlers are a solution to the large footprint issue of traditional sedimentation tanks (Chen et al., 1994). Both tube- and lamella settlers operate in the same manner as shown in Figure 2-5 (Timmons and Ebeling, 2007). These settlers are operated similarly to a sedimentation tank where the water flows through by gravity. The outlet level of the settler must be lower than the fish tank water overflow level for gravity flow to take place. The settler is inclined with tubes or plates (lamella) located in the settling zone, where the particles settle and run down to the sludge zone. Due to the internals, the effective settling surface area is increased, but the capital cost is often higher depending on the type of construction. Laminar flow in these settlers is essential to allow effective settling (Brandt et al., 2016). These settlers tend to get clogged and thus need to be cleared periodically (Timmons and Ebeling, 2007).

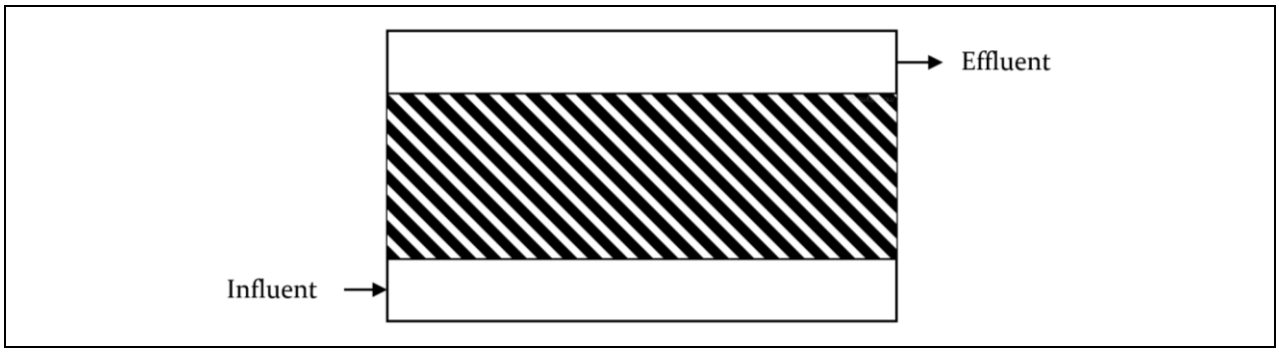

Figure 2-5: Tube- and lamella settler cross-section and flow. Redrawn from Timmons and Ebeling (2007)

2.3.2 Filtration

Solids filtration methods used in RAS are microscreens, granular filters and porous media (PM) filters.

2.3.2.1 Microscreen filters

Microscreens remove solids by obstructing them by certain mesh sizes, allowing the water and particles smaller than the mesh size to pass through. Backwashing of the screen is required. Backwashing frequency and head loss increase with decreasing mesh size. Mesh sizes are typically around 60 µm. Microscreen filters can be designed in various ways, namely stationary, triangle and rotary. Stationary filters simply obstruct the particles and require manual backwashing due to buildup of particles on the screen. Triangle filters incorporate continuous backwashing by letting the water run down an inclined screen, where water falls through and particles are caught and pushed down by the incoming water. The particles are washed away in a separate outlet by backwashing water that is added at the end of the screen (Chen et al., 1994). Rotary drum filters are mechanically driven filters with a horizontal drum rotating in a rectangular vessel. The drum wall is the microscreen mesh and the influent water is introduced inside the drum. The water passes through the mesh into the rectangular vessel and particles are caught in the mesh. As the drum rotates these particles are washed

off by high pressure water jets from the outside, being caught in a separate outlet stream. Other examples of microscreen filters are disc filters and inclined belt filters (Timmons and Ebeling, 2007).

Fernandes et al. (2015) investigated the effects of different drum filter mesh sizes on particle count, nitrification kinetics and fish health. Although particle counts decreased, mesh sizes between 20 – 100 µm had no measurable impact on nitrification kinetics or fish health.

2.3.2.2 Granular filters

Granular filters capture particles by deposition onto media within the filter and can capture a wide range of particle sizes (> 20 µm). Three types of granular filters are typically used, namely downflow sand filters, upflow sand filters and bead filters (Chen et al., 1994). Due to the high head loss through granular filters, a pump is required to pressurize the water to enable flow through the filter (Lekang, 2007).

2.3.2.3 Porous media filters

Porous media (PM) filters have larger media and finer pore sizes than granular filters. The two types typically used are diatomaceous earth (DE) filters and cartridge filters. Both these types can remove particles even smaller than 1 µm. Therefore, PM filters have high backwashing frequencies and easily clog, making them unsuitable for continuous operation of a RAS (Chen et al., 1994).

2.3.3 Flotation

Flotation, also known as foam fractionation, is a process where surfactants attached to air bubbles capture small particles (< 30 µm). Firstly, air bubbles are created in a water column. Secondly, surfactants in the water attach to the air bubble due to surfactants having a hydrophobic end. The hydrophobic end exists due to surfactants having polar and non-polar parts and water being polar, making the non-polar part of the surfactant hydrophobic. This makes the air-water interface polar and attracts fine solids. Thirdly, the foam is removed at the top of the water column and discarded (Timmons, 1994). Foam fractionation only removes solids smaller than 30 µm, making it a suitable process for reduction of fine solids in RAS. An advantage of foam fractionation is that no backwashing is required (Chen et al., 1994). Typically, this degree of solids removal is only required in hatcheries where water quality requirements are stricter.

2.4 Aeration and oxygenation

Dissolved oxygen concentration (DO) is an important parameter for fish survival and is often the first factor limiting the carrying capacity of the system. The use of air to supply DO is the preferred option at moderate stocking densities, with pure oxygen only becoming financially viable at high stocking densities. Equipment used to contact air with water are (1) floating surface agitators, (2) submerged air diffusers, (3) water jet aerators, (4) packed columns with counter-current flow of air and water, (5) airlifts and (6) perforated tray cascades. Equipment used to contact pure oxygen with water are (1) packed columns, (2) multi-stage low-head oxygenators, (3) spray columns, (4) side-stream oxygen

injectors, (5) U-tubes, (6) down-flow bubble contactors and (7) enclosed surface agitators (Watten, 1994).

Air supply in aquaculture is most commonly provided by:

1) Rotary vane blowers, also known as roots blowers or positive displacement blowers (Ecotao Enterprises, 2019), are used when the backpressure of the aeration system exceeds 3 – 4 meters head (Watten, 1994).

2) Regenerative blowers, also known as axial blowers or side-channel blowers (CFW Fans, 2019a), are used when the backpressure of the aeration system is 2 meters head or lower and the airflow is more than 100 L/min (Watten, 1994).

It has been reported that aeration typically accounts for 20% of the energy usage in a small-scale RAS (d'Orbcastel et al., 2009).

Reliable supply of oxygen is crucial to the successful operation of a RAS, as the relatively high stocking density encountered in these systems will quickly deplete oxygen if the supply fails. There have been cases where the aeration of RAS water ceased for only 10 minutes due to power failure and resulted in total mortality of the fish population. This has led to past RAS facilities being forced to declare bankruptcy (Timmons and Ebeling, 2007). In the context of an experimental facility, failure of oxygen supply can lead to failed experiments and loss of funds. This can be used as motivation to include emergency oxygen supply equipment.

2.5 Carbon dioxide degassing

Carbon dioxide is produced by fish during the metabolism of fish feed. When oxygenation is used instead of aeration, carbon dioxide degassing is often required to prevent a build-up of dissolved carbon dioxide in the system. Carbon dioxide can be degassed in stripping columns designed specifically for carbon dioxide degassing (Vinci et al., 1996) or by using trickling filters as biofilters with forced ventilation (Eding et al., 2006).

2.6 Disinfection

Disinfection of RAS circulation water and RAS inlet water is important to reduce pathogen counts and prevent disease outbreaks. The main methods of disinfection are ozonation (introduction of ozone (O_3) into the water) and UV irradiation (exposure of water to ultraviolet light) (Lekang, 2007). A disadvantage of ozonation is that the ozone needs to be produced onsite and thus can be expensive in terms of both capital cost (ozone generator) and operating cost (electricity and maintenance) (Brazil et al., 1996). UV irradiation reduces the heterotrophic bacterial populations suspended in the water, benefiting the autotrophic bacteria in the biofilter by reducing competition for dissolved oxygen (Blancheton et al., 2013).

2.7 Water and air heating

Water heating systems used in RAS are (1) electric resistance heaters, (2) plate and frame heat exchangers, (3) shell and tube heat exchangers, (4) geothermal heat pumps, (5) water-cooled heat pumps, (6) air-cooled heat pumps, (7) solar collectors and (8) situating the RAS within a greenhouse (Badiola et al., 2018; Fuller, 2007). Water heating must always be done before the aeration step, since the heating of the water causes supersaturation of gases and aeration counters supersaturation at shallow water depths (Lekang, 2007). Supersaturation of nitrogen gas in water can be harmful to fish (Watten, 1994).

Air temperature inside RAS buildings is usually controlled to decrease heat losses from the recirculating water. The humidity inside RAS buildings is also often controlled to prevent condensation on the inner surfaces of the building that can cause structural damage over time. Greenhouses can be used as an electricity-free method to heat the air inside the RAS building (Badiola et al., 2018; Fuller, 2007). Air-cooled air conditioners are used to control air conditions when the sun is not available for greenhouse heating or when cooling of the air is required.

2.8 Waste management

Waste management of RAS effluent is required to prevent pollution of the environment and non-compliance to environmental regulations. This can be done by treatment of the liquid and solid effluent from the solids removal step. Van Rijn (2013) prepared a review of current methods of waste treatment, waste disposal, waste reduction and estimation of waste production. Schneider et al. (2007) designed and constructed a suspended growth bioreactor for treatment of a drum filter effluent of an African catfish RAS facility. The RAS effluent can also be used to produce biogas, which can reduce the electricity costs of the system (Yogev et al., 2017). However, treatment of the RAS effluent is out of the scope of this thesis as it will have negligible effects on equipment choices unless denitrification or biogas production is employed. It is strongly advised by the author that the RAS effluent from the solid removal steps be disposed of in a responsible manner such as contracting a waste management company for disposal or controlled composting of solid waste.

2.9 Conclusions

The literature survey was successful in establishing the target limits of the critical water quality parameters to enable the designed RAS to culture both African catfish and tilapia. It can be concluded that there are several existing technologies available for each unit operation with which to put a RAS together, which means that it can be complex to put it all together. For this reason, each RAS will be unique based on the unique requirements. The discussion of each unit operation's options provided a basis for making design decisions on selection of technologies and provided focus when selecting appropriate modeling methods.

Chapter 3. Steady state RAS modeling methods

3.1 Introduction

Modeling a RAS is generally done using steady state models, meaning that the model equations assume constant water conditions over time (Timmons and Ebeling, 2007). Ideally, a RAS should be modelled dynamically where time steps in production are modelled with changing fish biomass and water quality parameters and has been done several times in literature (Caraman et al., 2010; Karimanzira et al., 2016; Wik and Lindén, 2004; Wik et al., 2009). However, these modeling exercises have not been verified with experimental data and therefore remain unsuited for the design of a new RAS.

The waste in the RAS water that needs to be removed by the various unit operations almost exclusively originates from the fish feed added to the system and thus the sizing of RAS wastewater treatment equipment is mainly a function of the feeding rate. For this reason, estimating the maximum feeding rate is a critical step in RAS design. As an overview of the methodology, the steady state modeling of a RAS can be divided into four sections. Additionally the reader can refer to Figure 4-1 and Figure 4-2 in Chapter 4, which show an overview of the variables and models used in the design. Compiling the models in this chapter aimed to achieve Objective 2 of the study (see section 1.4).

1) Feeding rate estimation

The feed fed on a certain day was based on the feed conversion ratio (FCR) and the fish biomass gained on that day. The FCR is defined as the mass ratio of dry feed fed to wet fish weight gain. The change in fish biomass is a function of total fish biomass, which is modelled by fish growth models. The maximum feeding rate is experienced at the end of an experimental growth trial as it is the time point where the system will have the highest total fish biomass. Fish mortalities are modelled to calculate the correct number of fish to be stocked initially to reach a target final fish biomass by accounting for fish mortalities during the trial.

2) Waste production estimation

Estimations of the waste production rates are made based on literature data for specific fish species and are generally a function of the feeding rate. These estimations are essential to be able to size the wastewater treatment section of the RAS.

3) Wastewater treatment modeling

The dimensions and capacity requirements of the wastewater treatment units are dependent on the amount of waste generated and need to be sized accordingly. This is done through various models for biofilter reaction rates, solids removal rates and aeration mass transfer.

4) Heat transfer modeling

The heating/cooling requirements of the system must be estimated to size the water and air temperature regulation equipment correctly. The heat transfer rates for the RAS process water and building air are estimated using standard heat transfer equations based on the geometry of the various heat transfer surfaces considered.

The modeling methods described in this chapter were used to inform the design and sizing of each unit operation required in the RAS (see Chapter 4). The uncertainty within each modeled parameter was assessed by looking at variation in literature values reported in this chapter and performing a sensitivity analysis in Chapter 4. The system was modeled according to data for African catfish due to it being the species with the higher commercial stocking density (see section 4.1.4) and thus more likely to be the species with the highest fish biomass at the end of an experimental growth trial.

3.2 Fish growth, mortality and feeding

3.2.1 Fish growth models

Fish growth is typically observed as having an S-shaped curve as shown in Figure 3-1, with a slow initial growth rate, followed by an exponential weight increase and finally a decrease in growth rate as the fish reaches maturity (Lugert et al., 2016).

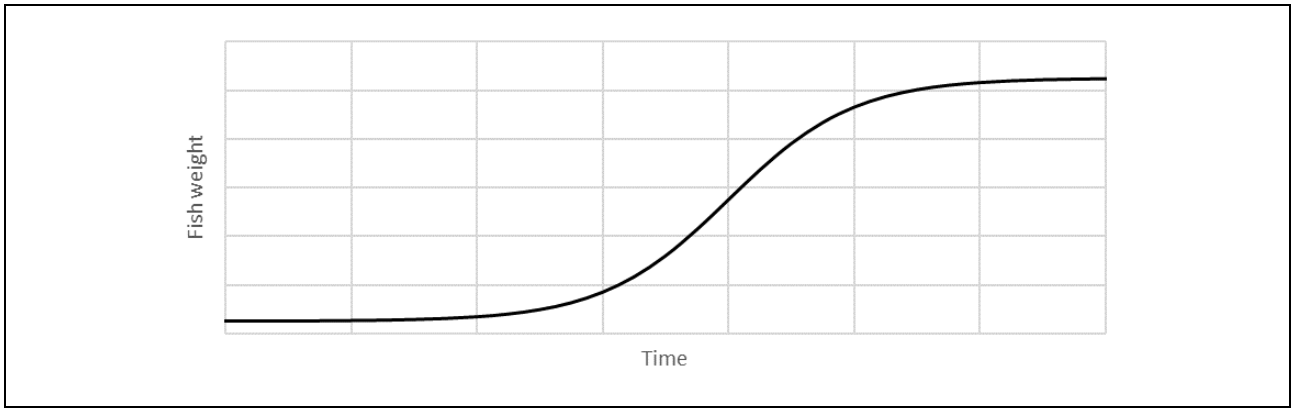

Figure 3-1: Typical fish growth curve (Lugert et al., 2016)

Various models have been developed to describe and predict fish growth. The fish growth models considered in this study were the absolute growth rate (AGR), specific growth rate (SGR), thermal growth coefficient (TGC) and the Von Bertalanffy growth function (VBGF). These models were chosen as they are the most commonly employed fish growth models in aquaculture. The objectives of the fish growth modeling had to be considered when choosing an appropriate model. The primary objective was to model the maximum gain in biomass the RAS will experience, which will provide an estimate of peak feeding rate when coupled with the estimated FCR. Estimating the peak feeding rate is critical for sizing the wastewater treatment equipment, since all waste production estimations are based on feeding rate. A secondary objective of the fish growth modeling was to estimate the final individual fish weight given an initial individual fish weight as input. This allows for estimation of the

number of fish that need to be stocked at the start of the trial to roughly reach the target commercial stocking density. Lugert et al. (2016) provided an excellent review of the considered fish growth models.

3.2.1.1 Absolute growth rate

The absolute growth rate (AGR) model is shown in equation (3.1).

$$AGR = \frac{w_t - w_i}{t} \tag{3.1}$$

where

AGR	=	Absolute growth rate $[g/day]$
w_t	=	Fish body weight at time t $[g]$
w_i	=	Initial fish body weight $[g]$
t	=	Production time $[days]$

Thus, if the AGR is determined experimentally by solving equation (3.1), the fish growth curve of weight vs time can be predicted.

$$w_t = AGR \cdot t + w_i \tag{3.2}$$

AGR is commonly used in experimental studies to compare treatments in a trial (Gericke, 2019; Goosen, 2014; Oluwaseyi, 2016; Suresh and Lin, 1992). Although it is a valid tool for comparing whether growth rates differ (e.g. in different experimental treatments in trials), it is a poor model of fish growth and not an accurate model for prediction of fish body weight as equation (3.2) describes a linear correlation. Lugert et al. (2016) found that the AGR model overestimated all intermediate fish weights between the initial and final weights in their data set. An experimentally determined AGR would be species and system specific.

3.2.1.2 Specific growth rate

The specific growth rate (SGR) model is shown in equation (3.3).

$$SGR = \frac{\log(w_t) - \log(w_i)}{t} \times 100 \tag{3.3}$$

The SGR models the fish growth as a percentage increase in weight per day. As with the AGR, it is also common in the comparison of treatments in experimental trials (Degani et al., 1989; Gericke, 2019; Goosen, 2014; Pruszyński, 2003; Rahmatullah et al., 2010; Salhi et al., 2004; van de Nieuwegiessen et al., 2008; Zhang et al., 2011). It has been suggested that SGR is suitable for prediction of the growth of younger fish, which are still in the exponential growth phase, however growth over different life stages is not well predicted. SGR was found to underestimate intermediate data whilst overestimating growth at later life stages (Lugert et al., 2016). An experimentally determined SGR would also be species and system specific.

3.2.1.3 Temperature growth coefficient

The temperature growth coefficient (TGC) model is given in equation (3.4).

$$w_t = \left(w_i^{1/b} + TGC \cdot \sum_{j=1}^{t} T_j \right)^b \quad (3.4)$$

where

TGC	=	Temperature growth coefficient $\left[g^{1/b}/(°C \cdot day)\right]$
b	=	Allometric exponent
T_j	=	Mean process water temperature at time step j [°C]

The TGC model assumes that "growth rate is allometrically related to fish body weight" and "the allometric constant of proportionality is directly related to mean daily water temperature averaged over the rearing period" (Dumas et al., 2007). The allometric constants (a and b in equation (3.5)) describe the relationship between fish length and body weight (Froese, 2006).

$$w = a \cdot l^b \quad (3.5)$$

where

w	=	Fish body weight $[kg]$
a	=	Allometric constant $[kg/m]$
b	=	Allometric exponent
l	=	Fish length $[m]$

Iwama and Tautz (1981) proposed an allometric exponent of $b = 3$ for finfish. This assumption has been verified experimentally for African catfish by Swanepoel (2017), and the TGC model has been validated for warm-water fish (Bureau et al., 2000). Assuming the process water temperature in a RAS is controlled at a constant value, equation (3.4) can be simplified to equation (3.6) (Lugert et al., 2016).

$$w_t = \left(w_i^{1/3} + TGC \cdot T \cdot t \right)^3 \quad (3.6)$$

Lugert et al. (2016) found the TGC model to fit their growth data better than both the AGR and SGR models and propose it to be a suitable model for fish growth prediction from the early life stages to the end of the exponential growth phase. The AGR and SGR models are only viable if the data is within the exact life stage of the production being modeled (Lugert et al., 2016). Experimental data gathered at water temperatures close to the desired temperature should be used to minimize errors in the prediction (Dumas et al., 2010). It should be noted that the TGC model will overestimate the weight of fish that are passing exponential growth. If the growth surpasses the exponential growth phase, a non-linear growth model such as VBGF is needed to predict the S-shaped growth curve (Figure 3-1).

3.2.1.4 Von Bertalanffy growth function

The Von Bertalanffy growth function (VBGF) model is shown in equation (3.7).

$$w_t = w_{inf} \cdot \left(1 - e^{(-k_{VBGF}(t-t_0))}\right)^b \quad (3.7)$$

where

w_{inf}	=	Asymptotic weight $[g]$
k_{VBGF}	=	Von Bertalanffy growth coefficient $[1/day]$
t_0	=	Point where the curve intersects the x-axis $[days]$
b	=	Allometric exponent

Assuming that the allometric exponent is constant, the VBGF model requires intermediate fish weight data to regress the growth coefficient k, unlike the AGR, SGR and TGC models that only require the initial and final fish weights. Although it was found to be the most accurate of the 4 growth models (Lugert et al., 2016), there was a lack of reliable literature data and thus the VBGF model was not used. However, the TGC model was deemed to be sufficiently accurate for this design and was used to model fish growth.

3.2.2 Fish mortality model

Fish mortalities were modelled to calculate the correct number of fish to be stocked initially to reach a target final fish biomass by accounting for fish mortalities during the experimental growth trial. Fish mortality was modeled by Wik and Lindén (2004) as a first-order death process, accounting for the higher amount of fish deaths observed at earlier stages of life. Number of fish (n) was modeled by equation (3.8).

$$n_t = n_i \cdot e^{-k_{death}t} \quad (3.8)$$

where

k_{death}	=	$-\frac{1}{t_p}\ln\left(1 - \frac{p_n}{100}\right)$ $[1/day]$
n_t	=	Number of fish at time t
n_i	=	Initial number of fish
t_p	=	Length of production cycle of mortality data $[days]$
p_n	=	Percentage of population that died in mortality data

A wide range of mortality rates have been observed in literature ranging from 6% to 50% for production lengths of 30 days to 90 days (Akinwole and Faturoti, 2007; Gericke, 2019; Oluwaseyi, 2016). However, this parameter will not have much effect on the system design other than the estimated number of fish that need to be stocked. An African catfish population in a typical trial at Welgevallen grown from 9 – 304 g in 84 days had a mortality of $p_{84} = 22\%$ (Oluwaseyi, 2016, p. 85). This resulted in an estimated $k_{death} = 2.96 \times 10^{-3}\ \frac{1}{day}$.

3.2.3 Fish growth modeling results and discussion

Lugert et al. (2016) recommended that TGC values should be determined using data from the RAS that is modeled. The fish species modelled was the African catfish as it has higher commercial stocking densities and thus more likely to be the limiting case in experimental trials (i.e. the highest probable final fish biomass). Previous studies done using the existing RAS (Welgevallen) have been used in the calculation of TGC values in Table 3-1. African catfish growth data from other studies have also been included.

Table 3-1: African catfish growth data and calculated TGC's

Source	Initial fish weight [g]	Final fish weight [g]	Growth period [days]	Temperature [°C]	TGC [$g^{1/3}$/°C.day]
Akinwole and Faturoti (2007)	12	981	154	25	1.99×10^{-3}
Akinwole and Faturoti (2007)	12	787	154	25	1.80×10^{-3}
Akinwole and Faturoti (2007)	12	717	154	25	1.73×10^{-3}
Besson et al. (2014)	13	1300	119	27	2.66×10^{-3}
Bovendeur et al. (1987)	136	265	60	25	0.84×10^{-3}
DAFF (2018)	10	1000	240	27	1.21×10^{-3}
Schram et al. (2010)	141	412	34	27	2.44×10^{-3}
Schram et al. (2010)	141	468	34	27	2.79×10^{-3}
Welgevallen: Gericke (2019)	562	803	91	27	0.42×10^{-3}
Welgevallen: Swanepoel (2017)	0.96	31.16	70	26	1.19×10^{-3}
Welgevallen: Swanepoel (2017)	61.75	97.07	14	26	1.77×10^{-3}

The highest TGC values shaded orange in Table 3-1 were predicted by the more recent data from The Netherlands (Besson et al., 2014; Schram et al., 2014). African catfish bred in The Netherlands have been selectively bred for improvement of genetics for about 30 years. However, in comparison to the other data in Table 3-1, it is apparent that the TGC values of these studies are notably higher than what has been achieved in South African conditions and were therefore not deemed likely to be replicated in the RAS being designed. The remaining sources are all from Africa (Akinwole and Faturoti, 2007; DAFF, 2018; Gericke, 2019; Swanepoel, 2017) and an early Dutch study (Bovendeur et al., 1987). These relevant TGC values shaded green in Table 3-1 varied from 0.42×10^{-3} to 1.99×10^{-3} with an average of 1.37×10^{-3}. The design TGC value was 1.21×10^{-3}, estimated using the DAFF data from a recent feasibility study for African catfish production in South Africa (DAFF, 2018), which also closely matched one of the TGC estimations from Welgevallen of 1.19×10^{-3}. The effect of TGC on the system design was considered using a sensitivity analysis reported in Chapter 4. The results of using TGC = 1.21×10^{-3} is shown in Figure 3-2 (fish production length for design is 91 days).

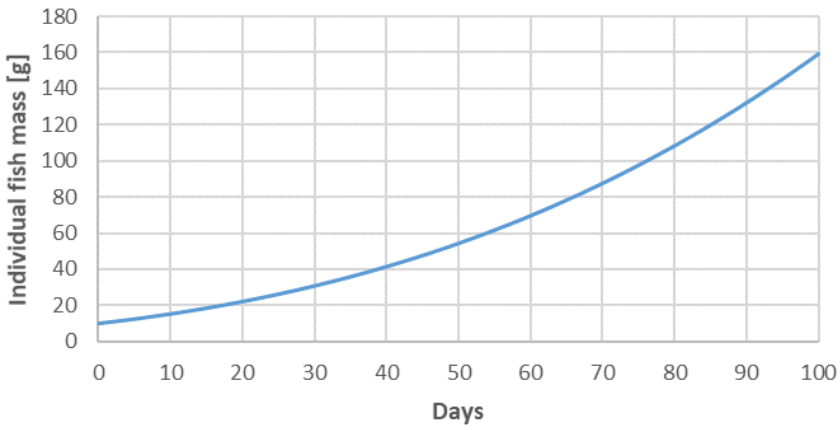

Figure 3-2: Fish growth curve at 27°C with a TGC = 1.21 x 10^{-3} $g^{1/3}$/°C.day

3.2.4 Feeding rate

Total ammonia nitrogen (TAN), total suspended solids (TSS), carbon dioxide and organic matter are all waste products entering the RAS water through fish metabolism of fish feed, or through biological degradation of uneaten feed. Oxygen consumption is also directly related to fish feed metabolism (Machiels and Henken, 1986). Thus, it is important to model the feeding rate as it will determine the production rates of all the above-mentioned waste products and consequently also the required sizes of the respective wastewater treatment unit operations. Two approaches can be used to model feeding rate:

1) Variable feeding levels (% body weight (BW) fed per day) depending on the life stage of the fish.

2) Fixed expected feed conversion ratio (FCR). FCR is defined as the mass ratio of dry feed fed to wet fish weight gain. The FCR can be used to estimate the feeding rate based on daily weight gains from the TGC fish growth model using equation (3.9), which also compensates for feed that is left uneaten. FCR is reported in numerous articles and therefore data for FCR are plentiful.

$$m_{feed}(t) = \frac{(w_t - w_{t-1}) \cdot FCR \cdot n_t}{(x_{protein} + x_{carb} + x_{fat} + x_{ash})(1 - \varepsilon_{feed\ lost})} \quad (3.9)$$

where

$m_{feed}(t)$	=	Mass of feed fed in period spanning $t-1$ to t $[g]$
w_t	=	Fish body weight at time t $[g]$
w_{t-1}	=	Fish body weight at time $t-1$ $[g]$
FCR	=	Feed conversion ratio $[g\ dry\ feed/g\ fish\ weight]$
n_t	=	Number of fish at time t
$x_{protein}$	=	Protein content of feed $[g/g\ feed]$
x_{carb}	=	Carbohydrate content of feed $[g/g\ feed]$
x_{fat}	=	Fat content of feed $[g/g\ feed]$
x_{ash}	=	Ash content of feed $[g/g\ feed]$
$\varepsilon_{feed\ lost}$	=	Fraction of feed not consumed by fish $[g/g\ feed]$

FCR is dependent on fish size (Robinson and Li, 2010), exposure of African catfish to light (Adewolu et al., 2008) and various other factors. Table 3-2 lists feeding levels and observed FCR's from previous Welgevallen studies as well as recommended feeding rates found in literature.

Table 3-2: Feeding levels and observed FCR's in African catfish systems

Feeding level [% BW fed/day]	FCR [kg dry feed/kg weight gain]	Reference
5.0%	0.81 – 1.16	Welgevallen: Swanepoel (2017, p. 36)
3.18%	1.39	Welgevallen: Oluwaseyi (2016, p. 85)
2.34% ± 0.14%	5.38 ± 0.70	Welgevallen: Gericke (2019, p. 83,85)
0.5%	Not reported	Buttle et al. (1995)
0.5%	0.97 – 1.0	Bovendeur et al. (1987)
See Table 3-3	0.9 – 1.3	DAFF (2018, p. 48)

Some studies propose an optimal feeding level of 0.5% BW per day for African catfish growth (Bovendeur et al., 1987; Buttle et al., 1995). These low proposed feeding levels were intended for growout fish masses, which are not the fish sizes used at Welgevallen (see section 4.1.3). The Welgevallen RAS will use smaller fish sizes, which have higher relative feeding rates compared to mature fish.

South Africa's Department of Agriculture Forestry and Fisheries (DAFF) compiled a feasibility study for the growth of African catfish from 10g to 1000g in 8 months, recommending feeding levels which are listed in Table 3-3.

Table 3-3: Feeding levels proposed for African catfish growth from 10g to 1000g in 8 months (DAFF, 2018, p. 48)

Month	1	2	3	4	5	6	7	8
Feeding level [%BW/day]	4.8%	4.1%	3.7%	2.0%	1.6%	1.3%	1.2%	1.2%

The 1 to 3 month feeding levels proposed by DAFF are appropriate to model the system since the design basis trial duration is 3 months (see section 4.1.2) and are based on a starting fish mass of 10g, which is the same as the design basis value (see section 4.1.3). The 1 to 3 month feeding levels of 3.7% - 4.8% are also similar to prior Welgevallen experimental studies (2.3% - 5.0%). Modeling the feeding rate was more convenient by using a fixed FCR and likely more accurate as FCR literature data was plentiful. In order to determine if a fixed FCR can be used instead of feeding levels based on fish biomass, the fish growth was modelled and feeding rates over time were calculated using the DAFF feeding levels (Table 3-3) and a fixed FCR of 1.5. The results of the two feeding rate estimation methods are plotted in Figure 3-3.

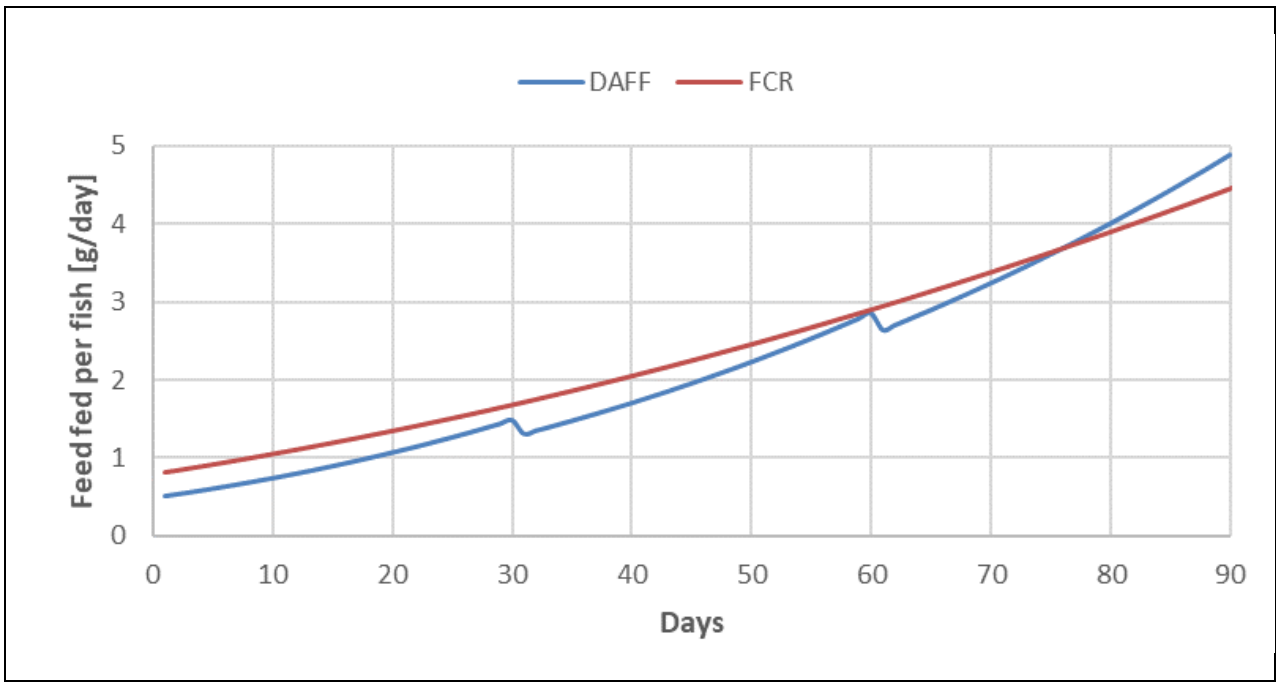

Figure 3-3: Specific fish feeding rates estimated using DAFF feeding levels and FCR, both with TGC model estimated fish weights

There can be seen in Figure 3-3 that the fixed FCR model accurately matches the predicted feeding rates of the DAFF feeding levels when using an FCR of 1.5. The step changes seen in the DAFF feeding level feeding rates is due to changing feeding levels at a certain fish weight. An FCR of 1.5 is seen as a conservative estimate of typical FCR's observed in literature and equivalent to 3.3% BW per day during peak loading and was thus used in the design for estimating the feeding rate.

3.3 Waste production models

3.3.1 TAN production

Ammonia is produced as a waste product from the breakdown of the protein contained in the fish feed. The combined concentrations of ammonia and ammonium is expressed as total ammonia nitrogen (TAN) (see section 2.1.3). Reported TAN production rates in literature are highly variable and can differ by as much as a factor of 10 (Wheaton et al., 1994b). This is evidenced in observed TAN production ratios of 3 – 7 g TAN/kg feed (Pruszyński, 2003), 38 – 81 g TAN/kg feed (Buttle et al., 1995), 40 g TAN/kg feed (Nijhof and Bovendeur, 1990) and 56 g TAN/kg feed (Bovendeur et al., 1987) in African catfish culture. A rule of thumb used in industry for Atlantic salmon (*Salmo salar*) RAS is a TAN production ratio of 35 – 45 kg TAN/kg feed (Gråkjær, 2019). Thus, care must be taken when sizing equipment based on TAN production ratios from literature. This was done by doing a sensitivity analysis (see section 4.5.4.3) to account for the uncertainty in the TAN production ratio.

As a starting design value for TAN production ratio, a theoretical estimation can be made. Essentially all the nitrogen in the fish feed is contained in the proteins. A generally accepted assumption is that the nitrogen content of protein is 0.16 grams N per gram protein (Besson et al., 2014; Mariotti et al.,

2008; Wik and Lindén, 2004). Since protein is the only significant source of nitrogen in fish feed, the theoretical maximum TAN production can be calculated given the protein content of the feed. The expected TAN production can be calculated by subtracting the expected nitrogen retention (NR) of the fish (g N retained in fish/g N in consumed feed) from the theoretical maximum TAN production. Observed levels of NR in African catfish has been reported in literature as 31% (Farhat and Khan, 2011), 34 – 38% (van Weerd et al., 2003), 37 – 38% (Torreele et al., 1993) and 42% (Lim et al., 2001). Trials done with black catfish (*Rhamdia quelen*) resulted in NRs of 32 – 40%. Possible reasons for these differences in observed NR's are that (1) the life stages and hence the digestive capabilities of the fish and the feed formulations differed between the studies and (2) uneaten feed can skew the results of a study due to the difficulty of measuring uneaten feed mass, which must be accounted for when calculating NR. A lower NR will result in more nitrogen being excreted by the fish, increasing TAN production. An average nitrogen retention of 35% was chosen to model the RAS.

The typical protein contents of commercial and experimental fish feed are listed in Table 3-4. The information in Table 3-4 shows the protein contents vary from around 40% to 50%. An average of 45% protein content was chosen to model the RAS. The conservative upper value was not chosen due to the design including a sensitivity analysis on the design parameters, which will account for conservative estimates.

Table 3-4: Protein content of fish feeds in literature

Fish species	Protein content % [g protein/g feed]	Source
African catfish	45%	Besson et al. (2014)
	47.1%	Bovendeur et al. (1987)
	45%	Akinwole and Faturoti (2007)
	49%	Schram et al. (2010)
	36.9 – 38.4%	Swanepoel (2017, p. 43)
	37%	Gericke (2019, p. 117)
	41%	Talamuk (2016, p. 27)
	41 – 50%	Buttle et al. (1995)
	44%	Palm et al. (2018)
Atlantic salmon	44%	Wik and Lindén (2004)
Mozambique tilapia	40 – 45%	Goosen (2014, pp. 56, 93)

The excreted nitrogen is in two forms namely urine and feces. The nitrogen in the urine is regarded as TAN directly excreted into the process water, while the nitrogen in the feces slowly diffuses into the water over time. Buttle et al. (1995) found that 80% of the excreted nitrogen enters the water as TAN. For the purposes of this model, a conservative estimate is taken by assuming that 100% of the excreted nitrogen enters the water immediately as TAN.

As the above described methodology would suggest, TAN production ratio (grams TAN produced per gram feed fed) is a function of feed protein content, nitrogen content of protein, nitrogen retention in the fish and mass of feed fed. The TAN production ratio model is given in Equation (3.10).

$$\left(m_{prod}\right)_{TAN} = m_{feed} \times C_{protein} \times C_{N,protein} \times (1 - NR) \quad (3.10)$$

where

$\left(m_{prod}\right)_{TAN}$	=	Total ammonia-nitrogen added to water $[g\ N/day]$
m_{feed}	=	Feeding rate $[g\ feed/day]$
$C_{protein}$	=	Feed protein content $[g\ protein/g\ feed]$
$C_{N,protein}$	=	Nitrogen content of protein $[g\ N/g\ protein]$
NR	=	Nitrogen retention in the fish $[g\ N\ retained/g\ N\ intake]$

Given the assumptions of $C_{protein} = 45\%$, $C_{N,protein} = 0.16$, and $NR = 35\%$, the TAN production ratio was calculated as $\frac{(m_{prod})_{TAN}}{m_{feed}} = 0.047 \frac{g\ TAN}{g\ feed}$

3.3.2 Oxygen consumption and carbon dioxide production

Dissolved oxygen in a RAS is consumed by fish, autotrophic bacteria and heterotrophic bacteria, which all need to be estimated in order to size the aeration system correctly. Oxygen consumption in the fish tanks is mainly through fish respiration with oxygen consumption due to bacterial growth being negligible. A rule of thumb for oxygen consumption by fish respiration has been proposed where 0.25 kg O_2 is consumed per kg of feed consumed by the fish (Timmons and Ebeling, 2007, p. 87). This estimate is supported by similar findings for African catfish ranging between 0.235 – 0.255 kg O_2/kg feed (Bovendeur et al., 1987; Machiels and Henken, 1986).

Oxygen in the biofilter water is consumed by both autotrophic and heterotrophic bacteria. Autotrophic bacteria consume oxygen during nitrification. The stoichiometry of the oxidation of ammonia to nitrate with nitrite as intermediate results in 4.25 g O_2 consumed per g TAN converted (Eding et al., 2006; Losordo and Westers, 1994). Heterotrophic bacteria consume oxygen when breaking down organics. General design guidelines are proposed to be between 0.13 – 0.50 kg O_2 per kg of feed fed (Timmons and Ebeling, 2007, p. 87). However, a more accurate estimation was done by modeling the organic matter production rates (see section 3.3.4).

Dissolved carbon dioxide is produced by fish respiration with 1 mol CO_2 produced per 1 mol O_2 consumed. Converting to a mass basis yields a ratio of 1.375 g CO_2/g O_2 (Timmons and Ebeling, 2007; Wik et al., 2009). A similar ratio of 1.27 g CO_2/g O_2 was found experimentally (Bovendeur et al., 1987). It was decided to use the higher value of 1.375 g CO_2/g O_2 to model the RAS. Dissolved carbon dioxide is also produced by heterotrophic bacterial aerobic digestion of organic carbon matter. This is produced in the same ratio as above (Gallert and Winter, 2008).

3.3.3 Total suspended solids production

Feces and uneaten feed are the main sources of TSS in water. Various levels of TSS production have been observed in literature, all being reported as a percentage of the dry feed mass being converted to

TSS. A general rule of thumb where 25% of the dry feed mass is converted to TSS has been proposed (Timmons and Ebeling, 2007, p. 87). Studies on channel catfish (*Ictalurus punctatus*) have found varying results, with one study finding 18% of dry feed mass converted to TSS whilst another found that 43% was converted. Studies on salmonids have found that 25 – 30% of the dry feed is converted to TSS (Chen et al., 1994, pp. 62–63). A 20% conversion of dry feed to TSS was estimated as the TSS production rate in a rainbow trout (*Oncorhynchus mykiss*) system (Lekang, 2007, p. 58).

Based on the above literature observations, it was concluded that the rule of thumb where 25% of the dry feed is converted to TSS is a reasonable average design value assumption given that a sensitivity analysis was done to account for more conservative values.

3.3.4 Particulate and dissolved organic matter

Organic matter is excreted by fish in particulate and dissolved form. This organic matter contributes to the BOD_5 within the system, which negatively affects nitrification rates (Eding et al., 2006). Therefore, the overall BOD_5 production rate within the system needed to be modeled.

Bovendeur et al. (1987, p. 351) found that the distribution of excreted organic matter in a typical African catfish RAS was 65% particulate organic matter (POM) and 35% dissolved organic matter (DOM). This can also be expressed as a DOM to POM ratio of 0.54:1. Another study found that almost all organic matter in a rainbow trout (*Oncorhynchus mykiss*) RAS was dissolved (Rojas-Tirado et al., 2017). They did not include particles removed in solids removal steps though. Bovendeur et al. (1987, p. 351) was the only literature source found that reports the excreted distribution of organic matter.

For this study, it was assumed that all excreted TSS will be organic matter. The POM production can then be regarded to be equal to TSS production. DOM production can then be calculated using the assumed DOM to POM ratio of 0.54:1. Bovendeur et al. (1987, p. 335) found African catfish waste organic matter to have a COD to organic matter (POM + DOM) ratio of 1.4:1, and a biodegradability (BOD/COD) of 80%. Additional data for COD and BOD_5 originating from African catfish excreted organic matter were not available to the knowledge of the author. Estimation of BOD_5 was done by calculating the COD of the organic matter (POM + DOM) using the 1.4:1 ratio and assuming 80% of that will be BOD_5.

3.4 Biofiltration modeling

Two types of biofilters were modeled in this design. A tricking filter was modeled to determine whether it is necessary to replace the current trickling filters based on the TAN removal capacity of the current system. A moving bed bioreactor (MBBR) was modeled for the purpose of replacing the existing tricking filters with MBBRs. Described in this section are the various approaches considered for modeling trickling filters and MBBRs. Eventually trickling filter model approach 4 (plug-flow model) and MBBR model approach 2 was used in the design.

3.4.1 Trickling filter model approach 1: Well-mixed reactor models

Trickling filters have been modeled as a continuously stirred-tank reactor (CSTR), which assumes that the reactor is well-mixed (Bovendeur et al., 1987; Lastiri et al., 2018). In other words, the concentration of the reactant (ammonia in this case) is the same everywhere inside the reactor. This assumption would mean that the TAN concentration exiting the trickling filter at the bottom of the reactor is the same as the TAN concentration near the top of the column. However, a trickling filter cannot be modeled as a CSTR due to the TAN concentration clearly decreasing as the water flows through the column. This is supported by experiments done by Nijhof (1995). Therefore, this approach was not considered further.

3.4.2 Trickling filter model approach 2: System specific empirical data

Liao and Mayo (1974) proposed an empirical approach to determine the TAN removal rate in trickling filters based on experimental data. However, this model is only applicable to specific trickling filter systems with Koch rings as packing, hydraulic loadings ranging from 86.4 – 147 m^3/m^2.day and TAN concentrations ≤ 1 mg/L. This would not be applicable to the proposed RAS which has a TAN limit ranging up to 3 mg/L, or the current existing trickling filter, which has structured packing. Manufacturers of various biofilters use experience based estimates for the TAN removal rate (Drennan et al., 2006). These estimates are only valid for applications with a specific fish species, water quality conditions and system configuration (Eding et al., 2006). The system specific empirical approaches were thus not further considered to model a trickling filter.

3.4.3 Trickling filter model approach 3: Activated sludge model

Wik (1999) took a more complex approach to modeling trickling filters by using the activated sludge models (ASM) of Henze et al. (1987). The activated sludge models dynamically predict the following:

- Bacterial growth – Both autotrophs and heterotrophs.
- Utilization of oxygen.
- Consumption of ammonia and organic matter.
- Diffusion of substrates from the bulk fluid into the biofilm and vice versa.
- Diffusion of substrates within the biofilm.

Although this model provides good predictive capability, it is complex and requires estimates for a large number of parameters and it is unclear whether estimates generated through this method hold significant advantage over simpler models. For the purposes of this design, a simpler model which delivers sufficiently accurate biofiltration estimates, but which is less complex, was preferred to assess the capacity of the trickling filters in the current system.

3.4.4 Trickling filter model approach 4: Plug-flow model

A plug flow model proposed by Nijhof (1995) predicts nitrification rates using TAN concentration, hydraulic surface loading and trickling filter height and model parameter as model inputs. Due to the simplicity of the model and applicability to the system being modeled, this model was chosen to assess the capacity of the existing trickling filters in the system.

The nitrification reaction kinetics used in the model by Nijhof (1995) are half-order/zero-order kinetics, which are commonly used to model biofilters (Eding et al., 2006). The main ways that the nitrification rate can be limited or impacted in this kinetic model are:

1) Limited by TAN concentration – TAN diffusion limitation (Case 1 in Table 3-5)
2) Limited by oxygen concentration – Oxygen diffusion limitation (Case 2 in Table 3-5)
3) Limited by intrinsic reaction rate – Reaction rate limited (Case 3 in Table 3-5)

Transition concentrations for TAN and oxygen where reaction kinetics change from zero-order to half-order are defined as $C_{TAN}{}^{*}$ and $C_{O_2}{}^{*}$. If the actual substrate concentration is above its respective transition concentration, the nitrification rate cannot be limited by the respective substrate. If both substrates are in abundance, the nitrification rate is limited by the intrinsic reaction rate of the nitrification reaction. The TAN diffusion limitation case was modeled as half-order kinetics with model parameters a_1 and a_2 (Equation (3.11)) and oxygen diffusion limitation as zero-order kinetics with model parameter a_3 (Equation (3.12)). Studies done in freshwater RAS have consistently found that the ratio of the transition concentrations ($C_{O_2}{}^{*}/C_{TAN}{}^{*}$) range between 3.4 and 3.8 (Bovendeur et al., 1987; Bovendeur and Klapwijk, 1986; Nijhof and Bovendeur, 1990).

Table 3-5: Half-order/zero-order kinetics for nitrification reactions in a trickling filter (Bovendeur et al., 1987; Eding et al., 2006; Nijhof, 1995)

Case 1:	If	$C_{TAN} < C_{TAN}^*$ $C_{O_2} > C_{O_2}^*$ $C_{O_2} = constant$	$r_{TAN} = a_1 \cdot \sqrt{C_{TAN}} - a_2$	**(3.11)**
Case 2:	If	$C_{TAN} > C_{TAN}^*$ $C_{O_2} < C_{O_2}^*$ $C_{O_2} = constant$	$r_{TAN} = a_3$	**(3.12)**
Case 3:	If	$C_{TAN} > C_{TAN}^*$ $C_{O_2} > C_{O_2}^*$	$r_{TAN} = r_{TAN,max}$	**(3.13)**

where

C_{TAN}	=	TAN concentration in bulk fluid $[mg/L]$
C_{TAN}^*	=	Transition TAN concentration between half-order and zero-order kinetics $[mg/L]$
C_{O_2}	=	Oxygen concentration in bulk fluid $[mg/L]$
$C_{O_2}^*$	=	Transition oxygen concentration between half-order and zero-order kinetics $[mg/L]$
r_{TAN}	=	Nitrification reaction rate $\left[g/(m^2(biofilm) \cdot day)\right]$
a_1	=	Kinetic coefficient $\left[g^{0.5}/(m^{0.5} \cdot day)\right]$
a_2	=	Kinetic coefficient $\left[g/(m^2 \cdot day)\right]$
a_3	=	Kinetic coefficient $\left[g/(m^2 \cdot day)\right]$

Nijhof (1995) found that stratification of the bacterial population within a trickling filter caused a decrease in C_{TAN}^* lower in the column. He proposed that lower bacterial populations down the column were found due to lower TAN concentrations down the column. The lower TAN concentrations were due to the high bacterial population at the top converting TAN to NO_2-N and NO_3-N. Nijhof (1995) proposed equation (3.14) as a correlation between C_{TAN}^* and distance from the top of the column (h_{tf}).

$$C_{TAN}^* = 5 - 1.25h_{tf} \quad \textbf{(3.14)}$$

where

h_{tf}	=	Distance from the top of the trickling filter $[m]$

Kamstra et al. (1998) evaluated the model by Nijhof (1995) using data from trickling filters on various eel farms. They discarded the use of equation (3.14) and assumed C_{TAN}^* was constant. This was due to the small effect stratification has on the overall efficiency of the filter and the lack of information regarding stratification from full-scale farms. Equation (3.14) was incorporated in this study, as the correction ensures that any estimates are slightly more conservative.

3.4.4.1 Case 1: TAN diffusion limitation

For this case, the trickling filter was assumed to operate under TAN diffusion limitation conditions if $C_{TAN} < C_{TAN}^{*}$. Nijhof (1995) proposed a correlation between the half-order nitrification rate coefficient a in equation (3.11) and the hydraulic surface loading rate (HSL) of the trickling filter. This correlation is given in equation (3.15). The second kinetic coefficient b was regressed as a constant of $a_2 = 0.1\ g/(m^2 \cdot day)$.

$$a_1 = 7.81 \times 10^{-4} HSL + 0.261 \quad (3.15)$$

where

HSL = Hydraulic surface loading rate $[m^3/(m^2 \cdot day)]$

The HSL is calculated by dividing the recirculating flow rate by the cross-sectional area of the trickling filter. A minimum HSL is required to keep the biofilm surface area wet, but this does not determine the minimum HSL. Clogging can occur when solids attach to the biofilm and buildup occurs with insufficient scouring of the biofilm. Therefore, it is recommended that HSL must be kept above 300 m^3/m^2.day to prevent clogging of the filter (Eding et al., 2006). Within the proposed model (equation (3.15)), the high and low values of HSL will overestimate and underestimate the nitrification rate respectively. Greiner and Timmons (1998) tested hydraulic loading rates in a trickling filter ranging from 469 to 1231 $m^3/(m^2$.day) and found no increase in nitrification rates. This suggests that there is an upper limit above which hydraulic loading rates have no further effect on nitrification rates. Equation (3.15) was regressed from data collected at HSLs of 75, 150 and 300 m^3/m^2.day (Nijhof, 1995). Since HSLs higher than 300 m^3/m^2.day are recommended to prevent clogging, the desired HSL would be higher than the range investigated when the model parameters were regressed, which introduces the possibility of nitrification rates being overestimated by the model.

3.4.4.2 Case 2: Oxygen diffusion limitation

The trickling filter was assumed to operate under oxygen diffusion limitation conditions if $C_{TAN} > C_{TAN}^{*}$. This would result in a zero-order nitrification rate with respect to TAN concentration and is determined by the oxygen concentration. The oxygen concentrations used in the study by Nijhof (1995) varied from 7.4 – 8.2 mg/L., The TAN concentration did not fall below the zero-order transition TAN concentration during the modeling of the trickling filters (see section 4.5.1). Thus, the zero-order nitrification rate and bulk water oxygen concentration in the trickling filters was not estimated in this study.

Oxygen diffusion limitation could exist if the BOD_5 from organic matter in the water was sufficiently high. Nitrification can only occur if the BOD_5 < 110 mg/L and is due to heterotrophic bacteria overgrowing the autotrophic bacteria when there is a high organic carbon concentration in the water (Gallert and Winter, 2008). A 30% reduction of nitrification rates in submerged filters due to organic loading has been observed in literature (Zhu and Chen, 2001). The effect of BOD_5 on trickling filter performance was not modeled and is motivated in section 4.5.1.

3.4.4.3 Case 3: Intrinsic reaction rate limitation

When both the TAN and oxygen substrates are in excess, the nitrification rate will be limited by the intrinsic reaction rate limit. Intrinsic reaction rate limits of 1.2 – 2.9 g/m^2·day have been observed, although the temperature ranges are not reported. The predicted nitrification rates in this study did not fall centrally into this range and thus no further literature review of this case was done.

3.4.5 Moving bed bioreactor model approach 1: Activated sludge model

The activated sludge models developed by Henze et al. (1987) was implemented by Wik et al. (2009) to model MBBRs for nitrification of Atlantic salmon waste. The model is the same as described in section 3.4.3. For the purposes of this stage in the design, a simpler model was preferred to calculate the required MBBR volume.

3.4.6 Moving bed bioreactor model approach 2: TAN/oxygen diffusion limiting

The chosen MBBR model was based on evaluating the same 3 cases as in section 3.4.4. These cases (described below) are each evaluated and for the purposes of ensuring a conservative design, the case with the lowest estimated nitrification rate is assumed to be the actual nitrification rate. An MBBR can be assumed as a continuously stirred tank reactor (CSTR), which implies that the liquid mixture inside the reactor is homogenous in all its properties (Rusten et al., 2006).

3.4.6.1 Case 1: TAN diffusion limitation

Rusten et al. (2006) proposed equation (3.16), which predicts nitrification rate at TAN diffusion limiting conditions.

$$r_{TAN} = k_{MBBR} {C_{TAN}}^{n_r} \quad (3.16)$$

where

k_{MBBR} = Reaction rate constant $[g^{1-n_r} m^{3n_r-2}/day]$

n_r = Reaction order

The observed reaction order for TAN diffusion limitation was found to be $n = 0.7$ for MBBRs (Hem et al., 1994). This is notably different to the half-order reaction rates used to describe nitrification rates in trickling filters. The reaction rate constant depends on water temperature and other system variables that affect nitrification rates other than oxygen and TAN. A reaction rate constant of $k_{MBBR} =$ 1.3 was recommended by an MBBR biomedia manufacturer for nitrification in an MBBR at a temperature of 24°C (Drennan et al., 2006). The predictions of the model with the above parameters is compared to literature data (Kamstra et al., 2017) in Figure 3-4. Kamstra et al. (2017) operated at $C_{O_2} = 6.9\ mg/L$, corresponding with a $C_{O_2}/C_{TAN} = 3.5$ at $C_{TAN} = 2\ mg/L$. Thus, the MBBR would be oxygen diffusion limited at $C_{TAN} > 2\ mg/L$.

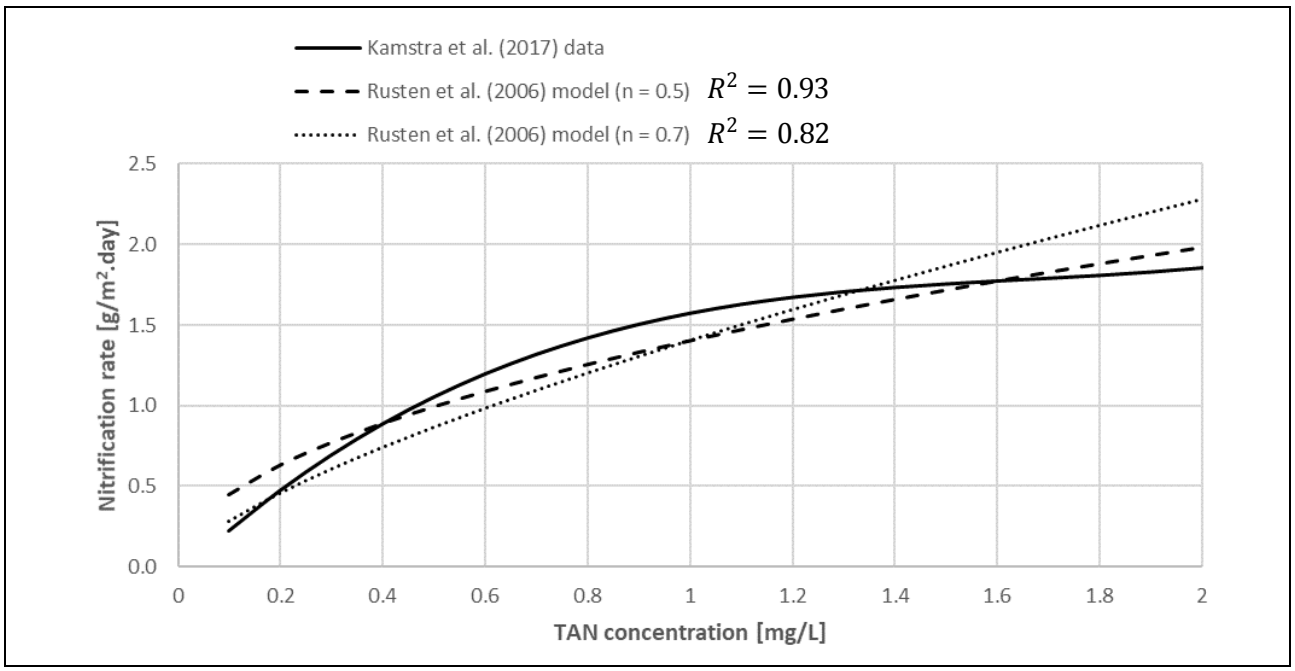

Figure 3-4: Nitrification rates observed in literature compared to the TAN diffusion limiting model equation (3.16)

Half-order kinetics ($n_r = 0.5$) describes the variation in literature data overall better than $n_r = 0.7$, with R-squared values of 0.93 and 0.82 respectively. This is due to the overestimation of nitrification rates at $C_{TAN} > 1.3\,mg/L$ when using $n_r = 0.7$. The estimated MBBR outflow TAN concentration and also the internal TAN concentration due to the CSTR assumption in this study was $C_{TAN} < 0.4\,mg/L$, where both $n_r = 0.5$ and $n_r = 0.7$ provides similar estimations of nitrification rates. Therefore, the MBBR specifically derived reaction order of $n_r = 0.7$ was used in the design.

3.4.6.2 Case 2: Oxygen diffusion limitation

Increased organic loading on the biofilm causes growth of heterotrophic bacteria in the outer biofilm layer. This decreases the effective oxygen concentration in the biofilm that is available for nitrifying bacteria, decreasing the nitrification rate (Rusten et al., 2006). A study quantified this oxygen concentration decrease as 0.5 mg/L at low organic loadings and 2.5 mg/L at 1.5 g BOD_5/m^2·day (Rusten et al., 1995). Instead of modeling the decrease in oxygen concentration in the biofilm, it was more convenient to use empirical data (Table 3-6) of nitrification rates observed at different bulk water oxygen concentrations and organic loadings (Hem et al., 1994).

Table 3-6: Nitrification rates observed in an MBBR at various oxygen concentrations and organic loadings at a water temperature of 15°C (Hem et al., 1994)

Nitrification rate [g/m²·day]	Organic loading [g BOD_5/m²·day]						
Bulk Oxygen concentration [mg/L]	**0**	**1**	**2**	**3**	**4**	**5**	**6**
2	0.55	0.20	0.20	0.20	0.20	0.20	0.20
3	0.80	0.45	0.20	0.20	0.20	0.20	0.20
4	1.05	0.70	0.30	0.20	0.20	0.20	0.20
5	1.30	0.95	0.55	0.20	0.20	0.20	0.20
6	1.55	1.20	0.80	0.45	0.20	0.20	0.20
7	1.80	1.45	1.05	0.70	0.30	0.20	0.20
8	2.05	1.70	1.30	0.95	0.55	0.20	0.20

In order to model the MBBR for the warm-water application, the observed nitrification rates in Table 3-6 had to be corrected for temperature and interpolated between organic loadings. The organic loading was calculated to be equal to the daily BOD_5 production divided by the biofilm area (equation (3.17)).

$$Z = \frac{BOD_{5,prod}}{A_{biofilm}} \quad (3.17)$$

where

Z	=	Organic loading $\left[g\ BOD_5/\left(m^2 \cdot day\right)\right]$
$BOD_{5,prod}$	=	Daily BOD_5 production $[g\ BOD_5/day]$
$A_{biofilm}$	=	Biofilm area $\left[m^2\right]$

Equation (3.17) is based on the conservative assumption that all the biodegradable organic matter is oxidized in the biofilm. Biofilter manufacturers assume as a rule of thumb that only 10 – 15% of the bacterial activity occurs outside the biofilter, i.e. in the fish tanks, piping and pump sump (Drennan et al., 2006), making the above assumption reasonable and also the worst case scenario for biofilter sizing.

3.4.6.3 Case 3: Intrinsic reaction rate limitation

Intrinsic reaction rate limits were not found in literature for MBBRs specifically and it was assumed that the rates would either be TAN diffusion limited due to low TAN concentrations (case 1) or oxygen diffusion limited due to organic loading (case 2).

3.4.7 Effect of scale on moving bed bioreactor performance

Kamstra et al. (2017) tested MBBRs of various scales (0.8L, 200L, 20 000L and 280 000L) and found that scaling up an MBBR causes an increase in nitrification rates. This was explained by lower friction losses on the sides of larger reactors, where there is less wall surface area per water volume, resulting

in more turbulence. They found the 0.8L MBBR to have a nitrification rate 20% lower than the 200L MBBR. However, no model was proposed to predict these effects and was not considered in this study.

3.4.8 Effect of temperature on nitrification

The nitrification rates of the biofilter models needed to be corrected for temperature due to higher reaction rates being observed at higher temperatures. This was done using the following equation (Eding et al., 2006; Rusten et al., 2006):

$$r_{T_2} = r_{T_1}\theta^{(T_2-T_1)} \quad \textbf{(3.18)}$$

where

r_{T_1}	=	Reaction rate at water temperature 1 $[g/(m^2 \cdot day)]$
r_{T_1}	=	Reaction rate at water temperature 2 $[g/(m^2 \cdot day)]$
T_1	=	Water temperature of system 1 [°C]
T_2	=	Water temperature of system 2 [°C]
θ	=	Temperature activity coefficient

Observed values for θ in trickling filters range from 1.02 to 1.08 (Eding et al., 2006). Rusten et al. (1995) found a θ value of 1.09 to describe temperature variations in nitrification rates in MBBRs. Kinyage and Pedersen (2016) found a θ value of 1.079 to be valid for MBBRs at temperatures ranging from 6 – 30°C. Bovendeur et al. (1987) regressed a θ value of 1.08 from trickling filter data when rearing African catfish at 25°C, and consequently a θ value of 1.08 was also used for this design. The effect of lower temperature activity coefficients is investigated in a sensitivity analysis (see section 4.5.4.3).

Linear methods of adjusting nitrification rate for temperature effects have been proposed (Wortman and Wheaton, 1991; Zhu and Chen, 2002), but equation (3.18) was the most commonly used in literature and also gives the most conservative estimates.

3.4.9 Effect of pH on nitrification

Nitrification of ammonium consumes HCO_3^-, which decreases the pH (Eding et al., 2006). This is true at a pH ranging from 4.3 to 8.3 (see APPENDIX E). Lower nitrification rates are observed for bulk water with lower pH (Rusten et al., 2006). A model valid for pH 6 – 8 to calculate the percentage reduction of nitrification rates caused by pH was proposed (Bovendeur, 1989), and is given in equation (3.19) and plotted in Figure 3-5.

$$y = 0.148(pH)^2 - 2.43(pH) + 9.972 \quad \textbf{(3.19)}$$

where

y	=	Franctional reduction in nitrification rate relative to pH 8

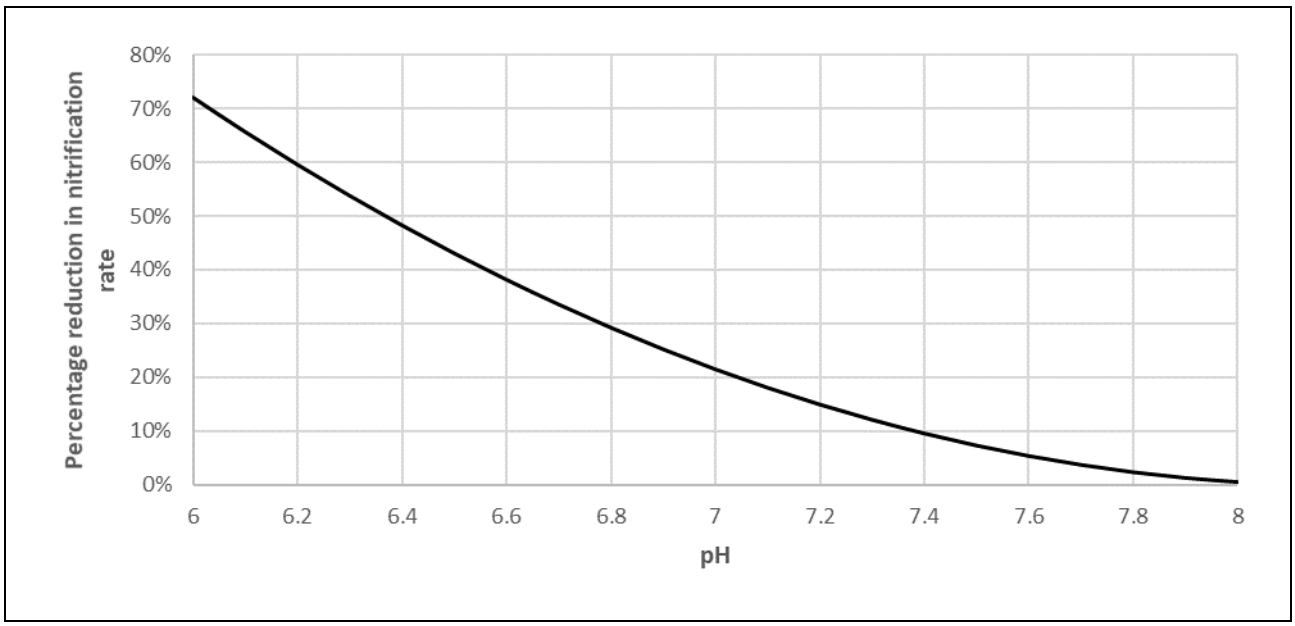

Figure 3-5: Percentage reduction in nitrification rates caused by lowered pH values

Nitrification rates are estimated to be lowered by 70% at pH 6 relative to nitrification rates at pH of 8. Since pH was usually not reported in nitrification models, it was assumed that the models used in this study were derived at a very commonly used RAS pH of 7.

3.5 Solids removal modeling

3.5.1 Sedimentation model

The fundamental principle of sedimentation is that a solid particle denser than the surrounding fluid will accelerate downwards under the effect of gravity. The settling particle will eventually reach a terminal velocity when the downward gravitational force and the upward drag forces cancel out.

A well accepted method for modeling settling (except for swirl separators) is the overflow rate method (Chen et al., 1994). The overflow rate (u_o) is defined as the volumetric flow rate divided by the horizontally projected settling area A_{settle}. The model assumes that all particles with a settling velocity (u_s) faster than the overflow rate will settle to the bottom of the sedimentation tank. Additionally, the particles with slower settling velocities will settle out in the ratio of u_s/u_o due to a number of them being lower in the suspension at the moment of entering the settler (Hazen, 1904). Because of this vertical height difference in particle position, the effect of removing particles with $u_s < u_o$ is only significant if the sedimentation tank has a significant water height. When modeling tube settlers or lamella settlers, which have short settling paths due to the internals, this effect is likely small and was assumed to be negligible. For years residence time inside a sedimentation tank has been thought to impact the design, but has been proven to not have any effect (Chen et al., 1994).

Laminar flow must be maintained when operating settlers. Turbulence in the water will cause particles to be resuspended, reducing the solids removal efficiency of the settler. The flow regime is characterized by the Reynolds number defined in equation (3.20) (Cengel and Cimbala, 2014).

$$Re = \frac{u_{avg} D_h}{v_w} = \frac{\rho_w u_{avg} D_h}{\mu_w} \tag{3.20}$$

where

Re	=	Reynolds number
u_{avg}	=	Average flow velocity $[m/s]$
D_h	=	Hydraulic diameter of the geometry $[m]$
v_w	=	Kinematic viscosity of water $\left[m^2/s\right]$
ρ_w	=	Density of water $\left[kg/m^3\right]$
μ_w	=	Dynamic viscosity of water $[Pa \cdot s]$

As a rule of thumb in circular pipes, laminar flow occurs at $Re < 2300$, transitional flow at $2300 < Re < 4000$ and turbulent flow at $Re > 4000$ (Cengel and Cimbala, 2014). A recommended design limit for Reynolds numbers in tube- and lamella settlers are to maintain $Re < 800$ to ensure that flow does not resuspend settled particles (Faraji et al., 2013). The hydraulic diameter in lamella settlers is the distance between the plates due to the width of the plates being considerably larger than the distance between the plates (Seshadri and Williams, 1978).

In order to estimate the efficiency of a designed settler, the settling rate of the suspension needs to be determined. The simplest method to predict the settling rate of a particle is by Stokes' Law (Stokes, 1851). Stokes' Law only applies to particles with a very low particle Reynolds Number (< 1), which is the case for suspended solids produced in aquaculture systems. Stokes' Law is given by equation (3.21).

$$u_s = \frac{g(\rho_p - \rho_w){D_p}^2}{18\mu_w} \quad (3.21)$$

where

u_s	=	Settling velocity $[m/s]$
g	=	Gravitational acceleration $[m/s^2]$
ρ_p	=	Particle density $[kg/m^3]$
D_p	=	Particle diameter $[m]$

The specific gravity is used to represent the particle density. Chen et al. (1993) studied two RAS and determined that the average SG of the suspended solids was 1.19, equaling an average particle density of 1190 kg/m^3.

Knowledge of the particle size distribution of the suspension is required to calculate the settling rates for the entire suspension. Various studies have investigated the particle size distributions. Chen et al. (1993) found that more than half of the number of particles were smaller than 10 µm, but particles larger than 200 µm were excluded by pre-filtering. They also found that 50% of the particle mass is contained in particles smaller than 20 µm. Fernandes et al. (2014) found that 50% of the particle mass is contained in particles smaller than 60 µm, however it should be noted that pre-filtering was not done in this study. The larger mass contained in the smaller particles could be due to breakages of particles by pumping. It should also be noted that the particle size distribution can vary greatly from system to system depending on the fish species, feed formulation and system configuration. No particle size distribution data from a RAS similar to the RAS of focus in this study was found, and therefore, due to the inability to obtain the required data an alternative method other than Stoke's Law had to be found for determining expected settling rates.

3.5.2 Solids settling characterization experiment

In order to determine settling rates to design a suitable solid settling unit, an experimental approach was followed to measure the settling rates of the solids likely to be encountered in the designed RAS.

3.5.2.1 Methodology

Wong and Piedrahita (2000) proposed an experimental methodology for characterizing settling rates of a RAS solids suspension. Using their methodology, the mass distribution of particles with different settling rates can be experimentally determined for a specific RAS solids sample. A specific species had to be chosen to be characterized for the design. It was decided to measure data for African catfish solids due to observations at Welgevallen of African catfish feces breaking more readily into finer solids than tilapia, meaning that African catfish solids are likely to have slower settling rates than

tilapia solids. In order to perform settling experiments, a sample of African catfish solids was collected from a large sedimentation tank at the Welgevallen experimental RAS facility in Stellenbosch, South Africa. A settling test was performed using the experimental setup shown in Figure 3-6.

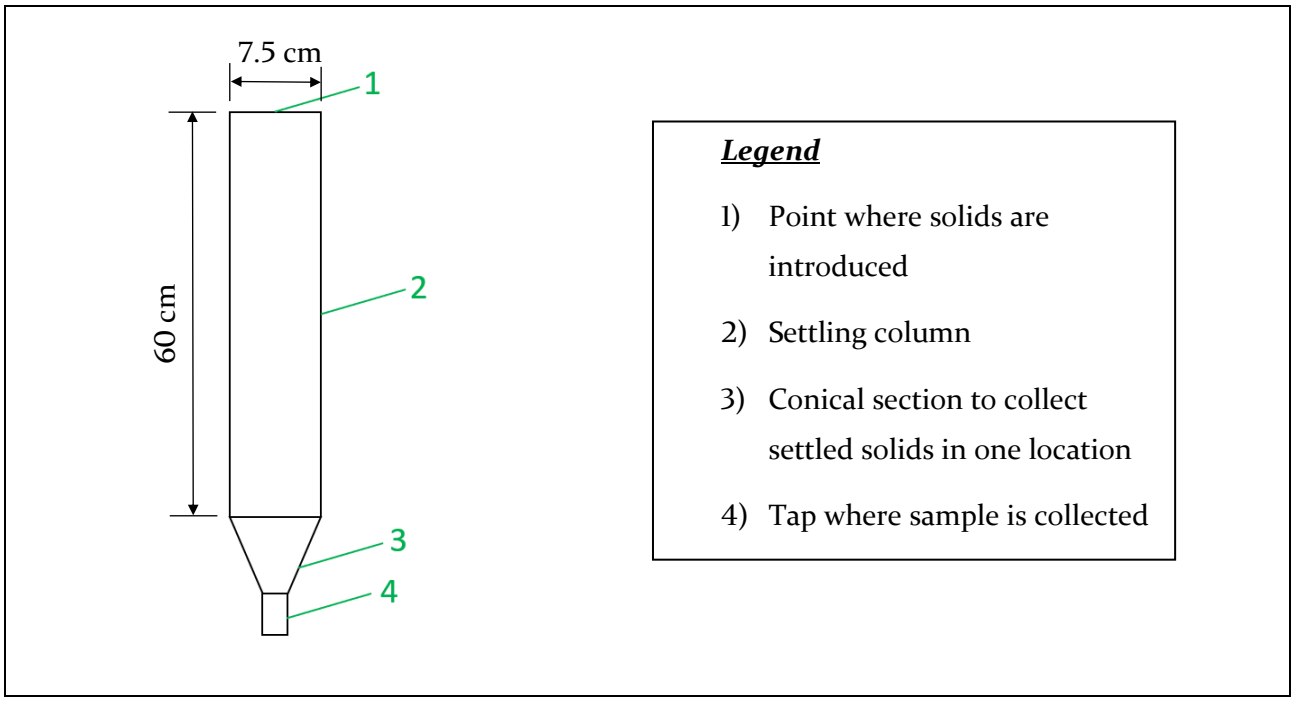

Figure 3-6: Experimental rig used to conduct a settling test for characterization of African catfish solids

The solids sample was loaded at point 1 in Figure 3-6 and the timer started. Solids samples settled into the conical section (3 in Figure 3-6) were collected using a valve (4 in Figure 3-6). The samples were filtered using Grade 292 filter paper that retains particles larger than 5 µm. The filter paper was dried and weighted before filtration. The sample retained on the filter paper was dried at 103 – 105°C for 1 hour as per the standard methodology for measuring TSS in wastewater (APHA, 1998). The water volume of each sample was measured.

Settling velocities were calculated for each sample using equation (3.22), which also compensated for the decrease in water level in the experimental settler caused by all the previous samplings. If the decrease in water level is not compensated for, all subsequent settling velocities will be overestimated due to the remaining particles in the column moving downwards during a sampling without actually settling that distance.

$$u_{s,n} = \frac{h_w - \sum_{i=1}^{n-1}(\frac{V_n}{A_c})}{t_n} \quad (3.22)$$

where

$u_{s,n}$	=	Settling velocity of sample collected at t_n $[cm/s]$
t_n	=	Elapsed time since beginning of the test $[s]$
h_w	=	Total water height at the beginning of the test $[cm]$
V_n	=	Volume of sample collected at t_n $[mL]$
A_c	=	Cross-sectional area of settling column $[cm^2]$

The settling column was 7.5 cm in diameter and a cross-sectional area of 44 cm^2. The water height at the beginning of the test was 60 cm after addition of the solids sample. Samples were collected at the following elapsed times: 1 min, 2 min, 3 min, 5 min, 10 min, 15 min, 20 min, 30 min. The unsettled solids after 30 minutes were also collected by draining the entire column and filtering out the solids.

3.5.2.2 Results and discussion

The measured cumulative mass fractions removed after each sampling is plotted at the respective settling rate in Figure 3-7.

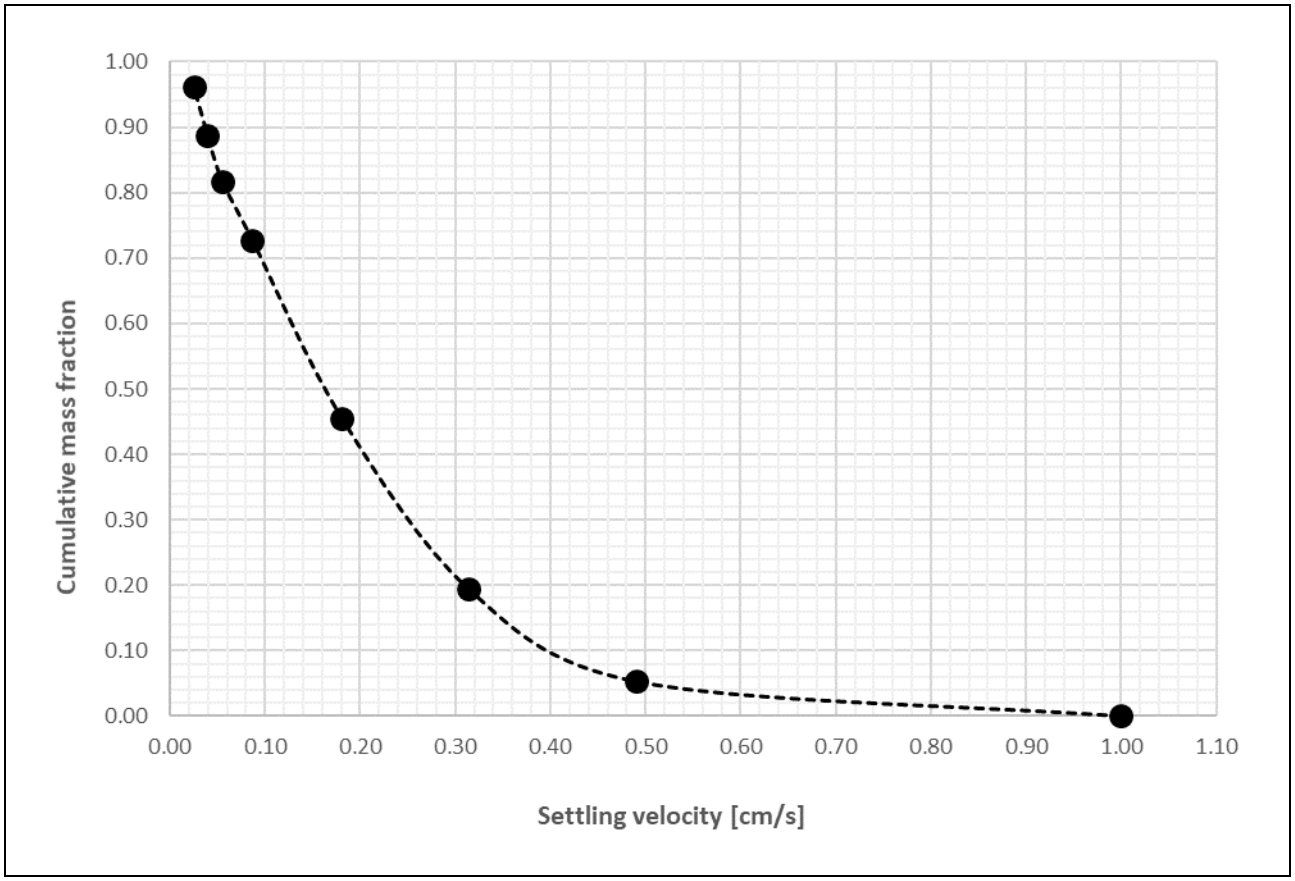

Figure 3-7: Solids characterization of African catfish solids collected at Welgevallen, South Africa

A study by Stechey and Trudell (1990) observed TSS removal efficiencies 65% to 85% in a settling basin operating at overflow rates of 0.046 – 0.092 cm/s. At the same overflow rates, the TSS removal efficiencies predicted by the characterization curve (Figure 3-7) would be 72% at 0.092 cm/s and 82% at 0.046 cm/s. This would suggest that the TSS removal efficiencies predicted by Figure 3-7 are accurate for the level of detail required in this study.

3.5.3 Lamella settlers

Lamella settlers have slanted plates to increase effective settling area within the same amount of equipment footprint. The total effective settling area is defined as the horizontally projected surface areas of the plates and is calculated by trigonometry using equation (3.23).

$$A_{settle} = n_{plate} \cdot L_{plate\ length} \cdot L_{plate\ width} \cdot \cos \Phi \quad (3.23)$$

where

n_{plate}	=	Number of plates
A_{settle}	=	Horizontally projected settling area $[m^2]$
$L_{plate\ length}$	=	Lamella settler plate length $[m]$
$L_{plate\ width}$	=	Lamella settler plate width $[m]$
Φ	=	Lamella settler plate inclination with the horizontal plane $[degrees]$

3.5.4 Sand filter model

Sand filters have a typical TSS removal efficiency of 95%. As a rule of thumb, 95% of particles larger than 6 µm and 15 µm are removed when using 0.3 mm and 0.5 mm sand grains respectively (Lekang, 2007). Pressure drop over a sand filter will increase as the solids are entrapped. The minimum and maximum pressure drop experienced in a sand filter was obtained from manufacturers and not modeled.

3.6 Aeration and degassing models

3.6.1 Aeration modeling

Aeration by submerged air diffusers, also known as airstones, was modeled in this study due to (1) general use in experimental RAS and (2) widespread availability and low cost of the technology. Fundamentally the diffusion mass transfer of oxygen to and from water can be modeled using equation (3.24) (Wik et al., 2009).

$$m_{O_2} = V \cdot K_L a_{O_2} \cdot \left({C_{O_2}}^{sat} - C_{O_2}\right) \tag{3.24}$$

where

m_{O_2}	=	Mass transfer rate of oxygen into the water $[g/day]$
V	=	Volume of the vessel $[m^3]$
$K_L a_{O_2}$	=	Overall oxygen mass transfer coefficient $[1/day]$
${C_{O_2}}^{sat}$	=	Saturation concentration of oxygen in water $[mg/L]$
C_{O_2}	=	Dissolved oxygen concentration $[mg/L]$

The saturation concentration of oxygen in clean water can be estimated using equation (3.25) (Timmons and Ebeling, 2007).

$$\left({C_{O_2}}^{sat}\right)_{CW} = \frac{1\,003\,200}{\left(\frac{9}{5} \cdot T + 32\right)^{0.625} \cdot \left(760 + \frac{\zeta}{107.6}\right)} \tag{3.25}$$

where

$\left({C_{O_2}}^{sat}\right)_{CW}$	=	Oxygen saturation concentration under clean conditions $[mg/L]$
T	=	Water temperature [°C]
ζ	=	Altitude of the site $[m]$

${C_{O_2}}^{sat}$ at field conditions can differ from ${C_{O_2}}^{sat}$ in clean water due to TDS and TSS (Stenstrom and Gilbert, 1981). This is quantified by the beta factor (β) as in equation (3.26). A beta factor of 1.0 was observed in catfish ponds (Shelton and Boyd, 1983).

$$\beta = \frac{\left({C_{O_2}}^{sat}\right)_{FW}}{\left({C_{O_2}}^{sat}\right)_{CW}} \tag{3.26}$$

where

$\left({C_{O_2}}^{sat}\right)_{FW}$	=	Oxygen saturation concentration under field conditions $[mg/L]$

The ratio of the oxygen transfer coefficients at field and clean water conditions is represented by the alpha factor (α) as in equation (3.27). An alpha factor of 1.00 has been observed in catfish ponds (Shelton and Boyd, 1983).

$$\alpha = \frac{\left(K_L a_{O_2}\right)_{FW}}{\left(K_L a_{O_2}\right)_{CW}} \quad (3.27)$$

where

$\left(K_L a_{O_2}\right)_{FW}$	=	Overall oxygen mass transfer coefficient under field conditions $[1/day]$
$\left(K_L a_{O_2}\right)_{CW}$	=	Overall oxygen mass transfer coefficient under clean water conditions $[1/day]$

For provision of aeration to RAS, regenerative blowers are generally employed. The approximate blower power consumption (P_{blower}) can be estimated using the transfer efficiency of the submerged diffusers. This is used for optimization of aeration processes and was used in the optimization of the oxygen concentration in the MBBRs (see section 4.5.4.1). The approximate blower power is estimated using equations (3.28), (3.29) and (3.30) (Colt and Tchobanoglous, 1981; Huguenin and Colt, 2002).

$$P_{blower} = \frac{m_{O_2}}{N_{FW} \cdot \eta_{blower}} \quad (3.28)$$

$$N_{FW} = \frac{N_{std} \cdot \left(\beta\left(C_{O_2}{}^{sat}\right)_{eff} - C_{O_2}\right) \cdot 1.024^{T-20} \cdot \alpha}{\left(C_{O_2}{}^{sat}\right)_{CW}} \quad (3.29)$$

$$\left(C_{O_2}{}^{sat}\right)_{eff} = \left(C_{O_2}{}^{sat}\right)_{FW} \cdot \left(1.00 + \varphi h_{diffuser}\right) \quad (3.30)$$

where

P_{blower}	=	Blower input power $[hp]$
N_{FW}	=	Oxygen transfer efficiency at field conditions $[kg\ O_2/(kW \cdot h)]$
η_{blower}	=	Blower efficiency
m_{O_2}	=	Mass transfer rate of oxygen into the water $[kg\ O_2/h]$
N_{std}	=	Oxygen transfer efficiency at standard conditions $[kg\ O_2/(kW \cdot h)]$
$\left(C_{O_2}{}^{sat}\right)_{eff}$	=	Mean effective dissolved oxygen saturation concentration $[mg/L]$
T	=	Temperature [°C]
φ	=	0.008 for coarse bubble diffusers, 0.016 for fine bubble diffusers
$h_{diffuser}$	=	Diffuser depth $[m]$

Regenerative blowers typically have an efficiency of 66% (CFW Fans, 2019a; Huguenin and Colt, 2002). For the purposes of conceptual design, standard oxygen transfer efficiencies of 0.6 $kg\ O_2/(kW \cdot h)$ and 1.2 $kg\ O_2/(kW \cdot h)$ can be used for coarse and fine bubble diffusers respectively (Huguenin and Colt, 2002).

Predicting the oxygen mass transfer rate using equation (3.24) requires modeling $K_L a_{O_2}$. The overall oxygen mass transfer coefficient, $K_L a_{O_2}$, is determined by gas bubble size, water turbulence, system geometry, water depth, temperature, air flow rate, air flow rate per diffuser and tank water surface

area (Ashley et al., 1991; Watten, 1994; Wik et al., 2009). Due to the number of variables that determines $K_L a_{O_2}$, the prediction thereof through modeling is complex (Al Ba'ba'a, 2015). Typically, the $K_L a_{O_2}$ is experimentally determined for a specific system (Watten, 1994).

A simpler method of estimating the oxygen transfer rate was proposed by Huguenin and Colt (2002). The model is based on experimental data of oxygen absorption efficiencies gathered by Mavinic and Bewtra (1976) in a freshwater aeration system shown in Figure 3-8.

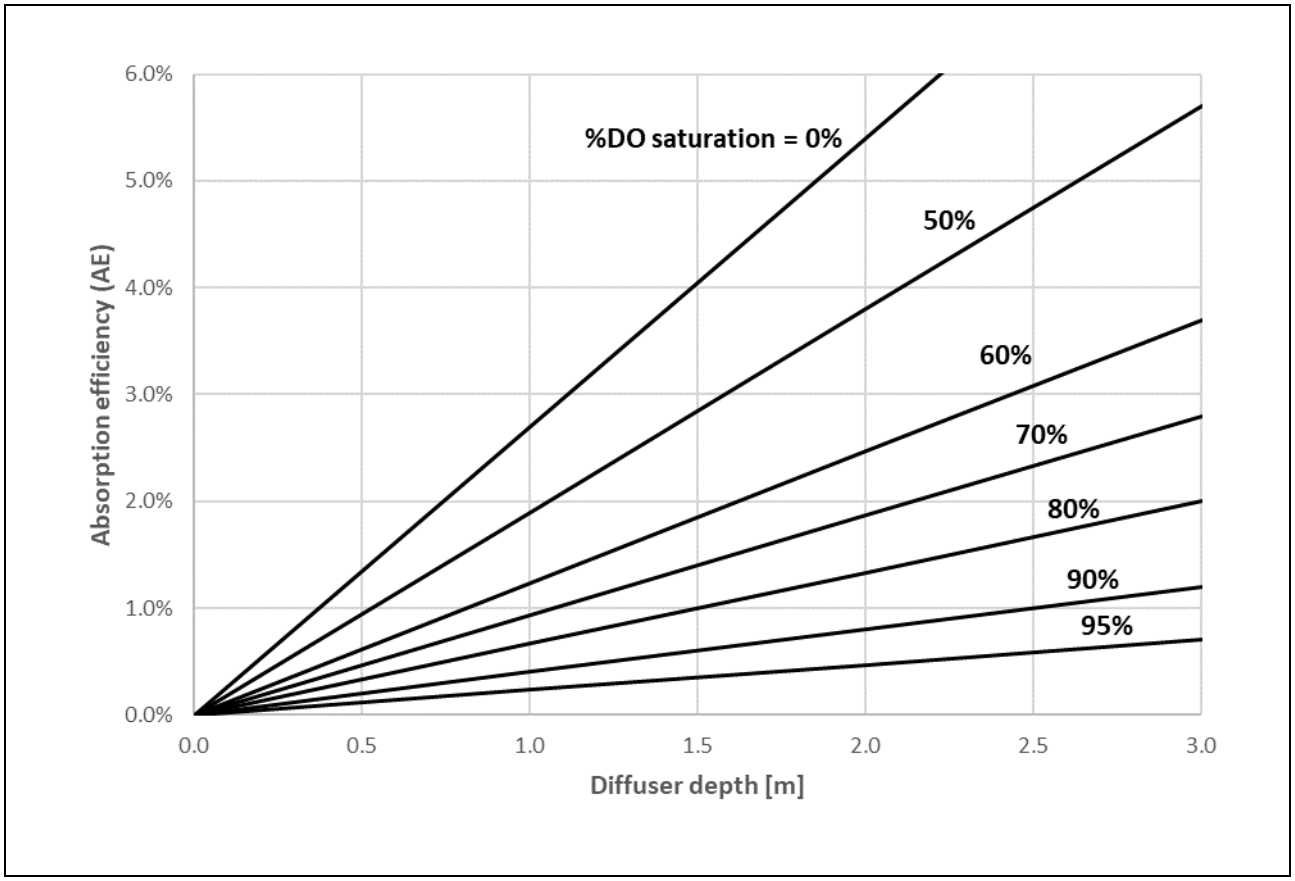

Figure 3-8: Oxygen absorption efficiencies at various diffuser depths and DO saturation levels. Data by Mavinic and Bewtra (1976). Redrawn from Huguenin and Colt (2002)

The DO saturation level is calculated by dividing C_{O_2} by $\left({C_{O_2}}^{sat}\right)_{FW}$. Although $\left({C_{O_2}}^{sat}\right)_{FW}$ will increase at deeper diffuser depths to $\left({C_{O_2}}^{sat}\right)_{eff}$ as modeled by equation (3.30), $\left({C_{O_2}}^{sat}\right)_{FW}$ was used for added conservativity. The oxygen mass transfer rate to the water is modeled by equation (3.31) (Huguenin and Colt, 2002).

$$m_{O_2} = 0.162 \cdot \eta_a \cdot Q_{air} \quad \textbf{(3.31)}$$

where

m_{O_2}	=	Mass transfer rate of oxygen into the water $[kg/day]$
η_a	=	Absorption efficiency from Figure 3-8
Q_{air}	=	Air volumetric flow rate at STP of 0°C and 101 325 Pa $[m^3/h]$

3.6.2 Gas supersaturation

Total dissolved gas pressure (TGP) is determined by the summing the gas tensions (also known as partial pressure) of the dissolved gases as in equation (3.33) after calculating each individual gas tension using equation (3.32). Carbon dioxide was not included due to its low concentration observed in this study making its contribution to TGP negligible.

$$\tau_i = F_i C_i \tag{3.32}$$

$$TGP = \sum \tau_i \tag{3.33}$$

where

τ_i	=	Gas tension of component i $[mmHg]$
F_i	=	Gas tension factor of component i $[mmHg/(mg/L)]$
C_i	=	Concentration of component i $[mg/L]$
TGP	=	Total dissolved gas pressure $[mmHg]$

The gas tension factors and solubilities of oxygen and nitrogen are given in APPENDIX F.

3.6.3 Carbon dioxide degassing model

Carbon dioxide degassing due to aeration was modeled according to the method by Wik et al. (2009) using equation (3.34).

$$m_{CO_2} = V \cdot K_L a_{CO_2} \cdot \left({C_{CO_2}}^{sat} - C_{CO_2}\right) \tag{3.34}$$

where

m_{CO_2}	=	Mass transfer rate of carbon dioxide into the water $[g/day]$
V	=	Volume of the vessel $[m^3]$
$K_L a_{CO_2}$	=	Overall carbon dioxide mass transfer coefficient $[1/day]$
${C_{CO_2}}^{sat}$	=	Saturation concentration of carbon dioxide in water $[mg/L]$
C_{CO_2}	=	Dissolved carbon dioxide concentration $[mg/L]$

${C_{CO_2}}^{sat}$ is equal to 0.5 mg/L due to it being the concentration of CO_2 in ambient air (Timmons and Ebeling, 2007, p. 107). $K_L a_{CO_2}$ can be estimated using a ratio of $\frac{K_L a_{CO_2}}{K_L a_{O_2}} = 0.9$, and $K_L a_{O_2}$ can be estimated by rearranging equation (3.24) to yield equation (3.35).

$$K_L a_{O_2} = \frac{m_{O_2}}{V \cdot \left({C_{O_2}}^{sat} - C_{O_2}\right)} \tag{3.35}$$

Comprehensive models for CO_2 degassers are available (Grace and Piedrahita, 1994; Vinci et al., 1996). However, within the design parameters of the current study, a dedicated CO_2 degassing unit was not required as enough CO_2 was removed by aeration in the fish tanks and biofilters (see section 4.6.5).

3.7 Pipe flow pressure drop

Pressure drop in pipes is determined by the flow velocity, pipe diameter, surface roughness of the pipe, pipe length, fluid properties and flow regime (Cengel and Cimbala, 2014). Pressure drop is also expressed in terms of equivalent water body height known as head loss. Head loss is calculated using equation (3.36).

$$h_L = \frac{f \cdot L_{pipe} \cdot {u_{avg}}^2}{2g \cdot D_{pipe}} \tag{3.36}$$

where

h_L	=	Head loss $[m]$
f	=	Darcy friction factor
L_{pipe}	=	Pipe length $[m]$
u_{avg}	=	Average flow velocity $[m/s]$
g	=	Gravitational acceleration $[m/s^2]$
D_{pipe}	=	Pipe diameter $[m]$

The effect of wall friction is accounted for using the Darcy friction factor (f). The following methods were used to calculate the friction factor.

Laminar flow through circular pipe:
$$f = \frac{64.00}{Re} \tag{3.37}$$

Turbulent flow through circular pipe:
$$f = \left(\frac{1}{-1.8 \log\left(\frac{6.9}{Re} + \left(\frac{\xi / D_{pipe}}{3.7} \right)^{1.11} \right)} \right)^2 \tag{3.38}$$

Laminar flow between parallel plates:
$$f = \frac{96.00}{Re} \tag{3.39}$$

where

Re	=	Reynolds number (see section 3.5.1)
ξ	=	Pipe surface roughness $[m]$

Minor head losses are introduced by components such as valves and heat exchangers and changes in flow geometry such as bends and pipe diameter expansion or contraction. Except for heat exchangers, the minor head losses were assumed to be negligible due to the early stage of design and lack of minor losses that can be expected in the system.

Hydraulic head is the head loss introduced when pumping from a water surface with a lower elevation than the destination, and the value is equal to the height difference between the two points. When gravity flow occurs, the difference in water level of the two free water surfaces will be equal to the total head loss within the piping system where the gravity flow occurs.

3.8 Fish tank mass balances

A mass balance over a RAS system volume is expressed as $mass\ accumulation = mass\ in - mass\ out$. Mass balances were needed in this design to size the recirculation pumps to allow enough circulation to avoid accumulation of waste products in the fish tanks. Thus, the chosen system volume was the fish tanks. Due to the low make-up flow rates in RAS culture (99% of water is recycled), the effect of waste removal by effluent water was assumed to be negligible and omitted from the mass balance calculations.

The general mass balance of a material over the fish tanks is expressed as:

$$(m_{acc})_i = \left(m_{recirc,in}\right)_i + \left(m_{prod}\right)_i - \left(m_{recirc,out}\right)_i - (m_{cons})_i \quad (3.40)$$

where

$(m_{acc})_i$	=	Mass accumulation rate of component i $[g/day]$
$\left(m_{recirc,in}\right)_i$	=	Influent mass flow rate of component i $[g/day]$
$\left(m_{prod}\right)_i$	=	Production rate of component i $[g/day]$
$\left(m_{recirc,out}\right)_i$	=	Effluent mass flow rate of component i $[g/day]$
$(m_{cons})_i$	=	Consumption rate of component i $[g/day]$

Applying equation (3.40) to the major components of interest, namely oxygen, carbon dioxide, total suspended solids and total ammonia nitrogen yields the following equations. It is assumed that the mass accumulation rate of each component in the fish tanks is zero. The influent and effluent mass flow rates are shown in terms of recirculating flow rate and component concentration.

$$Q_{recirc} \cdot C_{O_2,in} + \left(m_{prod}\right)_{O_2} - Q_{recirc} \cdot C_{O_2,out} - (m_{cons})_{O_2} = 0 \quad (3.41)$$

$$Q_{recirc} \cdot C_{CO_2,in} + \left(m_{prod}\right)_{CO_2} - Q_{recirc} \cdot C_{CO_2,out} - (m_{cons})_{CO_2} = 0 \quad (3.42)$$

$$Q_{recirc} \cdot C_{TSS,in} + \left(m_{prod}\right)_{TSS} - Q_{recirc} \cdot C_{TSS,out} = 0 \quad (3.43)$$

$$Q_{recirc} \cdot C_{TAN,in} + \left(m_{prod}\right)_{TAN} - Q_{recirc} \cdot C_{TAN,out} = 0 \quad (3.44)$$

where

Q_{recirc}	=	Recirculation flow rate $\left[m^3/day\right]$
$C_{i,in}$	=	Concentration of influent component i $[mg/L]$
$C_{i,out}$	=	Concentration of effluent component i $[mg/L]$
$\left(m_{prod}\right)_{O_2}$	=	Oxygen added by aeration $[g/day]$
$(m_{cons})_{O_2}$	=	Oxygen consumed by fish metabolism $[g/day]$
$\left(m_{prod}\right)_{CO_2}$	=	Carbon dioxide excreted by fish $[g/day]$
$(m_{cons})_{CO_2}$	=	Carbon dioxide removed by aeration $[g/day]$
$\left(m_{prod}\right)_{TSS}$	=	Total suspended solids produced by feeding $[g/day]$
$\left(m_{prod}\right)_{TAN}$	=	Total ammonia nitrogen produced by feeding $[g/day]$

Rearranging the above equations to solve for Q_{recirc} yields the equations below, which can be used to calculate the required recirculating flow rates to ensure no accumulation of waste products in the fish tanks at the maximum allowable waste concentrations. The minimum required recirculating flow rate will be equal to the Q_{recirc} with the highest value.

Dissolved oxygen: $$Q_{recirc} = \frac{(m_{cons})_{O_2} - (m_{prod})_{O_2}}{C_{O_2,in} - C_{O_2,out}} \quad \textbf{(3.45)}$$

Dissolved carbon dioxide: $$Q_{recirc} = \frac{(m_{cons})_{CO_2} - (m_{prod})_{CO_2}}{C_{CO_2,in} - C_{CO_2,out}} \quad \textbf{(3.46)}$$

Total suspended solids: $$Q_{recirc} = \frac{(m_{prod})_{TSS}}{C_{TSS,out} - C_{TSS,in}} \quad \textbf{(3.47)}$$

Total ammonia nitrogen: $$Q_{recirc} = \frac{(m_{prod})_{TAN}}{C_{TAN,out} - C_{TAN,in}} \quad \textbf{(3.48)}$$

Nitrate is the product of complete nitrification of ammonium and will build up in the system if it is not removed by the process of denitrification or by exchanging RAS water with fresh make-up water. This study did not focus on denitrification due to the complexity of operating such a system. A preferred solution was to calculate the required make-up water to ensure that nitrate-nitrogen levels remain below a desired concentration is calculated using equation (3.49). The production rate of NO_3-N was assumed to be equal to the removal rate of TAN in the biofilters.

$$Q_{makeup} = \frac{(m_{prod})_{NO_3-N}}{C_{NO_3-N,max}} \quad \textbf{(3.49)}$$

where

Q_{makeup} = Make-up water volumetric flow rate $[m^3/day]$

$C_{NO_3-N,max}$ = Maximum allowable nitrate concentration $[mg/L]$

3.9 Water and air heat transfer models

3.9.1 Process water heat and mass transfer models

In order to estimate the heating requirements for process water, the heat flows in and out of the process water had to be modeled. The system boundary is defined as the entire process water volume. Refer to Chapter 4 for descriptions of the proposed system and building. Heat transfer out of the water is represented by a positive value and heat transfer into the water a negative value.

3.9.1.1 Make-up water

Makeup water is added to the system to balance with the effluent water lost from the system. The makeup water will result in either a removal or addition of energy to the water, causing heating or cooling. This was calculated by considering the temperatures of the makeup stream and process water, the makeup water flow rate and the heat capacity of water as in equation (3.50).

$$H_{makeup} = Q_{makeup} \cdot \rho_w \cdot c_{p,w} \cdot (T_{PW} - T_{makeup}) \quad (3.50)$$

where

H_{makeup}	=	Heat transfer rate due to make-up water addition $[W]$
Q_{makeup}	=	Make-up water volumetric flow rate $[m^3/s]$
ρ_w	=	Density of water $[kg/m^3]$
$c_{p,w}$	=	Specific heat capacity of water $[J/(kg \cdot K)]$
T_{makeup}	=	Make-up water temperature [°C]
T_{PW}	=	Process water temperature [°C]

Municipal water with a conservative temperature of 15°C was assumed to be used. $c_{p,w}$ was assumed to be 4179 $J/kg \cdot K$ at 27°C and varies by less than 0.5% over the range of 10°C to 30°C (Cengel and Ghajar, 2015).

3.9.1.2 Fish tank and MBBR wall heat loss

Heat transfer through solid objects occur by conduction in the solid material and by convection and radiation on the outer surfaces of the solid material (Cengel and Ghajar, 2015). These mechanisms were used to model heat transfer through the walls of the fish tanks and MBBRs. Heat transfer by conduction is modeled by equation (3.51).

$$H_{cond} = \frac{\kappa_{wall} \cdot A_s \cdot (T_s - T_\infty)}{L_{wall}} \quad (3.51)$$

where

H_{cond}	=	Heat transfer by conduction $[W]$
κ_{wall}	=	Thermal conductivity of wall material $[W/(m \cdot K)]$
A_s	=	Heat transfer surface area $[m^2]$
T_∞	=	Air temperature sufficiently far away from the surface [°C]
T_s	=	Surface temperature [°C]
L_{wall}	=	Wall thickness $[m]$

Heat transfer between surfaces and their environment occurs by two mechanisms in parallel, namely radiation and convection, which is modeled in equations (3.52) and (3.53).

$$H_{conv} = \psi_{conv} \cdot A_s \cdot (T_s - T_\infty) \tag{3.52}$$

$$H_{rad} = \psi_{rad} \cdot A_s \cdot (T_s - T_\infty) \tag{3.53}$$

where

H_{conv}	=	Heat transfer by convection $[W]$
ψ_{conv}	=	Convection heat transfer coefficient $\left[W/\left(m^2 \cdot K\right)\right]$
H_{rad}	=	Heat transfer by radiation $[W]$
ψ_{rad}	=	Radiation heat transfer coefficient $\left[W/\left(m^2 \cdot K\right)\right]$
T_s	=	Surface temperature [°C]
T_{surr}	=	Temperature of the surrounding environment [°C]

The driving force of both these mechanisms is the temperature difference between the surface and its surroundings. The intensity of each mechanism is represented by its respective heat transfer coefficient (ψ).

Heat transfer by convection can occur in two different regimes, natural convection and forced convection. Forced convection results in higher heat transfer rates and occurs when the fluid (air) velocity over the heat transfer surface is significant. Natural convection occurs when the bulk fluid velocity effects are negligible. To determine which type of convection will occur, the Grashof number (Gr_L) and Reynolds number (Re_L) needs to be calculated to determine the ratio Gr_L/Re_L^2. If $Gr_L/Re_L^2 < 0.1$, forced convection will dominate. If $Gr_L/Re_L^2 > 10$, natural convection will dominate. If $0.1 < Gr_L/Re_L^2 < 10$, both natural convection and forced convection needs to be considered (Cengel and Ghajar, 2015, p. 560). All fluid properties are evaluated at the air film temperature, which is the average of the surface temperature and bulk fluid temperature: $T_{film} = (T_s + T_\infty)/2$

$$Gr_L = \frac{g \cdot B \cdot (T_s - T_\infty) \cdot {L_c}^3}{v^2} \tag{3.54}$$

$$Re_L = \frac{u_{air} \cdot L_c}{v} \tag{3.55}$$

where

Gr_L	=	Grashof number
B	=	Coefficient of volume expansion $[1/K]$
g	=	Gravitational acceleration $\left[m/s^2\right]$
L_c	=	Characteristic length of the geometry $[m]$
v	=	Kinematic viscosity of the air $\left[m^2/s\right]$
u_{air}	=	Air velocity $[m/s]$

Estimating the air velocity in the RAS building accurately is not a straightforward calculation as there are multiple air inlets (aeration points) inside the building and the air outlet will be leaks in the greenhouse construction. As a conservative approximation of the air velocity, the air change rate of the building (building volume per hour) was multiplied by the path length from the center of the room to one of the corners, which is the maximum possible path length of evacuating air. The building air change rate was 1.6l, which took into account air changes by leaks in the greenhouse construction (see section 3.9.2.2) and the aeration rate of the fish tanks and biofilters (see section 4.6). The path length was calculated to be 5.8 m and thereby the air velocity was estimated to be 0.0026 m/s. The characteristic length was assumed to be equal to the path length. The Gr_L/Re_L^2 ratio was calculated to be 85 000, which is much larger than 10 and indicated that, at the assumed air change rate and geometry, natural convection effects will dominate on all surfaces in the RAS building. Thus, only the equations describing heat transfer by natural convection are discussed.

The convection heat transfer coefficient is commonly calculated using the dimensionless Nusselt number (Nu) shown in equation (3.56).

$$Nu = \frac{\psi_{conv} \cdot L_c}{\kappa_{air}} \tag{3.56}$$

where

Nu	=	Nusselt number
κ_{air}	=	Thermal conductivity of air $[W/(m \cdot K)]$

The Nusselt number is generally calculated using the Rayleigh number (Ra), which is the product of the Grashof number and Prandtl number (Pr). The Prandtl number is a temperature dependent property of the fluid.

$$Ra_L = Gr_L Pr \tag{3.57}$$

where

Ra_L	=	Rayleigh number
Pr	=	Prandtl number

Empirically derived Nusselt number relations for natural convection over various geometries is given in Table 3-7.

Table 3-7: Nusselt number relations for natural convection over various geometries. Redrawn from Cengel and Ghajar (2015).

Geometry	Characteristic length (L_c)	Nusselt number (Nu)
Vertical flat plate	Length of plate	$Nu = \left(0.825 + \frac{0.387 \cdot Ra_L^{1/6}}{\left(1+\left(\frac{0.492}{Pr}\right)^{9/16}\right)^{8/27}} \right)^2$ **(3.58)**
Horizontal flat plate with upward heat flow	$\frac{A_s}{perimeter}$	$Nu = 0.54 \cdot Ra_L^{1/4}$ if $10^4 < Ra_L < 10^7$ **(3.59)** $Nu = 0.15 \cdot Ra_L^{1/3}$ if $10^7 < Ra_L < 10^{11}$ **(3.60)**
Horizontal flat plate with downward heat flow	$\frac{A_s}{perimeter}$	$Nu = 0.27 \cdot Ra_L^{1/4}$ if $10^5 < Ra_L < 10^{11}$ **(3.61)**
Vertical cylinder	Height of cylinder	Treated as a vertical plate if $D \geq \frac{35 \cdot L}{Gr_L^{1/4}}$
Horizontal cylinder	Diameter of cylinder	$Nu = \left(0.6 + \frac{0.387 Ra_L^{1/6}}{\left(1+\left(\frac{0.559}{Pr}\right)^{9/16}\right)^{8/27}} \right)^2$ **(3.62)**

The radiation heat transfer coefficient is calculated using equation (3.63).

$$\psi_{rad} = \varepsilon \cdot \sigma \cdot A_s \left(T_s + T_{surr}\right)\left(T_s^2 + T_{surr}^2\right) \quad \textbf{(3.63)}$$

where

ε	=	Emissivity of surface
σ	=	Stefan-Boltzmann constant = $5.670 \times 10^{-8}\ W/\left(m^2 \cdot K^4\right)$
T_s	=	Surface temperature $[K]$
T_{surr}	=	Temperature of the surrounding environment $[K]$

In order to simplify the combination of the three different heat transfer mechanisms, the thermal resistance network method was used. The thermal resistance network method was used throughout this study to account for heat transfer mechanism both in series and parallel (Cengel and Ghajar, 2015, p. 144). The thermal resistance (Λ) network is analogous to Ohm's Law for an electrical circuit such that $H \times \Lambda = \Delta T$. The thermal resistances are defined as:

$$\Lambda_{cond} = \frac{L_{wall}}{\kappa_{wall} A_s} \quad \textbf{(3.64)}$$

$$\Lambda_{conv} = \frac{1}{\psi_{conv}\, A_s} \quad \textbf{(3.65)}$$

$$\Lambda_{rad} = \frac{1}{\psi_{rad}\, A_s} \quad \textbf{(3.66)}$$

where

Λ_{cond}	=	Thermal resistance against heat transfer by conduction $[K/W]$
Λ_{conv}	=	Thermal resistance against heat transfer by convection $[K/W]$
Λ_{rad}	=	Thermal resistance against heat transfer by radiation $[K/W]$

After the overall thermal resistance (Λ_{total}) has been calculated (equation (3.67)) using the same method as adding up parallel and series resistors, the heat transfer rate can be calculated using equation (3.68).

$$\Lambda_{total} = \frac{\Lambda_{conv}\,\Lambda_{rad}}{\Lambda_{conv} + \Lambda_{rad}} + \Lambda_{cond} \tag{3.67}$$

$$H = \frac{T_s - T_{surr}}{\Lambda_{total}} \tag{3.68}$$

where

Λ_{total} = Overall thermal resistance against heat transfer $[K/W]$

3.9.1.3 Water surface heat transfer and evaporation

Disturbances of the water surface by water flows or fish movement will increase the surface area available for heat and mass transfer. The increased surface area will result in increased heat and mass transfer rates. This is evidenced by observations of higher swimming pool surface evaporation rates when occupied with people as opposed to unoccupied pools (Shah, 2014). However, no correlations for surface evaporation in aquaculture tanks were found in literature and thus the water surface was assumed to be equivalent to a horizontal flat plate. The fish tanks in this study were assumed to be open with no lids covering the water surface. The addition of a lid will decrease heat loss from the fish tank water surface due to evaporation and should be considered during construction as a means of reducing water heating demands.

The heat and mass transfer were assumed to be by the mechanism of natural convection. Under the assumption of a horizontal flat plate and natural convection, the correlations in Table 3-7 were used to calculate the heat transfer coefficient. The mass transfer rate by convection was modeled using equation (3.69), where the driving force of the mass transfer is the difference in water vapor density between the air at the water surface and the bulk air water vapor density (Cengel and Ghajar, 2015). Radiation heat transfer was also included and was calculated as described for the fish tank walls (see section 3.9.1.2).

$$m_{evap} = \psi_{mass} \cdot A_s \cdot (\rho_{v,s} - \rho_{v,\infty}) \tag{3.69}$$

where

m_{evap} = Evaporation rate $[kg/s]$

ψ_{mass} = Convection mass transfer coefficient $\left[W/\left(m^2 \cdot K\right)\right]$

$\rho_{v,s}$ = Water vapor density at water surface $\left[kg/m^3\right]$

$\rho_{v,\infty}$ = Water vapor density of bulk air $\left[kg/m^3\right]$

The convection mass transfer coefficient is commonly calculated using the dimensionless Sherwood number (Sh) shown in equation (3.70) (Cengel and Ghajar, 2015).

$$Sh = \frac{\psi_{mass} L_c}{D_{AB}} \tag{3.70}$$

where

Sh = Sherwood number

D_{AB} = Mass diffusivity of water in air $[m^2/s]$

Empirically derived Sherwood number relations for natural convection over a horizontal flat plate with upwards heat flow is given in equations (3.71) and (3.72). The Schmidt number (Sc) used in the correlations is calculated using equation (3.73) (Cengel and Ghajar, 2015).

$$Sh = 0.54 \cdot (Gr_L \cdot Sc)^{1/4} \qquad \text{if } 10^4 < Gr_L \cdot Sc < 10^7 \tag{3.71}$$

$$Sh = 0.15 \cdot (Gr_L \cdot Sc)^{1/3} \qquad \text{if } 10^7 < Gr_L \cdot Sc < 10^{11} \tag{3.72}$$

$$Sc = \frac{v}{D_{AB}} \tag{3.73}$$

where

Sc = Schmidt number

The heat loss by evaporation is quantified by the latent heat of vaporization of water ($\lambda_w = 2437.6\ kJ/kg$) and is calculated using equation (3.74).

$$H_{evap} = \lambda_w \cdot m_{evap} \tag{3.74}$$

where

H_{evap} = Heat transfer due to evaporation $[W]$

λ_w = Latent heat of vaporization of water $[kJ/kg]$

3.9.1.4 Pipe heat loss

The thermal resistance network method was used for heat loss through piping. Thermal resistance against heat transfer by conduction through a circular pipe wall was calculated using equation (3.75) (Cengel and Ghajar, 2015).

$$\Lambda_{cond,pipe} = \frac{\ln\left(\frac{D_{outer}}{D_{inner}}\right)}{2\pi \cdot L_{pipe} \cdot \kappa_{wall}} \tag{3.75}$$

where

$\Lambda_{cond,pipe}$ = Thermal resistance against heat conduction through a circular pipe wall $[kg/s]$

D_{outer} = Outer pipe diameter $[m]$

D_{inner} = Inner pipe diameter $[m]$

L_{pipe} = Pipe length $[m]$

It was assumed that forced convection effects dominate inside the pipes as a worst case. The thermal resistance against heat transfer by forced convection inside the pipes was calculated using the Nusselt number correlation below (equation (3.76)).

$$Nu = \frac{\left(\frac{f}{8}\right) \cdot (Re - 1000) \cdot Pr}{1 + 12.7\left(\frac{f}{8}\right)^{0.5} \cdot \left(Pr^{2/3} - 1\right)} \quad \textbf{(3.76)}$$

The thermal resistance against heat transfer by natural convection on the outer surface of the pipe was calculated using the horizontal cylinder correlation for the Nusselt number (equation (3.62)) shown in Table 3-7. The thermal resistance against heat transfer by radiation was calculated similarly to the fish tank walls.

3.9.1.5 Sump heat loss

Overall heat transfer coefficients for heat losses from a concrete sump with 12 inch walls is reported by Talati (1988). Wet ground has a higher heat transfer coefficient than dry ground and the ground was thus assumed to be wet. Given that the above assumption applies to the system being modelled, the wall and floor overall heat transfer coefficients are 1.42 $W/(m^2 \cdot K)$ and 0.68 $W/(m^2 \cdot K)$ respectively.

Heat loss from the sump water surface was calculated using the same equations as for the fish tanks (see section 3.9.1.3). Evaporation from the sump water surface was assumed to be negligible due to the low ventilation rate inside the sump room.

3.9.1.6 Aeration heat transfer and evaporation

Air bubbles entering the water columns of the fish tanks and MBBRs have a high interfacial surface area with the water. Thereby it was assumed that the air temperature will be the same as the water temperature when the air bubble exits the water column (Talati, 1988). It was also assumed that the relative humidity inside the air bubble will be 100% when the air bubble exits the water column.

The air temperature discharged from the submerged diffusers will have a higher temperature than the air at the suction side of the blower due to compression. The discharge air temperature can be calculated by assuming a value for the isentropic efficiency of the blower. The isentropic efficiency of a blower is defined as “the ratio of the work input required to raise the pressure of a gas to a specified value in an isentropic manner to the actual work input”. It was assumed that the heat loss from the blower and pipes will be negligible as the gas velocity is high. Due to this assumption the system from the suction end of the blower to the submerged diffuser is assumed to be adiabatic. The isentropic efficiency in an adiabatic blower is expressed in equation (3.77) (Cengel and Boles, 2015).

$$\eta_{blower} = \frac{E_{2s} - E_1}{E_{2a} - E_1} \tag{3.77}$$

where

η_{blower}	=	Isentropic efficiency of the blower
E_1	=	Enthalpy of the inlet air $[kJ/kg]$
E_{2s}	=	Enthalpy of the air after isentropic compression $[kJ/kg]$
E_{2a}	=	Actual enthalpy of the air after compression $[kJ/kg]$

Isentropic efficiencies of the regenerative blowers considered for this design were 66% (CFW Fans, 2019b). Air properties were read from property tables in Cengel and Boles (2015)(see APPENDIX F). The inlet enthalpy (E_1) was read at the inlet air temperature. In order to obtain the enthalpy after isentropic compression (E_{2s}), the pressure of the inlet and discharge (P_1, P_2) needs to be known, which is determined by the design. P_1 and P_2 were assumed to be 101 325 Pa and 126 325 Pa respectively, with P_1 being the standard ambient pressure at sea level and P_2 being P_1 plus the head loss through the aeration process. A dimensionless quantity known as the relative pressure (P_r), which is a function of temperature, aids in determining the state after an isentropic compression process. Firstly, P_{r1} is read from the property tables at the inlet air temperature, which was assumed to be 6°C (see section 4.1.7.1). Secondly, P_{r2} is calculated using equation (3.78). Lastly, E_{2s} is read from the property table at P_{r2}.

$$\frac{P_2}{P_1} = \frac{P_{r2}}{P_{r1}} \tag{3.78}$$

where

P_1	=	Absolute pressure of the inlet air $[Pa]$
P_2	=	Absolute pressure of the discharged air $[Pa]$
P_{r1}	=	Relative pressure of the inlet air
P_{r2}	=	Relative pressure of the discharged air

When η_{blower} is assumed and both E_1 and E_{2s} obtained using property tables, E_{2a} was calculated by rearranging equation (3.77) and solving it. Finally, when E_{2a} is known, the temperature of the discharged air (T_2) can be read from the property tables at E_{2a}. The sensible heat loss from the water by aeration was calculated by estimating the mass flows of air and water vapor entering the column (using equations (F.1), (F.2) and (F.3) in APPENDIX F) and calculating the heat transfer using equation (3.79).

$$H_{aeration\ (sensible)} = (m_{air} \cdot c_{p,a} + m_w \cdot c_{p,w}) \cdot (T_{PW} - T_2) \quad \textbf{(3.79)}$$

where

$H_{aeration\ (sensible)}$	=	Sensible heat transfer due to aeration $[W]$
m_{air}	=	Mass flow rate of dry air $[kg/s]$
$c_{p,a}$	=	Specific heat capacity of air $[J/(kg \cdot K)]$
m_w	=	Mass flow rate of water vapor before evaporation $[kg/s]$
T_2	=	Temperature of discharged air [°C]

The heat transfer due to evaporation of water into the air bubble was calculated similarly to the water surface evaporation after estimating the evaporation rate by assuming 100% relative humidity and calculating the evaporation rate required to achieve 100% relative humidity. Inlet relative humidity at 6°C was assumed to be 73% (see section 4.1.7.2).

$$H_{aeration\ (latent)} = \lambda_w \cdot m_{evap} \quad \textbf{(3.80)}$$

where

$H_{aeration\ (latent)}$	=	Latent heat transfer due to aeration $[W]$

3.9.1.7 Fish heat production

Energy is released by fish into the water as part of losses by metabolism (van Weerd et al., 2003). Metabolic heat production will increase as the feeding rate increases, resulting in the highest metabolic heat production being observed at peaking stocking densities. As the temperature must be maintained constant throughout the entire production duration, the metabolic heat production was assumed to be zero to account for negligible metabolic heat production at the start of a trial, where the stocking density will be low. Metabolic heat production can only be included in the design if stocking densities are high throughout the entire production duration, which is more common in commercial farms that operate using high stocking densities on a continuous basis. Experimental trials can be regarded as similar to batch operations of a chemical process with dynamic product concentrations, whereas commercial farms can be regarded as similar to a chemical process operating continuously with constant product concentrations.

3.9.1.8 Pump heat production

Centrifugal pumps typically have a hydraulic efficiency of 73% and a motor efficiency of 90% (Grundfos, 2019), which results in 33% of the input power being lost to the water as heat. This heat gain will reduce the water heating requirements.

3.9.2 Internal building air heat transfer models

In order to estimate the heating requirements for air conditioning, the heat flows in and out of the RAS building had to be modeled. The system boundary is defined as the entire air volume within the RAS building. Heat transfer to the internal building air is thus represented by a positive value and heat

transfer out of the water a negative value. The design case was defined as being at night in the winter to (1) determine the required heating value during the time of year requiring the highest input, and (2) compare these values to the existing heating facilities at the Welgevallen experimental RAS to determine the suitability of the currently installed air conditioner.

3.9.2.1 Heat transfer through building walls

Heat entering the building through the walls and roof was considered. Due to the design case being defined as operation during nighttime, solar heating through the greenhouse panels did not need to be modeled. The following mechanisms of heat transfer were considered:

- Radiation (surroundings) – Absorbed by outer building surface
- Convection (outside) – Forced convection by wind
- Conduction (through brick walls or greenhouse panels)
- Convection (internal) – Natural convection at inner surface
- Radiation (surroundings) – Emitted by inner surface to the inside of the building

The following assumptions were made:

- The internal combined (convection + radiation) heat transfer coefficients (h_i) on a vertical surface and horizontal surface were assumed to be 8.29 $W/(m^2 \cdot ℃)$ and 6.13 $W/(m^2 \cdot ℃)$ respectively. Still air conditions are assumed for this value to apply (Çengel and Ghajar, 2013).
- The external combined (convection + radiation) heat transfer coefficient (h_o) was assumed to be 34.0 $W/(m^2 \cdot ℃)$. An emissivity of 0.9 and average wind speeds of 6.7 m/s are assumed for this value to apply (Çengel and Ghajar, 2013).
- The R-value of the 8 mm thick twin-wall polycarbonate sheeting is 0.30 $(m^2 \cdot ℃)/W$ (Palram, 2019).
- The R-value of the double brick wall with 13 mm air space is 0.40 $(m^2 \cdot ℃)/W$ (Cengel and Ghajar, 2015).

Based on the listed assumptions, 3 thermal resistances were calculated for each surface. These thermal resistances were the thermal resistance of the outer surface, wall material and inner surface. Rates of heat transfer were calculated for each surface and a Solver routine in Microsoft Excel was used to adjust the outer and inner surface temperatures to make all the rates of heat transfer equal.

3.9.2.2 Air infiltration

Cold air entering the building will contribute to the heating duty of the building air. The two primary sources of external air entering the building is by leaks between the greenhouse panels and by aeration coming from the blower. The aeration will enter the building air at the same temperature as the water (see section 3.9.1.6). The air infiltration by leaks in paneled greenhouse construction is reported to result in the air volume of the room being replaced once per hour (NGMA, 2010). The same method

as used for the make-up was used to calculate the heating duty contribution of the air infiltration (see section 3.9.1.1).

3.9.2.3 Heat transfer through ground

Heat transfer through the ground into a building can be modeled by dividing the heat transfer path through the ground up into multiple layers as shown in Figure 3-9. The path length was calculated for each layer and the thermal resistance against heat conduction calculated. Thermal resistance against convection and radiation on either side of the ground was assumed to be negligible. The thermal conductivity of the ground was assumed to be similar to that of sand, which is typically 2 $W/(m \cdot K)$ (Zhang and Wang, 2017). The ground heat transfer was considered on three sides of the fish tank room and the building is raised on a foundation as seen in Figure 3-9.

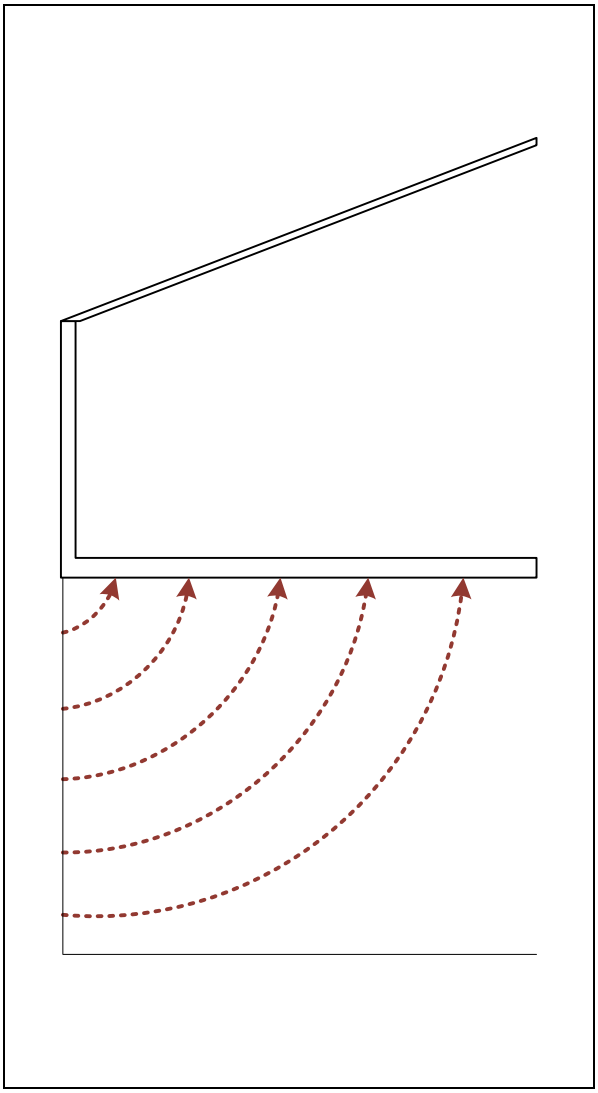

Figure 3-9: Heat transfer paths through the ground

3.9.2.4 Heat transfer from water

Heat transfer to the air from the water surface is described in the section 3.9.1.3 and will be the negative of the heat transfer to the water. Heat transfer from the fish tank walls, MBBR walls and piping is also included as calculated in the previous sections.

Chapter 4. Conceptual design results

This chapter sets out to formulate a design basis for the Welgevallen experimental RAS, and to apply the models described in the previous chapter to complete the design. Existing infrastructure and equipment were reused in the design where feasible to achieve Objective 3 of the study (see section 1.4).

To begin the conceptual design process, a design basis was formulated to give the design a solid foundation to work from. The subsequent steps, not necessarily in order, were:

1) Selection of technology based on extensive literature review discussed in Chapter 2.
2) Sizing of the various equipment using the models described in Chapter 3.
3) Design of a floor plan layout based on the building dimensions and equipment footprints.

Figure 4-1 and Figure 4-2 are graphical representations of the temperature control and wastewater treatment conceptual design processes respectively that show the flow of information, the inputs, technology choices and where existing infrastructure exists at the particular facility.

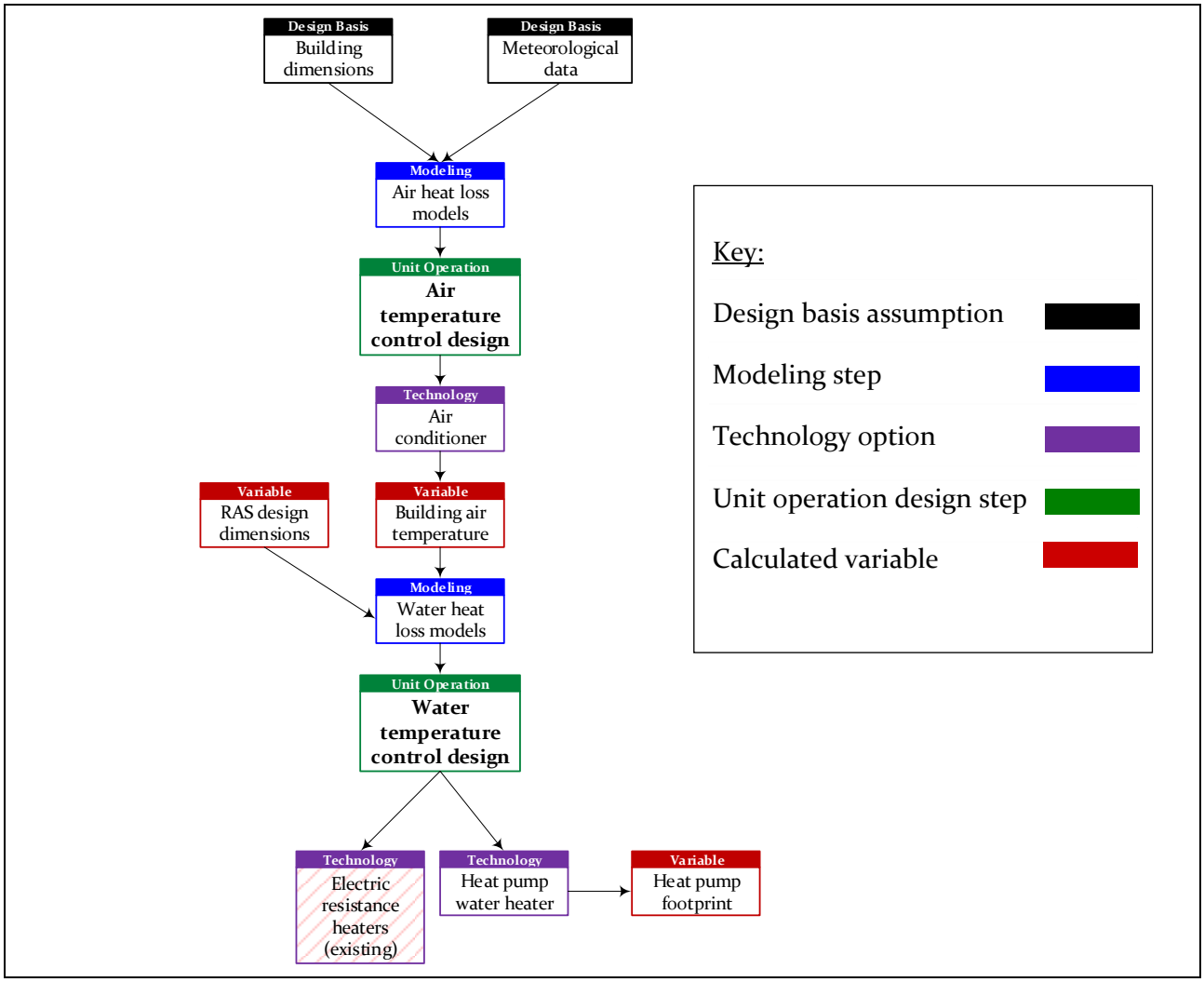

Figure 4-1: Temperature control conceptual design process

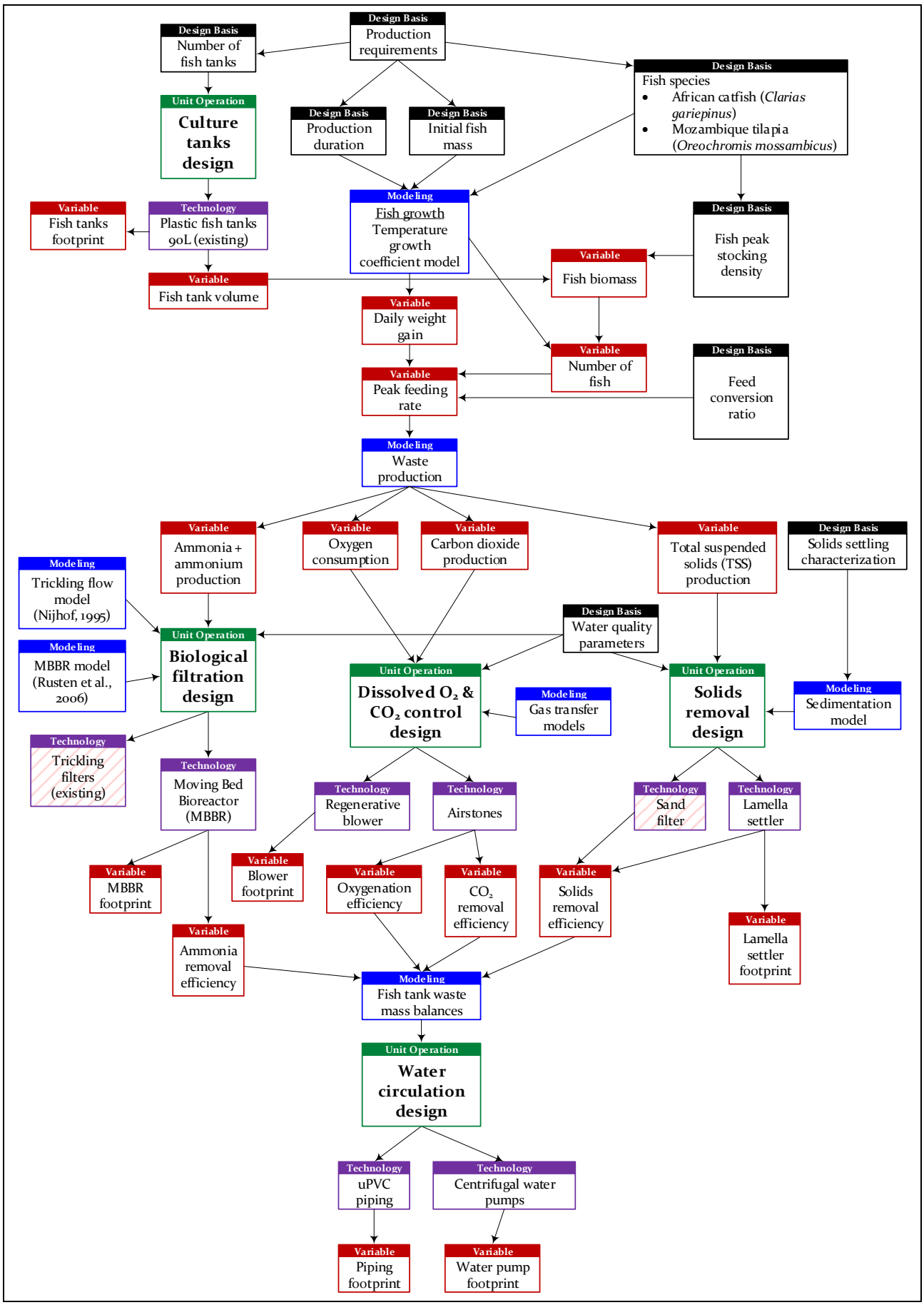

Figure 4-2: Wastewater treatment conceptual design process

4.1 Design basis

4.1.1 Description of current existing RAS

The current existing RAS was included in the design basis since one of the objectives of the study was to reuse as many of the equipment and buildings as possible.

4.1.1.1 Inventory of equipment

The process equipment in the current existing RAS is listed in Table 4-1.

Table 4-1: List of equipment in the current existing RAS

Equipment type	Description	Amount	Dimensions/rating
Plastic fish tanks	Water inlet is from an overhanging pipe. Water outlet is through an overflow. Tanks are on steel tables.	88	Length = 700 mm Width = 390 mm Height = 330 mm Volume = 90 L
Sump	Concrete sump.	1	Length = 2600 mm Width = 2250 mm Height = 500 mm
Electric resistance water heaters	Heaters have an element suspended in the water which heats up the water according to the setpoint of the device.	2	Power input = 4 kW
Water circulation pumps	Self-priming water circulation pumps Manufacturer: BADU Model: Porpoise 10	2	Power input = 0.45 kW 12 m^3/h @ 7 m head
Trickling filters	Trickling bed biofilters with crossflow media structured packing	4	Length = 850 mm Width = 650 mm Height = 1700 mm
Air blower	Air blower connected to air diffusers in each fish tank. Manufacturer: FPZ Model: SCL V4	1	Power input = 1.1 kW Max. flow = 137 m^3/h Max. pressure = 200 mbar
Air handling unit	Air handling unit situated outside the building that controls the temperature of air inside the fish tank building. Manufacturer: Daikin Model: UATY15K	1	Cooling capacity = 43.9 kW Heating capacity = 46.1 kW

Certain piping can be reused such as the underground pipe going to the sump and the pipe running back to the fish tank room from the sump. The piping inside the fish tank room were damaged and will have to be replaced.

Figure 4-3 shows how the equipment is connected to form the current existing RAS as of the writing of this thesis.

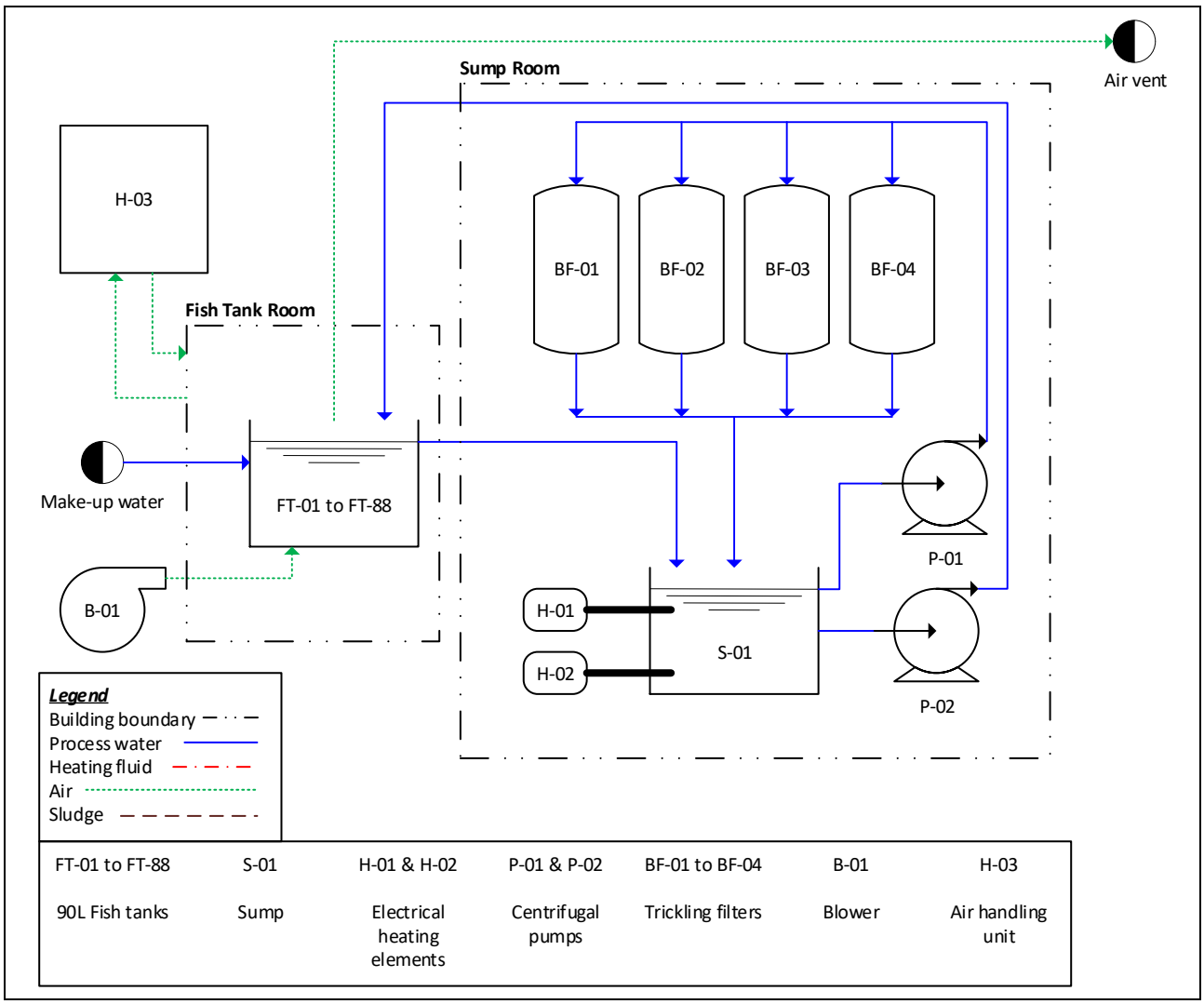

Figure 4-3: Process flow diagram of current existing RAS

It was noted that the RAS has two circulation loops, which is not standard and increases electrical energy requirements by pumping the water vertically twice instead of the standard one vertical lift observed in all RASs in literature. In this particular system the water first has to be pumped up to the top of the trickling filters from where it gravitates back into the sump. The reason for the water being pumped from the sump again is to return it from the sump to the fish tanks, and the piping layout requires that the water return line going back to the fish tanks has to be lifted over a walkway that separates the fish tanks and the sump. The water cannot gravitate directly to the fish tanks from the trickling filters, as the trickling filter outlets are below the walkway height and thus the return water has to be pumped from the sump.

4.1.1.2 Building dimensions

The RAS design process included considering the available footprint of the existing facilities. The fish tank room floor has a floor space of 9600mm x 6550mm, whereas the floor next to the sump in the sump room is 2600mm x 900mm. The sump is 2600mm long, 2250mm wide and 500mm deep.

The largest access doors available for carrying equipment into the fish tank room and sump room are 845mm x 2000mm and 690mm x 2000mm respectively.

4.1.2 Fish tanks and production length

The number of required fish tanks was determined by examining previous studies done at Welgevallen. Studies typically test a certain amount of different treatments to observe the effects of feed additives, water mineralization and various other parameters on the fish. The same treatment is replicated in more fish tanks to increase the statistical significance of the findings. Table 3-4 shows the experimental design of previous studies by listing the number of treatments, replicates and fish tanks used in addition to the production length of each study.

Table 4-2: Experimental design of previous studies at Welgevallen

Source	Species	Number of treatments	Number of replicates	Total fish tanks used	Production length [days]
Goosen (2014, p. 42)	Mozambique tilapia	2	5	10	52
Goosen (2014, p. 69)	Mozambique tilapia	4	5	20	52
Goosen (2014, p. 93)	Mozambique tilapia	7	6	42	61
Swanepoel (2017, p. 34)	African catfish	8	6	48	70
Talamuk (2016)	African catfish	4	6	24	91
Oluwaseyi (2016, p. 74 & 78)	African catfish	12	7	84	84
Oluwaseyi (2016, p. 109)	African catfish	9	7	63	70
Gericke (2019, p. 69)	African catfish	4	6	24	91
Gericke (2019, p. 115)	African catfish	4	6	24	91

On average, both the number of treatments and replicates were 6, which was assumed for future studies. Thereby a total of 36 fish tanks are used for a typical experimental study consisting of 6 treatments with 6 replicates each. It was decided that the existing 90-liter plastic fish tanks can be reused for the new RAS. The current number of installed tanks in the existing RAS is 88. However, this was deemed to be surplus to requirement for the typical set of fish trials done within this facility. It is estimated that 72 tanks is a more appropriate number, as this will allow two simultaneous experiments using 36 tanks each, whilst still accommodating for possible larger experiments should the need arise.

Production length in the above studies ranged from 52 to 91 days. Since the production length variable goes into fish growth modeling and dynamic modeling, the longest time period of 91 days was chosen as a basis for modeling of these parameters.

4.1.3 Initial fish weight

Initial fish weights used in trials have ranged from 0.96 g (Swanepoel, 2017) to 562 g (Gericke, 2019). As a design basis 10 g was taken as the starting weight for the fish as this is similar to commercial starting weights (Akinwole and Faturoti, 2007; Besson et al., 2014) and African catfish fingerlings are

widely available for purchase at 10 g from commercial hatcheries, to be used in trials. 10 g African catfish has also been used in a study at Welgevallen (Oluwaseyi, 2016).

4.1.4 Stocking density

Fish stocking density, defined as kg fish per m^3 of tank volume, is a critical parameter dictating the design, as it influences the amount of feed given per day and hence the waste production rates. As is standard for experimental RAS systems, the experimental trials to be done using the RAS will stock a fixed number of fish at the start and observe growth over time with minimal exchange of fish during the experiment. Fish that are removed from the system for sampling purposes are replaced to maintain the biomass in the trial. Thus, the stocking density within the RAS will increase as biomass increases, and the peak stocking density will be observed at the end of the trial due to fish growth. Trials should preferably be done at stocking densities close to that of commercial systems to eliminate stocking density effects on the results if applied in industry.

An intensive tilapia RAS in the USA is reported to operate at 82 kg/m^3 (Watanabe et al., 2002). A guide for recirculating aquaculture reported commercial stocking densities for tilapia of 20 to 120 kg/m^3 (Negroni, 2013). Table 4-3 shows allowable stocking densities reported for tilapia (Timmons and Ebeling, 2007, p. 121).

Table 4-3: Allowable stocking densities for tilapia RAS culture at different fish masses (Timmons and Ebeling, 2007, p. 121)

Fish mass [g]	Allowable stocking density [kg/m^3]
0.2	8.4
1.4	17
11	34
38	50
75	63
83	83
346	105
599	126
951	147

African catfish RAS culture in the Netherlands is typically done in two phases. Phase 1 grows 10g fish to a mass of 150g at peak stocking densities between 100 and 300 kg/m^3. Phase 2 grows 150g fish to a mass of 1500g which is suitable for market consumption. Phase 2 has peak stocking densities between 200 and 500 kg/m^3 (van de Nieuwegiessen et al., 2009, 2008). An African catfish RAS in Nigeria reported rearing adult fish at 176.6 kg/m^3 (Akinwole and Faturoti, 2007). A guide for recirculating aquaculture reported commercial stocking densities for African catfish of 300 kg/m^3 (Negroni, 2013). A semi-commercial experimental African catfish RAS in Germany operated at intensive aquaculture conditions with a stocking density of 200 kg/m^3 (Strauch et al., 2018).

Based on the above information, the first design iteration designed a RAS for an African catfish peak stocking density of 200 kg/m^3. Commercial tilapia peak stocking densities are considerably lower than that of African catfish. If operated at a peak stocking density of 200 kg/m^3, the new RAS would represent the conditions of commercial farms. However, after several iterations in the design process, it became apparent that the biofiltration demands of operating the RAS at a commercial stocking density of 200 kg/m^3 exceeded the existing floor space of the Welgevallen experimental facilities. Consequently, the design stocking density was reduced to 50 kg/m^3. This implied that the RAS was to be designed for utilization of all tanks at a peak stocking density of 50 kg/m^3. If the researchers desire to operate at a peak stocking density of 200 kg/m^3, only a quarter of the tank need to be used to achieve the same peak biomass and feeding rate for which the RAS was designed.

4.1.5 Feed composition and feeding rate

Feed composition and feeding rate have a large influence on waste production and therefore need to be carefully determined. Particularly the protein content of the feed is important, as it is the main source of nitrogenous wastes produced in the RAS. Feed protein content was assumed to be 45% (see section 3.3.1). The remaining feed components were assumed to be that of a typical fish feed (Wik and Lindén, 2004) and are listed in Table 4-4.

Table 4-4: Fish feed composition

Component	Feed content [g/g feed]
Protein	0.45
Carbohydrates	0.14
Fat	0.24
Ash	0.08
Water	0.09

A feed conversion ratio (FCR) of 1.5 has been chosen to model the feeding rate (see section 3.2.4). The maximum feeding rate was estimated to be 10.3 kg/day under the assumption of operating all tanks simultaneously, at conditions that will result in the maximum allowable stocking density to be reached at the last day of a 91-day growth trial. A peak stocking density of 50 kg/m^3 was used. Figure 4-4 shows the estimated daily feeding rate of each day of production.

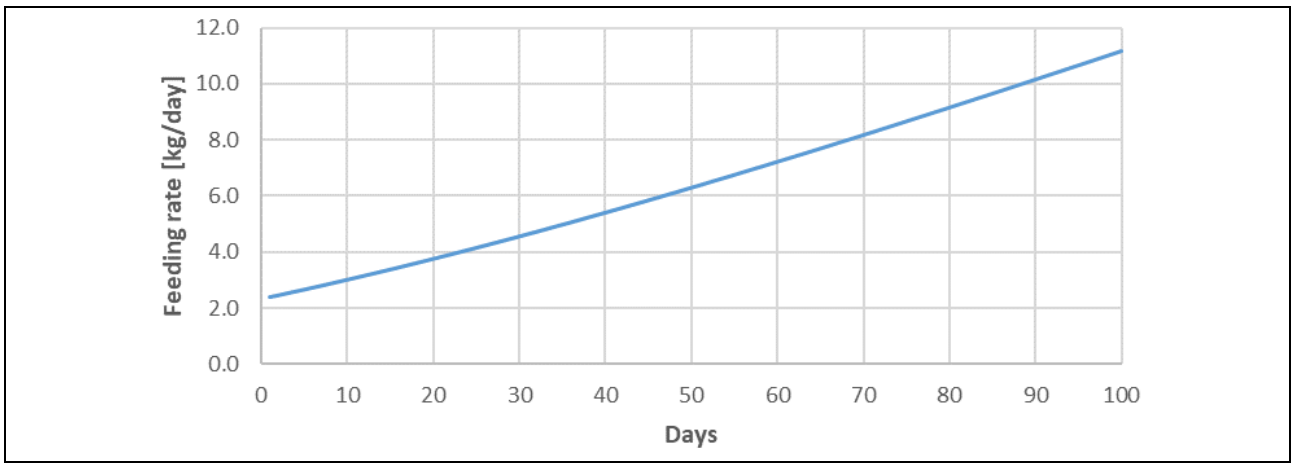

Figure 4-4: Total estimated daily feeding rate over time

From Figure 4-4 it was observed that the peak daily feeding rate is experienced at the end of a production period, as is expected.

4.1.6 Water quality

The target design water quality parameters suitable for both African catfish and tilapia motivated in section 2.1 are given in Table 4-5.

Table 4-5: Chosen design water quality parameters for rearing tilapia and African catfish

Water quality parameter	Limit
Dissolved oxygen [mg/L]	> 4; optimal = 5
Temperature [°C]	27°C ±1 °C
NH_3-N [mg/L]	< 0.06
TAN [mg/L]	< 3.0
NO_2-N [mg/L]	< 1.0
NO_3-N [mg/L]	< 140
pH	7.0 ±0.2
Alkalinity [mg equiv. $CaCO_3$/L]	Will depend on CO_2 production
Hardness [mg equiv. $CaCO_3$/L]	> 100
Dissolved CO_2 [mg/L]	< 15 (rough guideline)
Salinity [ppm]	2000 - 3000
TSS [mg/L]	< 25; optimally < 10
BOD_5 [mg/L]	< 110

4.1.7 Meteorological data

Meteorological data such as air temperatures and humidity were required as inputs for the energy balance calculations. The meteorological station closest to the Welgevallen site was a solar radiation monitoring station at Stellenbosch University (SAURAN, 2019).

4.1.7.1 Dry bulb temperature

Dry bulb temperature data of the ambient air at the site was required for the building air heating design and was contained in the SAURAN data spanning from February 2012 to August 2019. The data from winter months were of interest as the heating requirements are higher at low temperatures. Figure 4-5 shows the probabilities that a dry bulb temperature will not be exceeded (probability of non-exceedance).

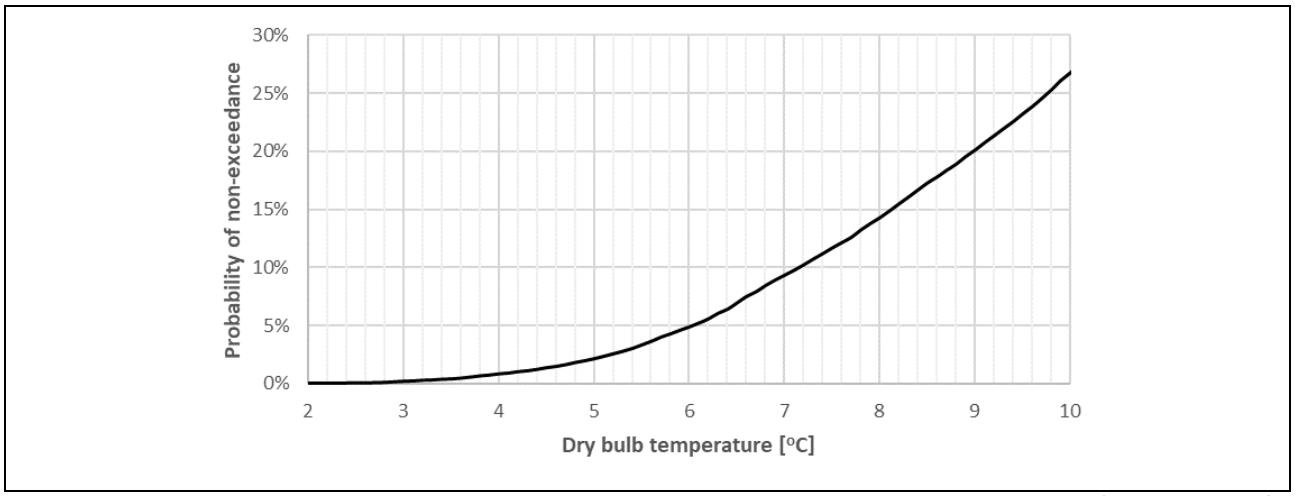

Figure 4-5: Probability of non-exceedance of dry bulb temperatures from SAURAN dataset (SAURAN, 2019) **during winter months (June – August)**

It was decided to design for the 5% probability case and concluded that a suitable design dry bulb temperature for the site is 6°C.

4.1.7.2 Humidity

Humidity of the ambient air was important as it determined the humidity inside the RAS buildings due to regular air changes. The lowest probable humidity was of interest as the heat loss due to water surface evaporation will be high in this case. The SAURAN dataset was used to determine the 5% probability of non-exceedance case for the site (SAURAN, 2019). Due to the large dataset (64420 data points), a count of the relative humidity in 1% increments at each temperature in 1°C was done. These counts were represented as probabilities of non-exceedance. The relative humidity at each temperature with a probability of non-exceedance of 5% is given in Table 4-6.

Table 4-6: Relative humidity and absolute humidity with 5% probability of non-exceedance

Dry bulb temperature [°C]	Relative humidity	Absolute humidity [g/m³]	Dry bulb temperature [°C]	Relative humidity	Absolute humidity [g/m³]
3	79%	4.7	17	45%	6.5
4	78%	5.0	18	43%	6.6
5	76%	5.2	19	41%	6.7
6	73%	5.3	20	38%	6.6
7	73%	5.7	21	36%	6.6
8	70%	5.8	22	35%	6.8
9	69%	6.1	23	32%	6.6
10	67%	6.3	24	28%	6.1
11	61%	6.1	25	26%	6.0
12	60%	6.4	26	25%	6.1
13	56%	6.4	27	24%	6.2
14	52%	6.3	28	23%	6.3
15	50%	6.4	29	21%	6.0
16	48%	6.5	30	20%	6.1

From the above data, the design dry bulb temperature of 6°C has a 5% probability of not exceeding a relative humidity of 73%. This corresponded with an absolute humidity of 5.3 g H_2O/m^3 dry air.

4.1.8 Water and electricity costs

The water and electricity costs in 2018 were obtained from Stellenbosch University accounts and were R 62,96 per m^3 and R 1,3652 per kWh respectively. Inflation of municipal water costs was not considered as no comparative payback calculations were done that included water use. An annual inflation rate of 15% was used to correct for increases in electricity price, reflecting the disproportionate escalation of electricity prices in South Africa during recent years. All operating costs were based on 10 months or 300 days of operation per year, which is typical for the experimental system.

4.2 Initial site layout

It should be noted that no structural alterations can be made to the buildings. The floor space in the sump room is very limited (900 mm x 2600 mm) and thus not suitable to house major WWT equipment. However, the number of active fish tanks in the fish tank room was reduced from 88 to 72 (see section 4.1.2), freeing up space for a WWT system to be installed. The available footprint in the fish tank room is shown in Figure 4-6.

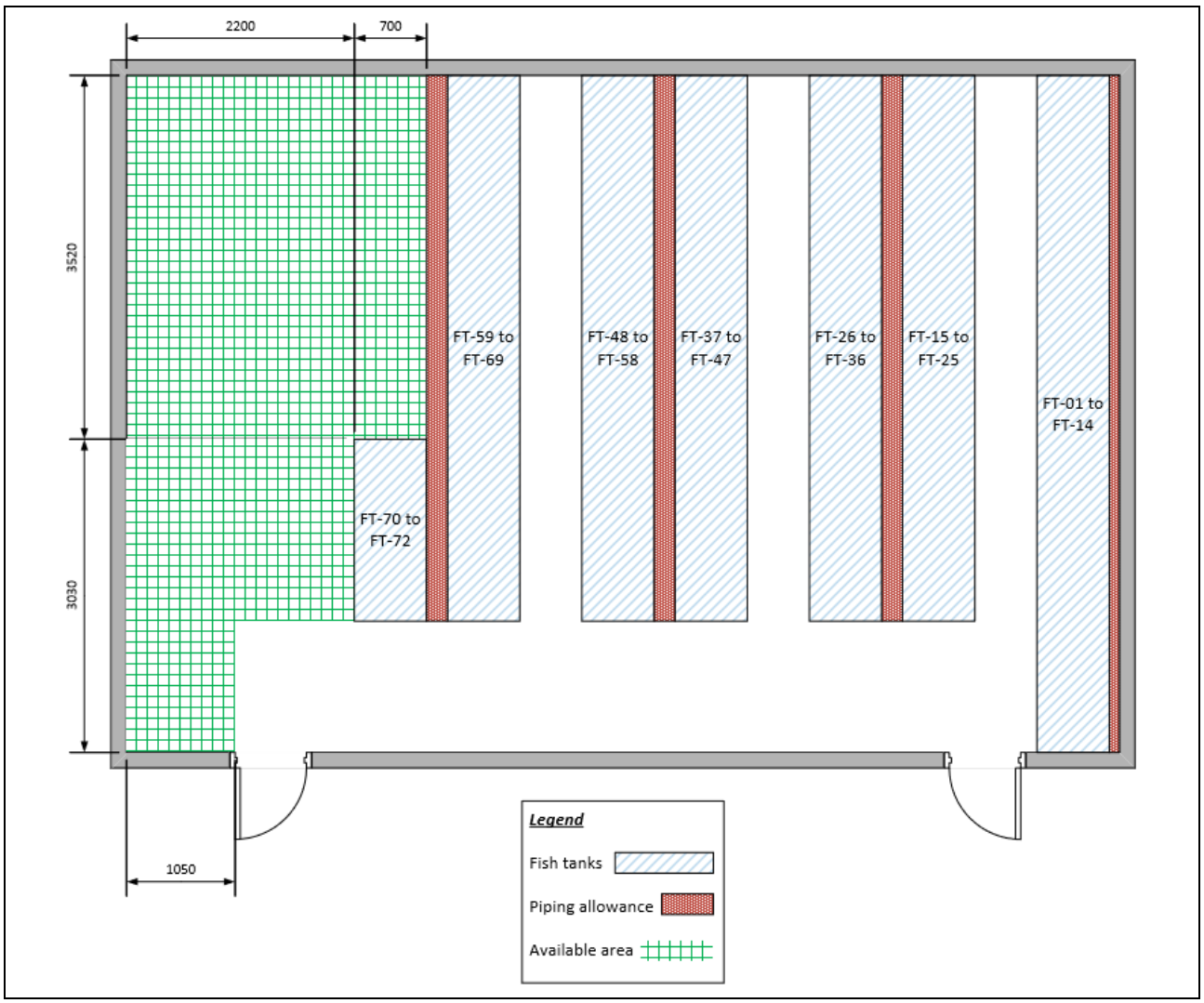

Figure 4-6: Fish tank room layout before addition of WWT equipment (top view)

4.3 Fish tank design

From discussions with system operators and postgraduate students who completed experiments in the existing Welgevallen RAS, it was observed that solids tend to remain at the bottom of the fish tanks. An improved fish tank outlet design was therefore proposed and is shown in Figure 4-7 with the blue arrows indicating the water flow during normal operation.

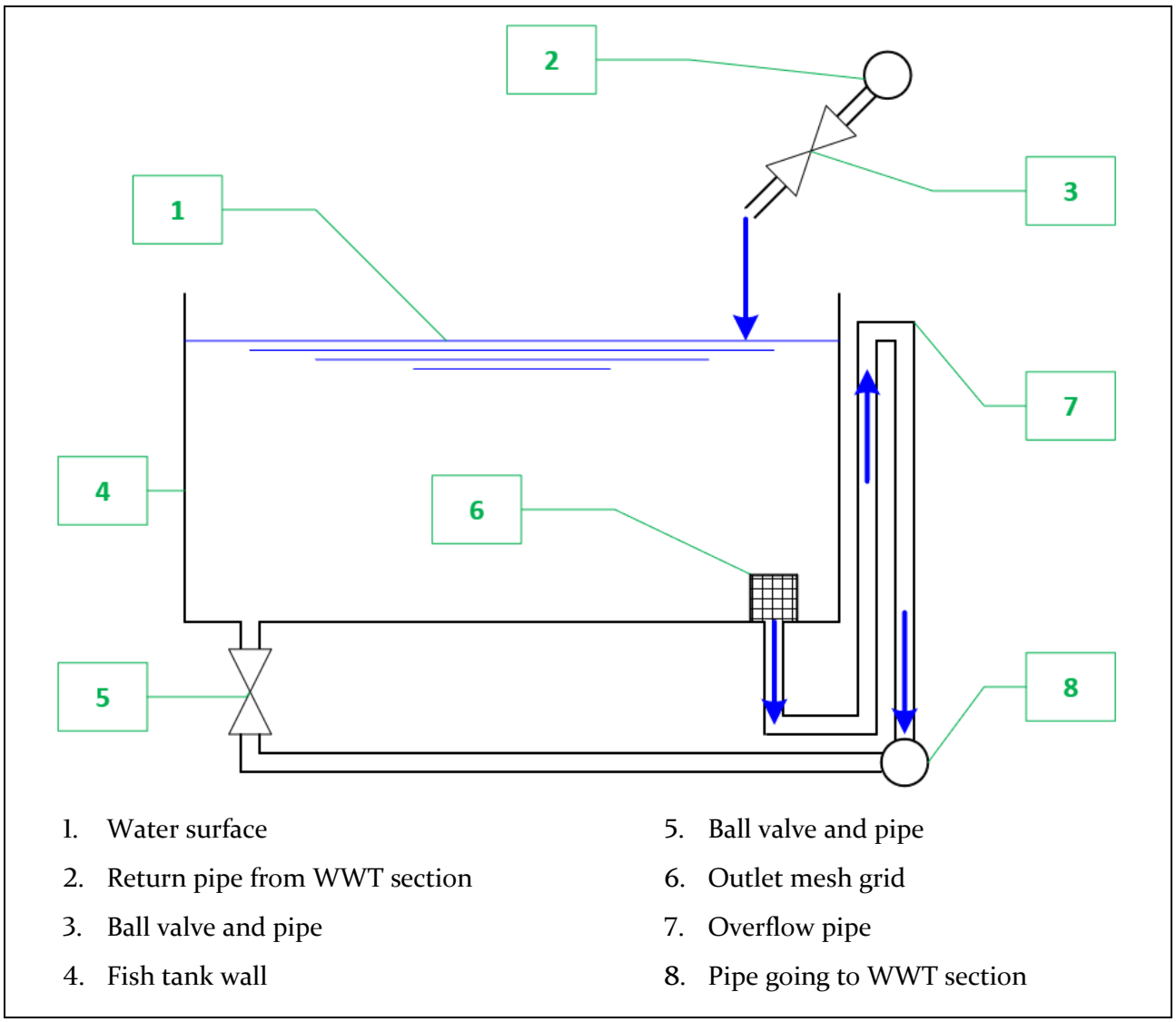

1. Water surface
2. Return pipe from WWT section
3. Ball valve and pipe
4. Fish tank wall
5. Ball valve and pipe
6. Outlet mesh grid
7. Overflow pipe
8. Pipe going to WWT section

Figure 4-7: Fish tank inlet and outlet design cross sectional side view

The fish tank outlet was designed to allow solids to be sucked into the overflow pipe (7 in Figure 4-7) that is connected to the pipe going to the WWT section (8 in Figure 4-7). A mesh grid (6 in Figure 4-7) is attached to the outlet to prevent fish from entering the overflow pipe. A separate pipe and ball valve (5 in Figure 4-7) connected to the bottom of each tank needs to be added to allow for complete drainage of the tank during system cleaning and maintenance. The ball valve can be manually opened to drain the tank.

The return stream from the WWT section enters each fish tank from an overhanging pipe (2 in Figure 4-7) as per existing infrastructure. Flow patterns induced by the fish tank inlet were not deemed important in this design due to the small scale of each tank. A ball valve (3 in Figure 4-7) needs to be installed in each of the inlet pipes to allow for shutdown of any individual fish tank. There is no risk of a surge of inlet water inducing a siphoning effect that will drain all the water from the tanks, because the overflow pipe of the fish tanks is buffered by a subsequent weir overflow at the lamella settler (see section 4.4.3), which cannot experience the siphoning effect. Therefore, the water level in the fish tanks cannot fall below the level of the lamella settler overflow weir.

In-tank aeration is done by submerged air diffusers, also known as airstones. The design for the in-tank aeration is presented in section 4.6.

4.4 Solids removal design

4.4.1 Selection of solids removal technology

Chen et al. (1994) have summarized potential applications and disadvantages of various solids removal configurations and is listed in Table 4-7 along with other configurations deduced from extensive literature review.

Table 4-7: Disadvantages and potential applications of various solids removal configurations (Chen et al., 1994)

Configuration	Disadvantages	Potential applications
Settling tank	High space requirements, poor fines removal	Hardy fish such as carp and tilapia
Tube settler/lamella settler	Poor fines removal, biofouling	Warm-water fish such as catfish at moderate stocking densities
Settler + microscreen filter	Backwashing required	High density fish production
Settler + granular filter	High head loss, backwashing required	High density fish production
Granular filter	High head loss, backwashing required	Fingerling production
Granular filter + cartridge filter	High head loss, backwashing required, cartridge costs	Larvae development
Granular filter + DE filter	High head loss, backwashing required	Larvae development

Sedimentation is a required processing step even if finer solids removal such as a microscreen filter or granular filter is used. This is due to the finer solids removal devices getting clogged and requiring substantial amounts of backwashing if coarse particles are not removed first by sedimentation. An exception is in small systems such as for larvae or fingerling production where fine solids must be removed, and the total solids production is low. Therefore, the approach to selecting the solids removal technology was to design a solids settler and add additional solids removal steps if the settler was not efficient in preventing accumulation of solids in the fish tanks.

For this particular design, a lamella settler was preferred to a tube settler due to (1) ease of cleaning and (2) the possibility of easily increasing the settling area by incorporation of additional plates.

4.4.2 Sizing of a rectangular sedimentation tank

The desired TSS removal efficiency was chosen as 80%, which can theoretically be achieved by operating a sedimentation stage at an overflow rate of 0.06 cm/s according to Figure 3-7 (see section 3.5.2.2). The required settling area was calculated to be 5.5 m^2 at a recirculating flow rate of 12 m^3/h as determined in section 4.7. At a length to width ratio of 1:1, the settling zone of the rectangular sedimentation tank will have to be 2.3 meters in length and width, which excludes the inlet and outlet

zones. A minimum depth of 1 meter is recommended (Liao and Mayo, 1974). However, a length to width ratio of 1:1 is not ideal as the recommended rectangular sedimentation tank length to width ratios range from 4:1 to 8:1 (Arceivala, 1983). The minimum length and width of 2.3 meters fills most of the available area shown in Figure 4-6, and therefore a lamella settler was chosen, which is a lower footprint solution.

4.4.3 Sizing of a lamella settler

The desired TSS removal efficiency was chosen as 80%, which can theoretically be achieved by operating a sedimentation at an overflow rate of 0.06 cm/s according to Figure 3-7 (see section 3.5.2.2). The required settling area was calculated to be 5.5 m^2 at a recirculating flow rate of 12 m^3/h as determined in section 4.5.4.3. The dimensioning of the lamella settler was an iterative process due to the following conditions and design recommendations that had to be met:

Condition 1. The horizontally projected settling area must be at least 5.5 m^2.

Condition 2. Ideally, the unit should be assembled off-site and be ready for installation, and therefore the unit must fit through the access door with dimensions 845 mm x 2000 mm.

Condition 3. The overflow level must be lower than the fish tank water level, which is 1.2 m.

Condition 4. The horizontal spacing between plates inside the settler must be between 50 mm and 80 mm to allow for cleaning access (Brandt et al., 2016).

Condition 5. The inclination of the plates is 55 – 60° to the horizontal plane (Brandt et al., 2016).

Condition 6. The Reynolds number inside the settler must not exceed 800 (Faraji et al., 2013).

Condition 7. The sludge zone (see Figure 2-4) must be designed for optimal accumulation of solids at the drainage point.

The lamella settler designed to meet all of the conditions above is shown in Figure 4-8. The dimensions of the lamella settler are given in APPENDIX G. The horizontally projected settling area was calculated to be 5.5 m^2. The bulk settler dimensions were 1190 mm high, 820 mm wide and 2000 mm long. Horizontal spacing between the plates were 61 mm, which is within the recommended range of 50 mm and 80 mm. The inclination of the plates is 55°, which is the minimum recommended value and yielded the most horizontally projected settling area per plate. The Reynolds number in the settler was kept as low as possible to avoid entrainment of settled particles and was calculated to be 244, which is considerably lower than the maximum of 800.

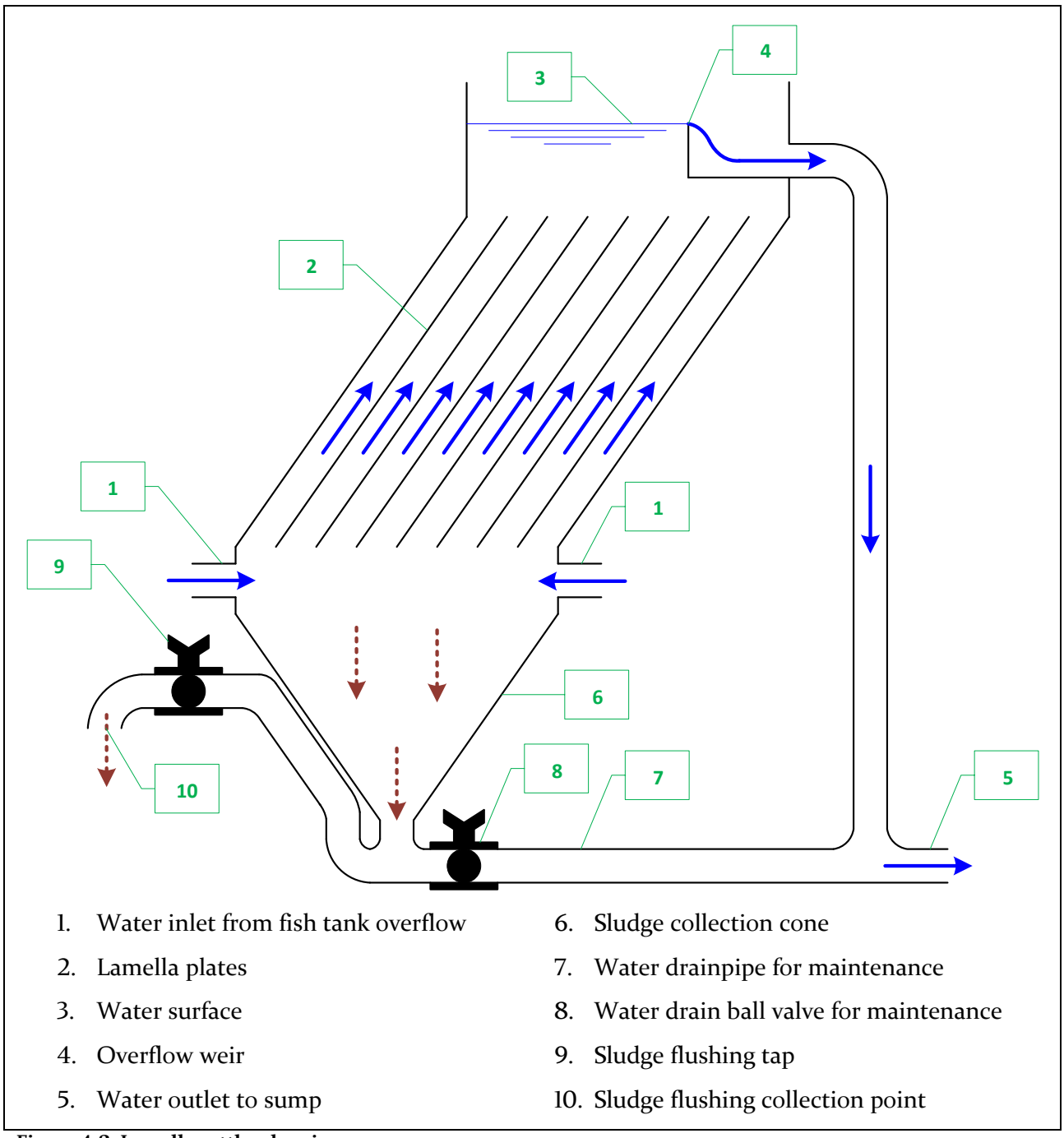

1. Water inlet from fish tank overflow
2. Lamella plates
3. Water surface
4. Overflow weir
5. Water outlet to sump
6. Sludge collection cone
7. Water drainpipe for maintenance
8. Water drain ball valve for maintenance
9. Sludge flushing tap
10. Sludge flushing collection point

Figure 4-8: Lamella settler drawing

The flow hydraulics between the fish tanks and the settler was assessed to ensure that water level remains at the overflow level. If the head loss through the connecting piping is more than the difference in overflow levels, the water will accumulate in the fish tanks until the head loss is equal to the height difference between the water levels. The fish tank furthest from the settler was assessed as it will have the flow with the most head loss. After adjusting the pipe sizes, it was estimated that the minimum elevation difference between the fish tank overflows and the settler overflow should be 32 mm. A decrease in specified pipe sizes will result in a rise in water levels in the fish tanks and possibly complete overflow. Therefore, it is critical to construct the system as specified.

The sludge zone was designed to have steep walls to allow for solids to accumulation at the flushing ports. Flushing of settled solids must be done regularly by connecting a portable hose to the flushing ports (10 in Figure 4-8). The regularity of flushing must be determined through experience of working with the RAS. Water loss due to drainage of the settled solids could not be estimated due to insufficient knowledge of the settled particle density. However, the water loss is expected to be negligible compared to overall system volume.

The smallest particle size estimated to be removed in the lamella settler at a settling rate of 0.06 cm/s was calculated to be 70 µm. This was calculated by solving for the particle diameter in Stoke's Law (equation (3.21)) and assuming an average particle density of 1190 kg/m^3 (Chen et al., 1993). A TSS removal efficiency of 80% has been observed in a study using a tube settler system with particles larger than 70 µm being removed (Easter, 1992). This is identical to the estimations made in the current design and adds credibility to the estimations made for the lamella settler efficiency.

4.4.4 Sensitivity analysis

A sensitivity analysis (summarized in Figure 4-9 and Figure 4-10) was done to determine the effect of TSS removal efficiency and the TSS production ratio on the TSS concentration in the tanks given a constant recirculation flow rate of 12 m^3/h. The optimal TSS limit of 10 mg/L and maximum TSS limit of 25 mg/L is included in the figures.

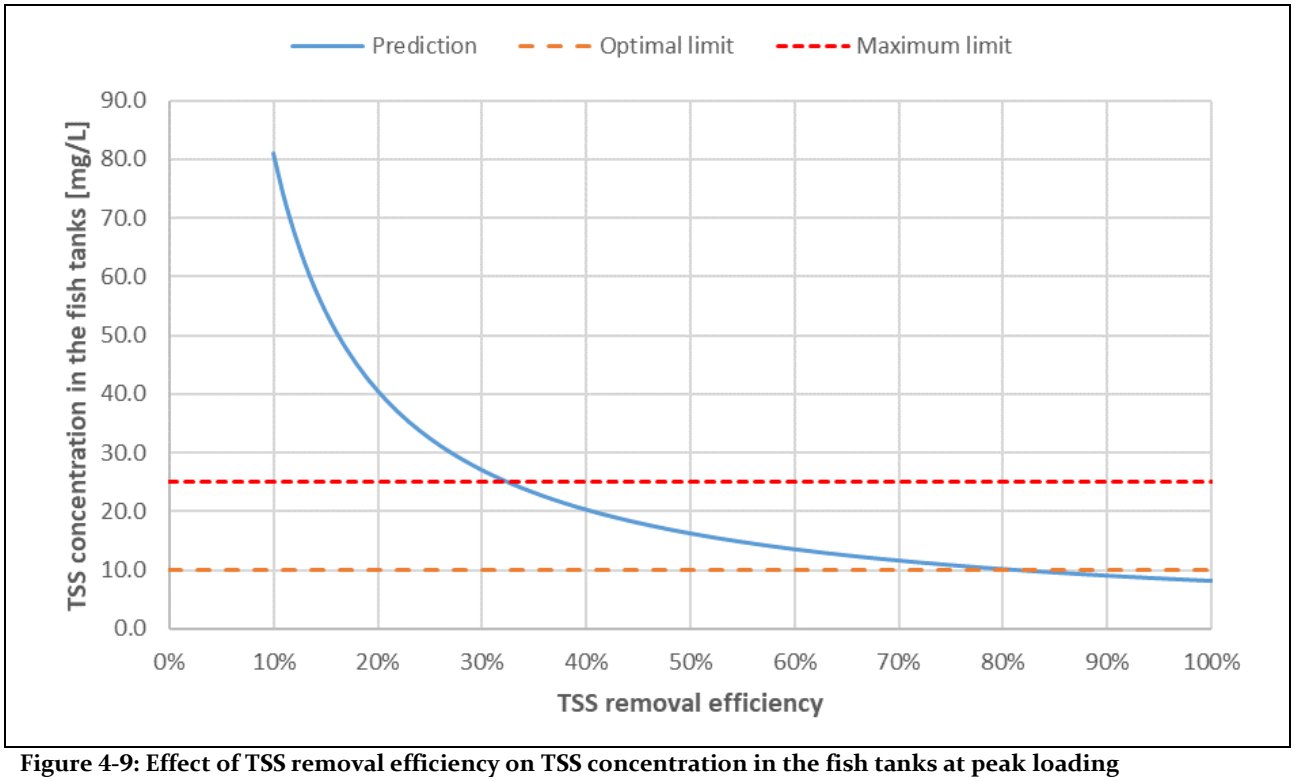

Figure 4-9: Effect of TSS removal efficiency on TSS concentration in the fish tanks at peak loading

Figure 4-9 illustrates that the TSS concentration in the fish tanks increases exponentially with a decrease in TSS removal efficiency. However, the maximum TSS limit is only exceeded at TSS removal

efficiencies below 33%. Such a low removal efficiency is unlikely to be observed as the solids settling model predicts a removal efficiency of 80% and was verified using literature data (see section 3.5.2).

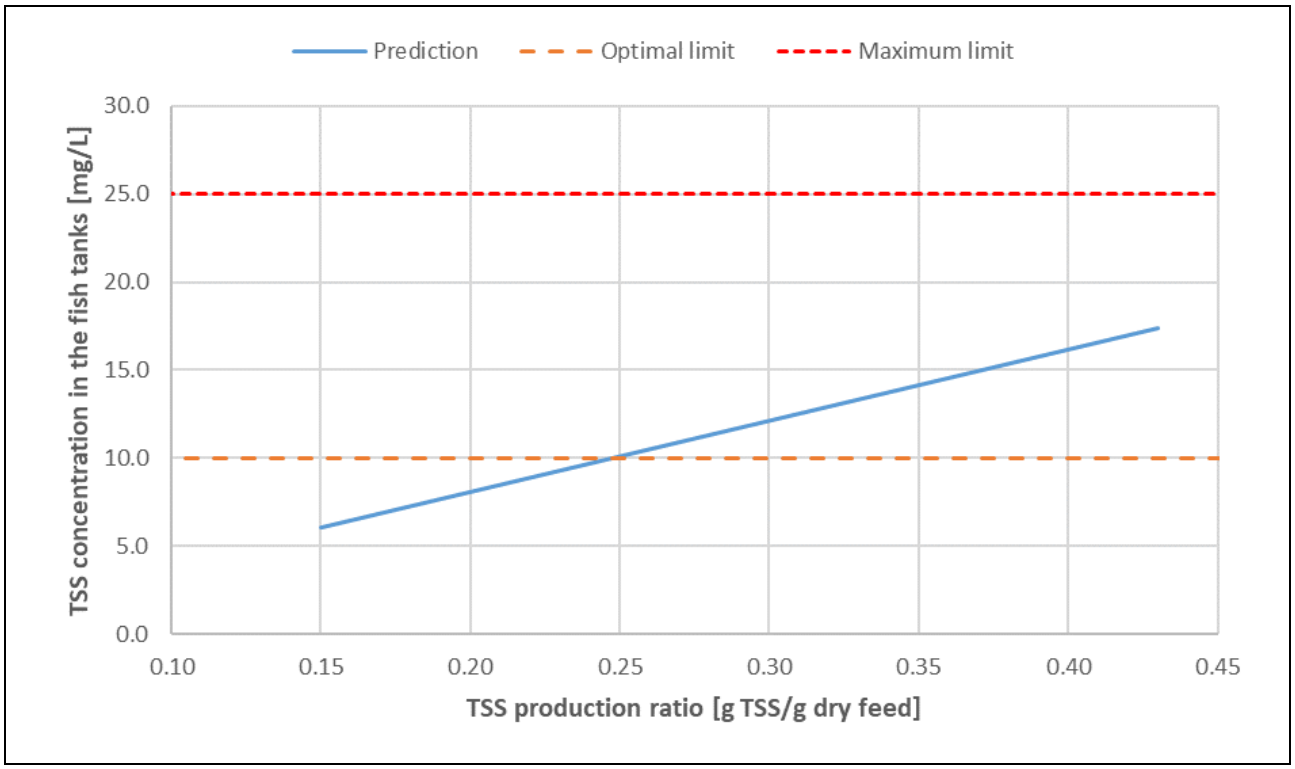

Figure 4-10: Effect of TSS production ratio on TSS concentration in the fish tanks at peak loading

Figure 4-10 illustrates that the TSS concentration increases linearly with an increase in the TSS production ratio. The maximum TSS limit is not exceeded at any TSS production ratio reported in literature.

The sensitivity analysis above shows that the proposed lamella settler geometry is highly likely to provide sufficient TSS removal for the RAS.

4.4.5 Costing of a lamella settler

The lamella settler can be costed by (1) equipment purchase quote from a supplier, (2) scaling factors based on previous projects or (3) estimate based on construction cost from basic materials and labor estimates. Option 3 was used as method for cost estimation due to the specific geometry required for the design. The lamella settler shell is to be constructed by welding pieces of 304 stainless steel (304SS) together. 304SS was chosen as material of construction due to its corrosion resistance when constantly exposed to water. The plates inside the lamella settler is proposed to be 304SS cut sheets welded into the settling zone of the settler shell. As the plates are not loading bearing, they do not need to be 304SS sheets and thus cheaper alternatives can be considered during construction. From the dimensions, it was determined that four 304SS sheets with dimensions 3000mm x 1500mm x 2.0mm each will be needed to construct the lamella settler shell and plates (see APPENDIX G). The cost of these sheets is R 3 674,25 each (as quoted by Stalcor, a local supplier) with delivery price included. As

four sheets are required, the minimum cost of the lamella settler will be R 14 697, under the assumption that the construction can be done internally at Stellenbosch University at no extra cost.

4.4.6 Financial feasibility of fine solids removal

Fine solids filtration by microscreen filters or sand filters was considered as an additional solids removal step after the sedimentation process. Microscreen filters were found to be unfeasible due to the high backwashing required, which means high amounts of water is lost during a backwashing step. At a typical backwash flow rate of 0.2% - 2.0% of the recirculating flow (Lekang, 2007), purchase of the backwash water would cost from R 10 900 to R 109 000 per year, showing that operation of a microscreen filter is costly. This estimate was made assuming 300 days per year operation, 12 m^3/h recirculating flow and a cost of R 62,96 per m^3 municipal water.

A sand filter was considered as an additional solids removal step by assessing the financial feasibility through a cost-benefit analysis. Introduction of a sand filter will increase TSS removal efficiency and therefore also decrease the required aeration to the downstream MBBR, but it will require additional pumping power to overcome head loss in the sand filter. Important variables for each process option are listed in Table 4-8.

Table 4-8: Comparison of designs including and excluding a sand filter

Variable	Sand filter + lamella settler	Lamella settler
TSS removal efficiency	95%	80%
MBBR aeration rate [m^3/h]	16	18
Blower power [kW]	0.43	0.48
Total dynamic head [m]	12.9	4.7
Selected recirculation pump	BADU Porpoise 22	BADU Porpoise 10
Pump power [kW]	1.10	0.45
Organic loading [g O_2/(m^2.day)]	2.4	2.5
Nitrification rate [g TAN/(m^2.day)]	0.74	0.63
Biomedia volume [m^3]	2.14	2.52
Biomedia cost [ZAR]	16 992	20 017
Number of 1000L biofilters	4	4
Biofilter tank cost [ZAR]	9 200	9 200
Biofilter total cost [ZAR]	26 192	29 217

The higher TSS removal efficiency of the sand filter decreased the overall organic matter in the system, making the biofilters more efficient. This is evidenced by the lower organic loading, higher nitrification

rate and lower biomedia volume required to treat the wastewater. The addition of the sand filter decreased the overall capital cost of the biofilters by approximately R 3 000. The cost of purchasing a sand filter operating at flow rates of 12 m^3/h from online suppliers is R 2699 (Takealot, 2019). The addition of a sand filter after the lamella settler seemed feasible from purely a capital cost point of view.

Blower power operating requirements are decreased by 0.05 kW by the addition of a sand filter due to less organic matter having to be oxidized by heterotrophic bacteria in the biofilter. However, the pressure drop over the sand filter is estimated to be approximately 80 kPa and thus require specifying a larger pump. The pump power will be 0.65 kW higher with the addition of a sand filter. The net power supply required increases by 0.60 kW when adding a sand filter, resulting in an additional annual operating cost of approximately R 5 900. The savings in capital costs by installing a sand filter were therefore far outweighed by the significant increases in operating expenditure, and it was concluded that a sand filter is not a financially feasible addition to the RAS. It should be noted that backwash water costs associated with periodic backwashing of the sand filter were not included in the cost benefit analysis due to insufficient information on backwashing frequency, but it is clear from the analysis that the large increase in electricity costs were enough to deem the sand filter unfeasible.

4.4.7 Conclusion

For the solids removal step in the designed RAS, it was concluded that a lamella settler was the preferred piece of equipment. A lamella settler was designed to remove coarse suspended particles and sized by considering various design conditions and performing a sensitivity analysis on the performance capacity by varying the TSS removal efficiency and the TSS production ratio. Additional fine solids removal was eliminated by a cost benefit analysis.

4.5 Biological filtration design

4.5.1 Evaluation of the existing trickling filters

A previous feeding trial using the existing RAS observed toxic levels of ammonia and nitrite, resulting in increased water replacement where system water volume was replaced every two weeks (Gericke, 2019). This scenario is undesirable due to the scarcity of freshwater with sufficient water quality in the area and the high cost of municipal water. The poor performance of the trickling filters in the study by Gericke (2019) can possibly be attributed to the lack of solids removal resulting in high BOD_5 and thus inhibition of effective nitrification. Another likely cause is the need for trickling filters to be ventilated properly, ensuring that anaerobic conditions are not present (Eding et al., 2006). The existing trickling filters are housed in an enclosed chamber and are operated under conditions of zero forced ventilation, making lack of ventilation a likely cause for the poor nitrification performance. Therefore, in order to consider the reuse of the existing trickling filters, forced ventilation will need to be installed.

For the assessment of the existing trickling filters, the trickling filters were assumed to be TAN diffusion limited and modeled as described in section 3.4.4. When modeling the RAS, the peak daily TAN production was estimated to be 477 g TAN/day. Nitrification rates are determined by the hydraulic surface loading rate (HSL) within the model. The minimum required HSL to treat the TAN produced was estimated to be 381 $m^3/m^2 \cdot day$. Given that the total combined cross-sectional area of the trickling filters is 2.21 m^2, a recirculation flow rate of 35 m^3/h is required to achieve the required HSL. The estimated nitrification rates, bulk fluid TAN concentrations and zero-order transition TAN concentrations (TAN*) within each of the modeled layers of the trickling filters are shown in Figure 4-11. The modeled zero-order transition TAN concentrations were higher than the bulk water TAN concentrations as seen in Figure 4-11, thereby indicating that the trickling filters would be TAN diffusion limited throughout. The predicted nitrification rates were adjusted for the effects of temperature (see section 3.4.8).

The model by Nijhof (1995) used to model the trickling filters did not consider the effect of BOD_5 on the nitrification rate. It is highly probable that lower nitrification rates would be observed in the existing RAS than the estimated rates (Figure 4-11) due to oxygen diffusion limitation by organic loading not being taken into account by the trickling filter model. This is supported by comparing the TAN diffusion limited nitrification rates estimated for the trickling filters (Figure 4-11) with the oxygen diffusion limited nitrification rates used in the MBBR modeling (see section 3.4.6.2). Applying the MBBR nitrification rates directly to the trickling filter modeling could be inaccurate since the hydraulic and aeration operation of the two filters types are vastly different. However, the possibility of lower nitrification rates than those in Figure 4-11 remains a concern that requires more research.

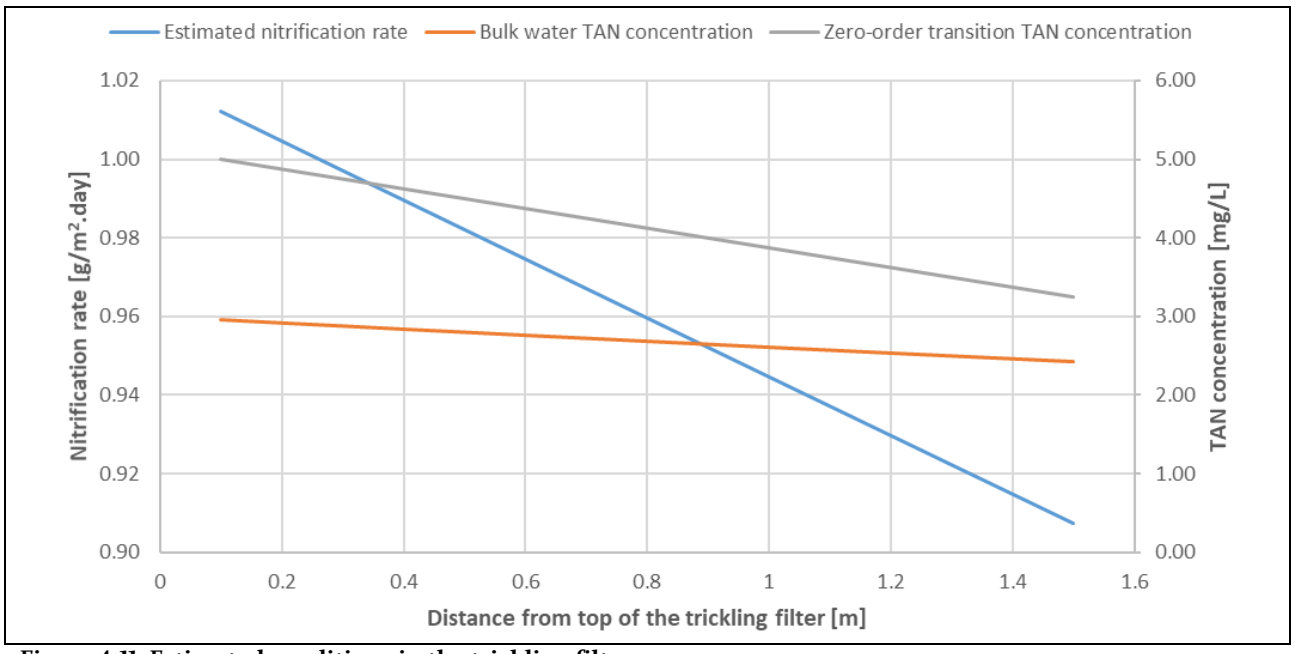

Figure 4-11: Estimated conditions in the trickling filters

4.5.2 Selection of biofilter technology

Even though the modeling indicated that the trickling filters could theoretically remove the TAN produced in the proposed RAS, the financial feasibility of the existing trickling filters compared to alternative biofilters had to be assessed. The rotating biological contactor (RBC), fluidized sand biofilter (FSB), floating bead bioclarifiers (FBB) and moving bed bioreactor (MBBR) were considered as possible replacements for the existing trickling filters.

RBC: The possibility for mechanical failures in the rotating shaft make RBCs an undesirable choice and was not further considered.

FSB: One of the disadvantages of FSBs is that they experience reduced nitrification rates after 6 – 24 hours of zero flow, due to anaerobic conditions developing in the filter. This will constantly happen in an experimental facility when the recirculation in the RAS is shut down between experiments. Maintaining the flow rate through an FSB within the acceptable range (maintaining fluidization) makes FSBs more difficult to operate than other biofilters.

FBB: FBBs have a high head loss, which increases pumping costs. The specific surface area of these filters is low and thus will likely require a large biofilter volume. Period backwashing is required.

MBBR: The MBBR biofilter technology was selected as the most appropriate replacement biofilter. Reasons for the choice were that (1) mechanical failure of MBBRs is minimal, (2) upkeep of the MBBR during RAS downtime is possible with aeration and ammonia dosing, (3) efficiency of an MBBR is not sensitive to recirculation flow rates, (4) MBBRs have low head loss, (5) MBBR media with high specific surface area is available, (6) backwashing is not required and (7) MBBRs do not clog. These points all address the negative aspects of the other biofilters considered, and it was therefore selected as the technology of choice.

4.5.3 Selection of equipment and costing

The MBBRs are to be placed in the fish tank room as there is not enough space in the sump room. The MBBR tanks will have to fit through the access door (dimensions 845 mm x 2000 mm) in order to be installed in the fish tank room. Slim water storage tanks of 1000L each have been identified as the largest water tanks able to fit through the access door and this tank was thus chosen as the water tank of choice for the MBBRs. Concrete tanks built on site were not considered due to the wall strength required to build high enough concrete MBBRs to cater to the requirement of gravity flow from the MBBRs back to the fish tanks. Many different water storage tanks are available on the market and the 1000L tank offered by Nel Tanks (2019) was selected for the design due to it being the lowest price. Heat loss between the tank types were not compared due to the similarities in the construction. No other factors needed to be considered for the selection of the tank.

Many different types of biomedia for MBBRs are available commercially (Ecotao Enterprises, 2018a; Pfeiffer and Wills, 2011). Performance amongst the different types of biomedia can vary due to specific biofilm surface area and hydraulic differences that can impact diffusion. It was therefore decided that biomedia similar to that used to derive the MBBR models (Hem et al., 1994; Rusten et al., 2006) should be used in the design to prevent possible inaccuracies in the prediction of the models. The chosen biomedia is shown in Figure 4-12. Although the biomedia supplier reported specific biofilm areas exceeding 700 m^2/m^3, the effective biofilm area of the biomedia was calculated to be 300 m^2/m^3 by carefully measuring the geometry of an individual carrier and measuring the packing density by filling a known volume with a counted number of carriers. The cost of the biomedia is R 7 935 per cubic meter (Ecotao Enterprises, 2017, 2018a).

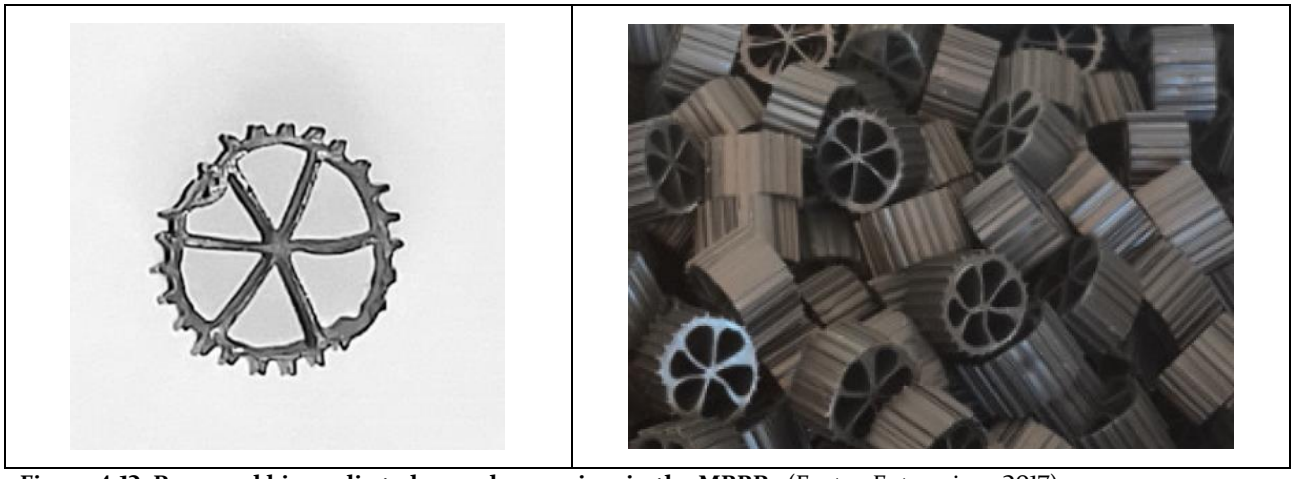

Figure 4-12: Proposed biomedia to be used as carriers in the MBBRs (Ecotao Enterprises, 2017)

4.5.4 Sizing of the MBBR

4.5.4.1 Optimization of the oxygen concentration

The oxygen concentration inside the MBBR is a critical variable in the oxygen diffusion limiting model (see section 3.4.6.2). Higher oxygen concentrations will result in more efficient MBBRs and thus lower capital cost but will require higher blower power to achieve the desired oxygen concentration in the

MBBR. The aeration rate of both the MBBRs and fish tanks was considered, as an increase in oxygen concentration in the MBBRs decreased the required air flow to the fish tanks slightly. Blower power was estimated as described in section 3.6.1.

A discounted cash flow analysis was done to determine the financially optimal oxygen concentration over various years of operation. The analysis considered the capital cost of the biofilter tanks and biomedia, and the electricity cost of the aeration blower to maintain the MBBR oxygen concentration as well as the optimal oxygen concentration in the fish tanks. The discounted cash flow arising from these costs was used to calculate the annual net present value (NPV) over 10 years for various MBBR oxygen concentrations ranging from 2.0 mg/L to 8.0 mg/L. The optimal oxygen concentration after a certain period of operation is represented by the NPV that is least negative as no revenue stream is included in the discounted cash flow. Figure 4-13 illustrates the optimal oxygen concentration as a function of the investment period as determined by the discounted cash flow analysis. The optimal oxygen concentration did not change when varying the discount rate between 5% and 15% and it was thus assumed that a discount rate of 10% was reasonable. The detailed results are reported in APPENDIX H.

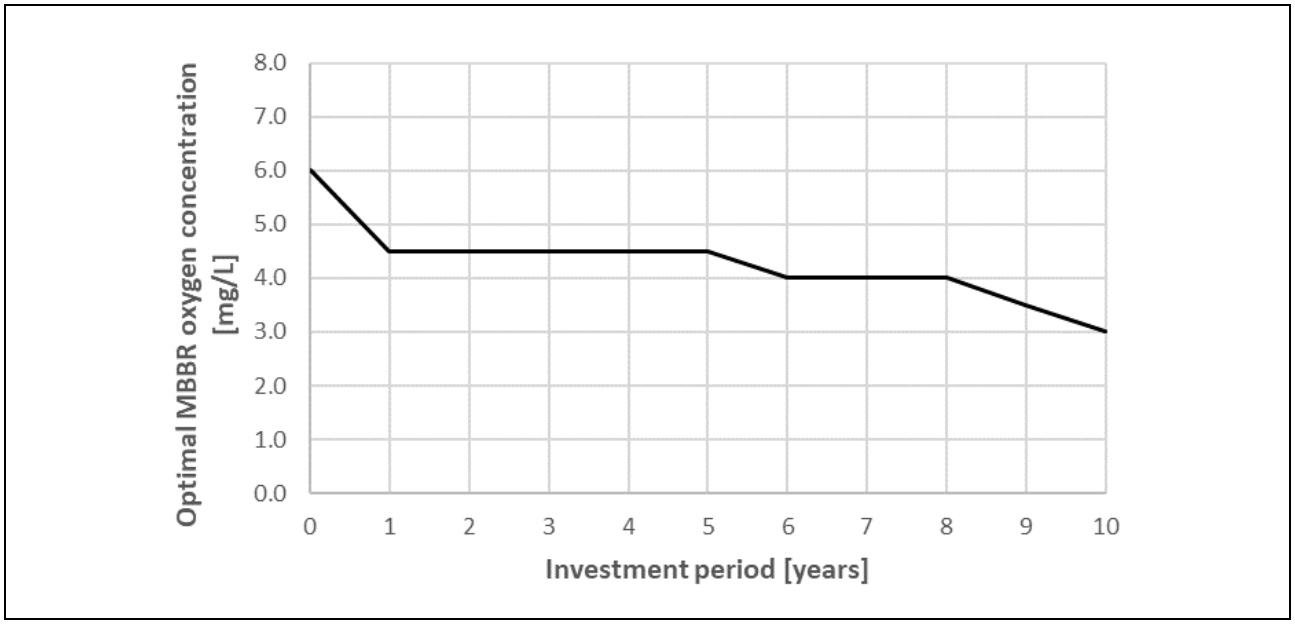

Figure 4-13: Optimal MBBR oxygen concentrations as a function of investment period. Discount rate = 10%

The optimal oxygen concentration decreases from 6 mg/L to 4.5 mg/L within the first year and remains constant for 5 years. Only after 5 years does the optimal oxygen concentration decrease to 4 mg/L and to 3 mg/L after an investment period of 10 years. The gradual decrease in optimal oxygen concentration over time is difficult to explain explicitly but could be due to the relative decrease in blower power required at low DO concentrations having more of a financial impact over time than the relative increase in capital cost of the biofilters. The financial optimal oxygen concentration in the MBBR remains 4.5 mg/L for 5 years after the initial investment, indicating that it is the most economical option during the first 5 years of operation. The footprint of the MBBRs required when operating at

4.5 mg O_2/L was found to fit into the footprint available for the WWT section. Thus, it was decided to operate the MBBRs at 4.5 mg/L.

4.5.4.2 Initial sizing

Initial MBBR sizing was based on an estimated peak daily TAN production of 477 g TAN/day that is estimated to be produced on the 91st day of a growth trial at maximum fish stocking density. The peak daily production of DOM and POM was estimated as 2333 g/day and 1930 g/day respectively. The POM production was assumed to be equal to the TSS production and thus the effective daily POM production is reduced by the solids removal steps. Given the TSS removal efficiency of 80%, the POM production contributing to BOD_5 is only 467 g/day at peak loading. Peak daily BOD_5 production reaching the biofilters was estimated to be 1930 g O_2/day, where 1407 g O_2/day can be attributed to DOM and 523 g O_2/day can be attributed to POM. The percentage filling of the MBBRs with biomedia was assumed to be 65%.

The models used to model the MBBR (see section 3.4.6) depend on TAN concentration in the MBBR (TAN diffusion limiting) or oxygen concentration and organic loading (oxygen diffusion limiting). The model with the lowest nitrification rate prediction was assumed to be the observed nitrification rate. Decreasing the biofilm area in the MBBR increased the organic loading per biofilm surface area and thus decreased the nitrification capacity of the MBBR. The MBBR was sized by running a Solver routine on the model using Microsoft Excel to minimize the biofilm area whilst maintaining the required nitrification capacity. The results of this initial sizing are given in Table 4-9.

Table 4-9: Initial sizing results for the MBBR design

Variable	Value
Organic loading [g O_2/(m^2.day)]	2.4
Nitrification rate [g TAN/(m^2.day)]	0.63
MBBR TAN outlet concentration [mg/L]	0.26
MBBR TAN removal efficiency	91.5%
Biomedia volume [m^3]	2.52
Number of 1000L biofilters	4
Combined total residence time of biofilters [min]	32
Required recirculation flow rate [m^3/h]	7.3

4.5.4.3 Sensitivity analysis

The sizing described above did not consider the possible variations in the input variables. The effects on the design when changing the input variables within their ranges observed in literature was investigated in the sensitivity analysis below in Table 4-10.

The sensitivity analysis showed that the MBBRs need to be oversized for the maximum possible TSS production ratio case. This is explained by the profound effect of TSS on the organic loading inside the MBBR. A TSS production ratio of 0.43 g TSS/g dry feed will result in an estimated nitrification rate

of 0.41 g/(m^2.day) and biomedia volume of 3.88 m^3. The maximum possible TAN production ratio in the sensitivity analysis determined the required recirculating flow rate to prevent accumulation of TAN in the fish tanks and thus the minimum required recirculation flow rate of the RAS was estimated to be 12 m^3/h.

Table 4-10: Biofilter sensitivity analysis

Variable	Minimum value	Design Value	Maximum value	Required recirculation flow rate [m^3/h]	Nitrification rate [g TAN/m^2.day]	Biomedia volume [m^3]
FCR	1.0	1.5	2.0	4.8 - 9.7	0.63 - 0.63	1.68 - 3.36
TGC	0.00042	0.00121	0.00199	4.1 - 8.7	0.63 - 0.63	1.41 - 3.02
Water temperature [°C]	22	27	32	6.9 - 7.5	0.56 - 0.68	2.59 - 2.50
TAN production ratio [g TAN/g feed consumed]	0.030	0.047	0.070	4.5 - 11.3	0.43 - 0.83	2.34 - 2.86
Stocking density [kg/m^3]	25	50	75	3.6 - 10.9	0.63 - 0.63	1.26 - 3.78
Biofilter media specific surface area [m^2/m^3]	240	300	360	7.2 - 7.2	0.63 - 0.63	3.15 - 2.10
Nitrification temperature correction (θ)	1.02	1.08	1.09	7.2 - 7.2	0.51 - 0.65	3.14 - 2.46
TSS removal efficiency	60%	80%	90%	6.9 - 7.4	0.52 - 0.70	3.08 - 2.27
TSS production ratio [g TSS/g dry feed fed]	0.15	0.25	0.43	7.7 - 6.9	0.91 - 0.41	1.75 - 3.88
Initial individual fish mass [g]	5	10	15	7.9 - 6.8	0.63 - 0.63	2.76 - 2.38

4.5.5 Feasibility of trickling filters vs MBBRs

The operating expenses of the existing trickling filters in the existing RAS configuration (dual pump operation) were compared to that of the newly designed MBBRs (single pump operation + biofilter aeration). The trickling filter RAS (Figure 4-3) pumps the water twice within the recirculation loop. This is due to the sump of the trickling filters being at a lower level than the fish tanks, preventing water from returning to the fish tanks by gravity. Due to the available space in existing facilities, positioning of the trickling filter sump level above fish tank water level would not be possible.

Therefore, two pumps will be needed to continue operating the trickling filters. The pump selection and operating costs for the trickling filter RAS and MBBR RAS is summarized in Table 4-11.

Table 4-11: Pump selection and operating costs for trickling filter RAS and MBBR RAS

Variable	Trickling filters	MBBRs
Recirculating flow rate [m^3/h]	35	12
Total dynamic head [m]	4.3	3.3
Selected recirculation pump model	BADU Galaxy 23 (1.50kW)	BADU Porpoise 10 (0.45kW)
Number of pumps	2	1
Total pump power [kW]	3.00	0.45
Pumping energy [kWh/year]	21 600	3 240
Pumping operating cost [ZAR/year]	29 500	4 400
Blower operating cost [ZAR/year]	0	13 400
Total operating cost [ZAR/year]	29 500	17 800

From the results in Table 4-11 it was determined that investing in MBBRs will result in annual savings of approximately R 11 700. Based on these values, the payback period of the R 45 500 MBBR investment was calculated to be 3.9 years, which is considered a feasible investment. Additionally, the performance evaluation of the trickling filters was not based on any sensitivity analysis, which means that it is not as conservative an estimate as the MBBR design and will most probably be undersized for the designed system. Further potential knock-on effects of utilizing the existing trickling filters lies with the lamella settler: since the trickling filter configuration requires a much higher recirculating flow rate, the settling area of the lamella settler will also need to increase to achieve the desired 80% TSS removal efficiency.

4.5.6 Final biofilter design and cost

The final MBBR design is based on the results of the modeling and sensitivity analysis considerations. The MBBR design results are described by the specifications in Table 4-12. Assuming that the biomedia are only available in discrete batch sizes of 1 m^3 each at a cost of R 7 935/m^3 and that 3.88 m^3 is required for 65% filling of the MBBRs, the required biomedia will cost R 31 740 with 100L of biomedia unused. Six MBBR tanks of 1 m^3 each are required to contain 3.88 m^3 of biomedia with a 65% filling. The total capital cost of the MBBR tanks and biomedia will be R 45 500.

Table 4-12: Final sizing results for the MBBR design

Variable	Value
Biomedia volume [m^3]	3.88
Filling fraction [m^3 biomedia/m^3 biofilter]	65%
Number of 1000L biofilters	6
Overall biofilter volume [m^3]	6.00
Overall effective biofilm area [m^2]	1164
Required recirculation flow rate [m^3/h]	12.0

The 1000L MBBRs will be connected in series to allow recirculating water to contact all the biofilm area for maximum TAN removal. According to Suhr and Pedersen (2010), it is advantageous to connect multiple biofilters in series rather than a single large biofilter due to dominance of heterotrophic bacteria in the first biofilter. This results in increased nitrifier populations in the later biofilters, potentially increasing nitrification rates. Also, according to standard reactor engineering theory, CSTRs in series start to approximate plug flow reactor behavior (Fogler, 2014).

The MBBR piping, internals and flow pattern is illustrated in Figure 4-14. Each MBBR vessel has a diameter of 0.75 m, is 2.23 m high and has a volume of 1000L.

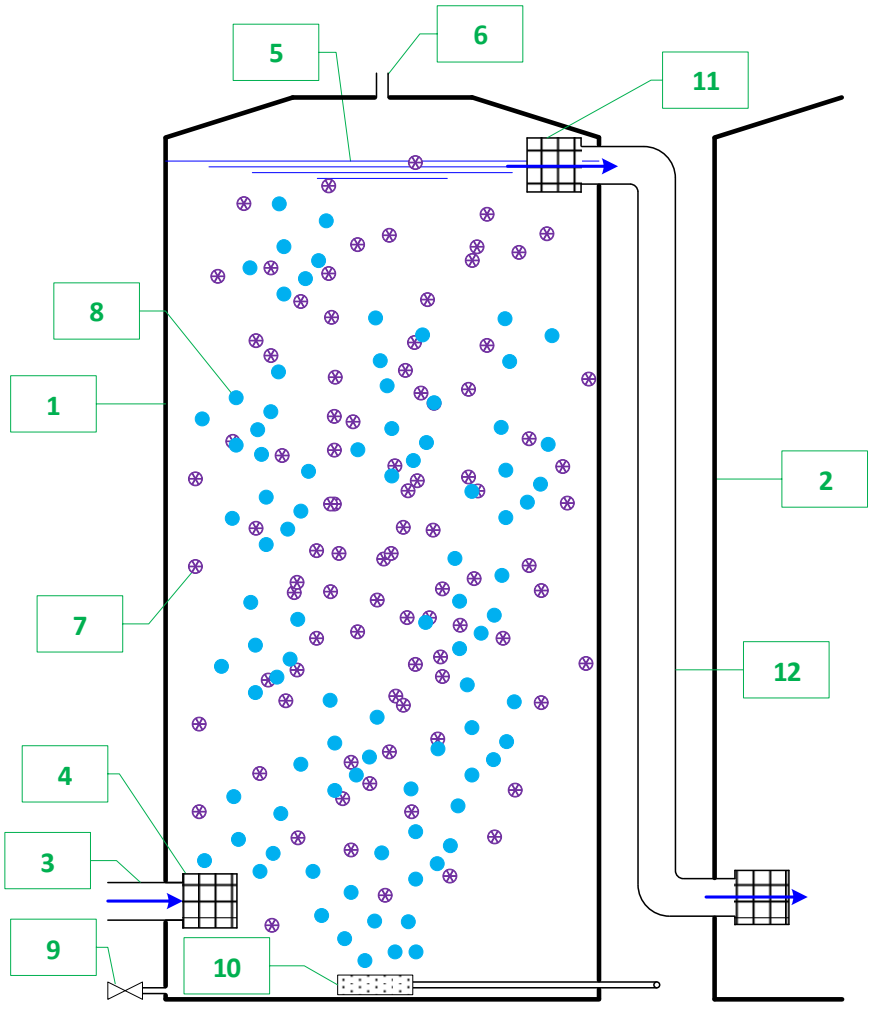

1. MBBR wall
2. Adjacent MBBR
3. Return pipe from sump
4. Inlet mesh grid
5. Water surface
6. Air vent
7. Biomedia (not to scale)
8. Air bubble (not to scale)
9. Drainage valve
10. Air diffuser connected to air supply pipe
11. Outlet mesh grid
12. Outlet pipe going to the next MBBR

Figure 4-14: First MBBR (BF-01) internals, piping and flow pattern design cross sectional side view

The internals, pipe sizes and vessel diameter are shown to scale, but the height of the vessel in the image has been reduced and biomedia and bubble size increased for practical depiction. The inlet of each MBBR is at the bottom and the overflow outlet pipe is at the top. Both the MBBR inlet and outlet have mesh grids to prevent biomedia from leaving the MBBR vessel. A drainage valve is located at the bottom of the MBBR vessel to allow drainage of the entire water volume. Aeration is provided by submerged diffusers at the bottom whose design is discussed in section 4.6. The roof of the MBBR has a hole in it to allow venting of the aeration air. A non-return valve is located at each aeration inlet to prevent backflow of water through the air supply pipes.

4.6 Aeration design

4.6.1 Selection of aeration technology

Submerged air diffusers, also known as airstones, were selected as the method of aeration in the design. Airstones are commonly used in indoor RAS as the final diffusing mechanism, and thus many options are commercially available on the market. A benefit of aerating the water with submerged air diffusers is that the blower increases the temperature of the air, decreasing the overall water heating requirements of the system. Aeration by surface agitation or cascades were not preferred due to no heating benefits and additional space footprint required for implementation. The submerged air diffusers can be placed directly in the fish tanks and MBBR.

4.6.2 Sizing of the air diffusers

The first step in sizing the air diffusers was to calculate the oxygen consumption in each fish tank (consumption by fish) and MBBR (consumption by autotrophic and heterotrophic bacteria). The air flow required to replace the oxygen consumption rates was calculated using equation (3.31) and Figure 3-8. The initial model variables and results are listed in Table 4-13.

Table 4-13: Initial air diffuser sizing

Variable	Fish tanks	MBBRs
Oxygen consumption rate [g/day]	2 538	3 958
Net oxygen supply by water flow [g/day]	-144	144
Required oxygen supply by aeration [g/day]	2 682	3 814
Bulk fluid oxygen concentration [mg/L]	5.0	4.5
%DO saturation	60%	54%
Diffuser depth [m]	0.3	2.2
Oxygen absorption efficiency (from Figure 3-8)	0.5%	3.2%
Total required air flow [std m^3/h]	80.7	18.1
Required air flow per vessel [std m^3/h]	1.1	3.0

A sensitivity analysis to the model input variables was done on the required air flows by changing the input variables within their ranges observed in literature. The results of the sensitivity analysis are presented in Table 4-14.

Table 4-14: Fish tank and MBBR air flow sensitivity analysis

Variable	Minimum value	Design Value	Maximum value	Fish tanks required air flow [std m^3/h]	MBBRs required air flow [std m^3/h]
FCR	1.0	1.5	2.0	55.2 - 106.1	11.9 - 24.3
TGC	0.00042	0.00121	0.00199	47.1 - 95.6	10.0 - 21.8
Water temperature [°C]	22	27	32	74.0 - 86.0	16.5 - 19.4
TAN production ratio [g TAN/g feed consumed]	0.030	0.047	0.070	80.7 - 80.7	14.7 - 22.8
Stocking density [kg/m^3]	25	50	75	42.5 - 118.8	8.8 - 27.4
TSS removal efficiency	60%	80%	90%	80.7 - 80.7	20.6 - 16.9
TSS production ratio [g TSS/g dry feed fed]	0.15	0.25	0.43	80.7 - 80.7	14.5 - 24.7
Fish oxygen consumption ratio [g O_2/g feed consumed]	0.235	0.250	0.255	76.1 - 82.2	18.1 - 18.1
Initial individual fish mass [g]	5	10	15	87.9 - 76.3	19.9 - 17.1

Although the stocking density of 75 kg/m^3 required the highest air flows in the sensitivity analysis, correct management of the RAS can avoid such high stocking densities. Thus, the sensitivity to stocking density was not considered for the final sizing. The maximum possible FCR determined the required air flow to the fish tanks to be 106.1 std m^3/h. The maximum possible TSS production ratio determined the required air flow to the MBBRs to be 24.7 std m^3/h. It was decided that the design air flow rates to the fish tanks and MBBRs will be 110 std m^3/h and 25 std m^3/h respectively.

By way of comparison, an existing RAS (Guerdat et al., 2010) using MBBRs has an air flow of 4.9 std m^3/h per m^3 reactor volume. The proposed MBBR aeration system for this design has an air flow of 4.2 std m^3/h per m^3 reactor volume, which is 14% less than the air flow used by Guerdat *et al.* (2010). The difference is explained by the difference in MBBR water depths, the fact that they observed a higher oxygen concentration of 5.2 mg/L and the uncertainty in the aeration model. However, despite the differences, the values are of the same magnitude which serves as validation of the current design.

An important function of the aeration inside an MBBR is mixing of the biomedia. This is critical for efficient operation of an MBBR by maintaining well-mixed CSTR-type conditions. A study by (Kamstra

et al., 2017) has found that the superficial gas velocity, defined as the volumetric air flow rate per free water surface area, needs to be higher than 5.0 m/h to ensure sufficient mixing of the biomedia. The superficial gas velocity was calculated to be 9.4 m/h in each of the six MBBRs given that the design air flow is 25 m^3/h and the total water surface area of the six MBBRs equals 2.7 m^2. The high superficial gas velocity indicated that the aeration in the MBBRs will provide sufficient mixing of the biomedia.

After considering the points discussed above, it was concluded that the design air flow rates to the fish tanks and MBBRs of 110 std m^3/h and 25 std m^3/h respectively will be sufficient to maintain water quality at the required levels throughout a typical set of growth conditions experienced during experimental trials. The chosen submerged air diffuser suited for this application is the HB016 submerged air diffuser (Ecotao Enterprises, 2018b). The HB016 (shown in Figure 4-15) has a diameter of 30 mm, length of 130 mm, air flow rate of 13 L/min and bubble sizes of 0.3 mm to 0.5 mm.

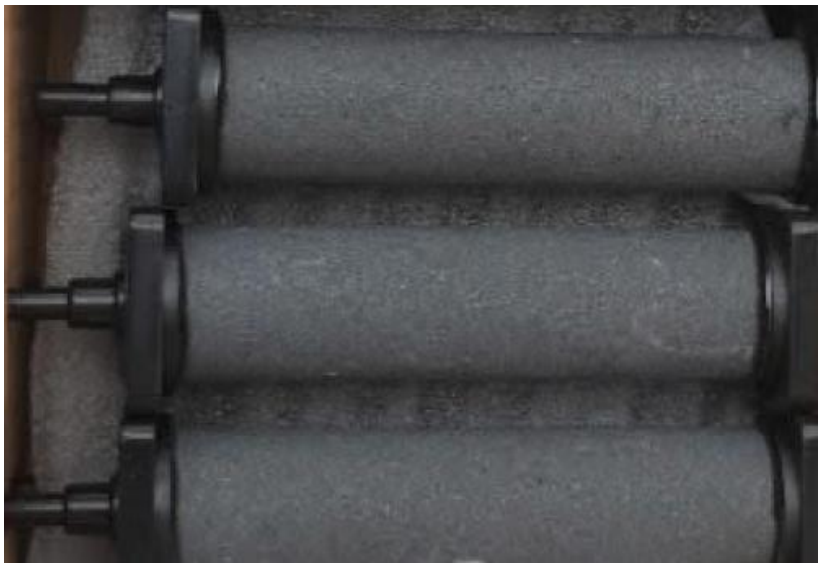

Figure 4-15: Chosen submerged air diffuser model HB016

Each fish tank will have 2 submerged diffusers supplying 13 std L/min of air each. Each MBBR will have 6 submerged diffusers supplying 13 std L/min of air each. To aerate a total of 72 fish tanks and 6 MBBRs, 180 HB016 submerged diffuser are required. The diffusers cost R 31,54 each (Ecotao Enterprises, 2018b), which results in a total cost of R 5 677 for 180 diffusers.

4.6.3 Blower selection

The blower selection required calculation of the total pressure drop that the blower must overcome. A certain pressure drop in the line will result in a certain air flow rate based on the blower performance curve of a specific blower. The submerged diffuser head loss was assumed to be 0.20 m (Aquarius Technologies Inc., 2011). The hydraulic head loss was the actual height of the water columns, being 0.3 m and 2.2 m for the fish tanks and MBBRs respectively. The head loss inside the HDPE air distribution pipes was calculated as 1.45 m for the furthest fish tank from the blower and 0.15 m for the furthest MBBR from the blower. The total head loss and pressure drop for the fish tank line was

estimated to be 1.95 m and 191 mbar respectively. The total head loss and pressure drop for the MBBR line was estimated to be 2.55 m and 250 mbar respectively. The variables of the air distribution system design are given in APPENDIX I.

It was decided to supply all the fish tanks and MBBRs using a single regenerative blower. This will require air taps/valves to be installed before each air diffuser in order to equalize the air pressures, allowing equal air flow through all air diffusers regardless of location. The operating pressure of each submerged air diffuser will thus be about 250 mbar. The correct blower was identified as the ZXB 710-3.0kW-50Hz regenerative blower supplied by CFW Fans. Its performance curve is shown in Figure 4-16 with the operating point indicated where the green dashed lines intersect the blower performance curve.

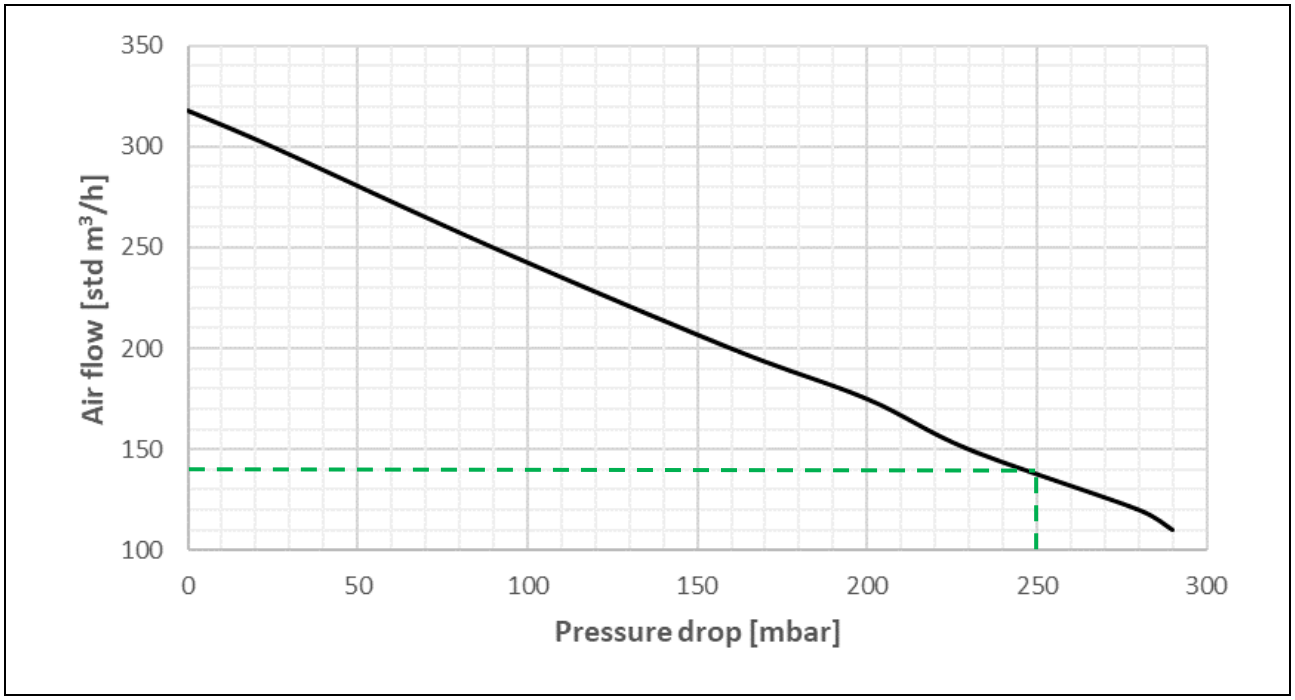

Figure 4-16: CFW Fans regenerative blower model ZXB 710-3.0kW-50Hz performance curve showing the operating discharge air flow of the blower

From Figure 4-16 it was determined that the proposed blower and aeration system will be able to deliver up to 140 std m^3/h of air to the fish tanks and MBBRs combined. The proposed blower setup is estimated to cost a total of R 15 867, which includes the blower, inlet manifold, air filter, pressure gauge and pressure relief valve. Redundancy in the aeration system was not included due to costs and the high resilience of tilapia and African catfish to low oxygen concentrations but can be included by the investors if they want to reduce risks of fish mortalities during breakdowns.

4.6.4 Gas supersaturation

The aeration within the MBBRs will cause supersaturation of dissolved nitrogen due to the water depth (2.2m). However, gas supersaturation is only important for the fish health. It was assumed that the nitrogen concentration will be reduced in the fish tanks. This is due to the low water depth of the

tanks causing lower nitrogen saturation concentrations and the vigorous aeration in the fish tanks causing equilibrium conditions for dissolved nitrogen.

The φ-value for fine bubble diffusers was used for nitrogen saturation concentration correction using equation (3.30) as fine bubble diffusers will account the most of the supersaturation. The results of the gas supersaturation evaluation in the fish tanks are given in Table 4-15.

Table 4-15: Gas supersaturation results

Variable	Value	Units
Effective nitrogen saturation concentration	14.1	mg/L
Nitrogen gas tension	611	$mmHg$
Local barometric pressure (BP)	760	$mmHg$
Case 1: Normal operation, fish tank DO concentration = 5.0 mg/L		
Oxygen gas tension	97	$mmHg$
Total dissolved gas pressure (TGP)	708	$mmHg$
DP (TGP – BP)	-52	$mmHg$
%TGP	93%	
Case 2: 100% oxygen saturation, fish tank DO concentration = 8.8 mg/L		
Oxygen gas tension	170	$mmHg$
Total dissolved gas pressure (TGP)	781	$mmHg$
DP (TGP – BP)	21	$mmHg$
%TGP	103%	

The two cases considered in Table 4-15 were the design oxygen concentration of 5 mg/L and a worst-case scenario of the fish tank water being saturated with oxygen to determine if there is any risk of gas supersaturation in the fish tanks. The water is not supersaturated with gas at case 1 because DP < 0. Thus, no risk of gas bubble disease is present in case 1. It was found that the water is supersaturated with gas in case 2 due to DP > 0. However, the DP exceeds the recommended limit of 20 mmHg by only 1 mmHg. The %TGP is below the literature limit of 106%. Case 2 is extremely unlikely due to constant consumption of oxygen by the fish and the fact that air is used for oxygenation instead of pure oxygen. Air flow rates required to achieve near 100% oxygen saturation is exceptionally high in the presence of intensive fish culture (Timmons and Ebeling, 2007). In conclusion, there is no risk of gas bubble disease in the proposed system.

4.6.5 Carbon dioxide degassing

At the estimated oxygen consumption rate in the fish tanks of 2538 g O_2/day, the carbon dioxide production rate was estimated to be 3490 g CO_2/day by considering the stoichiometry of the respiration (see section 3.3.2). $K_L a_{O_2}$ was calculated to be 130 day^{-1} and using the ratio of $\frac{K_L a_{CO_2}}{K_L a_{O_2}} = 0.9$, $K_L a_{CO_2}$ was calculated to be 117 day^{-1}. To find the steady state carbon dioxide concentration in the fish tanks, a carbon dioxide mass balance was done over the fish tanks. The effect of water inflow and outflow was assumed to be negligible. The removal of carbon dioxide by degassing and production of carbon dioxide by fish respiration were the only flows of carbon dioxide considered in the mass balance. Thereby steady state will be reached when the removal rate is equal to the production rate.

The carbon dioxide concentration was varied until this condition was met. It was found that the steady state carbon dioxide concentration in the fish tank at peak loading will be 5.3 mg/L, which is well below the recommended limit of 15 mg/L. It was concluded that the in-tank aeration is sufficient to maintain desirable carbon dioxide concentrations in the fish tanks.

4.7 Water and air distribution design

4.7.1 Sizing and selection of water pumps

The pumps were designed based on an accumulation of zero for each waste product inside the fish tanks and the largest required pump size resulted in the final sizing. According to the sensitivity analyses described in section 4.5.4.3, a recirculation flow rate of 12 m^3/h is sufficient.

Typically for such small-scale RAS, pool water circulation centrifugal pumps are used for water recirculation. The BADU Porpoise 10 was selected as the appropriate pump when operating at a total dynamic head of 7 m or lower as illustrated by its performance curve (Figure 4-17).

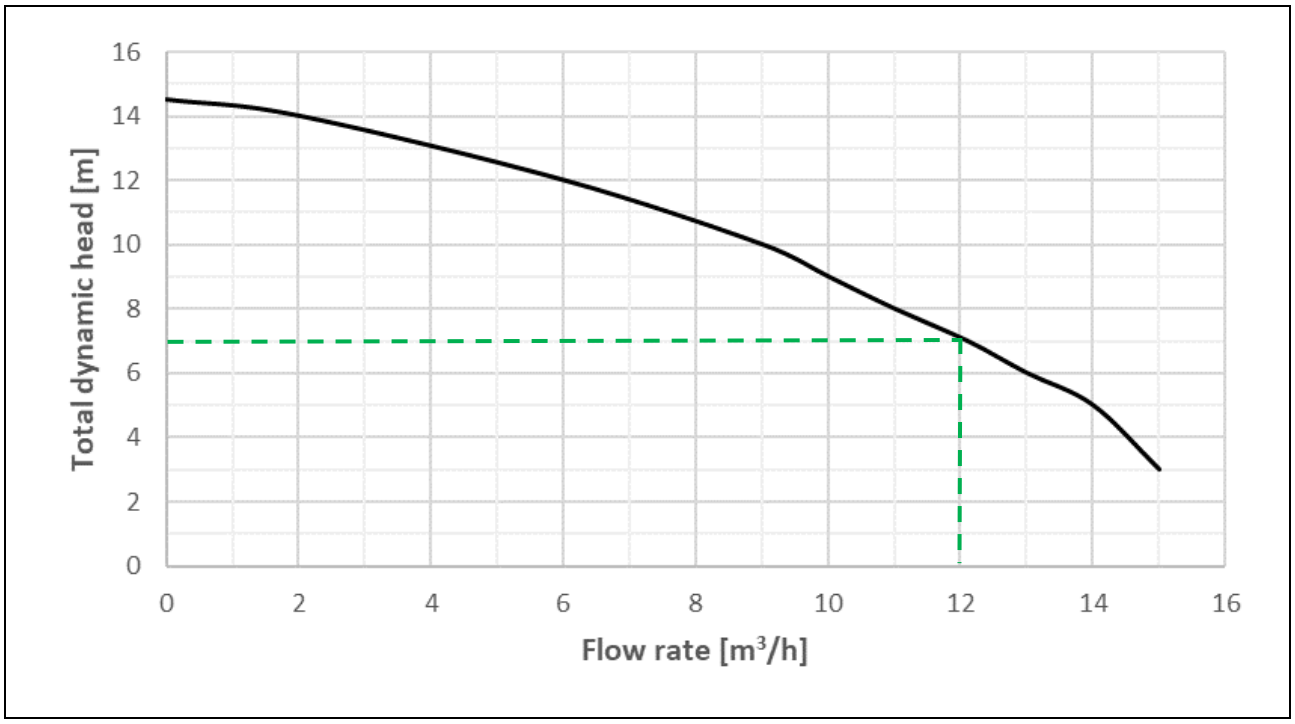

Figure 4-17: BADU Porpoise 10 pump performance curve

The total dynamic head consisted of the hydraulic elevation head, heat pump pressure head and the head loss introduced by friction in the pipe from the pump to the MBBR, where the subsequent flow is by gravity. The hydraulic head required to pump the water over the walkway and to the MBBRs was 2.6 m. The pressure drop over the chosen heat pump heat exchanger tubes (see section 4.8.2.2) is 6 kPa, which is equal to 0.6 m head loss. The friction head loss over 5 m of PVC pipe with an inner diameter of 60 mm was estimated to be 0.1 m. Thereby the total dynamic head operating point will be 3.3 m, which is lower than the maximum of 7 m needed to achieve a flow of 12 m^3/h. The overdesign introduced by this allows the system to be operated at between 14 m^3/h and 15 m^3/h if necessary. A

valve and flow meter will need to be installed at the pump to manually control the recirculating flow at 12 m^3/h as high flows can decrease the efficiency of the lamella settler.

A backup pump is required in case of pump failure or maintenance as the build-up of ammonia and solids inside the fish tanks could be fatal to the fish and needs to be transported to the solids removal and biofiltration unit operations. The current existing system does have two BADU Porpoise 10 pumps and thus no new pumps have to be purchased.

4.7.2 Water and air piping design

The chosen water pipes were uPVC piping, which is the standard pipe material used for RAS in South Africa. The chosen air pipes were HDPE piping. Both the water and air pipe diameters were chosen to minimize head loss and not allowing water velocities faster than 2.5 m/s. Higher water velocities in pipes can cause noise and damage to pipes if flow stops suddenly. The complete water and air distribution design is described by the piping and instrumentation diagrams (P&IDs) in APPENDIX C. The general layout of the water and air piping is shown in Figure 4-18.

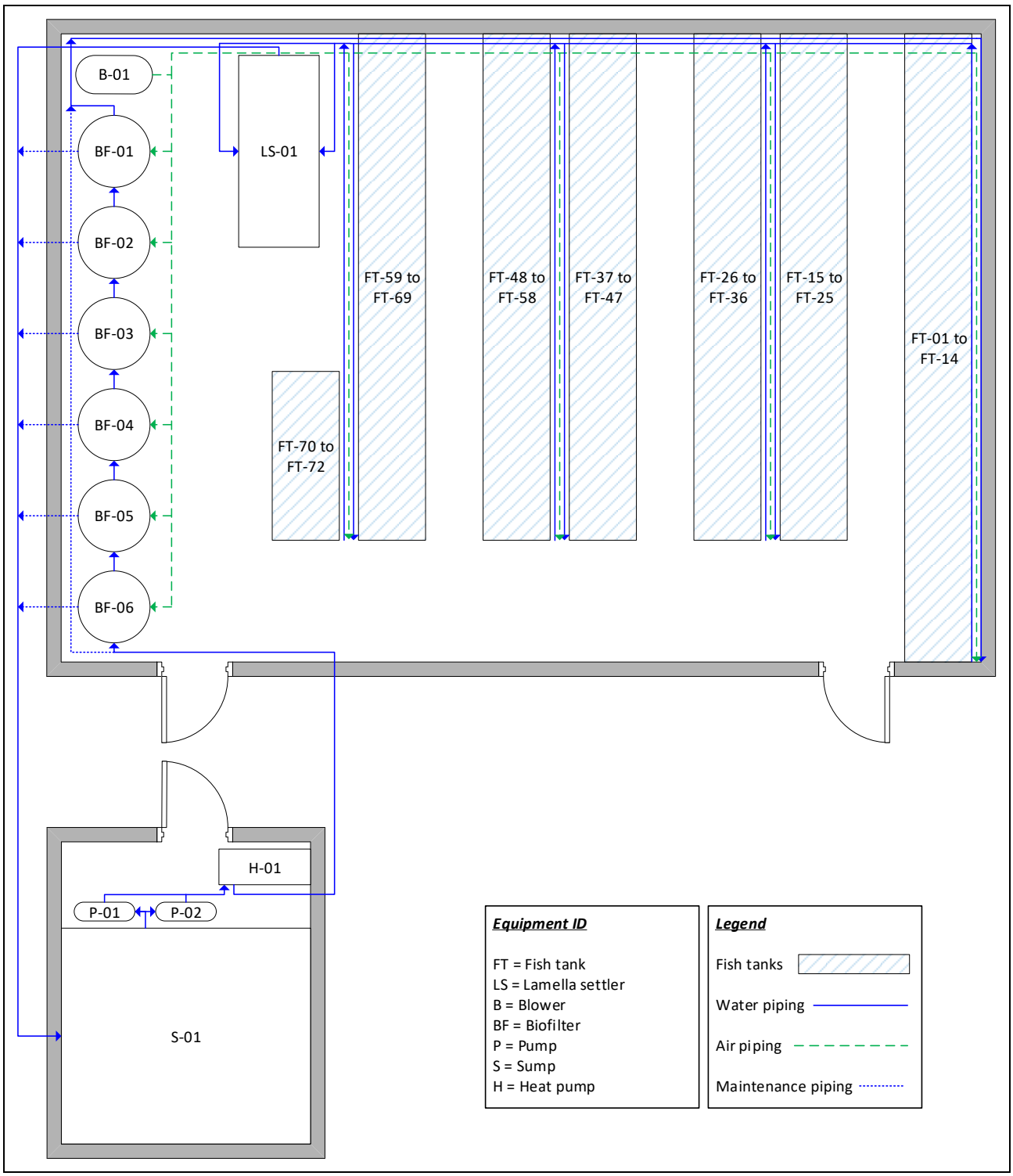

Figure 4-18: Water and air piping layout

The breakdown of specifications and costing of the piping, pipe fittings and valves are given in APPENDIX D. The capital cost of the piping was estimated to be R 8 687. The capital cost of the pipe fittings was estimated to be R 5 789. The capital cost of the valves was estimated to be R 8 409.

4.8 Temperature regulation design

The heat flows of the process water are, among other variables, dependent on the internal building air temperature. Therefore, the first step in designing the temperature regulation of the RAS was to determine the internal building air temperature that can be maintained.

4.8.1 Air handling design

The limiting case for the currently installed air handling unit would be its heating capacity at the design dry bulb temperature. This limiting case is defined as zero heating from the sun (nighttime) and a design dry bulb temperature of 6°C (see section 4.1.7.1). The building air temperature was assumed to be maintained at 24°C due to it being the rated temperature during heating for the current existing air conditioner. The building air heat losses were modeled as described in section 3.9.2 and resulted in the air heat losses presented in Figure 4-19.

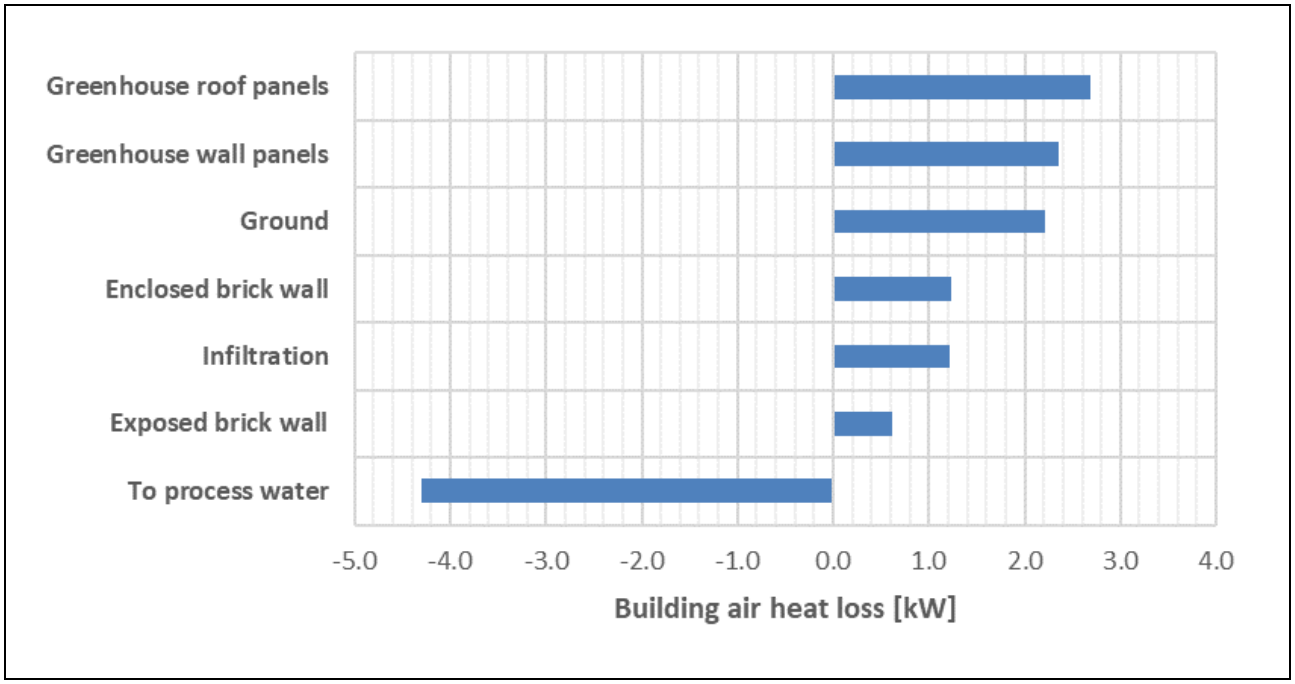

Figure 4-19: Building air heat losses at the design case

Building air heat losses were highest through the greenhouse panels and the ground, which is due to those surfaces having the most surface area available for heat transfer. The building air heat loss to the process water is negative due to the process water being at a higher temperature (27°C) than the building air (24°C). The sump room is separate from the fish tank room and does not share airspace. Air temperature and humidity in the sump room was assumed to be equal to the ambient atmospheric air conditions.

The total building air heat loss at design conditions was estimated to be 6.0 kW and is significantly less than the heating capacity of the already installed UATY15K Daikin air conditioner, which is 46.1 kW. In conclusion, this proved that the air conditioner is capable of maintaining a building air temperature of 24°C.

The fish tank room also has an ED24 Munters extraction fans capable of removing air from the building at roughly 10 000 m^3/h if the air temperature exceeds a certain value to protect equipment from overheating. The air temperature upper limit needs to be specified during construction.

4.8.2 Water heating design

4.8.2.1 Water heating requirements

The process water heat losses were modeled as described in section 3.9.1 and resulted in the air heat losses presented in Figure 4-20. The total estimated process water heat loss was 8.9 kW.

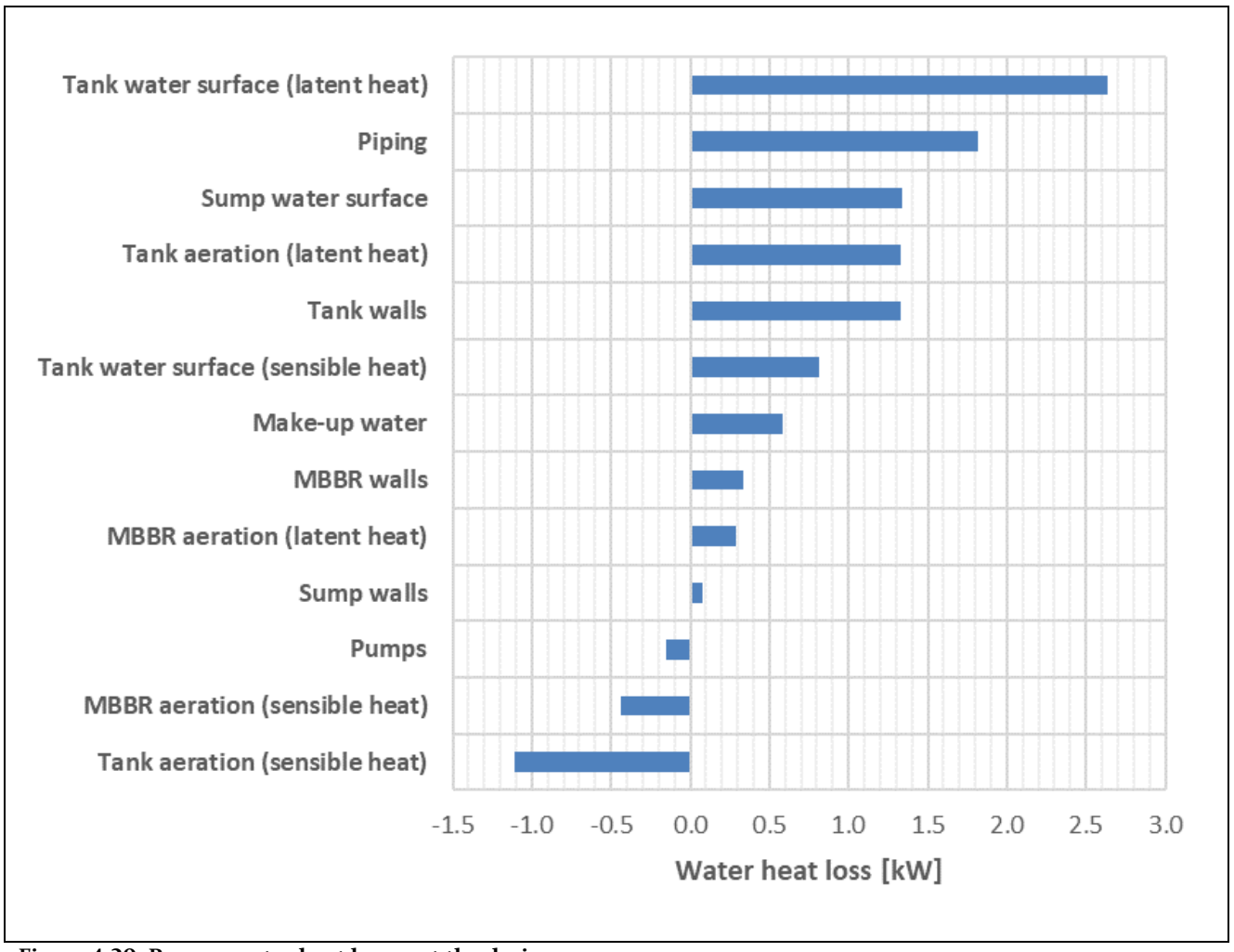

Figure 4-20: Process water heat losses at the design case

The largest source of heat loss in the RAS was predicted to be evaporation at the fish tank water surfaces. This is due to the large surface area of the fish tank water surfaces, the temperature difference between the water and air and the high latent heat of vaporization of water. Covering the tanks with a lid could possibly reduce the heat losses from fish tank water surfaces by reducing contact with the internal building air. This was not considered in this study but can be considered during construction of the facility as a means of reducing water heating demands. The second largest source of heat loss in the RAS was predicted to be through the un-insulated piping. This is due to the large number of pipes involved in the construction (see section 4.7.2). Heat is gained from pumps and sensible heating from

aeration due to the pump and blower inefficiencies and compression heating of the air entering the water. A sensitivity analysis was not necessary as the above results were obtained by modeling the system at design conditions defined in section 4.1.7 and the maximum required make-up water flow at peak loading, which is conservative and unlikely to occur at the same time.

4.8.2.2 Selection of water heating technology

The current existing electric resistance heaters can provide a total heating duty of 8 kW, which is lower than the maximum predicted required heating duty of 8.9 kW. Water heat pumps driven by a rotary compressor were considered as an alternative to the current existing electric resistance heaters. The chosen heat pump was an Aquaheat Premier SF020P single phase heat pump with a heating capacity of 9.2 kW in order to maintain 27°C even at worst case conditions used in the heating requirement estimation of 8.9 kW. The coefficient of performance (COP) of the heat pump is 6.1, which means that 6.1 kW of heating is obtained for every 1.0 kW of electrical power delivered to the unit. This is significantly more energy efficient than the electric resistance heaters, which have a COP of 1.

4.8.2.3 Financial feasibility of electric resistance heaters vs heat pump

The heating duty at the average dry bulb temperature of the site (16.4°C) was estimated to be 6.3 kW and was used to compare the electric resistance heaters with the proposed heat pump. The financial feasibility of replacing the electric resistance heaters with a heat pump was assessed by the cost-benefit analysis summarized in Table 4-16.

Table 4-16: Cost-benefit analysis of a heat pump vs electric resistance heater

Variable	Electric resistance heater	Aquaheat SF020P heat pump
Capital cost [ZAR]	0	30 360
Coefficient of performance (COP)	1.0	6.1
Average power requirement [kW]	6.3	1.03
Annual energy use [kWh/year]	45 360	7 396
Annual electricity cost [ZAR/year]	61 925	10 097
Annual savings [ZAR/year]		51 829
Payback period [years]		0.59

The payback period of 0.59 years (7 months) is considered a feasible investment and is sufficient motivation for the replacement of the electric resistance heaters. In conclusion, the proposed heat pump is the recommended method of water heating for the new RAS.

4.9 Disinfection design

UV sterilization was selected as the simplest solution to disinfection in the system. A UV sterilizer rated for a maximum flow of 18 m^3/h was selected known as the Pond Medic 55W UV sterilizer and

will cost R 1 099 (Futurama, 2019). The UV sterilizer will be installed in-line at the sump room after the pump discharge.

4.10 Water quality measurements

For regular monitoring of water quality, the critical water quality parameters must be measured namely, DO, pH, ammonia, nitrite, nitrate and CO_2. Due to the effort required to measure suspended solids, TSS only needs to be measured if water quality issues arise as part of the troubleshooting process (see section 5.4.10). Dissolved oxygen concentration measurements can be done manually using an IP67 DO meter that will cost R 3 750 (MyAquaponics, 2019a). pH and temperature measurements can be done manually using a pH and temperature meter that will cost R 1 695 (MyAquaponics, 2019b). Online measurement of ammonia, nitrite and nitrate is expensive and therefore daily manual measurement of these concentrations using low-cost spectrophotometric methods is required to ensure optimal operations. The costs of these manual measurement methods were excluded from the cost estimate for the project as the necessary equipment already exists at the present facility. Carbon dioxide concentrations can be inferred by the pH and total alkalinity.

Chapter 5. System design proposal

5.1 Required equipment and costs

The following major equipment listed in Table 5-1 needs to be procured or reused for the proposed RAS design to be implemented. A more detailed breakdown of the bill of quantities is presented in APPENDIX D.

Table 5-1: Equipment list and capital costs

Item	Description	Cost [ZAR]
P-01 & P-02	BADU Porpoise 10 recirculation pumps	Reuse existing
FT-01 to FT-72	90L fish tanks	Reuse
S-01	Sump	Reuse
B-01	ZXB 710-3.0kW-50Hz blower	15 867
Airstones	Fish tank and MBBR submerged diffusers	5 677
LS-01	Lamella settler	14 697
H-01	Aquaheat Premier SF020P single phase heat pump	30 360
H-02	Daikin UATY15K air conditioner	Reuse
BF-01 to BF-06	Moving bed bioreactors with 65% filling of biomedia	45 500
Piping and valves	Water and air distribution pipes and valves	22 883
UV sterilizer	Pond medic UV sterilizer 55W, 18000L/H	1 099
Measurement devices	DO meter, pH/temperature meter, flow meter (FI-01)	8 845
	TOTAL	145 000

Table 5-2: Operating cost estimates

Item	Description	Cost [ZAR]
Electricity	P-01 = 0.45 kW H-01 = 1.03 kW B-01 = 3.0 kW Air conditioner (H-02) excluded from estimate. Assumed operational days per year = 300 days Annual energy usage = 32 256 kWh @ R 1,3652 per kWh	44 036
Make-up water	Assumed 3 typical experimental trial lasting 91 days and using all 72 tanks occurs per year. Annual make-up water to control nitrate concentration = 184 m^3 @ R62,96 per m^3	34 754
Alkalinity control	Assumed 80 grams of sodium bicarbonate is added per kilogram of feed. Assumed 3 typical experimental trial lasting 91 days and using all 72 tanks occurs per year. Annual feed requirement = 550 kg Annual sodium bicarbonate requirement = 44 kg $NaHCO_3$ @ R 4,57 per kg $NaHCO_3$ (Alibaba, 2019)	201
	TOTAL	79 000

The estimated capital cost of implementing the proposed RAS design is R 145 000.

Based on the operating estimates described in Table 5-2, the total annual operating cost of the proposed RAS will be R 79 000. It should noted that the estimated annual operating cost of the RAS is more than 50% the total estimated capital cost, which further highlights the importance of considering operating costs versus capital costs of RAS equipment to achieve a financially optimal design.

5.2 Drawings of proposed facility

The process flow diagram (PFD) of the proposed RAS (Figure 5-1) summarizes the entire design. The piping and instrumentation diagrams that show more detail is found in APPENDIX C.

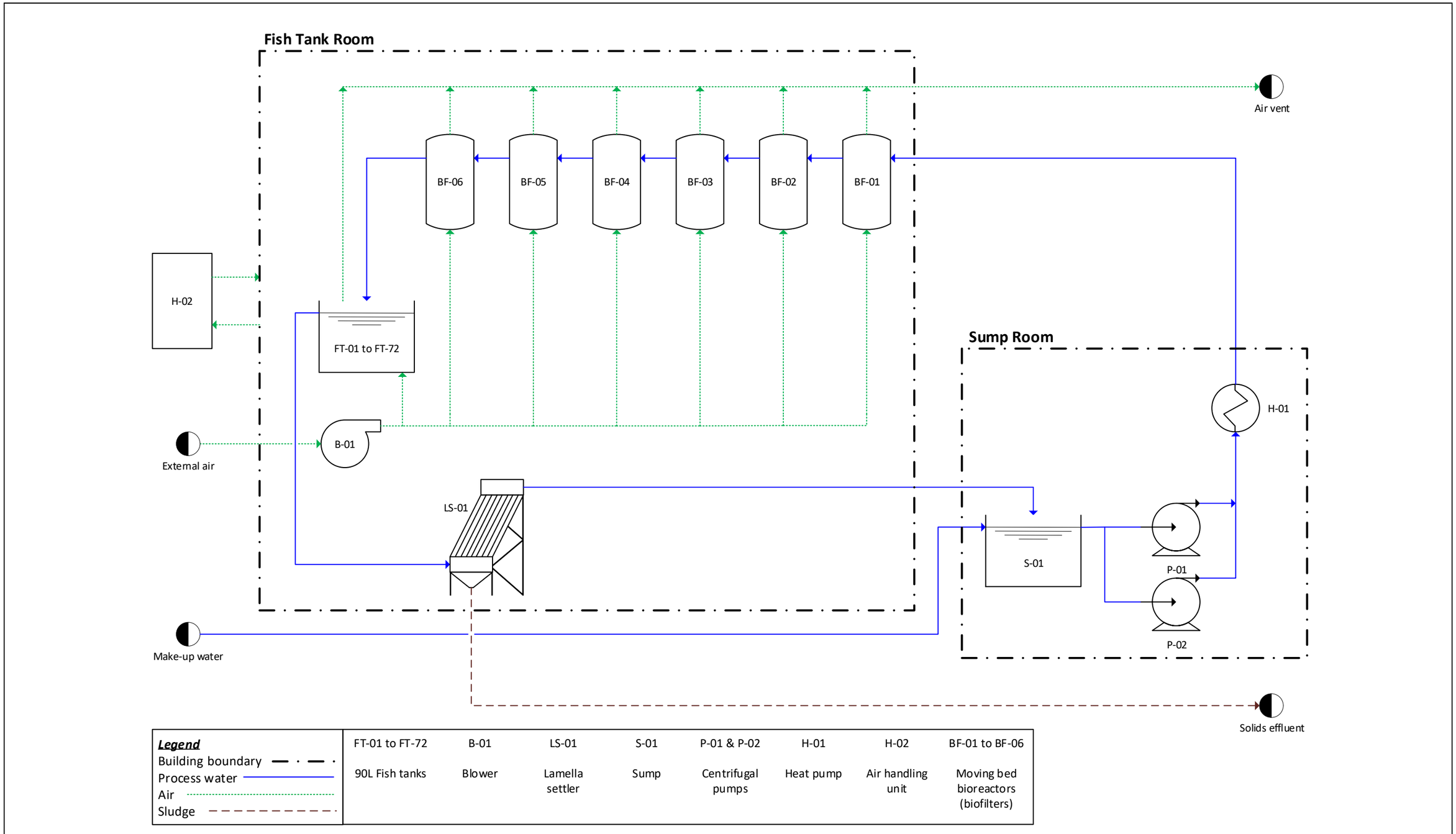

Figure 5-1: Process flow diagram of the proposed RAS design

5.3 RAS dimensioning heuristics

The proposed RAS design was based on a fish stocking density of 50 kg/m^3. If any other stocking density is desired the recirculation, biofilter, solids settling and aeration designs can be adjusted using the heuristic equations below in Table 5-3. These equations were derived based on the assumption that feeding rate and waste production rates are linearly related to stocking density and that all 72 90L fish tanks are utilized.

Table 5-3: RAS equipment sizing heuristics

$$Q_{recirc} = 0.24 \cdot \rho_{stocking} \quad (5.1)$$

$$A_{biofilm} = 23.28 \cdot \rho_{stocking} \quad (5.2)$$

$$A_{settle} = 0.11 \cdot \rho_{stocking} \quad (5.3)$$

$$Q_{air} = 2.7 \cdot \rho_{stocking} \quad (5.4)$$

where

Q_{recirc}	=	Required recirculation flow rate $[m^3/h]$
$A_{biofilm}$	=	Required biofilm area in MBBRs $[m^2]$
A_{settle}	=	Required horizontally projected settling surface area $[m^2]$
Q_{air}	=	Required air flow at standard conditions for aeration of fish tanks and MBBRs $[std\ m^3/h]$
$\rho_{stocking}$	=	Peak fish stocking density $[kg/m^3]$

The water and air heating designs are not sensitive to the peak stocking density being altered. However, if the design geometry changes, the heat transfer will need to be remodeled.

5.4 RAS management plan

A RAS management plan is required to aid personnel in achieving successful operation of a RAS. The following RAS management plan was compiled to achieve Objective 4 of the study (see section 1.4).

5.4.1 Stocking the RAS with fish

The proposed RAS has been dimensioned based on African catfish waste production data and a fish growth model based on African catfish growth data. Figure 5-2 can be used as a guide for stocking African catfish to reach a peak stocking density of 50 kg/m^3, assuming all 72 fish tanks are utilized. As the RAS has been dimensioned to handle a peak stocking density of 50 kg/m^3, stocking more than the recommended amount of fish will potentially cause unstable water quality conditions.

If any other species is to be grown in the RAS, stocking amounts should be altered based on growth data for the species in question. If this precaution is not followed, the system might not be able to treat the waste produced if fish growth is faster than expected.

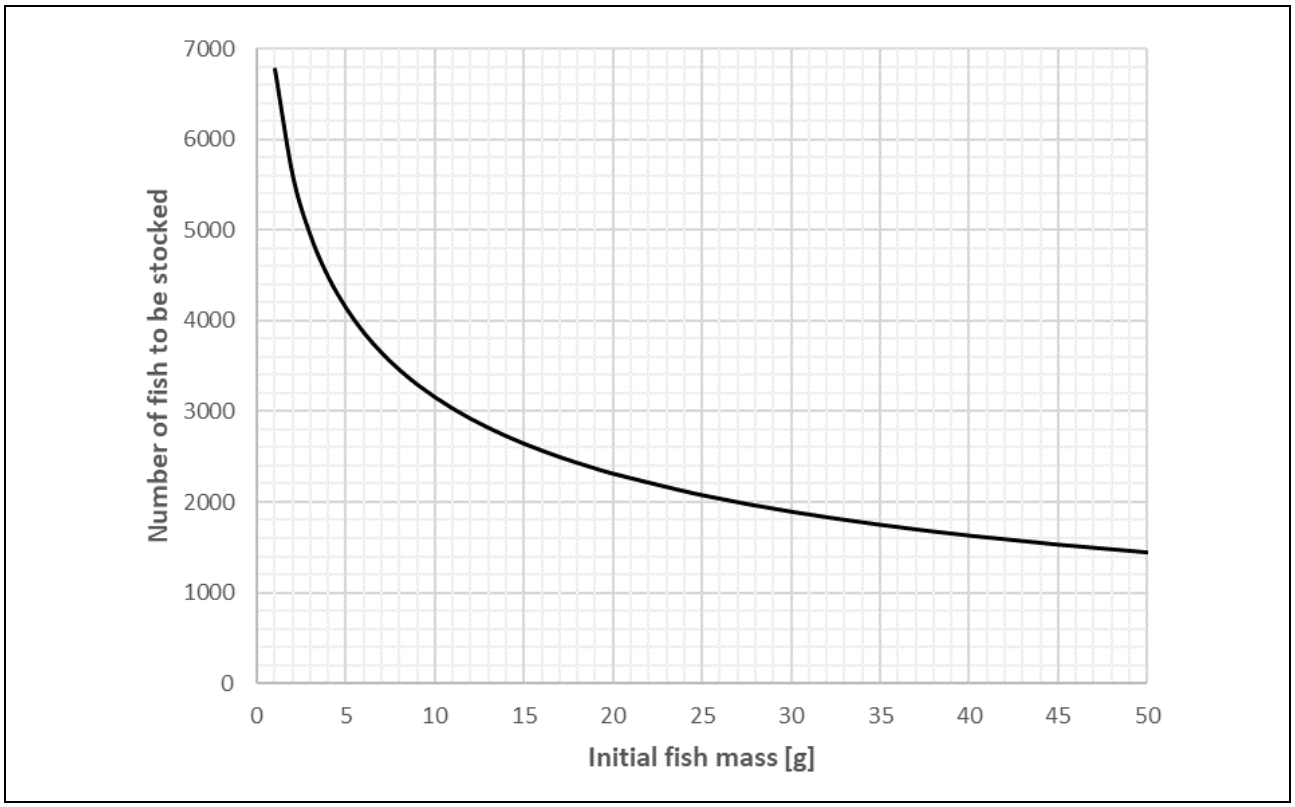

Figure 5-2: African catfish stocking limits

5.4.2 Water quality measurements

Dissolved oxygen, pH, temperature, ammonia, nitrite, nitrate, total alkalinity and hardness must preferably be measured daily. If the frequency of water quality parameter measurements can be increased, then it is advised to do so.

5.4.3 Biofilter management

When starting up the RAS, the biofilm in the MBBRs will be non-existent. Nitrifying bacteria, either bought or taken from another biofilter, can be dosed at the start of a trial to accelerate the growth of a healthy biofilm. Biofilms are known to take up to 4 months to fully develop (Pulkkinen et al., 2018; Rusten et al., 2006). Therefore, the users must use caution to prevent high RAS stocking densities early in the biofilm's development.

When the RAS is not being used for trials, it is advised to maintain MBBR aeration and dose ammonia into the MBBR to feed the nitrifying bacteria. Simply adding fish feed to the MBBR will likely cause an overgrowth of heterotrophic bacteria due to the increased organics in the water and is not recommended. If the MBBR aeration is stopped, anaerobic conditions will be reached in the MBBR, killing the nitrifying bacteria and thereby weakening the biofilm.

5.4.4 Flushing the lamella settler

Sludge from the lamella settler needs to be flushed daily to minimize ammonia leaching into the water from the settled solids. Flushed solids must be disposed of according to local regulations. Details on the disposal of the solids waste was out of the scope of this thesis. Regular checks of the plates inside the lamella settler is recommended and these should be cleaned using a long brush on a weekly basis.

5.4.5 Make-up water

The RAS requires regular make-up water to prevent buildup of nitrate in the water. Assuming no passive denitrification in the RAS, it was estimated that 332L of make-up water must be added for every kg of feed fed. At peak design stocking density and biomass, the make-up water flow rate was estimated to be 0.14 m^3/h

5.4.6 Alkalinity dosing

Alkalinity dosing needs to be done to keep the pH balanced. Bovendeur et al. (1987) recommended 80 g $NaHCO_3$ needs to be added per kg of feed. Regular pH measurements need to be done to ensure a constant pH of 7.0.

5.4.7 Nitrite toxicity prevention

Nitrite can be extremely toxic to fish, even in low concentrations. The main method of preventing this toxicity is by maintaining a sufficient chloride concentration in the water. The recommended ratio for safe operation is a minimum of 20g Cl per g NO_2^-. As an additional safety margin, chloride concentrations should be maintained at 100 mg/L. Salt (NaCl) can be added if the chloride concentration is too low. Weekly chloride measurements are recommended.

5.4.8 Effects of overfeeding the system

Overfeeding of the RAS can occur if the maximum design biomass is exceeded or extreme feeding levels are used. This will lead to the wastewater treatment units not removing waste at the same rate as what is being produced since the units were designed for a certain feeding rate. Ultimately this causes a net accumulation of waste products in the RAS and most importantly in the fish tanks. This effect is shown in Figure 5-3 where the predicted increase in TAN concentration is shown in the days following the peak loading.

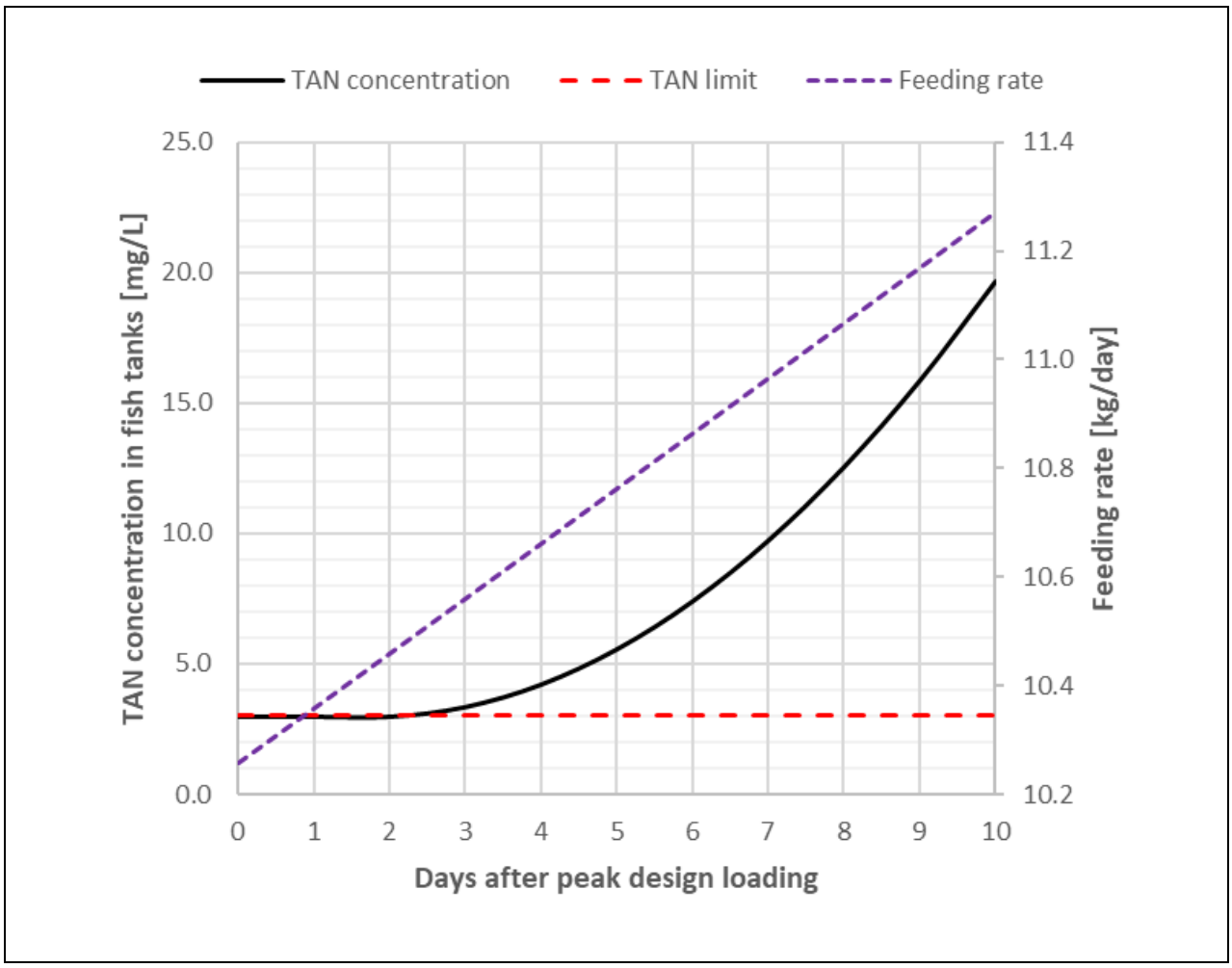

Figure 5-3: Increase in TAN concentrations due to overfeeding

The rapid predicted increase in TAN concentrations in Figure 5-3 demonstrates the importance of remaining below the design maximum feeding rate. This also shows that even though the biofilter is oversized for most of the production period, an exceedance of the maximum design feeding rate will quickly cause accumulation of TAN in the RAS.

5.4.9 Emergency power

Emergency power provided by a generator needs to be available in the case of power cuts.

5.4.10 Troubleshooting guide

Table 5-4 provides emergency remediation steps and long-term solutions to various potential issues that can be experienced when operating the RAS.

Table 5-4: RAS troubleshooting guide

Scenario description	Emergency remediation steps	Long-term solutions
High numbers of fish mortalities are observed.	If diseased fish are observed, quarantine of the diseased fish might be necessary to avoid population from being killed. Emergency RAS water replacement might be needed if water quality is identified as the cause of mortalities.	Measure TAN concentration and pH concentration. Use equations (2.2) and (2.3) to predict the concentration of unionized ammonia in the water. NH_3-N concentrations should not exceed 0.34 mg/L when rearing African catfish. If it exceeds 0.34 mg/L, identify which parameter (TAN or pH) is not within the allowable limits and take appropriate action. Measure nitrite nitrogen concentration. If NO_2-N > 1 mg/L, take appropriate action Measure DO concentration. If DO < 5 mg/L, take appropriate action. Measure TSS concentration. If TSS > 10 mg/L, take appropriate action. Measure nitrate nitrogen concentration. If NO_3-N > 140 mg/L, take appropriate action.
TAN > 3 mg/L	Add zeolite in a basket in the pump sump, to absorb ammonium ions in the recirculating water. This solution is considerably less economic than effective biofilter operation and should be viewed as an emergency measure only. If zeolite is unsuccessful, replace a considerable amount of process water to restore TAN concentrations below allowable limits.	Ensure that the system is not overstocked with fish or overfed. Analyze the BOD_5 of the water inside the MBBRs. If BOD_5 > 2.5 mg/L: • Flush the solids settler regularly. • Ensure that flow through the solids settler is not turbulent and that solids are settling out. Inspect the biofilm in the MBBR visually. If it appears to not be well formed, inoculate the MBBRs by manually adding nitrifying bacteria to the bulk water. Ensure that airflow through the MBBRs is steady and that vigorous mixing of the biomedia is occurring.
pH > 7.5	Add less sodium bicarbonate after feeding.	Optimize the amount of sodium bicarbonate to be added by trial and error.
pH < 6.5	Add more sodium bicarbonate after feeding.	Optimize the amount of sodium bicarbonate to be added by trial and error.
NO_2-N > 1 mg/L	Add salt (NaCl) to reduce nitrite toxicity.	Follow the same steps as with the TAN > 3 mg/L case.

Table 5-4: RAS troubleshooting guide (cont.)

Scenario description	Emergency remediation steps	Long-term solutions
DO < 5 mg/L	Close several of the MBBR air valves. This will supply the fish tanks with more air, increasing the DO concentration.	Check the airstones for possible clogging. If the airstones are clogged, remove the clogging material or replace the air stones. If the problem persists, consider adding a second blower and airstones to increase air supply.
Insufficient solids removal or TSS > 10 mg/L	Exchange the process water gradually, making sure that the water temperature is controlled at the setpoint.	Insufficient solids removal most probably means that the lamella settler is not operating as intended. The following measures can be taken: • Ensure that the flow through the lamella settler does not exceed 12 m^3/h. High volumetric flow through the settler causes only particles with fast settling rates to settle out. • Add more plates to the settler. This will increase the Reynolds number due to the smaller space between plates and thus a smaller characteristic length. If the lamella settler is inefficient at removing solids, the settling area can be increased by adding more plates to the lamella settler. This could increase turbulence inside the settling zone due to increased friction and thus must be done with caution.
NO_3-N > 140 mg/L	Exchange the process water gradually, making sure that the water temperature is controlled at the setpoint.	Ensure that the correct amount of daily make-up water is supplied to the system. It is estimated that 332L of make-up water must be added to the system for every kg of feed fed.

5.5 Conclusions

It can be concluded that the proposed RAS design presented in this thesis achieved all the objectives set out at the start of the study. The literature survey conducted provided sufficient background on the various technology option for each unit operations to make well-informed design decisions on technology selections. The literature survey also provided the water quality criteria for effectively operating a RAS with either African catfish or Mozambique tilapia. The fish growth models, waste production models and RAS unit operation models found in literature provided the methodology for accurately modeling various RAS configurations and allowed a cost-effective solution to be found. The study proposes a RAS design that is retrofitted into existing infrastructure, which was a major objective and constraint of the design. Various existing RAS equipment at the Welgevallen farm namely, the existing recirculation pumps, piping, fish tanks, sump and air conditioner could be reused in the proposed RAS design. An MBBR biofilter setup was found to be more financially feasible than the

existing trickling filters due to high pumping costs associated with the operation of the trickling filters. Additionally, the high flow rate required for trickling filter operation dramatically increased the solids settling unit size. The final objective was met by proposing an operating guide for effective operation of the proposed RAS. Finally, it can be concluded by the author that the proposed design is ready for implementation and the project is estimated to cost a total of approximately R 145 000.

5.6 Recommendations for process optimization

5.6.1 Floating feces technology

Since most TSS in water originate from feed excretion (Chen et al., 1994), research into floating feces technology has been conducted (Unger and Brinker, 2013). It was found that certain feed additives could lower the density of feces allowing it to float. The feces could then be easily removed by screening or skimming equipment before breaking up into smaller particles which are more difficult to remove. In a rainbow trout system, solids removal efficiency was found to increase from 25% to 59% when using floating feces feed additives (Schumann et al., 2017). No adverse effects on fish health was observed when feed additives were used in rainbow trout feed (Unger and Brinker, 2013; Schumann et al., 2017).

5.6.2 Automatic feeding

Feeding only 2 to 3 times a day (as is commonly done if manual feeding is employed during experimental trials) can cause drastic fluctuations in waste products in the water. This is due to higher mass of feed being fed at one time compared to if the feed is uniformly fed across 24 hours. This high feed mass entering the system is often eaten quickly and digested before the next feeding event, causing fluctuations in the waste stream entering the system. A solution to this is the use of automatic feeders, which can be loaded with feed pellets and programmed to feed the fish uniformly across 24 hours, increasing the stability of waste product concentrations in the RAS. This solution is expensive and should only be considered if the waste concentrations in the RAS is unstable and the user is sure that the WWT units are operating efficiently.

5.6.3 Energy usage

Energy usage in RAS is a topic that is rarely covered in most articles. However, a recent review by Badiola et al. (2018) on the topic of energy usage has identified several methods for reduction of energy usage and costs:

- Exploiting the height difference between unit operations to reduce pumping costs.
- Use of geothermal energy for heating.
- Use of pure oxygen to reduce flow rate requirements and thus pumping costs.

- Limiting the use of fine solids filtration to side-streams, which can be used intermittently. This can greatly reduce pumping costs due to the high head loss associated with fine solids filtration. An exception to this is foam fractionation.
- Use of solar energy for heating through solar collectors and/or greenhouses.
- Utilization of thermal wastewater from nearby industries.
- Use of airlift pumps.
- Use of axial pumps with variable speed control to reduce pumping costs when system is not at peak loading.
- Use of a surface aerator with variable speed control for carbon dioxide removal.

5.6.3.1 Blower air flow restriction

Process water heating requirements could be reduced be by restricting the blower air flow through the fish tanks and MBBRs using a valve. Restricting air flow will decrease heat loss by evaporation and decrease heat gains by heated blower air. Process water heating requirements would be reduced if there is an overall decrease in net heat loss. However, restricting the regenerative blower air flow will increase the current drawn by the blower motor, increasing energy usage. An investigation into these opposing effects can be done to assess the energy savings of restricting air flow. Due to the dynamic nature of the oxygen consumption through a trial, this optimization would be best done during operations.

5.6.3.2 Water heating versus air heating

Process water heating requirements decrease at higher building air temperatures. This fact creates a possible opportunity for optimization of energy usage by tuning the building air temperature set point to minimize the process water heating. This is best done during operation as the air heating requirements over time is difficult to model due to changing weather and solar heating of the building air by solar radiation penetrating the greenhouse panels.

5.6.3.3 Solar water heating

Utilizing solar energy for water heating has become popular and is a possible way of reducing the energy usage of the RAS (Fuller, 2007). Time series solar radiation data will need to be used in conjunction with various solar heating setups to determine the investment with the shortest payback period.

5.6.3.4 Variable speed drive pumps

As the operations in the proposed RAS will be for experimental trials, the stocking density and thus the required recirculation flow rate will be low at the start of a trial and gradually increase along with biomass increase as the trial progresses. Therefore, replacing the proposed recirculation pump with a variable speed drive pump could potentially decrease overall power costs if operated correctly.

5.6.3.5 Insulation

Heat losses can be reduced by installing insulation around process water piping.

References

Adewolu, M.A., Adeniji, C.A., Adejobi, A.B., 2008. Feed utilization, growth and survival of Clarias gariepinus (Burchell 1822) fingerlings cultured under different photoperiods. Aquaculture 283, 64–67.

Akinwole, A.O., Faturoti, E.O., 2007. Biological performance of African Catfish (Clarias gariepinus) cultured in recirculating system in Ibadan. Aquac. Eng. 36, 18–23.

Al Ba'ba'a, H.B.M., 2015. A New Correlation for Predicting Aeration Efficiency for Air Diffused Systems. University of Wisconsin.

Alibaba, 2019. Food Grade Sodium Bicarbonate [WWW Document]. URL https://www.alibaba.com/product-detail/China-Supplier-Factory-Sale-Food-Grade_60601890252.html (accessed 10.2.19).

APHA, 1998. Standard Methods for Examination of Water and Wastewater, 20th ed, Standard Methods. Association American Public Health.

Aquarius Technologies Inc., 2011. Aeration upgrade - Western Riverside County Regional WW Authority. Carlsbad.

Arceivala, S.J., 1983. Discussion of "Hydraulic Modeling for Waste Stabilization Ponds" by Raymond A. Ferrara and Donald R. F. Harleman (August, 1981). J. Environ. Eng. 109, 265–268.

Ashley, K.I., Hall, K.J., Mavinic, D.S., 1991. Factors influencing oxygen transfer in fine pore diffused aeration. Water Res. 25, 1479–1486.

Baccarin, A.E., Camargo, A.F.M., 2005. Characterization and evaluation of the impact of feed management on the effluents of Nile tilapia (Oreochromis niloticus) culture. Brazilian Arch. Biol. Technol. 48, 81–90.

Badiola, M., Basurko, O.C., Piedrahita, R., Hundley, P., Mendiola, D., 2018. Energy use in Recirculating Aquaculture Systems (RAS): A review. Aquac. Eng. 81, 57–70.

Béné, C., Arthur, R., Norbury, H., Allison, E.H., Beveridge, M., Bush, S., Campling, L., Leschen, W., Little, D., Squires, D., Thilsted, S.H., Troell, M., Williams, M., 2016. Contribution of Fisheries and Aquaculture to Food Security and Poverty Reduction: Assessing the Current Evidence. World Dev. 79, 177–196.

Besson, M., Komen, H., Aubin, J., De Boer, I.J.M., Poelman, M., Quillet, E., Vancoillie, C., Vandeputte, M., Van Arendonk, J.A., 2014. Economic values of growth and feed efficiency for fish farming in recirculating aquaculture system with density and nitrogen output limitations: A case study with African catfish (clarias gariepinus). J. Anim. Sci. 92, 5394–5405.

Blancheton, J.P., Attramadal, K.J.K., Michaud, L., D'Orbcastel, E.R., Vadstein, O., 2013. Insight into bacterial population in aquaculture systems and its implication. Aquac. Eng. 53, 30–39.

Bovendeur, J., 1989. Fixed-biofilm reactors applied to waste water treatment and aquacultural water recirculating systems. Wageningen University.

Bovendeur, J., Eding, E.H., Henken, A.M., 1987. Design and performance of a water recirculation system for high-density culture of the African catfish, Clarias gariepinus (Burchell 1822). Aquaculture 63, 329–353.

Bovendeur, J., Klapwijk, A., 1986. Zuivering en recirculatie van water in visteeltsystemen 1. H2O 19, 136–140.

Brandt, M.J., Johnson, K.J., Elphinston, A.J., Ratnayaka, D.D., 2016. Twort's Water Supply, 7th ed. Butterworth-Heinemann.

Brazil, B.L., 2006. Performance and operation of a rotating biological contactor in a tilapia

recirculating aquaculture system. Aquac. Eng. 34, 261–274.

Brazil, B.L., Summerfelt, S.T., Libey, G.S., 1996. Application of Ozone to Recirculating Aquaculture Systems, in: Successes and Failures in Commercial Recirculating Aquaculture.

Buentello, J.A., Gatlin, D.M., Neill, W.H., 2000. Effects of water temperature and dissolved oxygen on daily feed consumption, feed utilization and growth of channel catfish (Ictalurus punctatus). Aquaculture 182, 339–352.

Bureau, D., Azevedo, P., Tapia-salazar, M., Cuzon, G., 2000. Pattern and cost of growth and nutrient deposition in fish and shrimp: Potential implications and applications. Av. en Nutr. 111–140.

Buttle, L.G., Uglow, R., Cowx, I., 1995. Effect of dietary protein on the nitrogen excretion and growth of the African catfish, Clarias gariepinus. Aquat. Living Resour. 8, 407–414.

Camargo, J.A., Alonso, A., Salamanca, A., 2005. Nitrate toxicity to aquatic animals: a review with new data for freshwater invertebrates. Chemosphere 58, 1255–1267.

Caraman, S., Barbu, M., Ionescu, T., Ifrim, G., Cristea, V., Ceangă, E., 2010. The analysis of the dynamic properties of the wastewater treatment process in a recirculating aquaculture system. Rom. Biotechnol. Lett. 15, 5457–5466.

Çengel, J.A., Ghajar, A.J., 2013. Chapter 16: Heating and Cooling of Buildings, in: Heat and Mass Transfer: A Practical Approach.

Cengel, Y.A., Boles, M.A., 2015. Thermodynamics: An Engineering Approach, 8th ed. McGraw-Hill Education.

Cengel, Y.A., Cimbala, J.M., 2014. Fluid Mechanics: Fundamentals and Applications, 3rd ed. McGraw-Hill Education.

Cengel, Y.A., Ghajar, A.J., 2015. Heat and Mass Transfer: Fundamentals and Applications, 5th ed. McGraw-Hill Education, New York.

CFW Fans, 2019a. Regenerative blowers. Cape Town.

CFW Fans, 2019b. ZXB series catalogue: Side channel blowers and exhausters. Cape Town.

Chapman, P.M., Popham, J.D., Griffin, J., Leslie, D., Michaelson, J., 1987. Differentiation of physical from chemical toxicity in solid waste fish bioassays. Water. Air. Soil Pollut. 33, 295–308.

Chen, S., Coffin, D.E., Malone, R.F., 1993. Production, characteristics, and modeling of aquacultural sludge from a recirculating aquacultural system using a granular media biofilter, in: Wang, J.-K. (Ed.), Techniques for Modern Aquaculture. American Society of Agricultural Engineers, pp. 16–25.

Chen, S., Stechey, D., Malone, R.F., 1994. Suspended Solids Control in Recirculating Aquaculture Systems, in: Timmons, M.B., Losordo, T.M. (Eds.), Aquaculture Water Reuse Systems: Engineering Design and Management. Elsevier Science B.V., Amsterdam, pp. 61–100.

Colt, J.E., Tchobanoglous, G., 1981. Design of aeration systems for aquaculture, in: Proceedings of the Bioengineering Symposium for Fish Culture. American Fisheries Society, Bethesda, pp. 138–148.

d'Orbcastel, E.R., Blancheton, J., Aubin, J., 2009. Towards environmentally sustainable aquaculture: Comparison between two trout farming systems using Life Cycle Assessment. Aquac. Eng. 40, 113–119.

DAFF, 2018. African Sharptooth Catfish Feasibility Study [WWW Document]. URL https://www.nda.agric.za/doaDev/sideMenu/fisheries/03_areasofwork/Aquaculture/economics/Final Catfish Feasibility Study 2018_Formatted.pdf (accessed 7.31.19).

Davidson, J., Summerfelt, S.T., 2005. Solids removal from a coldwater recirculating system - Comparison of a swirl separator and a radial-flow settler. Aquac. Eng. 33, 47–61.

Degani, G., Ben-Zvi, Y., Levanon, D., 1989. The effect of different protein levels and temperatures on feed utilization, growth and body composition of Clarias gariepinus (Burchell 1822). Aquaculture 76, 293–301.

Drennan, D.G., Hosler, K.C., Francis, M., Weaver, D., Aneshansley, E., Beckman, G., Johnson, C.H., Cristina, C.M., 2006. Standardized evaluation and rating of biofilters. II. Manufacturer's and user's perspective. Aquac. Eng. 34, 403–416.

Dumas, A., France, J., Bureau, D., 2010. Modelling growth and body composition in fish nutrition: Where have we been and where are we going? Aquac. Res. 41, 161–181.

Dumas, A., France, J., Bureau, D.P., 2007. Evidence of three growth stanzas in rainbow trout (Oncorhynchus mykiss) across life stages and adaptation of the thermal-unit growth coefficient. Aquaculture 267, 139–146.

Easter, C., 1992. System component performance and water quality in a recirculating system produce hybrid striped bass, in: Aquacultural Expo V. New Orleans.

Ecotao Enterprises, 2019. Positive displacement blower: roots type [WWW Document]. URL https://www.ecotao.co.za/html/positivedisplacementblower.html (accessed 9.3.19).

Ecotao Enterprises, 2018a. Biomedia Quotation 2018/10/22.

Ecotao Enterprises, 2018b. Air stones - general stock.

Ecotao Enterprises, 2017. Biomedia Quotation 2017/02/15.

Eding, E.H., Kamstra, A., Verreth, J.A.J., Huisman, E.A., Klapwijk, A., 2006. Design and operation of nitrifying trickling filters in recirculating aquaculture: A review. Aquac. Eng. 34, 234–260.

Emerson, K., Russo, R.C., Lund, R.E., Thurston, R.V., 1975. Aqueous ammonia equilibrium calculations: Effect of pH and temperature. J. Fish. Res. Board Canada 32, 2379–2383.

FAOSTAT, 2017. FAO Yearbook: Fishery and Aquaculture Statistics. 2015, FAO Annual Yearbook.

Faraji, A., Asadollafardi, G., Shevidi, A., 2013. A pilot study for the application of one- and two-stage tube settlers as a secondary clarifier for wastewater treatment. Int. J. Civ. Eng. 11, 272–280.

Farhat, Khan, M.A., 2011. Growth, Feed Conversion, and Nutrient Retention Efficiency of African Catfish, Clarias gariepinus, (Burchell) Fingerling Fed Diets with Varying Levels of Protein. J. Appl. Aquac. 23, 304–316.

Fernandes, P., Pedersen, L.F., Pedersen, P.B., 2015. Microscreen effects on water quality in replicated recirculating aquaculture systems. Aquac. Eng. 65, 17–26.

Fernandes, P.M., Pedersen, L.F., Pedersen, P.B., 2017. Influence of fixed and moving bed biofilters on micro particle dynamics in a recirculating aquaculture system. Aquac. Eng. 78, 32–41.

Fernandes, P.M., Pedersen, L.F., Pedersen, P.B., 2014. Daily micro particle distribution of an experimental recirculating aquaculture system-A case study. Aquac. Eng. 60, 28–34.

Fogler, H.S., 2014. Elements of Chemical Reaction Engineering, 4th ed. Pearson.

Froese, R., 2006. Cube law, condition factor and weight–length relationships: history, meta-analysis and recommendations. J. Appl. Ichthyol. 22, 241–253.

Fuller, R.J., 2007. Solar heating systems for recirculation aquaculture. Aquac. Eng. 36, 250–260.

Futurama, 2019. Pond Medic 55W UV Sterilizer - 18000L/H [WWW Document]. URL https://www.futurama.co.za/pond-medic-55w-uv-sterilizer-18000l-h (accessed 10.2.19).

Gallert, C., Winter, J., 2008. Bacterial Metabolism in Wastewater Treatment Systems, Biotechnology: Second, Completely Revised Edition.

Gericke, S.J., 2019. The effects of xylanase and arabinoxylan- oligosaccharides on the growth performance , non- specific immunity , hindgut microbial diversity and hindgut short-chain fatty

acid production of African catfish , Clarias gariepinus by Master of Agricultural Sci.

Goosen, N.J., 2014. Investigation of potential bio- active properties and effects on production performance of aquafeed ingredients derived from fish processing waste by way of enzymatic autolysis 204.

Grace, G.., Piedrahita, R.H., 1994. Carbon Dioxide Control, in: Timmons, M.B., Losordo, T.M. (Eds.), Aquaculture Water Reuse Systems: Engineering Design and Management. Elsevier Science B.V., Amsterdam, pp. 209–234.

Gråkjær, 2019. Personal communication.

Greiner, A.D., Timmons, M.B., 1998. Evaluation of the nitrification rates of microbead and trickling filters in an intensive recirculating tilapia production facility. Aquac. Eng. 18, 189–200.

Grundfos, 2019. Grundfos Product Center [WWW Document]. URL product-selection.grundfos.com (accessed 10.1.19).

Guerdat, T.C., Losordo, T.M., Classen, J.J., Osborne, J.A., DeLong, D.P., 2010. An evaluation of commercially available biological filters for recirculating aquaculture systems. Aquac. Eng. 42, 38–49.

Hazen, A., 1904. On Sedimentation. Trans. ASCE.

Heinen, J.M., Hankins, J.A., Weber, A.L., Watten, B.J., 1996. A semi-closed recirculating water system for high-density culture of rainbow trout. Progress. Fish-Culturist 58, 11–22.

Hem, L.J., Rusten, B., Ødegaard, H., 1994. Nitrification in a moving bed biofilm reactor. Water Res. 28, 1425–1433.

Henze, M., Harremoës, P., la Cour Jansen, J., Arvin, E., 1997. Wastewater Treatment, 2nd ed. Springer, Berlin, Heidelberg, New York.

Henze, M., Jr, C.P.L.G., Gujer, W., Marais, G. v. R., Matsuo, T., 1987. Activated Sludge Model no. 1.

Hilmy, A.M., El-Domiaty, N.A., Wershana, K., 1987. Acute and chronic toxicity of nitrite to Clarias Lazera. Comp. Biochem. Physiol. - Part C Toxicol. Pharmacol. 86, 247–253.

Hochheimer, J.N., Wheaton, F., 2000. Biological Filters : Trickling and RBC Design 291–318.

Huguenin, J.E., Colt, J., 2002. Design and operating guide for aquaculture seawater systems. Elsevier.

Incropera, F.P., DeWitt, D.P., Bergman, T.L., Lavine, A.S., 2007. Fundamentals of Heat and Mass Transfer, 6th ed, International Journal of Heat and Mass Transfer. John Wiley & Sons.

Iwama, G.K., Tautz, A.F., 1981. A simple growth model for salmonids in hatcheries. Can. J. Fish. Aquat. Sci. 38, 649–656.

Kamstra, A., Blom, E., Terjesen, B.F., 2017. Mixing and scale affect moving bed biofilm reactor (MBBR) performance. Aquac. Eng. 78, 9–17.

Kamstra, A., van der Heul, J.., Nijhof, M., 1998. Performance and optimisation of trickling filters on eel farms. Aquac. Eng. 17, 175–192.

Karimanzira, D., Keesman, K.J., Kloas, W., Baganz, D., Rauschenbach, T., 2016. Dynamic modeling of the INAPRO aquaponic system. Aquac. Eng. 75, 29–45.

Kawan, J.A., Abu Hasan, H., Suja, F., Jaafar, O., Abd-Rahman, R., 2016. A review on sewage treatment and polishing using moving bed bioreactor (Mbbr). J. Eng. Sci. Technol. 11, 1098–1120.

Kinyage, J.P.H., Pedersen, L.F., 2016. Impact of temperature on ammonium and nitrite removal rates in RAS moving bed biofilters. Aquac. Eng. 75, 51–55.

Kroupova, H., Machova, J., Svobodova, Z., 2005. Nitrite influence on fish : a review. Vet Med 50, 461–471.

Lastiri, D.R., Geelen, C., Cappon, H.J., Rijnaarts, H.H.M., Baganz, D., Kloas, W., Karimanzira, D., Keesman, K.J., 2018. Model-based management strategy for resource efficient design and operation of an aquaponic system. Aquac. Eng. 83, 27–39.

Lekang, O.-I., 2007. Aquaculture Engineering, 1st ed. Blackwell Publishing Ltd, Oxford.

Liao, P.B., Mayo, R.D., 1974. Intensified fish culture combining water reconditioning with pollution abatement. Aquaculture 3, 61–85.

Lim, P.K., Boey, P.L., Ng, W.K., 2001. Dietary palm oil level affects growth performance, protein retention and tissue vitamin E concentration of African catfish, Clarias gariepinus. Aquaculture 202, 101–112.

Losordo, T.M., Hobbs, A.O., DeLong, D.P., 2000. The design and operational characteristics of the CP&L/EPRI fish barn: a demonstration of recirculating aquaculture technology. Aquac. Eng. 22, 3–16.

Losordo, T.M., Timmons, M.B., 1994. An Introduction to Water Reuse Systems, in: Timmons, M.B., Losordo, T.M. (Eds.), Aquaculture Water Reuse Systems: Engineering Design and Management. Elsevier Science B.V., Amsterdam, pp. 1–8.

Losordo, T.M., Westers, H., 1994. System Carrying Capacity and Flow Estimation, in: Timmons, M.B., Losordo, T.M. (Eds.), Aquaculture Water Reuse Systems: Engineering Design and Management. Elsevier Science B.V., Amsterdam, pp. 9–60.

Lugert, V., Thaller, G., Tetens, J., Schulz, C., Krieter, J., 2016. A review on fish growth calculation: Multiple functions in fish production and their specific application. Rev. Aquac. 8, 30–42.

Machiels, M.A.M., Henken, A.M., 1986. A Dynamic Simulation Model for Growth of the African Catfish, Clark gariepinus (Burchell 1822) I I. Effect of Feeding Level on Growth and Energy Metabolism. Aquac. Elsevier Sci. Publ. B.V 56, 29–52.

Malone, R.F., Pfeiffer, T.J., 2006. Rating fixed film nitrifying biofilters used in recirculating aquaculture systems. Aquac. Eng. 34, 389–402.

Mariotti, F., Tomé, D., Mirand, P.P., 2008. Converting nitrogen into protein - Beyond 6.25 and Jones' factors. Crit. Rev. Food Sci. Nutr. 48, 177–184.

Mavinic, D.S., Bewtra, J.K., 1976. Efficiency of diffused aeration systems in wastewater treatment. Water Pollut. Control Fed. 48, 2273–2283.

McDonald, J., 2006. Alkalinity and pH Relationships, CSTN.

McMillan, J.., Wheaton, F.., Hochheimer, J.., Soares, J., 2003. Pumping effect on particle sizes in a recirculating aquaculture system. Aquac. Eng. 27, 53–59.

Mota, V.C., Limbu, P., Martins, C.I.M., Eding, E.H., Verreth, J.A.J., 2015. The effect of nearly closed RAS on the feed intake and growth of Nile tilapia (Oreochromis niloticus), African catfish (Clarias gariepinus) and European eel (Anguilla anguilla). Aquac. Eng. 68, 1–5.

MyAquaponics, 2019a. IP67 Waterproof D.O. (Dissolved Oxygen) Meter [WWW Document]. URL https://myaquaponics.co.za/ip67-waterproof-d-o-dissolved-oxygen-meter-including-do-probe (accessed 10.2.19).

MyAquaponics, 2019b. pH meter Pen, ph5, ph and temperature meter [WWW Document]. URL https://myaquaponics.co.za/digital-ph-temperature-meter-ph5/ (accessed 10.2.19).

Negroni, G., 2013. Tilapia Farming Guide. Tilapia farming Introd. 44 pp.

Nel Tanks, 2019. OnlineStore - 1000L Slim Storage Water [WWW Document]. URL https://www.neltanks.co.za/en/Shop/OnlineStore/1000L_Slim_Water?gclid=Cj0KCQjw4s7qBRCzARIsAImcAxYQt7XXRWfS8q9tNXGlXIVx7LEIPbfXow83TrxiFdThcFKLh5N4d6kaAtcxEALw_wcB (accessed 8.28.19).

NGMA, 2010. National Greenhouse Manufacturers Association standards for heat loss in greenhouse structures. Harrisburg.

Nijhof, M., 1995. Bacterial stratification and hydraulic loading effects in a plug-flow model for nitrifying trickling filters applied in recirculating fish culture systems. Aquaculture 134, 49–64.

Nijhof, M., Bovendeur, J., 1990. Fixed film nitrification characteristics in sea-water recirculation fish culture systems. Aquaculture 87, 133–143.

Ødegaard, H., 1995. Method for purification of water. 5,458,779.

Oluwaseyi, A.M., 2016. Application of dietary clay as feed additive on feed quality, water quality and production performance of African catfish (Clarias gariepinus). Stellenbosch University.

Palm, H.W., Knaus, U., Wasenitz, B., Bischoff, A.A., Strauch, S.M., 2018. Proportional up scaling of African catfish (Clarias gariepinus Burchell, 1822) commercial recirculating aquaculture systems disproportionally affects nutrient dynamics. Aquaculture 491, 155–168.

Palram, 2019. Multiwall Polycarbonate Sheets For Greenhouse [WWW Document]. URL https://www.palram.com/us/sub-product/thermaglas-polycarbonate-multi-wall/ (accessed 10.2.19).

Pfeiffer, T.J., Wills, P.S., 2011. Evaluation of three types of structured floating plastic media in moving bed biofilters for total ammonia nitrogen removal in a low salinity hatchery recirculating aquaculture system. Aquac. Eng. 45, 51–59.

Piedrahita, R.H., Seland, A., 1995. Calculation of pH in fresh and sea water aquaculture systems. Aquac. Eng. 14, 331–346.

Pruszyński, T., 2003. Effects of feeding on ammonium excretion and growth of the African catfish (Clarias gariepinus) fry. Czech J. Anim. Sci. 48, 106–112.

Pulkkinen, J.T., Kiuru, T., Aalto, S.L., Koskela, J., Vielma, J., 2018. Startup and effects of relative water renewal rate on water quality and growth of rainbow trout (Oncorhynchus mykiss) in a unique RAS research platform. Aquac. Eng. 82, 38–45.

Rahmatullah, R., Das, M., Rahmatullah, S.M., 2010. Suitable stocking density of tilapia in an aquaponic system. Fish. Res 14, 29–35.

Robinson, E.H., Li, M.H., 2010. Channel Catfish, Ictalurus punctatus, Size and Feed Conversion Ratio. J. World Aquac. Soc. 41, 829–833.

Rojas-Tirado, P., Pedersen, P.B., Pedersen, L.F., 2017. Bacterial activity dynamics in the water phase during start-up of recirculating aquaculture systems. Aquac. Eng. 78, 24–31.

Rusten, B., Eikebrokk, B., Ulgenes, Y., Lygren, E., 2006. Design and operations of the Kaldnes moving bed biofilm reactors. Aquac. Eng. 34, 322–331.

Rusten, B., Hem, L.J., Ødegaard, H., 1995. Nitrification of municipal wastewater in moving-bed biofilm reactors. Water Environ. Res. 67, 75–86.

Salhi, M., Bessonart, M., Chediak, G., Bellagamba, M., Carnevia, D., 2004. Growth, feed utilization and body composition of black catfish, Rhamdia quelen, fry fed diets containing different protein and energy levels. Aquaculture 231, 435–444.

SalmonBusiness, 2018. New land-based fish farm for sea trout planned in South Africa [WWW Document]. Press Release. URL https://salmonbusiness.com/new-land-based-farm-for-sea-trout-planned-in-south-africa/

SAURAN, 2019. Southern African Universities Radiometric Network [WWW Document]. URL http://www.sauran.net/ShowStation.aspx?station=4 (accessed 8.21.19).

Schneider, O., Sereti, V., Eding, E.H., Verreth, J.A.J., Klapwijk, B., 2007. Kinetics, design and biomass production of a bacteria reactor treating RAS effluent streams. Aquac. Eng. 36, 24–35.

Schram, E., Roques, J.A.C., Abbink, W., Spanings, T., de Vries, P., Bierman, S., de Vis, H. van, Flik, G., 2010. The impact of elevated water ammonia concentration on physiology, growth and feed intake of African catfish (Clarias gariepinus). Aquaculture 306, 108–115.

Schram, E., Roques, J.A.C., Abbink, W., Yokohama, Y., 2014. The impact of elevated water nitrate concentration on physiology , growth and feed intake of African catfish Clarias gariepinus (Burchell 1822). Aquac. Res. 1499–1511.

Schumann, M., Unger, J., Brinker, A., 2017. Floating faeces: Effects on solid removal and particle size distribution in RAS. Aquac. Eng. 78, 75–84.

Seshadri, K., Williams, F.A., 1978. Laminar flow between parallel plates with injection of a reactant at high reynolds number. Int. J. Heat Mass Transf. 21, 251–253.

Shah, M.M., 2014. Methods for Calculation of Evaporation from Swimming Pools and Other Water Surfaces (PREPRINT). ASHRAE Trans. 120, 1–15.

Shelton, J.L., Boyd, C.E., 1983. Correction Factors for Calculating Oxygen-Transfer Rates of Pond Aerators. Trans. Am. Fish. Soc. 112, 120–122.

Stechey, D.M., Trudell, Y., 1990. Aquaculture wastewater treatment: Wastewater characterization and development of appropriate technologies for the New Brunswick smolt production industry.

Stenstrom, M.K., Gilbert, R.G., 1981. Effects of alpha, beta and theta factor upon the design, specification and operation of aeration systems. Water Res. 15, 643–654.

Stokes, G.G., 1851. X. On the effect of internal friction of fluids on the motion of pendulums. Trans. Cambridge Philos. Soc. 9, 52.

Strauch, S.M., Wenzel, L.C., Bischoff, A., Dellwig, O., Klein, J., Schüch, A., Wasenitz, B., Palm, H.W., 2018. Commercial African Catfish (Clarias gariepinus) recirculating aquaculture systems: Assessment of element and energy pathways with special focus on the phosphorus cycle. Sustain. 10.

Stumm, W., Morgan, J.J., 1995. Aquatic Chemistry: Chemical Equilibria and Rates in Natural Waters, 3rd ed. John Wiley & Sons.

Suhr, K.I., Pedersen, P.B., 2010. Nitrification in moving bed and fixed bed biofilters treating effluent water from a large commercial outdoor rainbow trout RAS. Aquac. Eng. 42, 31–37.

Summerfelt, S.T., 2006. Design and management of conventional fluidized-sand biofilters. Aquac. Eng. 34, 275–302.

Summerfelt, S.T., Wilton, G., Roberts, D., Rimmer, T., Fonkalsrud, K., 2004. Developments in recirculating systems for Arctic char culture in North America. Aquac. Eng. 30, 31–71.

Suresh, A. V., Lin, C.K., 1992. Effect of stocking density on water quality and production of red tilapia in a recirculated water system. Aquac. Eng. 11, 1–22.

Swanepoel, J.C., 2017. Determination of bioavailability and bioactivity of enzymatically hydrolysed fish protein and phosphates in the African catfish Clarias gariepinus. Stellenbosch University.

Takealot, 2019. Speck pumps sand filter [WWW Document]. URL https://www.takealot.com/speck-pumps-aquaswim-filter-high-rate-sand-filter-2 (accessed 9.1.19).

Talamuk, R., 2016. Comparisons of Growth Performance of African Catfish Fingerlings Fed Different Inclusion Levels of Black Soldier Fly Larvae Meal Diets. Stellenbosch University.

Talati, S., 1988. Heat Loss in Aeration Tanks. University of California.

Terjesen, B.F., Summerfelt, S.T., Nerland, S., Ulgenes, Y., Fjæra, S.O., Megård Reiten, B.K., Selset, R., Kolarevic, J., Brunsvik, P., Bæverfjord, G., Takle, H., Kittelsen, A.H., Åsgård, T., 2013. Design, dimensioning, and performance of a research facility for studies on the requirements of fish in RAS environments. Aquac. Eng. 54, 49–63.

Timmons, M.B., 1994. Use Of Foam Fractionators in Aquaculture, in: Timmons, M.B., Losordo, T.M. (Eds.), Aquaculture Water Reuse Systems: Engineering Design and Management. Elsevier Science B.V., Amsterdam, pp. 247–280.

Timmons, M.B., Ebeling, J.M., 2007. Recirculating Aquaculture. Cayuga Aqua Ventures.

Tomasso, J.R., Simco, B.A., Davis, K.B., 1979. Chloride Inhibition of Nitrite-Induced Methemoglobinemia in Channel Catfish (Icalurus punctatus). J. Fish. Res. Board Canada 36, 1141–1144.

Torreele, E., Sluiszen, A. van Der, Verreth, J., 1993. The effect of dietary L-carnitine on the growth performance in fingerlings of the african catfish (Clarias gariepinus) in relation to dietary lipid. Br. J. Nutr. 69, 289–299.

Tran-Duy, A., Schrama, J.W., van Dam, A.A., Verreth, J.A.J., 2008. Effects of oxygen concentration and body weight on maximum feed intake, growth and hematological parameters of Nile tilapia, Oreochromis niloticus. Aquaculture 275, 152–162.

Unger, J., Brinker, A., 2013. Floating feces: A new approach for efficient removal of solids in aquacultural management. Aquaculture 404–405, 85–94.

Vaisala, 2013. Humidity conversion formulas - Calculation formulas for humidity. Helsinki.

van de Nieuwegiessen, P.G., Boerlage, A.S., Verreth, J.A.J., Schrama, J.W., 2008. Assessing the effects of a chronic stressor, stocking density, on welfare indicators of juvenile African catfish, Clarias gariepinus Burchell. Appl. Anim. Behav. Sci. 115, 233–243.

van de Nieuwegiessen, P.G., Olwo, J., Khong, S., Verreth, J.A.J., Schrama, J.W., 2009. Effects of age and stocking density on the welfare of African catfish, Clarias gariepinus Burchell. Aquaculture 288, 69–75.

Van Gorder, S.D., Jug-Dujakovic, J., 2004. Performance characteristics of rotating biological contactors within two commercial recirculating aquaculture systems, in: Proceedings of the Fifth International Conference on Recirculating Aquaculture. pp. 22–24.

Van Rijn, J., 2013. Waste treatment in recirculating aquaculture systems. Aquac. Eng. 53, 49–56.

van Weerd, J.H., Khalaf, K.H.A., Aartsen, F.J., Tijssen, P.A.T., 2003. Balance trials with African catfish Clarias gariepinus fed phytase-treated soybean meal-based diets. Aquac. Nutr. 5, 135–142.

Vinci, B.J., Timmons, M.B., Summerfelt, S.T., Watten, B.J., 1996. Carbon Dioxide Control in Intensive Aquaculture: Design Tool Development. AES Tech. Sess. 1 Open Pap.

Watanabe, W.O., Losordo, T.M., Fitzsimmons, K., Hanley, F., 2002. Tilapia Production Systems in the Americas: Technological Advances, Trends, and Challenges. Rev. Fish. Sci. 10, 465–498.

Watten, B.J., 1994. Aeration and Oxygenation, in: Timmons, M.B., Losordo, T.M. (Eds.), Aquaculture Water Reuse Systems: Engineering Design and Management. Elsevier Science B.V., Amsterdam, pp. 173–208.

Weitkamp, D.E., Katz, M., 1980. A review of dissolved gas supersaturation literature. Trans. Am. Fish. Soc. 109, 659–702.

Wheaton, F.., Hochheimer, J.., Kaiser, G.E., Krones, M.J., Libey, G.S., Easter, C.C., 1994a. Nitrification filter principles, in: Timmons, M.B., Losordo, T.M. (Eds.), Aquaculture Water Reuse Systems: Engineering Design and Management. Elsevier Science B.V., Amsterdam, pp. 101–126.

Wheaton, F.., Hochheimer, J., Kaiser, G.E., Malone, R.F., Krones, M.J., Libey, G.S., Easter, C.C., 1994b. Nitrification Filter Design Methods, in: Timmons, M.B., Losordo, T.M. (Eds.), Aquaculture Water Reuse Systems: Engineering Design and Management. Elsevier Science B.V., Amsterdam, pp. 127–172.

Wik, T., 1999. On Modeling the Dynamics of Fixed Biofilm Reactors. Chalmers University of

Technology.

Wik, T., Lindén, B., 2004. Modeling, control and simulation of recirculating aquaculture systems. IFAC Proc. Vol. 37, 141–146.

Wik, T.E.I., Lindén, B.T., Wramner, P.I., 2009. Integrated dynamic aquaculture and wastewater treatment modelling for recirculating aquaculture systems. Aquaculture 287, 361–370.

Wills, B.A., Finch, J.A., 2016. Wills' Mineral Processing Technology, 8th ed. Elsevier Ltd.

Wong, K.B., Piedrahita, R.H., 2000. Settling velocity characterization of aquacultural solids. Aquac. Eng. 21, 233–246.

World Bank, 2011. The global program on fisheries: Strategic vision for fisheries and aquaculture.

Wortman, B., Wheaton, F., 1991. Temperature effects on biodrum nitrification. Aquac. Eng. 10, 183–205.

Yogev, U., Sowers, K.R., Mozes, N., Gross, A., 2017. Nitrogen and carbon balance in a novel near-zero water exchange saline recirculating aquaculture system. Aquaculture 467, 118–126.

Zhang, N., Wang, Z., 2017. Review of soil thermal conductivity and predictive models. Int. J. Therm. Sci. 117, 172–183.

Zhang, S.Y., Li, G., Wu, H.B., Liu, X.G., Yao, Y.H., Tao, L., Liu, H., 2011. An integrated recirculating aquaculture system (RAS) for land-based fish farming: The effects on water quality and fish production. Aquac. Eng. 45, 93–102.

Zhu, S., Chen, S., 2002. The impact of temperature on nitrification rate in fixed film biofilters. Aquac. Eng. 26.

Zhu, S., Chen, S., 2001. Effects of organic carbon on nitrification rate in fixed film biofilters. Aquac. Eng. 25, 1–11.

APPENDIX A : Design variables

The chosen input variables for the design as well as most important output variables are shown in Table A-1.

Table A-1: Input and output variables of the final RAS design

Variable	Value	Units	Variable type
Fish tanks			
Number of fish tanks	72		Input
Tank width	0.39	m	Input
Tank length	0.70	m	Input
Tank depth	0.33	m	Input
Tank volume – Individual	0.090	m^3	Input
Tank volume – Total	6.49	m^3	Input
Fish production			
Temperature growth coefficient (TGC)	0.00121	$g^{1/3}/^oC.day$	Input
Mortality rate (k_{death})	0.00296	1/day	Input
Production duration	91	days	Input
Fish mass – Initial (Individual)	10	g	Input
Fish mass – Final (Individual)	135	g	Output
Fish mass – Initial (Total)	31.5	kg	Output
Fish mass – Final (Total)	324	kg	Output
Stocking density – Initial	4.9	kg/m^3	Output
Stocking density – Final	50	kg/m^3	Input
Number of fish – Initial (Total)	3 150		Output
Number of fish – Initial (Per tank)	44		Output
Number of fish – Initial (Total)	2 406		Output
Number of fish – Initial (Per tank)	33		Output
Fish weight gain – Final (Individual)	2.56	g	Output
Fish weight gain – Final (Total)	6 160	g	Output
Feeding			
Feed composition – Protein	0.45	g/g feed	Input
Feed composition – Carbohydrates	0.14	g/g feed	Input
Feed composition – Fat	0.24	g/g feed	Input
Feed composition – Ash	0.08	g/g feed	Input
Feed composition – Water	0.09	g/g feed	Input
Feed lost to water	0.01	g/g feed	Input
Feed conversion ratio (FCR)	1.5	g dry feed/g weight gain	Input
Feeding rate – Peak (Total)	10.3	kg feed/day	Output
Feeding rate – Peak (Per tank)	142	g feed/day	Output
Water quality parameters in fish tanks			
Temperature	27	^oC	Input
Dissolved oxygen	≥ 5	mg/L	Input
Total ammonia nitrogen (TAN)	≤ 3	mg/L	Input
Dissolved CO_2	≤ 15	mg/L	Input
Total suspended solids (TSS)	≤ 10	mg/L	Input
Nitrate nitrogen (NO_3–N)	≤ 140	mg/L	Input

Table A-1: Input and output variables of the final RAS design (cont.)

Variable	Value	Units	Variable type
Waste production + Oxygen consumption			
TAN production ratio	0.047	g TAN/g feed consumed	Input
TAN production – Peak	505	g TAN/day	Output
TSS production ratio	0.25	g TSS/g dry feed fed	Input
TSS production – Peak	2 333	g TSS/day	Output
DOM to POM production ratio	0.54	g DOM/g POM	Input
COD to organic matter ratio	1.4	g COD/g organic matter	Input
BOD_5 to COD ratio	0.80	g BOD_5/g COD	Input
POM production – Peak	2 333	g/day	Output
DOM production – Peak	1 256	g/day	Output
Oxygen consumption by fish – Peak	2 538	g O_2/day	Output
Oxygen consumption by heterotrophic bacteria – Peak	1 930	g O_2/day	Output
Oxygen consumption by autotrophic bacteria – Peak	2 028	g O_2/day	Output
Carbon dioxide production by fish – Peak	3 490	g CO_2/day	Output
Solids removal – Lamella settler			
Number of lamella settlers	1		Input
Number of settling plates	8		Input
Plate width	2	m	Input
Plate length	0.6	m	Input
Plate angle	55	degrees	Input
Parallel space between plates	50	mm	Input
Horizontal space between plates	60	mm	Output
Cross sectional area of 1 plate space	0.1	m^2	Output
Hydraulic diameter of 1 plate space	50	mm	Output
Flow rate (total)	12	m^3/h	Output
Flow rate (per plate)	1.5	m^3/h	Output
Reynolds number	244		Output
Flow regime	Laminar		Output
Horizontally projected settling area	5.5	m^2	Output
Overflow rate	0.06	cm/s	Output
TSS removal efficiency	80%		Output
TSS outlet concentration	2	mg/L	Output
Smallest particle size removed	70	µm	Output
Biofiltration – Moving bed bioreactors			
Biomedia specific biofilm surface area	300	m^2/m^3	Input
Biomedia void fraction	50%		Input
Percentage filling with biomedia	65%		Input
MBBR oxygen concentration	4.5	mg/L	Input
Number of MBBRs	6		Output
Reactor volume – Individual	1.0	m^3	Input
Reactor volume – Total	6.0	m^3	Output
Biomedia volume	3.9	m^3	Output
Biofilm area	1170	m^2	Output
TAN removal efficiency	95.4%		Output
MBBR outlet concentration	0.14	mg/L	Output
BOD_5 loading (Organic loading)	1.6	g O_2/day	Output
Nitrification rate (TAN diffusion limited)	0.41	g TAN/(m^2.day)	Output
Nitrification rate (Oxygen diffusion limited)	1.47	g TAN/(m^2.day)	Output
Rate limiting substrate	Ammonium		Output
Volumetric flow rate	12	m^3/h	Output
MBBR residence time	52	minutes	Output
TAN concentration in the fish tanks	3.0	mg/L	Output

Table A-1: Input and output variables of the final RAS design (cont.)

Variable	Value	Units	Variable type
Aeration – Fish tanks			
DO saturation % in tank	60%		Input
Water depth	0.33	m	Input
Absorption efficiency	0.5%		Output
Aeration – Moving bed bioreactors			
DO saturation % in tank	54%		Input
Water depth	2.20	m	Input
Absorption efficiency	3.2%		Output
RAS general			
Recirculation flow rate	12	m^3/h	Output
Peak make-up water flow rate	0.14	m^3/h	Output
Recycle percentage at peak make-up ((Q_{recirc} - $Q_{make-up}$) / Q_{recirc})	99%		Output

APPENDIX B : Equipment data sheets

B.1. Lamella settler data sheet

Table B-1: Lamella settler data sheet

Parameter	Value	Units
Number of lamella settlers	1	
Number of settling plates	8	
Plate width	2	m
Plate length	0.6	m
Plate angle	55	degrees
Parallel space between plates	50	mm
Horizontal space between plates	60	mm
Horizontally projected settling area	5.5	m^2
Overflow rate	0.06	cm/s
TSS removal efficiency	80%	
Number of inlet pipes	8	
Inlet pipe connection diameter	63	mm
Number of overflow pipes	4	
Overflow pipe connection diameter	63	mm
Number of sludge collection points	4	

B.2. Moving bed bioreactor data sheet

Table B-2: Moving bed bioreactor data sheet

Parameter	Value	Units
Number of moving bed bioreactors	6	
Tank volume	1 000	L
Tank height	2.23	m
Tank diameter	0.75	m
Tank wall material	LLDPE	
Tank wall thickness	4	mm
Biomedia specific biofilm surface area	300	m^2/m^3
Biomedia void fraction	50%	
Percentage filling with biomedia	65%	
MBBR oxygen concentration	4.5	mg/L
Biofilm area	1170	m^2
Air flow per MBBR	4.2	m^3/h
Number of submerged air diffusers per MBBR	6	
Number of water inlet pipes	1	
Inlet pipe connection diameter	63	mm
Number of water overflow pipes	1	
Overflow pipe connection diameter	63	mm

B.3. Blower data sheet

Table B-3: Blower data sheet

Parameter	Value	Units
Model number	ZXB 710-7AH26	
Frequency	50	Hz
Rated output	3.0	kW
Rated voltage	200-240Δ / 345-415Y	V
Rated current	12.5Δ /7.2Y	A
Approximate weight	36	kg
Sound pressure level	69	dB(A)
Maximum airflow	318	m^3/h
Maximum vacuum	-270	mbar
Maximum pressure	290	mbar
Discharge pipe connection diameter	50	mm

B.4. Heat pump data sheet

Table B-4: Heat pump data sheet

Parameter	Value	Units
Heating capacity	9.2	kW
Heating power input	1.5	kW
Frequency	50	Hz
Rated voltage	230	V
Rated current	6.7	A
Number of compressors	1	
Compressor type	Rotary	
Heat exchanger type	Titanium in PVC	
Number of fans	1	
Fan power input	120	W
Fan rotate speed	850	RPM
Fan direction	Horizontal	
Noise level	51	dB(A)
Water inlet and outlet connection diameter	50	mm
Water side flow rate	3	m^3/h
Water side pressure drop	6	kPa
Heat pump length	956	mm
Heat pump width	334	mm
Heat pump height	600	mm
Heat pump weight	51	kg

B.5. Pump and blower performance curves

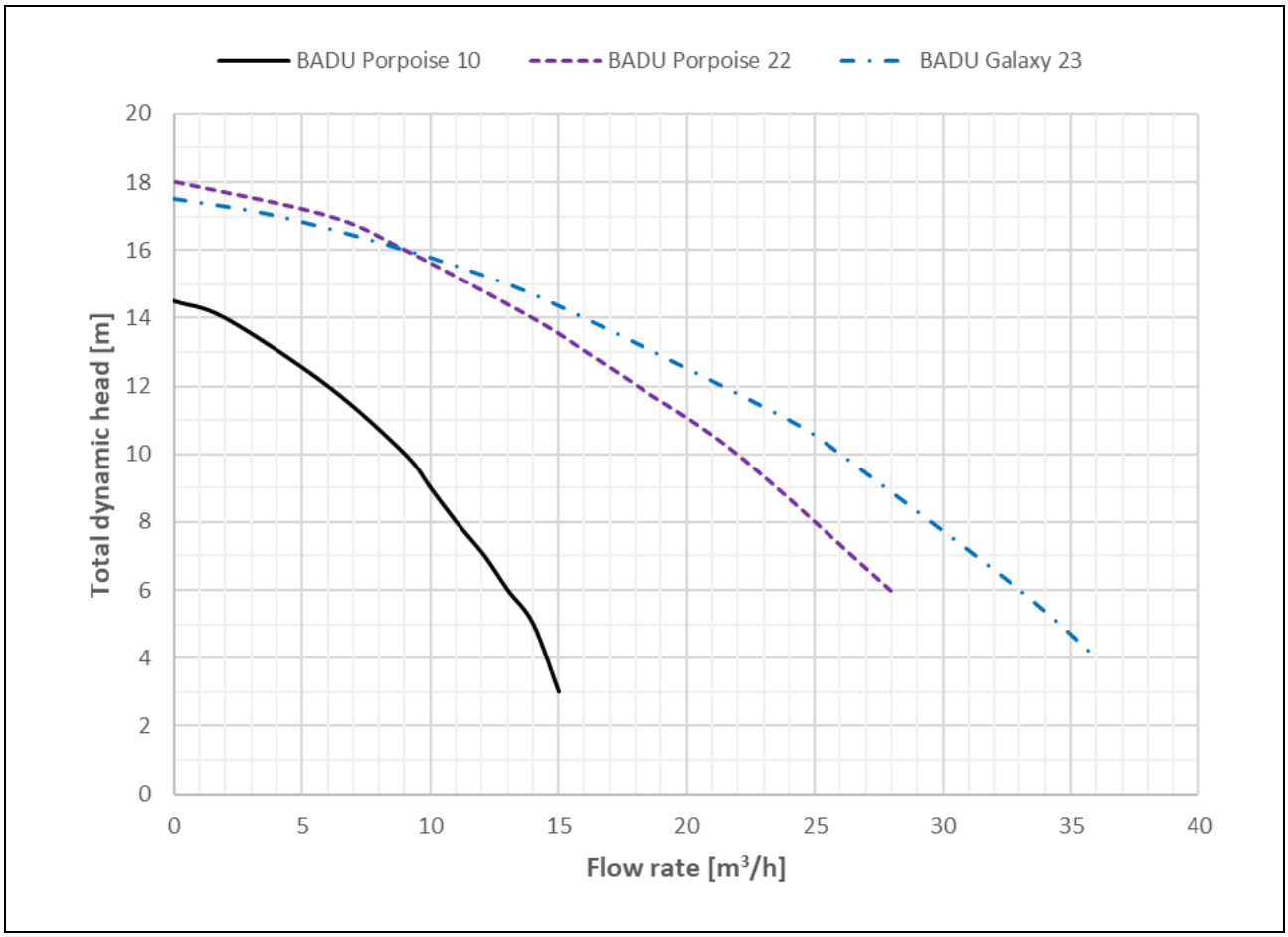

Figure B-1: BADU Porpoise 10, Porpoise 22 and Galaxy 23 pump performance curves

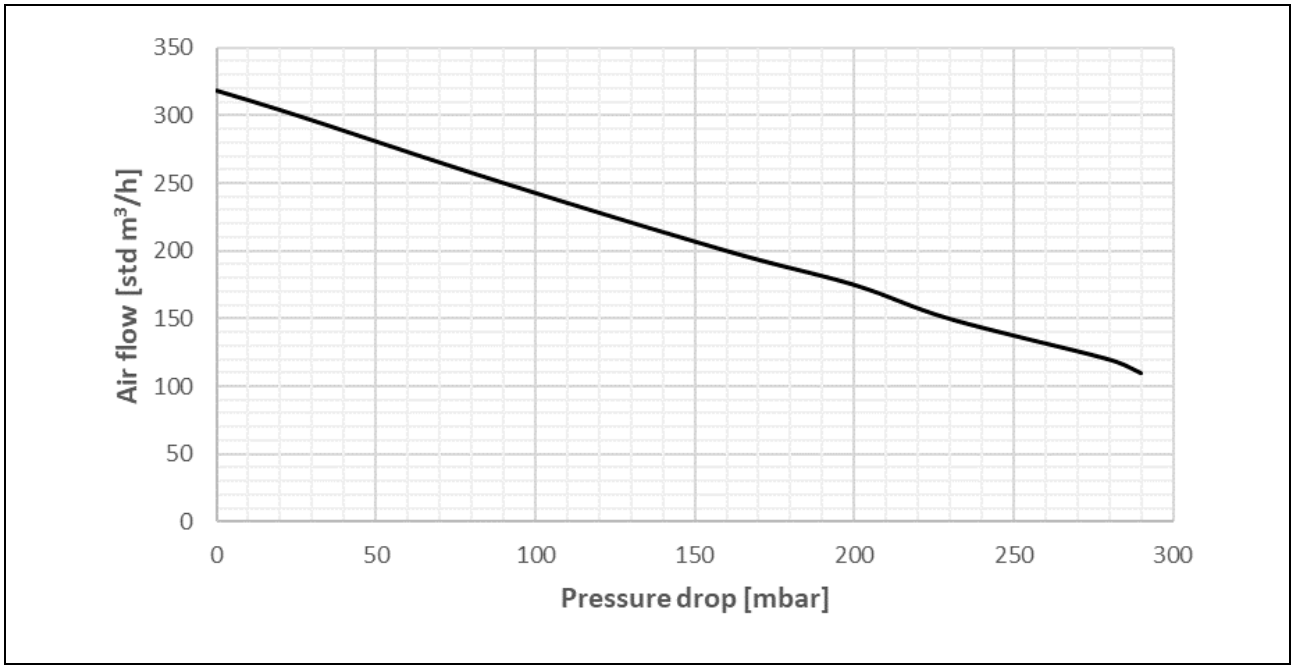

Figure B-2: CFW Fans regenerative blower model ZXB 710-3.0kW-50Hz performance curve

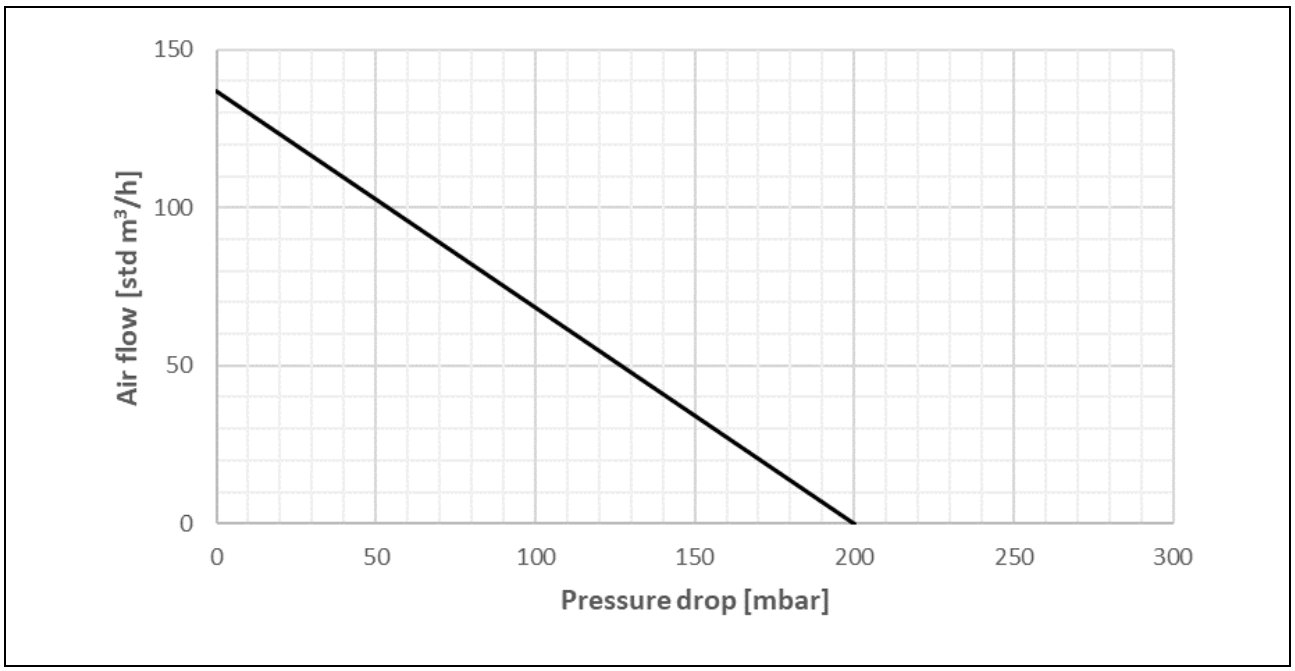

Figure B-3: SCL V4 1.1kW-50Hz regenerative blower performance curve

APPENDIX C : Piping and instrumentation diagrams (P&IDs)

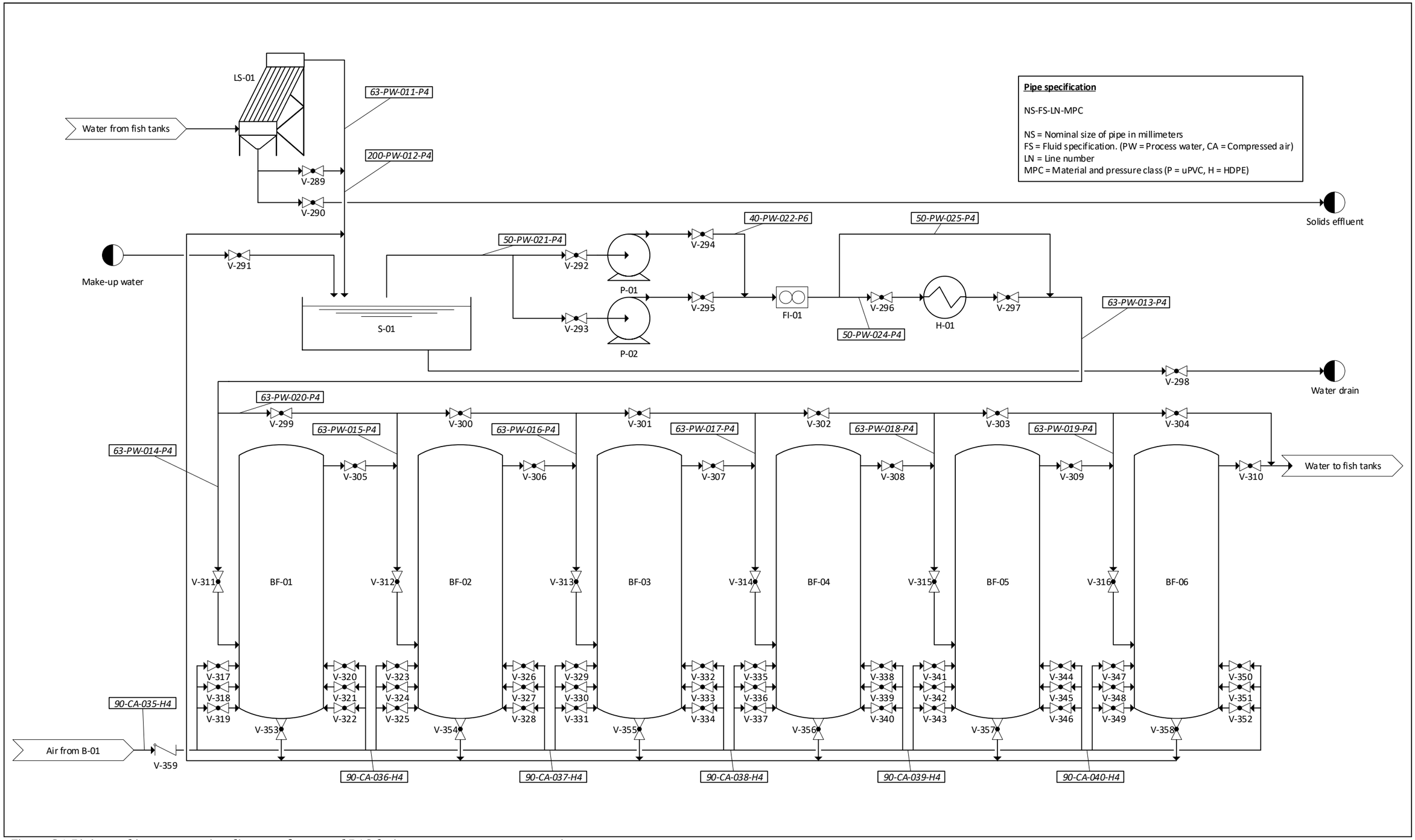

Figure C-1: Piping and instrumentation diagram of proposed RAS design wastewater treatment section

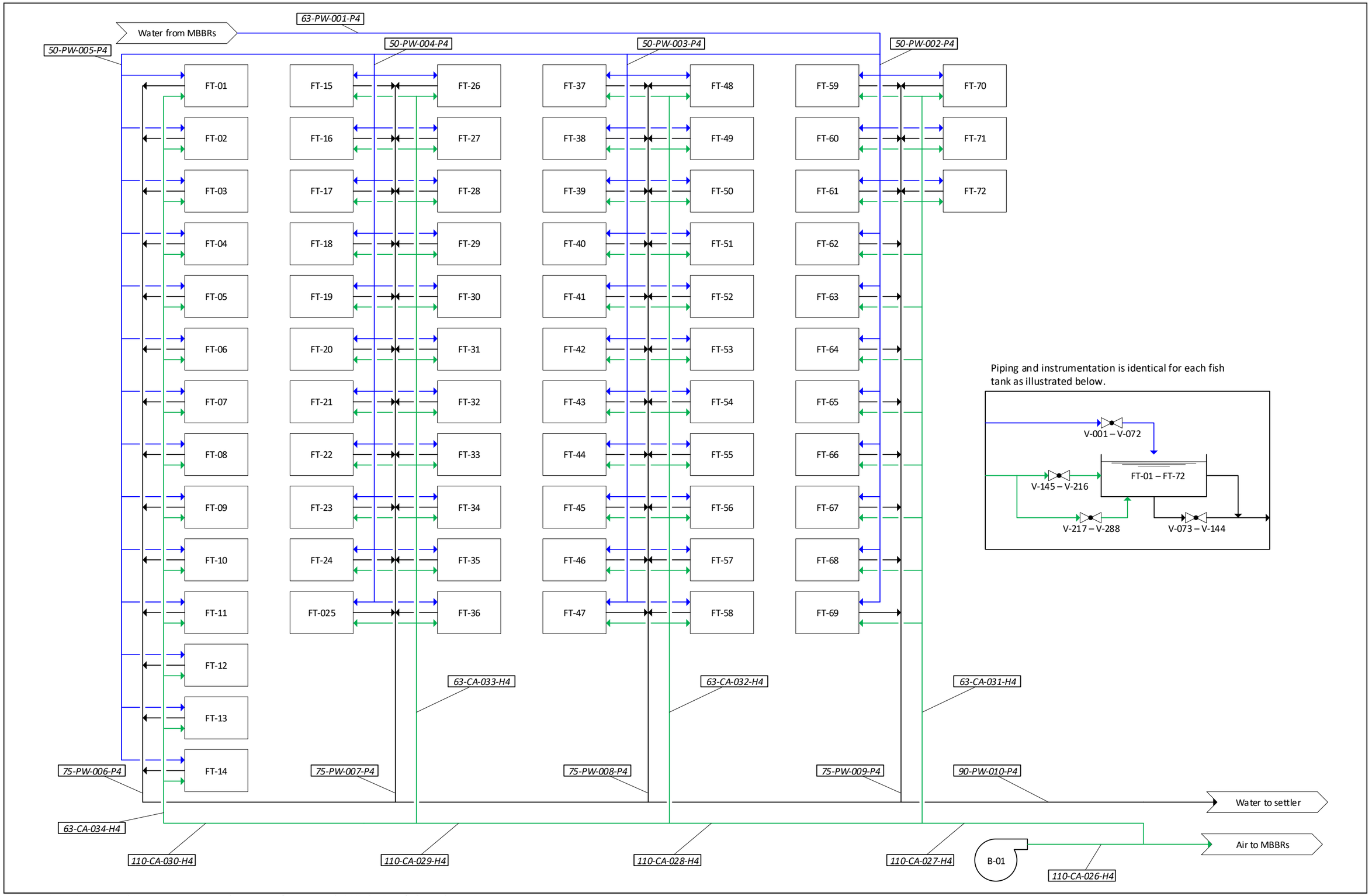

Figure C-2: Piping and instrumentation diagram of proposed RAS design fish tank section

APPENDIX D : Bill of quantities

Table D-1: Bill of quantities for the proposed RAS design (pipes, pipe fittings and valves)

Item	Item ID	Type	Location	Qty units	Qty	Cost per unit [ZAR]	Cost [ZAR]	Source
uPVC pipe, class 4, OD = 63 mm, wall thickness = 1.5 mm	63-PW-001-P4	Pipe	BF-06 to fish tanks	m	11.25	50.60	569.25	Effast
uPVC pipe, class 4, OD = 50 mm, wall thickness = 1.5 mm	50-PW-002-P4 50-PW-003-P4 50-PW-004-P4 50-PW-005-P4	Pipe	Fish tank rows return	m	22.1	43.70	965.77	Effast
uPVC pipe, class 16, OD = 25 mm, wall thickness = 1.9 mm		Pipe	Fish tank inlet	m	14.4	23.00	331.20	Effast
Ball valve 25 mm	V-001 to V-072	Valve	Fish tank inlet	#	72	24.15	1 738.80	Effast
Ball valve 25 mm	V-073 to V-144	Valve	Fish tank drain	#	72	24.15	1 738.80	Effast
90° elbow PVC fitting 25 mm		Pipe fitting	Fish tank drain	#	72	11.21	807.30	Effast
uPVC pipe, class 16, OD = 25 mm, wall thickness = 1.9 mm		Pipe	Fish tank drain	m	72	23.00	1 656.00	Effast
90° elbow PVC fitting 25 mm		Pipe fitting	Fish tank overflow	#	288	11.21	3 229.20	Effast
uPVC pipe, class 16, OD = 25 mm, wall thickness = 1.9 mm		Pipe	Fish tank overflow	m	72	23.00	1 656.00	Effast
uPVC pipe, class 4, OD = 75 mm, wall thickness = 1.5 mm	75-PW-006-P4 75-PW-007-P4 75-PW-008-P4 75-PW-009-P4	Pipe	Fish tank rows effluent	m	22.1	1.16	25.53	Effast
uPVC pipe, class 4, OD = 90 mm, wall thickness = 1.8 mm	90-PW-010-P4	Pipe	Fish tank to lamella settler	m	8	73.00	584.00	Effast
uPVC pipe, class 4, OD = 63 mm, wall thickness = 1.5 mm		Pipe	Lamella settler inlet	m	4	50.60	202.40	Effast
90° elbow PVC fitting 63 mm		Pipe fitting	Lamella settler inlet	#	3	41.29	123.86	Effast
90° tee PVC fitting 63 mm		Pipe fitting	Lamella settler inlet	#	7	56.81	397.67	Effast
uPVC pipe, class 4, OD = 63 mm, wall thickness = 1.5 mm	63-PW-011-P4	Pipe	Lamella settler overflow	m	10	50.60	506.00	Effast
90° elbow PVC fitting 63 mm		Pipe fitting	Lamella settler overflow	#	14	41.29	577.99	Effast
90° tee PVC fitting 63 mm		Pipe fitting	Lamella settler overflow	#	2	56.81	113.62	Effast
Solids flushing ball valve 63 mm	V-290	Valve	Lamella settler drain	#	4	111.55	446.20	Effast
Drain ball valve 63 mm	V-289	Valve	Lamella settler drain	#	4	111.55	446.20	Effast
uPVC pipe, class 4, OD = 50 mm, wall thickness = 1.5 mm	50-PW-021-P4	Pipe	Recirculation pumps inlet	m	0.5	43.70	21.85	Effast

Table D-1: Bill of quantities for the proposed RAS design (pipes, pipe fittings and valves) (cont.)

Item	Item ID	Type	Location	Qty units	Qty	Cost per unit [ZAR]	Cost [ZAR]	Source
Ball valve 50 mm	V-292, V-293	Valve	Recirculation pumps inlet	#	2	83.95	167.90	Effast
uPVC pipe, class 6, OD = 40 mm, wall thickness = 1.5 mm	40-PW-022-P6	Pipe	Recirculation pumps outlet	m	1.5	26.45	39.68	Effast
Ball valve 40 mm	V-294, V-295	Valve	Recirculation pumps outlet	#	2	55.20	110.40	Effast
Flowmeter 40 mm, range = 0 L/h - 16 000 L/h	FI-01	Meter	FI-01	#	1	3 400.00	3 400.00	J. Gey Van Pittius
Ball valve 50 mm	V-296	Valve	H-01 inlet	#	1	83.95	83.95	Effast
Ball valve 50 mm	V-297	Valve	H-01 outlet	#	1	83.95	83.95	Effast
uPVC pipe, class 4, OD = 50 mm, wall thickness = 1.5 mm	50-PW-025-P4	Pipe	H-01 bypass	m	1	43.70	43.70	Effast
uPVC pipe, class 4, OD = 63 mm, wall thickness = 1.5 mm	63-PW-014-P4	Pipe	H-01 to BF-01	m	5	50.60	253.00	Effast
90° elbow PVC fitting 63 mm		Pipe fitting	H-01 to BF-01	#	3	41.29	123.86	Effast
uPVC pipe, class 4, OD = 63 mm, wall thickness = 1.5 mm	63-PW-015-P4 63-PW-016-P4 63-PW-017-P4 63-PW-018-P4 63-PW-019-P4	Pipe	MBBR connections	m	10	50.60	506.00	Effast
90° elbow PVC fitting 63 mm		Pipe fitting	MBBR connections	#	10	41.29	412.85	Effast
Ball valve 63 mm	V-305, V-306, V-307, V-308, V-309, V-310, V-311, V-312, V-313, V-314, V-315, V-316	Valve	MBBR connections	#	12	111.55	1 338.60	Effast
uPVC pipe, class 4, OD = 63 mm, wall thickness = 1.5 mm	63-PW-020-P4	Pipe	MBBR bypass	m	6	50.60	303.60	Effast
Ball valve 63 mm	V-299, V-300, V-301, V-302, V-303, V-304	Valve	MBBR bypass	#	6	111.55	669.30	Effast
Ball valve 25 mm	V-353, V-354, V-355, V-356, V-357, V-358	Valve	MBBR drain	#	6	24.15	144.90	Effast
HDPE (PE63), class 4, OD = 90 mm, wall thickness = 3.5 mm	90-CA-035-H4 90-CA-036-H4 90-CA-037-H4 90-CA-038-H4 90-CA-039-H4 90-CA-040-H4	Pipe	MBBR aeration	m	6	33.67	202.00	Plastic Man Pipes
Air tap	V-317 to V-352	Valve	MBBR aeration	#	36	8.00	288.00	Ecotao
HDPE (PE63), class 4, OD = 110 mm, wall thickness = 4.2 mm	110-CA-026-H4 110-CA-027-H4 110-CA-028-H4 110-CA-029-H4 110-CA-030-H4	Pipe	Fish tank aeration	m	8.6	51.01	438.69	Plastic Man Pipes
HDPE (PE63), class 4, OD = 63 mm, wall thickness = 2.5 mm	63-CA-031-H4 63-CA-032-H4 63-CA-033-H4 63-CA-034-H4	Pipe	Fish tank aeration	m	22.5	17.00	382.58	Plastic Man Pipes
Air tap	V-145 to V-288	Valve	Fish tank aeration	#	144	8.00	1 152.00	Ecotao

APPENDIX E : Carbonate reaction equilibria

Carbon dioxide gas dissolved in water ($CO_{2(aq)}$) can react with water in a series of hydration and acid-base reactions to form $H_2CO_{3(aq)}$, $HCO_{3(aq)}^-$ and $CO_{3(aq)}^{2-}$ (Stumm and Morgan, 1995).

Carbonic acid is often represented by $H_2CO_3^*$ which includes both carbonic acid and dissolved carbon dioxide:

$$[H_2CO_3^*] = [H_2CO_{3(aq)}] + [CO_{2(aq)}]$$

The following equilibrium reactions describe the carbonate equilibria of the water (McDonald, 2006; Stumm and Morgan, 1995).

Reaction 1:	$H_2CO_3^* \leftrightarrow HCO_{3(aq)}^- + H_{(aq)}^+$	occurs at 4.3 < pH < 8.3
Reaction 2:	$HCO_{3(aq)}^- \leftrightarrow CO_{3(aq)}^{2-} + H_{(aq)}^+$	occurs at 8.3 < pH < 10.2
Reaction W:	$H_2O_{(l)} \leftrightarrow OH_{(aq)}^- + H_{(aq)}^+$	occurs at pH > 10.2

APPENDIX F : Gas properties

F.1. Nitrogen and oxygen properties

Table F-1: Nitrogen solubilities at different partial pressures, nitrogen and oxygen gas tension factors (Watten, 1994)

Water temperature [°C]	N_2 solubility @ 760mmHg [mg/L]	N_2 solubility @ 600mmHg [mg/L]	N_2 gas tension factor [mmHg/(mg/L)]	O_2 gas tension factor [mmHg/(mg/L)]
20	19.5	15.4	39.0	17.1
21	19.2	15.2	39.6	17.4
22	18.9	14.9	40.3	17.8
23	18.6	14.7	40.9	18.1
24	18.3	14.5	41.5	18.4
25	18.0	14.2	42.2	18.7
26	17.8	14.0	42.8	19.0
27	17.5	13.8	43.4	19.3
28	17.3	13.7	44.0	19.6
29	17.0	13.5	44.6	19.9
30	16.8	13.3	45.2	20.2

F.2. Air and water vapour properties

The absolute humidity was estimated using equation (F.1) for a known air temperature and relative humidity (Vaisala, 2013).

$$\mathcal{H} = 2.16679 \cdot \left(10^{\left(8.10765 - \frac{1750.286}{T_{air}+235}\right)} \cdot 133.322\right) \cdot \frac{\mathcal{R}}{T_{air} + 273.15} \quad \textbf{(F.1)}$$

where

$\mathcal{H}$ = Absolute humidity $[g\ H_2O/m^3]$

T_{air} = Air temperature [°C]

$\mathcal{R}$ = Relative humidity

The mixing ratio was calculated using equation (F.2) for a known air temperature, relative humidity and absolute air pressure (Vaisala, 2013).

$$x = 621.9907 \cdot \left(10^{\left(8.10765 - \frac{1750.286}{T_{air}+235}\right)} \cdot 133.322\right) \cdot \frac{\mathcal{R}}{P - \mathcal{R} \cdot \left(10^{\left(8.10765 - \frac{1750.286}{T_{air}+235}\right)} \cdot 133.322\right)} \quad \textbf{(F.2)}$$

where

x = Mixing ratio $[g\ H_2O/kg\ dry\ air]$

P = Absolute air pressure $[Pa]$

The relative humidity was calculated using equation (F.3) for a known air temperature, absolute air pressure and mixing ratio.

$$\mathcal{R} = x \cdot \frac{P}{\left(10^{\left(8.10765 - \frac{1750.286}{T_{air}+235}\right)} \cdot 133.322\right) \cdot (x + 621.9907)} \quad \textbf{(F.3)}$$

The ideal gas properties of air is given in Table F-2 (Cengel and Boles, 2015).

Table F-2: Ideal gas properties of air (Cengel and Boles, 2015)

Air temperature [K]	**Enthalpy** [kJ/kg]	**Relative pressure**
270	270.11	0.9590
280	280.13	1.0889
285	285.14	1.1584
290	290.16	1.2311
295	295.17	1.3068
300	300.19	1.3860
305	305.22	1.4686
310	310.24	1.5546
315	315.27	1.6442
320	320.29	1.7375

APPENDIX G : Lamella settler design

The stainless steel of grade 304 (304SS) specified for the lamella settler shell and plates is to be welded together. The 304SS sheets are 2.0mm thick, 3000mm long and 1500mm wide. Four sheets will be required to cut out all the required pieces that are to be welded together as determined by the proposed cutting layout illustrated in Figure G-1.

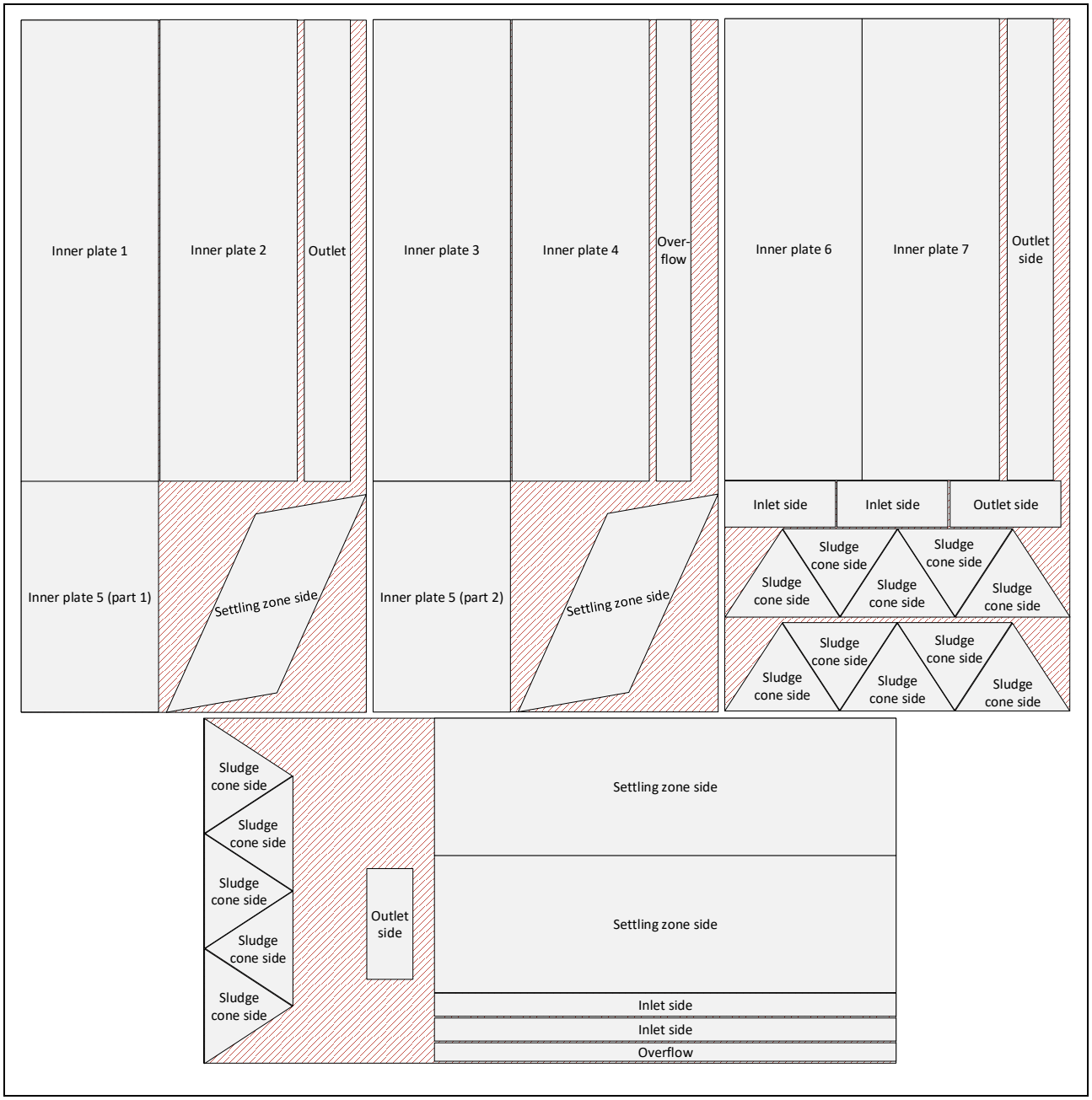

Figure G-1: Lamella settler sheet metal cutting pattern on four 3000mm x 1500mm 304SS sheets

The dimensions of the lamella settler seen from the side is given in Figure G-2.

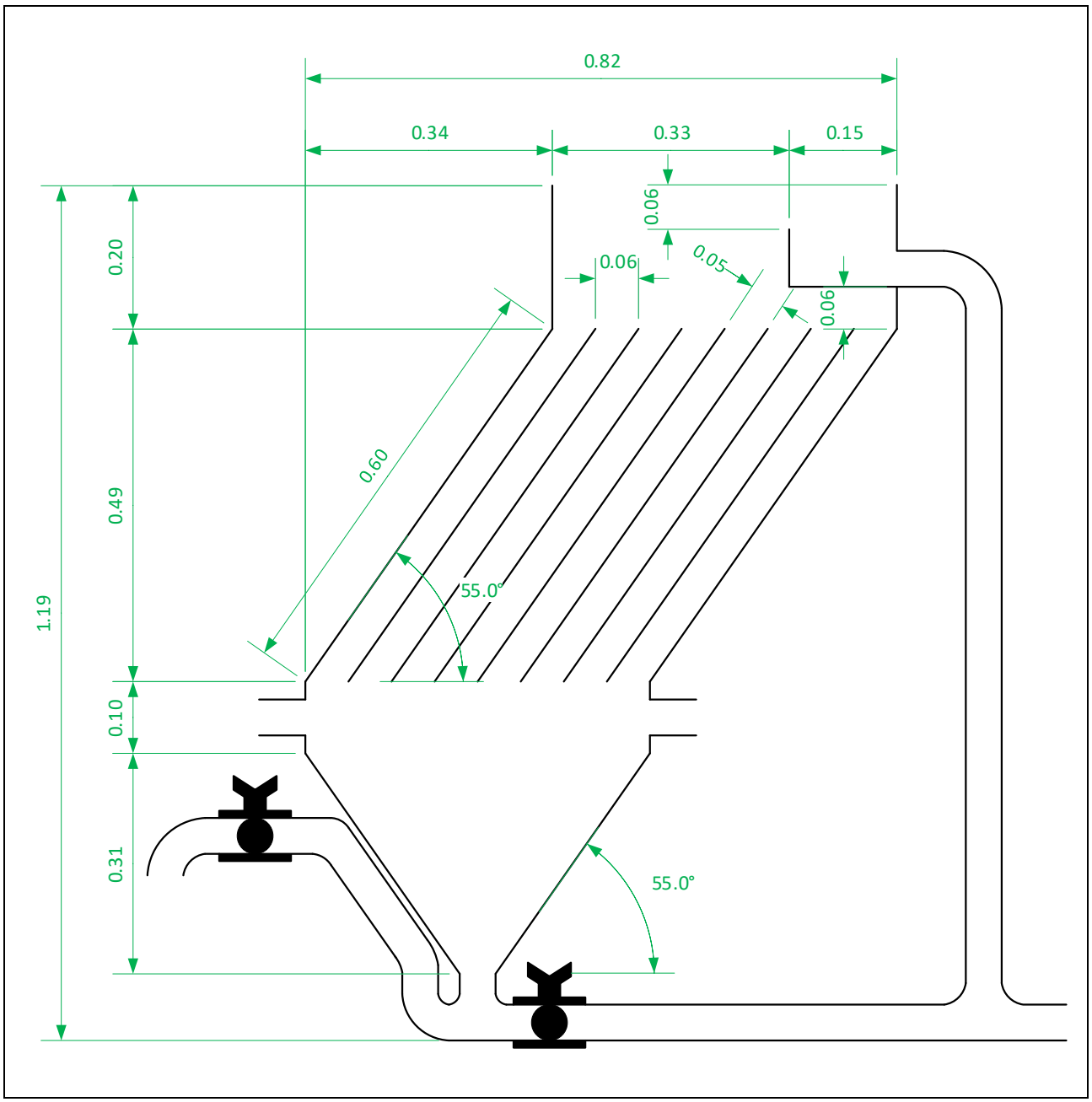

Figure G-2: Lamella settler dimensions

APPENDIX H : MBBR oxygen concentration optimization

Table H-1: Calculation results of blower operating costs

MBBR DO [mg/L]	MBBR Transfer efficiency (N) [lb/hp.h]	MBBR Air per mass oxygen supplied [m^3/lb]	MBBR Aeration rate [m^3/h]	MBBR Blower power [kW]	Fish Tank Aeration rate [m^3/h]	Fish Tank Blower power [kW]	Blower operating cost [ZAR/year]
2	0.87	33	10	0.4	94	0.7	11 307
2.5	0.80	35	11	0.4	91	0.7	11 519
3	0.74	36	12	0.5	88	0.7	11 806
3.5	0.68	39	13	0.6	85	0.7	12 189
4	0.61	41	14	0.6	82	0.7	12 700
4.5	0.55	51	18	0.7	79	0.6	13 380
5	0.48	65	24	0.8	76	0.6	14 299
5.5	0.42	74	28	1.0	73	0.6	15 563
6	0.36	82	31	1.2	71	0.6	17 358
6.5	0.29	109	43	1.5	68	0.5	20 026
7	0.23	136	54	2.0	65	0.5	24 290
7.5	0.17	182	74	2.8	62	0.5	31 978
8	0.10	327	136	4.6	59	0.5	49 411

Table H-2: Calculation results of biofilter capital costs

MBBR DO [mg/L]	Organic loading [g/m^2.day]	Nitrification rate [g/m^2.day]	Biomedia volume [m^3]	Biomedia cost [ZAR]	Number of biofilters	Biofilter tank cost [ZAR]	Biofilter total cost [ZAR]
2	1.3	0.33	4.77	37 811	8	18 400	56 211
2.5	1.5	0.38	4.15	32 932	7	16 100	49 032
3	1.6	0.41	3.90	30 936	6	13 800	44 736
3.5	1.9	0.48	3.30	26 177	6	13 800	39 977
4	2.2	0.56	2.86	22 686	5	11 500	34 186
4.5	2.5	0.63	2.52	20 017	4	9 200	29 217
5	2.7	0.68	2.34	18 562	4	9 200	27 762
5.5	3	0.75	2.11	16 736	4	9 200	25 936
6	3.3	0.83	1.92	15 237	3	6 900	22 137
6.5	3.5	0.88	1.81	14 379	3	6 900	21 279
7	3.8	0.95	1.67	13 258	3	6 900	20 158
7.5	4	1.00	1.59	12 604	3	6 900	19 504
8	4.3	1.08	1.48	11 734	3	6 900	18 634

Table H-3: Cashflow of various MBBR DO concentration cases

Cash flow [ZAR]	Year										
DO [mg/L]	0	1	2	3	4	5	6	7	8	9	10
2.0	-67 518	-13 125	-15 234	-17 683	-20 526	-23 826	-27 656	-32 102	-37 262	-43 252	-50 205
2.5	-60 551	-13 370	-15 520	-18 015	-20 910	-24 272	-28 174	-32 703	-37 960	-44 062	-51 145
3.0	-56 542	-13 704	-15 906	-18 463	-21 432	-24 877	-28 876	-33 518	-38 906	-45 160	-52 420
3.5	-52 166	-14 149	-16 423	-19 063	-22 128	-25 685	-29 814	-34 607	-40 170	-46 628	-54 123
4.0	-46 886	-14 741	-17 111	-19 861	-23 054	-26 760	-31 062	-36 055	-41 851	-48 579	-56 389
4.5	-42 598	-15 531	-18 028	-20 926	-24 290	-28 195	-32 727	-37 989	-44 095	-51 184	-59 412
5.0	-42 061	-16 598	-19 266	-22 363	-25 958	-30 131	-34 975	-40 597	-47 123	-54 698	-63 491
5.5	-41 499	-18 065	-20 969	-24 340	-28 253	-32 795	-38 067	-44 186	-51 290	-59 535	-69 105
6.0	-39 495	-20 148	-23 387	-27 146	-31 510	-36 576	-42 455	-49 280	-57 202	-66 398	-77 072
6.5	-41 304	-23 245	-26 981	-31 319	-36 353	-42 197	-48 981	-56 855	-65 994	-76 603	-88 918
7.0	-44 449	-28 195	-32 728	-37 989	-44 096	-51 184	-59 412	-68 963	-80 049	-92 917	-107 854
7.5	-51 481	-37 118	-43 085	-50 012	-58 051	-67 383	-78 215	-90 789	-105 383	-122 324	-141 989
8.0	-68 045	-57 354	-66 574	-77 276	-89 699	-104 118	-120 855	-140 284	-162 835	-189 011	-219 396

Table H-4: NPV over time of various MBBR DO concentration cases

NPV [ZAR]	Year										
DO [mg/L]	0	1	2	3	4	5	6	7	8	9	10
2.0	-67 500	-79 400	-92 000	-105 300	-119 300	-134 100	-149 700	-166 200	-183 600	-201 900	-221 300
2.5	-60 600	-72 700	-85 500	-99 100	-113 300	-128 400	-144 300	-161 100	-178 800	-197 500	-217 200
3.0	-56 500	-69 000	-82 100	-96 000	-110 700	-126 100	-142 400	-159 600	-177 800	-196 900	-217 100
3.5	-52 200	-65 000	-78 600	-92 900	-108 000	-124 000	-140 800	-158 600	-177 300	-197 100	-218 000
4.0	-46 900	-60 300	-74 400	-89 400	-105 100	-121 700	-139 200	-157 700	-177 300	-197 900	-219 600
4.5	-42 600	-56 700	-71 600	-87 300	-103 900	-121 400	-139 900	-159 400	-180 000	-201 700	-224 600
5.0	-42 100	-57 100	-73 100	-89 900	-107 600	-126 300	-146 100	-166 900	-188 900	-212 100	-236 500
5.5	-41 500	-57 900	-75 300	-93 500	-112 800	-133 200	-154 700	-177 400	-201 300	-226 500	-253 200
6.0	-39 500	-57 800	-77 100	-97 500	-119 100	-141 800	-165 700	-191 000	-217 700	-245 900	-275 600
6.5	-41 300	-62 400	-84 700	-108 300	-133 100	-159 300	-186 900	-216 100	-246 900	-279 400	-313 700
7.0	-44 400	-70 100	-97 100	-125 700	-155 800	-187 600	-221 100	-256 500	-293 800	-333 200	-374 800
7.5	-51 500	-85 200	-120 800	-158 400	-198 100	-239 900	-284 000	-330 600	-379 800	-431 700	-486 400
8.0	-68 000	-120 200	-175 200	-233 300	-294 500	-359 200	-427 400	-499 400	-575 300	-655 500	-740 100

APPENDIX I : Air distribution system sizing

The air distribution were all assumed to be HDPE pipes with a internal surface roughness of 0.007 mm (Marley Pipe Systems, 2010). The air distribution pipe coming from the blower immediately splits into two supply lines going to the fish tanks and MBBRs (see section 4.7.2). Each of these supply lines were sized to have the same head loss at the furthest air outlet on each end. The intermediate air outlets along each line will need to be tuned using valves to match the pressure drop experienced at the end of each line in order to allow air to discharge at those points.

Table I-1: Head loss calculation results of the fish tank air supply line

Line number	Diameter [mm]	Length [m]	Air flow [std m^3/h]	Air velocity [m/s]	Reynolds Number	Flow regime	Friction factor	Head loss [m]
1	101.6	2	110.0	3.77	25 528	Turbulent	0.024	0.35
2	101.6	2.2	88.6	3.04	20 564	Turbulent	0.026	0.26
3	101.6	2.2	55.0	1.88	12 764	Turbulent	0.029	0.11
4	101.6	2.2	21.4	0.73	4 964	Turbulent	0.038	0.02
5	58	0.48	21.4	2.25	8 695	Turbulent	0.032	0.07
6	58	0.48	19.9	2.09	8 074	Turbulent	0.033	0.06
7	58	0.48	18.3	1.93	7 453	Turbulent	0.034	0.05
8	58	0.48	16.8	1.77	6 832	Turbulent	0.034	0.05
9	58	0.48	15.3	1.61	6 211	Turbulent	0.035	0.04
10	58	0.48	13.8	1.45	5 590	Turbulent	0.037	0.03
11	58	0.48	12.2	1.28	4 969	Turbulent	0.038	0.03
12	58	0.48	10.7	1.12	4 348	Turbulent	0.039	0.02
13	58	0.48	9.2	0.96	3 726	Transitional	0.041	0.02
14	58	0.48	7.6	0.80	3 105	Transitional	0.044	0.01
15	58	0.48	6.1	0.64	2 484	Transitional	0.047	0.01
16	58	0.48	4.6	0.48	1 863	Laminar	0.034	0.00
17	58	0.48	3.1	0.32	1 242	Laminar	0.052	0.00
18	58	0.48	1.5	0.16	621	Laminar	0.103	0.00
Small pipe	12	0.5	0.8	1.88	1 501	Laminar	0.043	0.32

Table I-2: Head loss calculation results of the MBBR air supply line

Line number	**Diameter** [mm]	**Length** [m]	**Air flow** [std m^3/h]	**Air velocity** [m/s]	**Reynolds Number**	**Flow regime**	**Friction factor**	**Head loss** [m]
16	83	1	25.0	1.28	7 102	Turbulent	0.034	0.03
17	83	1	20.8	1.07	5 918	Turbulent	0.036	0.03
18	83	1	16.7	0.86	4 735	Turbulent	0.038	0.02
19	83	1	12.5	0.64	3 551	Transitional	0.042	0.01
20	83	1	8.3	0.43	2 367	Transitional	0.048	0.01
20	83	1	4.2	0.21	1 184	Laminar	0.054	0.00
Small pipe	12	0.1	0.7	1.71	1 364	Laminar	0.047	0.06